

The Role of Aliphatic and Aromatic Coal Structures and Macerals in Low Temperature Oxidation Processes

Yongseung Yun, Emma Jakab, William H. McClennen, George R. Hill
and Henk L.C. Meuzelaar

Biomaterials Profiling Center, University of Utah
Salt Lake City, Utah 84108

INTRODUCTION

Low temperature ($\leq 100^\circ\text{C}$) coal oxidation processes are known to have a pronounced effect on important coal properties such as coking and caking behavior (1,2,3), heat of combustion (3), floatability (2) slurry pH (2), tar yield and extractability (3). However, the mechanisms and kinetics of the chemical reactions underlying such "weathering" processes in coals are far from well understood. Among the most promising analytical methods for elucidating the structural and compositional changes during coal weathering are Fourier Transform infrared (FTIR) spectroscopy (4,5) and pyrolysis mass spectrometry (Py-MS) (6,7). FTIR studies performed by Painter et al. (8) show a strong increase in carbonyl as well as ester moieties. Recent Py-MS experiments by Jakab et al. (9) have demonstrated a pronounced decrease in the pyrolysis yields of phenolic and naphthalenic components accompanied by increased production of highly polar (carboxylic and carbonylic) short chain aliphatic moieties. Py-MS techniques based on the combination of Curie-point pyrolysis, low voltage mass spectrometry and computerized multivariate data analysis methods were found to be sensitive enough to detect changes in bituminous and lower rank coals after exposure to air at 80°C for only 1 or 2 days (9). Moreover, time-resolved Py-MS techniques capable of recording up to 10 spectra per second at heating rates of approx. 100°K/s were shown to provide valuable information about the mechanisms and kinetics of vacuum pyrolysis processes in fresh and weathered coal (9). Meuzelaar et al. (3) interpreted the pronounced decrease in extractable alkylnaphthalene moieties in high volatile B bituminous Hiawatha coal as a loss of "mobile phase" components by attachment to the "network phase". Under the conditions employed in those experiments, such "grafting" processes appear to be more prevalent than the often hypothesized crosslinking reactions between macromolecular components. These interpretations find support in recent studies by Larsen et al. (10) on the influence of weathering processes on coal swelling properties in solvents.

In the present article new Py-MS data on low temperature oxidation effects in several U.S. coals of different rank and origin will be discussed with special emphasis on the role of different coal macerals.

EXPERIMENTAL

Three separate experiments were performed: (a) oxidation under dynamic reactor flow conditions; (b) oxidation under static conditions; and (c) pyridine extraction of fresh and oxidized coal.

Under dynamic conditions, 20-24 g aliquots (-60 mesh) of four coals (Wyodak, Adaville #6, Hiawatha, Upper Freeport) were exposed to an air flow of 5.10 ml/min in a 100 ml glass reactor, at 100°C for 170-212 hours (11). Under static conditions, four maceral concentrates were oxidized with air, viz. vitrinite and semi-fusinite fractions prepared by density gradient centrifugation of Dakota seam coal (New Mexico, PSOC 858), sporinite prepared by density gradient centrifugation, from Brazil block seam, Indiana Eastern (PSOC 107) and a hand-picked resinite sample from the Wattis seam (Utah). Twenty five mg aliquots of these macerals were exposed to air at 100°C for 100 hours in sealed 2 l flasks.

Pyridine extraction was performed on Hiawatha coal in a regular Soxhlet extractor for 24 hours at room temperature. A weathered coal sample for pyridine

extraction was prepared by exposing a 15 g aliquot (-60 mesh) to air at 100°C for 212 hours (12) under dynamic flow conditions.

All whole coal samples as well as insoluble extraction residue were hand ground under nitrogen atmosphere into a fine, uniform suspension in Spectrograde methanol (5 mg of sample per ml of methanol). The pyridine-extracted fraction was dissolved in a mixture of benzene and methanol (3:1, v/v) at a concentration of 2 mg/ml. Five microliter drops of the above suspensions and the solution were coated on the ferromagnetic filaments used in Curie-point pyrolysis and air-dried under continuous rotation, resulting in approximately 20 µg of dry sample on the filament.

Pyrolysis MS runs were performed under the same conditions for all samples, i.e., electron energy 12 eV, mass range 20-260 m/z, scanning rate 1000 amu/s, temperature rise time about 6 s, equilibrium temperature 610°C, total heating time 10 s (13,14). In order to evaluate weathering-induced differences, computerized multivariate analysis techniques such as factor analysis and discriminant analysis were applied to the MS data (14,15).

RESULTS AND DISCUSSION

Low voltage pyrolysis mass spectra of fresh and weathered coals are shown in Figures 1-4. Comparison of the spectra of the four fresh coal samples in Figures 1a-4a shows the obvious effects of rank differences between the two subbituminous coals (Adaville #6 and Wyodak) and the two high volatile bituminous coals (Upper Freeport and Hiawatha). Whereas the spectra of the former (figs. 1a and 2a) are dominated by dihydroxybenzenes and phenols of various degrees of alkylsubstitution, the spectra of the latter (figs 3a and 4a) show a dramatic decrease in dihydroxybenzene signals coupled with a markedly higher abundance of aromatic hydrocarbon series such as naphthalenes and benzenes. This trend appears to be most pronounced in the Upper Freeport sample, perhaps due to its slightly higher rank (borderline hvAb/mvb) than the Hiawatha coal (hvBb/hvAb). However, the major differences in age and origin between the two samples (Upper Freeport - Carboniferous, Interior Province; Hiawatha - Cretaceous, Rocky Mountain Province) should also be kept in mind. As noted by Given et al. (16) Western coals tend to have lower hydroxyl content than Interior and Eastern Province coals of comparable rank. For a detailed discussion of rank effects on the low voltage pyrolysis mass spectra of 102 Western U.S. coals the interested reader is referred to previous publications (6,7).

The differences between the spectra of the two subbituminous coals (figs. 1a and 2a) are far less pronounced. Again a small rank effect may be present. On the basis of equilibrium moisture content some Wyodak coal samples could be classified as lignites (17) whereas the rank of the Adaville #6 coal is subbituminous B. Although the pyrolysis mass spectra of Western lignites and subbituminous coals do not show marked differences (7), the slightly higher relative abundance of the naphthalene series in the Adaville coal (Figure 2a) is rather typical as is the somewhat different distribution of phenols.

It should be pointed out here that chemical identification of the different peak series in the low voltage pyrolysis mass spectra of coals is tentative only and is based largely on supporting data obtained by GC/MS (18,19), MS/MS (20) and NMR (21) studies of similar coal pyrolyzates. Moreover, since every mass peak is likely to contain contributions from more than one chemical compound, the use of chemical labels is only meant to identify those components thought to contribute most strongly to the respective peak series.

The effects of low temperature oxidation on the four coals can be examined by "subtracting" the spectra of the weathered coal samples in Figures 1b-4b from those of the corresponding fresh samples using a discriminant analysis procedure (9) (Figures 1a-4a). This results in the discriminant spectra shown in Figures 1c-4c. Comparison of the latter reveals an intriguing, generalized trend. The aromatic components of the four coal pyrolyzates have decreased markedly, whereas the strong aliphatic signals (e.g., corresponding to C_nH_{2n+1} , C_nH_{2n} , C_nH_{2n-1} and C_nH_{2n-2} ; $n \leq 10$) in each spectrum appear to have remained constant. This apparently reflects a difference in susceptibility to weathering effects between those structural moieties

producing the abovementioned aliphatic peak series and those moieties giving rise to the aromatic hydrocarbon and hydroxyaromatic peak series.

A second, intriguing observation from Figures 1c-4c is the qualitative similarity between the low molecular weight ion signals found to increase upon weathering. In all four coals these peak series appear to represent highly polar short chain aliphatic compounds such as CO^+ (m/z 28), CO_2^+ (m/z 44), and CH_3COOH^+ (m/z 60). Furthermore, it is interesting to note the high intensity of m/z 32, thought to represent increased retention of the methanol solvent (used to prepare coal suspensions for Py-MS analysis) in the more polar, weathered coals.

First, let us concentrate on the differential loss of aromatic vs. aliphatic pyrolyzate components. It is tempting to try to explain this on the basis of possible differences in the susceptibility of the different coal maceral components. As evident from the averaged pyrolysis mass spectra of maceral concentrates in Figure 5, marked differences exist between the relative aliphaticity and aromaticity of pyrolyzates from fusinites (highly aromatic), vitrinites and sporinites (primarily aliphatic). Other liptinitic macerals such as alginite and cutinite provide even stronger aliphatic Py-MS patterns than sporinite (22), whereas resinites from Western U.S. coals are characterized by alicyclic and hydroaromatic series (23). Thus, in principle it would be possible that low temperature oxidation could effect primarily the more highly aromatic vitrinitic and/or fusinitic macerals while leaving the more aliphatic macerals relatively unaffected.

This brings up the interesting question which of the various liptinites are primarily responsible for the remarkably similar aliphatic patterns observed in all four coals in Figures 1-4. Although sporinite is likely to contribute to the Py-MS pattern of the Carboniferous Upper Freeport coal, Cretaceous (Adaville, Hiawatha) and Tertiary (Wyodak) Western coals generally contain only minor amounts of sporinite. Many Western coals, however, are known to contain marked amounts (e.g., 5-10%) of resinite (23). Nevertheless, typical Py-MS patterns of resinites are quite different from the prominent aliphatic hydrocarbon patterns in Figures 1-4. Consequently, the authors believe that two ubiquitous liptinitic macerals, namely alginite (or detrital forms such as bituminite) and cutinite are primarily responsible for the observed aliphatic Py-MS patterns and may well be present in much larger quantities than estimated by micropetrographic techniques. Evidence supporting the potentially important contributions of algal coal components has been presented (though not completely interpreted) in previous Py-MS studies of over 130 U.S. coals (7,17), whereas the grossly underestimated role of cutinitic macerals has recently been highlighted in several studies by De Leeuw and co-workers (24).

Pyridine extraction of Hiawatha coal before and after low temperature oxidation (Figure 6) not only shows a dramatic decrease in extraction yield (22% 4%) but also reveals a nearly complete separation between aromatic peak series (dominant in the extract) and aliphatic peak series (retained in the residue). Although it should be pointed out that the residue is likely to contain more or less highly condensed aromatic components as well (which may well have remained "invisible" to the Py-MS procedure), the apparent insolubility of the aliphatic hydrocarbon components is in line with the previous contention that alginite and/or cutinite derived macerals are likely to be responsible for the bulk of the observed aliphatic hydrocarbon signals in Py-MS patterns of whole coal. Both types of macerals are notoriously difficult to dissolve (cutinites and algal kerogens can be purified by means of strong acids!).

Careful examination of Figure 6 also provides an important clue with regard to the possible fate of the disappearing aromatic moieties during low temperature weathering. Py-MS analysis of the pyridine residue of the weathered coal sample reveals a clear series of alkylnaphthalenes, apparently liberated by the vacuum pyrolysis conditions. It is tempting to speculate that these aromatic moieties became linked ("grafted") to the macromolecular network during the weathering process. However, the possibility of physical entrapment (clathration) cannot be ruled out either. Present indications are that the grafted (or trapped) aromatic molecules alone cannot fully explain the marked loss of aromatic and hydroxyaromatic moieties but that some aromatic rings are destroyed by the oxidation process (in spite of the relatively low temperatures used), resulting in the formation of the

short chain aliphatic acids and ketones seen in Figures 1c-4c. Further support for this explanation is found in the results of low temperature oxidation studies on selected maceral concentrates of similar rank shown in Figures 7 and 8.

The factor score plot in Figure 7 reveals that the resinite and semifusinite concentrates underwent more severe oxidative changes, which resulted in the formation of oxygen containing aliphatic moieties, than the vitrinite concentrate. The sporinite concentrate showed the least severe weathering-induced degradation. This suggests that the abundant hydroaromatic and aromatic moieties in the resinite and semifusinite samples respectively, provide the most likely source for the short chain, carboxyl- and carbonyl-containing, aliphatic compounds observed in the Py-MS patterns of weathered coal.

In conclusion, aliphatic, hydrocarbon-rich coal structures thought to be derived from cutinitic or algal sources show little or no chemical changes under low temperature oxidation conditions whereas vitrinite and sporinite show a moderate oxidation tendency. Further oxidation experiments with coals and maceral concentrates from different sources will have to be carried out in order to determine the general validity of the observed phenomena for coals of different rank and depositional history.

ACKNOWLEDGEMENTS

The authors gratefully acknowledge gifts of fresh Upper Freeport and Wyodak samples by Dr. Karl Vorres (Argonne National Laboratory); of fresh Adaville #6 and Hiawatha samples by Utah Power and Light and of maceral concentrates by Drs. R. Pugmire and J. Karas (University of Utah). The work reported here was supported by DOE contract DE-FG22-84PC70798.

REFERENCES

1. Crelling, J.C., R.H. Schrader, and L.G. Benedict, *Fuel*, 58, 542 (1979).
2. Gray, R.J., A.H. Rhoades and D.T. King, *AIChE Transactions*, 260, 334-341 (1976).
3. Meuzelaar, H.L.C., W.H. McClennen, C.C. Cady, G.S. Metcalf, W. Windig, J.R. Thurgood, and G.R. Hill, in *ACS Preprints (Div. of Fuel Chem.)*, 29 (5), 166-177 (1984).
4. Rhoades, C.A., J.T. Senftle, M.M. Davis, and P.C. Painter, *Fuel*, 62, 1387 (1983).
5. Cronauer, D.C., R.G. Ruberto, R.S. Jenkins, A. Davis, and P.C. Painter, *Fuel*, 62, 1124 (1983).
6. Harper, A.M., H.L.C. Meuzelaar, *Fuel*, 63, 793 (1984).
7. Meuzelaar, H.L.C., A.M. Harper, G.R. Hill, and P.H. Given, *Fuel*, 63, 640-652 (1984).
8. Painter, P.C., R.W. Snyder, D.E. Pearson, and J. Kwong, *Fuel*, 59, 282 (1980).
9. Jakab, E., B. Hoesterey, W. Windig, G.R. Hill, and H.L.C. Meuzelaar, "Effects of Low Temperature Air Oxidation ("Weathering") Reactions on the Pyrolysis Mass Spectra of U.S. Coals" submitted to *Fuel* (1986).
10. Larsen, J.W., D. Lee, and T.E. Schmidt, "The Effect of Atmospheric Oxygen on the Structure of Coals", Final Report to GRI, Contract No. 5082-260-0907 (1985).
11. Meuzelaar, H.L.C., G.R. Hill, Y. Yun, and W. Windig, "Weathering Effects on Structure and Reactivity of U.S. Coals", Third Quarterly Report to DOE, Contract No. DE-FG22-84PC70798 (1986).
12. Hill, G.R., H.L.C. Meuzelaar, J.M. Futrell, A.M. Harper, and W.H. McClennen, "Role of Preasphaltenes in Coal Conversion Reactions", Final Report to DOE, Contract No. DE-FG22-82PC50970 (1984).
13. Meuzelaar, H.L.C., J.H. Haverkamp, and F.D. Hileman, *Pyrolysis Spectrometry of Recent and Fossil Biomaterials: Compendium and Atlas*, Elsevier Publishing Co., Amsterdam (1982).
14. Meuzelaar, H.L.C., W. Windig, A.M. Harper, S.M. Huff, W.H. McClennen, and J.M. Richards, *Science*, 226 (4672), 268-274 (1984).
15. Windig, W. and H.L.C. Meuzelaar, *Anal. Chem.*, 56, 2297-2303 (1984).
16. Yarzab, R.F., A. Abdel-Baset and P.H. Given, *Geochimica et Cosmochimica Acta*, 43, 281-287 (1979).

17. Metcalf, G.S. W. Windig, G.R. Hill, H.L.C. Meuzelaar, Characterization of U.S. Lignities by Pyrolysis Mass Spectrometry and Multivariate Analysis, Coal Geology, (1986) in press.
18. Blazso, M. and E. Jakab, J. Anal. Appl. Pyrol., 8, 189 (1982).
19. Nip, M., J.W. de Leeuw, P.A. Schenck, H.L.C. Meuzelaar, S.A. Stout, P.H. Given, and J.A. Boon, J. Anal. Appl. Pyrol., 8, 221 (1985).
20. Meuzelaar, H.L.C., W.H. McClennen, J.H. Tomlinson, and D.L. Pope, Proc. Int. Conf. on Coal Science, Dusseldorf, pp. 816-821 (1981).
21. Hoesterey, B.L., W. Windig, H.L.C. Meuzelaar, E.M. Eyring, D.M. Grant, and R.J. Pugmire, "An Integrated Spectroscopic Approach to the Chemical Characterization of Pyrolysis Oils" ACS Preprints (Div. of Fuel Chem.) Denver 1987.
22. Larter, S.R. and A.G. Douglas, J. Anal. Appl. Pyrol., 4, 1-19 (1982).
23. Crelling, J.C., personal communication.
24. Nip, M., E.W. Tegelaar, H. Brinkhuis, J.W. de Leeuw, and P.A. Schenck, Analysis of Recent and Fossil Plant Cuticles by Curie-point Pyrolysis-Gas Chromatography and Curie point pyrolysis-gas Chromatography-Mass Spectrometry: Recognition of a New, Highly Aliphatic and Resistant Biopolymer, in Adv. in Org. Geochem., (1986) in press.
25. Meuzelaar, H.L.C., Harper, A.M., Pugmire, R.J., and Karas, J., Int. J. Coal Geology, 4, 143-171 (1984).

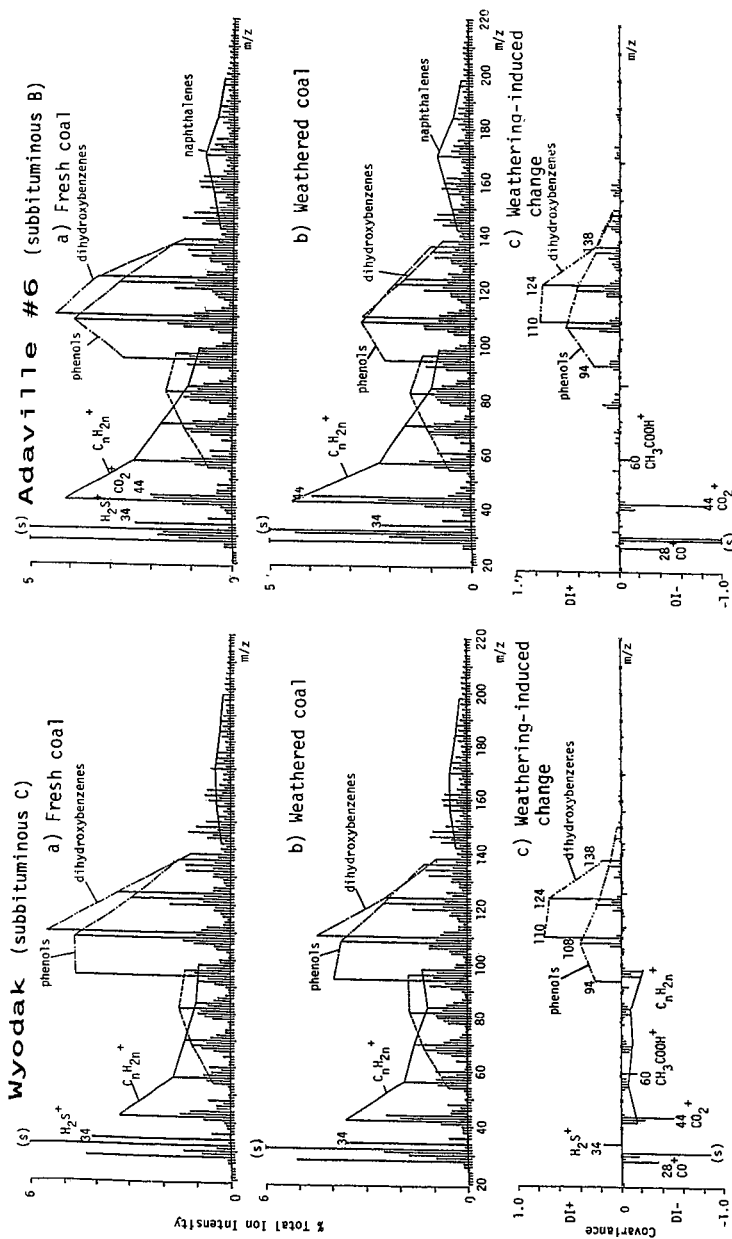


Figure 2. Curie-point pyrolysis mass spectra of (a) fresh, (b) weathered Adaville #6 coal, and (c) discriminant spectra. Positive components (DI⁺) represent mass peaks decreased in weathered sample and negative components (DI⁻) represent compounds increased in weathered sample. (s) denotes peak originating from solvent.

Figure 1. Curie-point pyrolysis mass spectra of (a) fresh, (b) weathered Wyodak coal, and (c) discriminant spectra. Positive components (DI⁺) represent mass peaks decreased in weathered sample and negative components (DI⁻) represent compounds increased in weathered sample. (s) denotes peak originating from solvent.

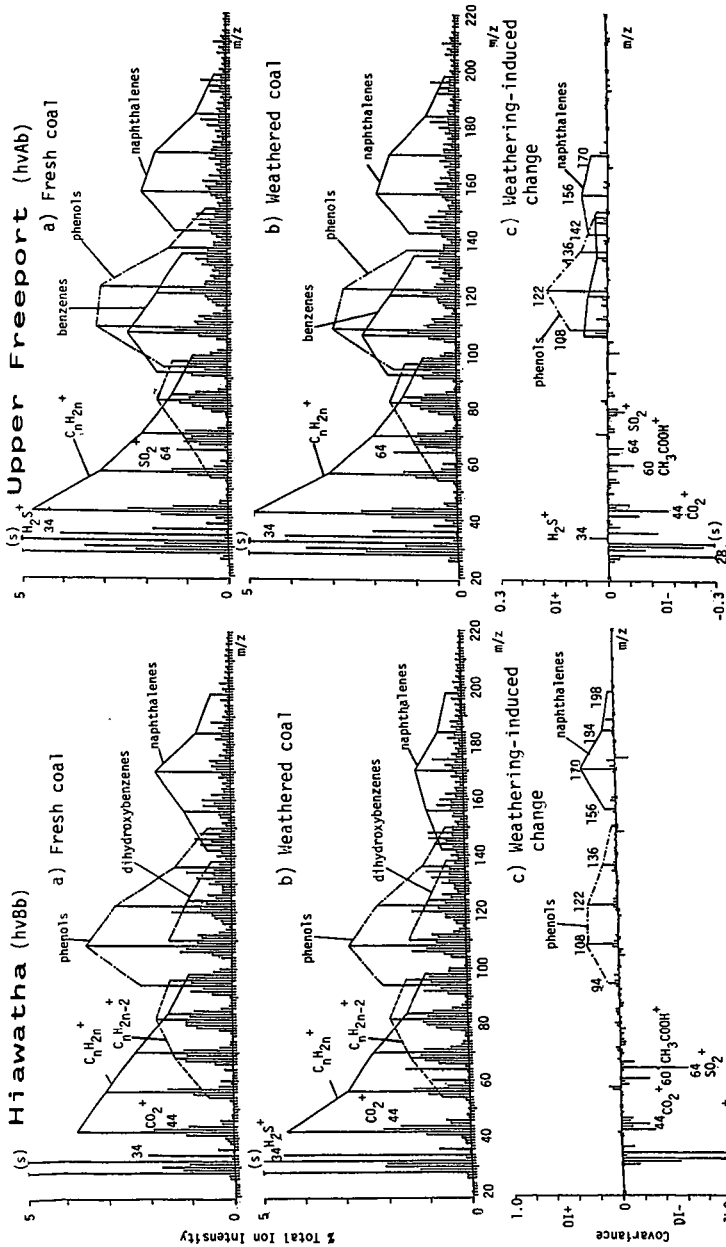


Figure 3. Curie-point pyrolysis mass spectra of (a) fresh, (b) weathered Hiawatha coal, and (c) discriminant spectra. Positive components (DI⁺) represent mass peaks decreased in weathered sample and negative components (DI⁻) represent compounds increased in weathered sample. (s) denotes peak originating from solvent.

Figure 4. Curie-point pyrolysis mass spectra of (a) fresh (b) weathered Upper Freeport coal, and (c) discriminant spectra. Positive components (DI⁺) represent mass peaks decreased in weathered sample and negative components (DI⁻) represent compounds increased in weathered sample. (s) denotes peak originating from solvent.

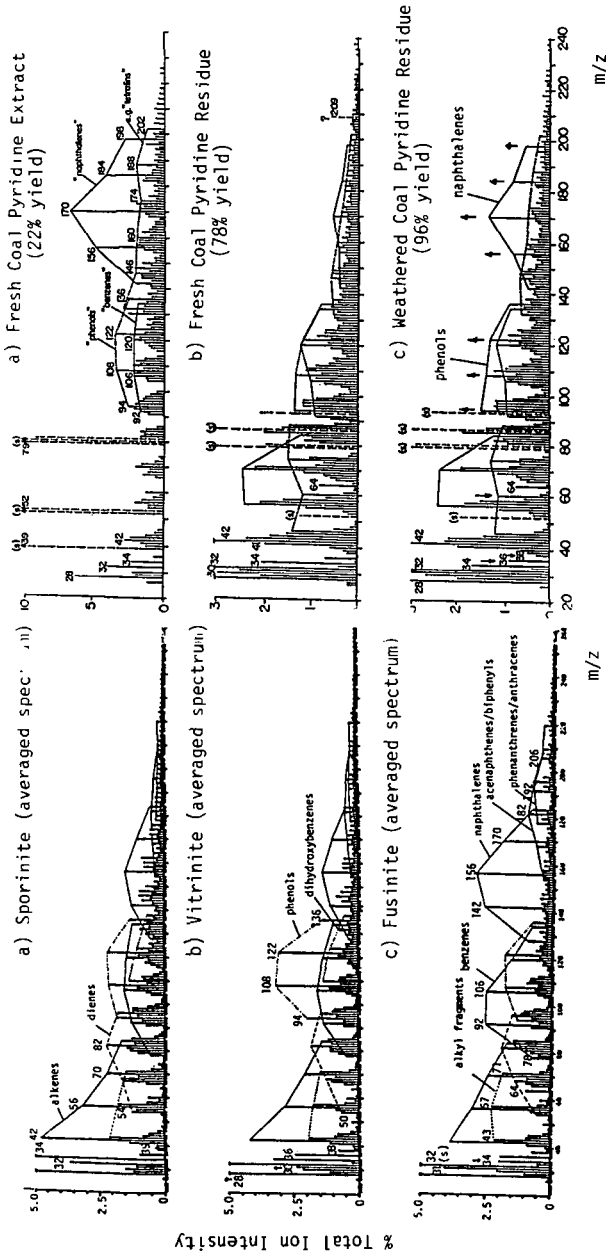


Figure 5. Typical pyrolysis mass spectra of three different maceral types obtained by averaging spectra of several different maceral concentrate samples, as obtained in an earlier study (25).

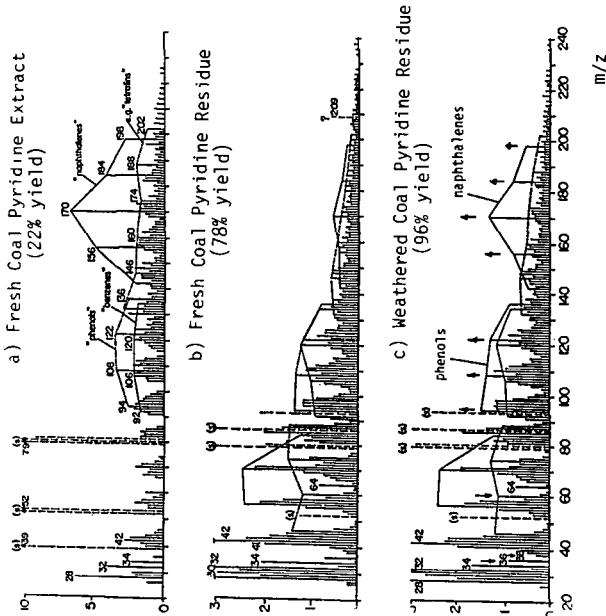


Figure 6. Low voltage desorption/pyrolysis mass spectra of pyridine extract and residues from Hiawatha coal. (s) denotes solvent peaks (pyridine solvent signals are indicated by dashed lines).

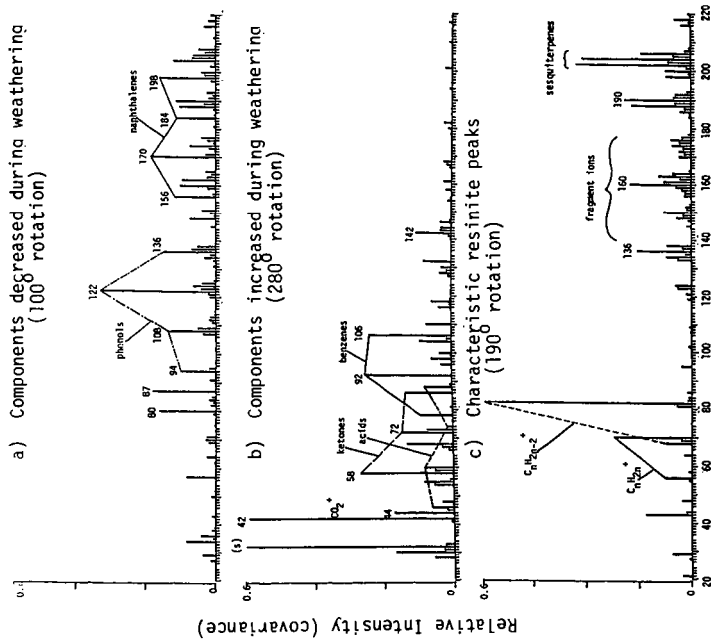


Figure 8. Discriminant spectra of macerals. 100° rotation is weathering direction and 280° rotation is resinite direction when compared with Figure 7.

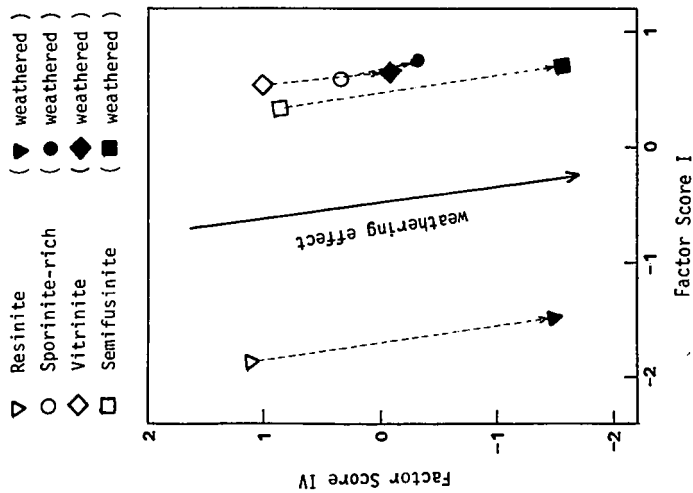


Figure 7. Factor score plot from Py-MS data sets on fresh and weathered macerals. 100° rotation clearly shows the weathering effect.

**CHARACTERIZATION OF SURFACE FUNCTIONALITY OF COALS BY
PHOTOACOUSTIC FTIR (PAIFT) SPECTROSCOPY, REFLECTANCE INFRARED
MICROSPECTROMETRY, AND X-RAY PHOTOELECTRON SPECTROSCOPY (XPS)**

**Brian M. Lynch, Lal-Im Lancaster,
and J. Anthony MacPhee***

**Department of Chemistry, St. Francis Xavier University,
Antigonish, Nova Scotia B2G 1C0, Canada**

This paper illustrates detection by the technique of PhotoAcoustic Infrared Fourier Transform (PAIFT) spectroscopy of new carbonyl-type functionality at the surfaces of powdered bituminous coals, generated by both base-promoted and by thermal decomposition of precursor peroxide species, postulated as ubiquitous constituents at the surfaces of all except the most freshly prepared samples. In artificially oxidized coals, there are quantitative associations between the level of carbonyl content revealed by PAIFT spectra and plastic properties of the coals. In additional, related studies, we have derivatized and quantified the hydroxyl group content of the oxidized coals by trifluoroacetylation, followed by hydrolysis and anion-chromatographic analyses for trifluoroacetate. PAIFT and Fluorine-XPS spectra of the trifluoroacetylated species are discussed. Maceral components and mineral inclusions have been identified and characterized in sectioned, polished surfaces of Canadian bituminous coals using reflection FTIR microspectrometry; this direct examination shows promise for real-time monitoring of various reactions at surfaces.

INTRODUCTION

Sensitivity enhancements in spectroscopy show promise of specific characterization of functional groups in coals and their chemical transformations. We have applied one of the newer techniques (PhotoAcoustic Infrared Fourier Transform spectroscopy (PAIFT spectroscopy)) to generate a data base of coal samples amounting to several thousand spectra. Various preliminary reports of our results have been published or presented (1-7).

Among the manifold advantages possessed by PAIFT spectroscopy for the study of coals are minimal sample preparation, insensitivity of signal to degree of subdivision, and the ability to observe surface features generated by chemical transformations. PAIFT spectra of coals do not exhibit the sloping baselines characteristic of alkali halide pellet spectra (contrast a recent report of such FTIR spectra of Canadian coals (8)), and subtraction to yield difference spectra revealing introduced features is straightforward and avoids arbitrary scaling procedures. The first paper of this series (7) reported detection by PAIFT spectroscopy of new carbonyl oxygen functions at the surfaces of powdered bituminous coals, derived from base-promoted or thermal decompositions of precursor peroxide species, which we suggested were present ubiquitously as surface entities for all except the most freshly prepared samples. In more recent work, we have discovered that thermal decompositions accompany a standard vacuum drying procedure.

* Energy Research Laboratories, CANMET, Energy, Mines and Resources Canada, Ottawa, Canada K1A 0G

EXPERIMENTAL

PhotoAcoustic Infrared Fourier Transform (PAIFT) Spectra

Spectra were obtained using a Bruker IFS110 purge-type Infrared Fourier System with a Ge on KBr beamsplitter. The interferometer compartment of the spectrometer was acoustically insulated from the sample compartment using a box fabricated from expanded polystyrene. The modulated source radiation was reflected into a E G & G Princeton Applied Research Model 6003 Photoacoustic accessory fitted with a zinc selenide window and the amplified photoacoustic output was transmitted to the data system of the IFS110. The nitrogen purge flow was interrupted during scanning.

In the standard operating mode, 10-50 mg of the dried coal were placed in the sample cup, and 128 photoacoustic interferograms were collected at 8 cm^{-1} resolution with a zero-filling factor of 2, corresponding to a final transformed spectrum encoded every 4 cm^{-1} . The photoacoustic spectra were obtained by ratioing against the energy output (black-body response) from a similarly dried sample of Fisher Carbon Lampblack C-198. The interferometer mirror velocity was $0.08333 \text{ cm s}^{-1}$, and spectra were acquired from 4000 to 400 cm^{-1} . The difference spectra illustrated in Figures 1 through 6 were obtained by least-squares subtraction over the range 2000 - 1400 cm^{-1} .

Preparation of Coal Samples for Spectroscopy

The coals were ground to the range 50-60 mesh under liquid nitrogen using a Brinkmann Pulverizer, and were dried at 100°C under vacuum for 6 h before transfer to the sample cup of the photoacoustic accessory.

High-Pressure Oxidations of Coal Samples

The coals were ground and sized to 50 mesh and were subjected to oxidation by air at 55°C and 9 MPa for periods ranging from 3 to 196 h. All samples were subjected to the standard drying procedure before PAIFT spectroscopic examination.

Analytical and fluidity data on the as-received coal samples are presented in Table 1.

FTIR Microspectrometry

Spectra were acquired (250-500 scans) using a Spectra-Tech IR-PLAN accessory and a Nicolet 20SX spectrometer, at a resolution of 4 cm^{-1} ; spectra are referenced against an equivalent area of a gold-surfaced mirror.

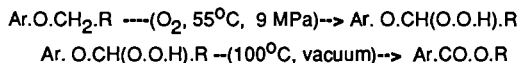
DISCUSSION AND RESULTS

(a) Generation of Carbonyl Functionalities from Thermal Decompositions of Peroxides at Surfaces of Coals Subjected to "Accelerated Oxidations" at High Pressure

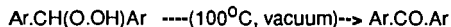
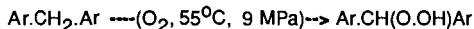
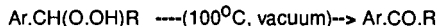
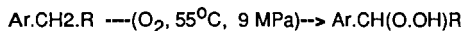
The recorded sensitivity of FTIR spectroscopy in detecting oxidative change in coals is significantly less than that of standard plasticity tests; thus, Painter and his colleagues (9), employing standard KBr pellet "transmission" FTIR spectroscopy, found less than a 1% increase in the ratioed intensity of carbonyl bands for coals oxidized at 60°C or 140°C for periods sufficient to decrease Gieseler fluidity by over 90%.

We have compressed the time scale of oxidative changes by subjecting powdered coals to pressurized air at slightly elevated temperatures. With such samples, we observe distinct, readily differentiated types of carbonyl absorptions (around 1750 , 1720 , 1690 , and 1650 cm^{-1}) whose relative proportions are *different* for different coals, and we propose that the carbonyl species are generated by the standard vacuum drying procedure from thermal decomposition of the assumed peroxide species. Representative difference spectra taken for the six coals of Table 1 at the stage of 48 hours oxidation are reproduced in Figures 1 through 6.

We suggest that these peaks arise from different, specific decompositions of peroxides occupying different structural sites in the coals. The 1750 cm^{-1} and 1720 cm^{-1} peaks are attributed to decompositions of α -hydroperoxyethers to yield cyclic or open-chain esters; the 1750 cm^{-1} (lactone species) from a cyclic ether precursor, and the 1720 cm^{-1} from an open-chain precursor, that is:



Stock and Wang (10) have recently postulated generation of lactone species from the ruthenium (VIII)-catalyzed oxidation of Illinois No. 6 bituminous coal by sodium periodate. The 1690 and 1650 cm^{-1} peaks are attributed to decompositions of α -hydroperoxy aralkanes or of hydroperoxy diarylalkanes, that is:



(b) *Associations of Carbonyl Absorption Intensities with Other Coal Properties*

The relative intensities of the four carbonyl absorptions for the six coals examined are dependent in a complex manner upon oxygen content, carbon/hydrogen ratio, and the progress of oxidation, but there are general *quantitative* associations of increasing carbonyl intensities with many characteristics of the behavior of the sequences of oxidized samples for a given coal. These include relationships between carbonyl intensity and oxygen content for the Greenhills coal (Western Canadian: bituminous high-volatile 'A'), carbonyl intensity and Gieseler fluidity for the Greenhills and Fording (Western Canadian: bituminous high-volatile 'A') coals, and for the Barton and McClure coals (U.S.A., bituminous high-volatile 'A' and medium-high volatile 'A'), illustrated in Figures 7 through 13. However, the coals are behaving in sufficiently different fashions (both in the quantitative distribution of the various introduced carbonyl species, in their qualitative rates of generation, and in the nature of the influence of changed functionality on the technical properties) that generalized treatment as a single data set would obscure the individual correlations. In view of our findings, we suggest that caution would be appropriate in using the approaches adopted by Fredericks and his co-workers (11), where attempts are made to make generalized predictions of technological properties using principal factor analyses of FTIR spectra of a wide range of coals.

(d) *Trifluoroacetylation as a Derivatization Technique for Hydroxyl Content of Coals*

Acetylation via acetic anhydride/pyridine is a standard derivatization method for analysis of hydroxyl content of coals, but the quantitative nature and the selectivity of these reactions are not established; there are significant difficulties in using FTIR difference spectroscopy and the acetate carbonyl intensity to define the nature of hydroxyl groups (that is, phenolic or alcoholic?). Since these differences arise in part from peak overlap of acetate carbonyl with the 1600 cm^{-1} absorption of coals, we have employed trifluoroacetylation (where the trifluoroacetate carbonyl absorbs around 1800 cm^{-1}) as an alternate technique. The trifluoroacetate ion may be analyzed readily by anion chromatography after hydrolysis of the trifluoroacetylated coal, and quantitation of the trifluoroacetyl group is also possible by calibration against the intensity of the fluorine and trifluoromethyl-carbon signals in the X-ray photoelectron spectra of such samples.

(e) *Reflection FTIR Microspectrometry of Coals*

We have conducted preliminary examinations of sectioned, polished surfaces of samples of Eastern and Western Canadian bituminous coals using the IR-PLAN accessory in the reflectance mode, referenced against a gold mirror. Representative spectra are reproduced as Figures 14 through 17. The significant differences among the microscopically distinguishable components, and the ease of detection and identification of mineral inclusions, suggest that direct examinations of coals undergoing chemical transformations (such as the base-promoted and thermal transformations discussed in this paper and our earlier work) could be profitably examined using this accessory FTIR device.

CONCLUSIONS

We have indicated the potential for surface characterization of several techniques under study in our laboratory. We suggest that the evidence for previously unquantified and undetected peroxide species on coal surfaces presented above and in an earlier Symposium (7) requires reconsideration of the influence of the proportion of surface peroxides upon the course(s) of coal pyrolyses, and provides strong support to recent proposals (12) recommending storage of laboratory samples of coals in sealed ampoules.

ACKNOWLEDGEMENTS

We thank Bob Durie, Jon Gethner, and Ron Liotta for useful discussions.

The reflection FTIR microspectrometric measurements were made at the Applications Laboratory, Spectra-Tech, Inc., Stamford, Connecticut, and we thank Joan Kwiatkowski and Cindy Friedman for their courtesy. The research work upon which this paper is based was supported by Energy, Mines, and Resources Canada through the Department of Supply and Services, Contract Serial Numbers OST83-00347 and OST85-00235, and under Research Agreements Nos. 230 (1985-1986) and 189 (1986-1987).

REFERENCES

- 1 Campbell, M., Lancaster, L., Lynch, B. M., and Mac Eachern, A. M. *Abstract 054, Pittsburgh Conference on Analytical Chemistry and Applied Spectroscopy*, 1983 (Atlantic City, New Jersey).
- 2 Lancaster, L., Lynch, B. M., Mac Eachern, A. M., Donini, J. C., Hamza, H. , and Michaelian, K. H. *Abstract 158, 57th Colloid & Surface Science Symposium, American Chemical Society*; 1983 (Toronto, Canada).
- 3 Lynch, B. M., and Mac Eachern, A. M. *Proc. 1983 Conference on Coal Science*, pp 653-654.
- 4 Lynch, B. M., Lancaster, L., Mac Eachern, A. M., and Khan, M. A. *Paper 161, Eastern Analytical Symposium, American Chemical Society*; 1983 (New York City, U. S. A.).
- 5 Lynch, B. M. *Bull. Am. Phys. Soc.* 1985, **30**, 504.
- 6 Lynch, B. M. *Proc. Soc. Photo-Optical Instr. Engineers* 1985, **553**, 320.
- 7 Lynch, B. M., Lancaster, L., and Fahey, J. T. *Prepr. Div. Fuel Chem. Am. Chem.Soc.* 1986, **31**, 43.
- 8 Cooke, N. E., Fuller, O. M., and Gaikwad, R. P. *Fuel* 1986, **65**, 1254.
- 9 Rhoads, C. A., Senville, J. T., Coleman, M. M., Davis, A., and Painter, P. C. *Fuel* 1983, **62**, 1387.
- 10 Stock, L. M. and Wang, S. H. *Prepr. Div. Fuel Chem. Am. Chem.Soc.* 1986, **31**, 49.
- 11 Fredericks, P. M., Osborn, P. R., and Swinkels, D. A. J. *Fuel* 1984, **63**, 139.
- 12 Larsen, J. W., and Schmidt, T. E. *Fuel* 1986, **65**, 131

Table 1
Coal Samples Subjected to High-Pressure Oxidations
Analytical and Fluidity Data on Fresh Coals

Coal Designation	Classification	C, %	H, %	O, %	Gieseler Fluidity (dd/min)
Greenhills (Western Canadian)	HV 'A'	81.56	4.75	4.79	24
Fording (Western Canadian)	HV 'A'	80.49	5.07	5.60	365
Barton (U. S. A.)	HV 'A'	81.81	5.08	4.34	20350
McClure (U. S. A.)	MV-HV 'A'	83.07	4.74	3.82	7900
Alto (Appalachian, U. S. A.)	HV 'A'	79.69	5.20	7.47	1580
Basset	L-MV	85.01	4.42	3.20	32

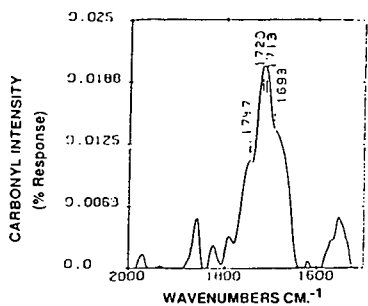


Figure 1
PAIFT Difference Spectrum
Greenhills Coal: (Oxidized 48 h) - (Fresh Coal)

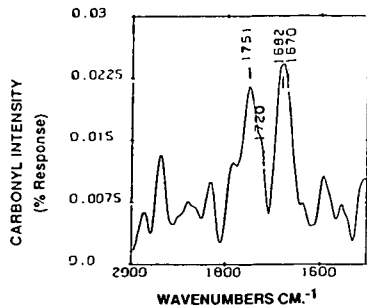


Figure 2
PAIFT Difference Spectrum
Fording Coal: (Oxidized 48 h) - (Fresh Coal)

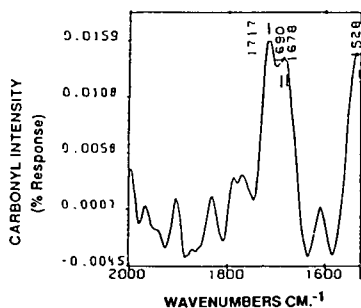


Figure 3
PAIFT Difference Spectrum
Barton Coal: (Oxidized 48 h) - (Fresh Coal)

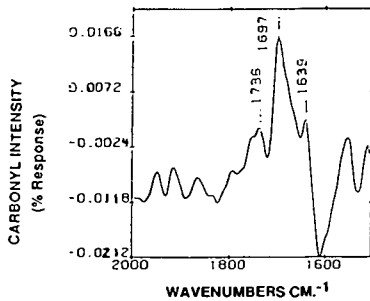


Figure 4
PAIFT Difference Spectrum
Alto Coal: (Oxidized 48 h) - (Fresh Coal)

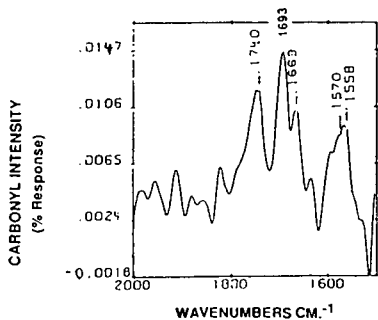


Figure 5
PAIFT Difference Spectrum
McClure Coal: (Oxidized 48 h) - (Fresh Coal)

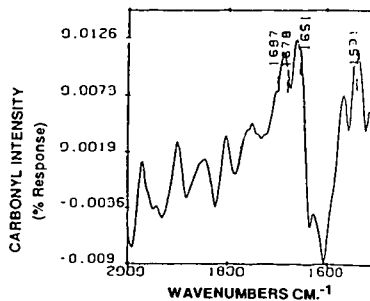


Figure 6
PAIFT Difference Spectrum
Basset Coal: (Oxidized 48 h) - (Fresh Coal)

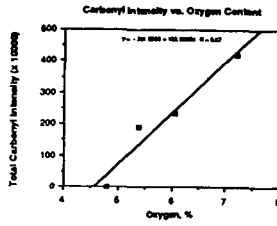


Figure 7
Greenhills Coal - Carbonyl Intensity (PAIFT Spectra) vs. Oxygen %

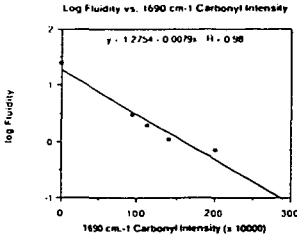


Figure 8
Greenhills Coal - log Fluidity vs. 1690 cm⁻¹ Carbonyl Intensity (PAIFT Spectra)

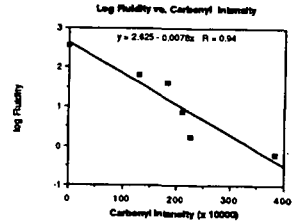


Figure 9
Fording Coal - log Fluidity vs. Carbonyl Intensity (PAIFT Spectra)

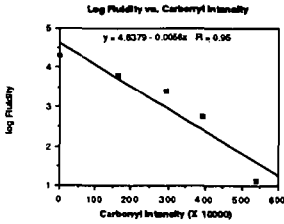


Figure 10
Barton Coal - log Fluidity vs. Carbonyl Intensity (PAIFT Spectra)

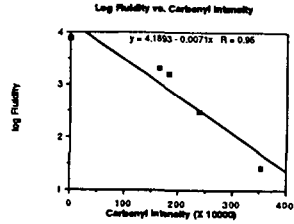


Figure 11
McClure Coal - log Fluidity vs. Carbonyl Intensity (PAIFT Spectra)

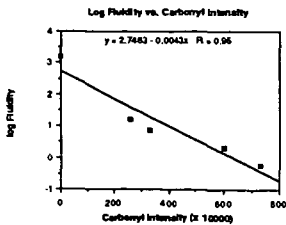


Figure 12
Ato Coal - log Fluidity vs. Carbonyl Intensity (PAIFT Spectra)

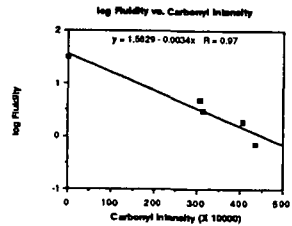


Figure 13
Besset Coal - log Fluidity vs. Carbonyl Intensity (PAIFT Spectra)

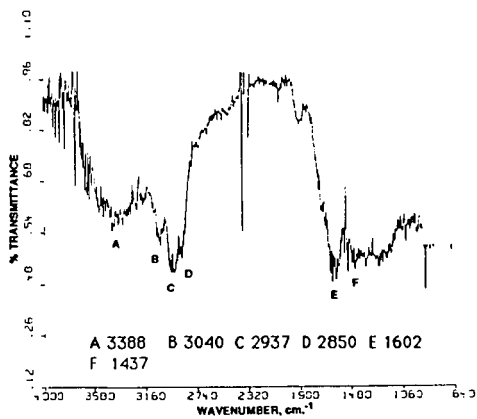


Figure 14

Western Canadian Bituminous Coal
FTIR Microspectrogram of Vitrinite Component

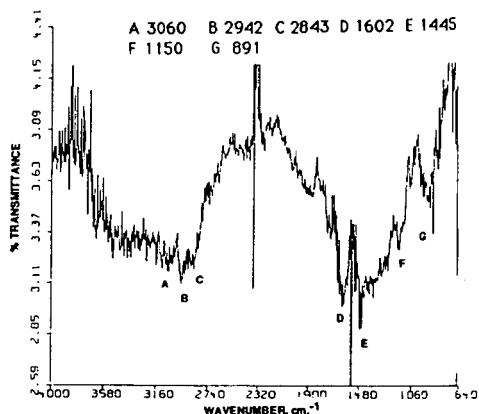


Figure 15

Western Canadian Bituminous Coal
FTIR Microspectrogram of Fusinite Component

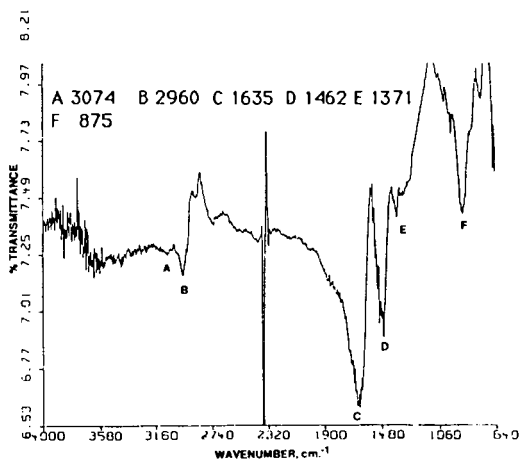


Figure 16

Cape Breton Bituminous Coal
FTIR Microspectrogram of Vitrinite Component

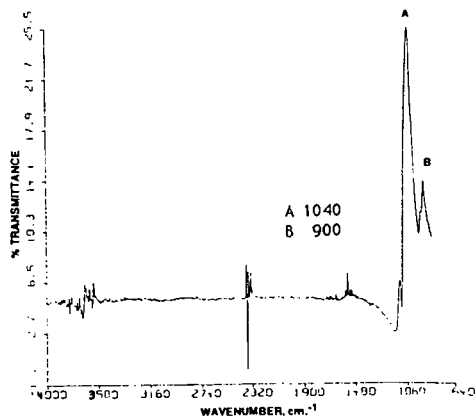


Figure 17

Cape Breton Island Bituminous Coal
FTIR Microspectrogram of Kaolinite Inclusion

EFFECT OF WEATHERING ON SOLVENT EXTRACTION OF COALS

David H. Buchanan, Linda C. Warfel, Wanping Mai, and Douglas Lucas

Chemistry Department
Eastern Illinois University
Charleston, IL 61920

INTRODUCTION

Ambient temperature air oxidation of coal (weathering) is a problem in storage, utilization, and characterization. This work grew out of our observations that toluene insoluble, pyridine soluble (TIPS) fractions of Illinois coals isolated by conventional Soxhlet extraction differed in number average molecular weights, phenol contents, and elemental analyses from the TIPS fractions isolated by the slurry/centrifugation method. Several Soxhlet fractions would not completely redissolve in the extraction solvent and phenol and oxygen contents were unreproducible. The problems have been traced to oxidation during extraction and subsequent work-up, unremoved extraction solvents, and contamination of Soxhlet extracts by colloids. The procedure described below avoids these problems and gives reproducible yields of soluble extracts with good material balances. Sequential extraction of coal with toluene followed by THF, DMF, and pyridine shows that weathering toward lowers the total extract yield, shifts the distribution from polar soluble toward non-polar solubles, and increases the amount of colloids in the crude extracts.

EXPERIMENTAL PROCEDURES

Coal samples were stored in argon flushed desiccators and handled in nitrogen flushed glove bags as much as possible. Samples ground to -100 mesh in a nitrogen flushed ball mill were dried to constant weight at 100° C and 0.05 Torr ("standard conditions") in a large Abderhalden apparatus(1) before use. Soxhlet thimbles were washed with the solvents to be used and dried to constant weight under standard conditions. Solvents were dried and distilled under an Ar atmosphere before use.

Soxhlet extraction of an 8-10 g sample of the coals described in Table 1 with approximately 120 mL of Ar purged solvent, under an Ar atmosphere, was continued for two to seven days with each solvent (Scheme). Two, 3 L RB flasks were attached to the inert gas system as ballast tanks; otherwise when the Soxhlet apparatus cycled, air was sucked back into the system through the oil bubbler at the gas exit. The insoluble residue was washed free of solvents with two or three cycles of 80% methanol/water for three hours each in the Soxhlet apparatus, followed by drying of the residue in the thimble to constant weight under standard conditions.

Soluble fractions were filtered, under an Ar blanket, through a Nylon Millipore AP pre-filter and a 0.45 μm Millipore filter, followed by removal of bulk solvent on the rotary evaporator and drying to constant weight under standard conditions. Colloidal material collected on the filter was counted as part of the residue. DMF and pyridine soluble fractions were washed three or four times with 80% methanol/water and recovered by centrifugation at 2800 G prior to Abderhalden drying. Removal of solvents was monitored by the loss of sharp IR bands at 1661 and 1386 cm^{-1} for DMF and at 1537, 1485, 1253, 750, and 650 cm^{-1} for pyridine, Figure 1.

FT-IR spectra of coal fractions, as KBr pellets (3.0 mg/300 mg), were recorded on a Nicolet 20-DXB spectrometer at 2 cm^{-1} resolution. Argon purged pyridine solutions of coal fractions were spun for 5 - 12 hrs at 24,000 rpm in a Beckman L3-50 Ultracentrifuge using stainless steel sample tubes in the SW27 rotor. The clearing

factor (k) for this experiment was 136; average Relative Centrifugal Field (RCF) = 76,000 G; maximum RCF = 104,000 G.(2) GPC analyses of coal fractions at 6.0 mg/mL in pyridine were performed on a three-column train of ASI Ultragel size exclusion columns (100, 500, 1000 Å) using HPLC grade pyridine at 1.8 mL/min as mobile phase with Refractive Index detection. The system has an efficiency of 7,150 for toluene and is currently calibrated with polystyrene (linear in the 20,000 to 100 dalton region). A 'bootstrap' calibration using narrow molecular weight distribution coal fractions is in progress. MW values were determined on a Knauer Model 11.00 Vapor Pressure Osmometer using pyridine at 90°C. Experimental values at three or four concentrations were extrapolated to infinite dilution.

RESULTS AND DISCUSSION

Most coals and especially oxidized coals produce colloidal material upon Soxhlet extraction by polar solvents which can be removed by centrifugation or Millipore, but not ordinary, filtration. Failure to remove this material from extracts has the consequence of defining 'soluble' as anything which will pass through a Soxhlet thimble. For the unoxidized coals in Table 1, less than 0.5% by weight of colloidal material was usually recovered on the Millipore filter. Oxidized coals produced over 2% colloidal material which completely clogged Millipore filters unless the Nylon Pre-filters were used. The FT-IR spectrum of a colloid isolated from the THF extract of coal 701 is shown in Figure 2. The bands at 1723, 1385, and 1177 cm^{-1} suggest esters of fatty acids.(3) Painter and Davis have previously noted FT-IR evidence for aliphatic esters in oxidized coals.(4) The band at 1035 and shoulder at 1130 cm^{-1} have been observed in coal minerals, however sharp kaolinite bands near 3660 cm^{-1} , visible in spectra of coals and residues, are missing in the colloids.(5)

Pyridine and DMF cannot be completely removed from coal by vacuum drying, resulting in high nitrogen contents, but best demonstrated by solvent peaks in the FT-IR spectrum of a water-washed residue after drying to constant weight (Figure 1 and Ref. 6). Since the residue had been extracted with pyridine after the DMF, this shows that both are tightly bound to the coal and that pyridine will not displace or wash out the DMF. Large volumes of 10% HCl or 5% THF in water (6d) will remove pyridine, but not DMF, from residues and extracts. Some mineral matter is lost to the acidic solution. The most efficient washing procedure uses several small portions of 80% (v/v) methanol/water followed by drying to constant weight under standard conditions. The choice of this mixture follows from the high wetting rates of coal in methanol/water and the large heat of immersion of coal in methanol compared with a variety of other solvents.(7) That these considerations lead to removal of DMF under mild conditions suggests that the binding of DMF, and possibly pyridine, to coals and residues may be a surface effect. Unoxidized samples bind pyridine and DMF more tightly than do oxidized samples.

Sequential solvent extractions of coal were carried out as shown in the Scheme and are summarized in Table 2. Total material balances were 92-98% and were 94-105% for individual elements. Several experiments in which the solvent order was changed indicate that each solvent in the Scheme dissolves everything soluble in the previous solvents plus additional material made soluble by both the increasing solvent power (8) and coal swelling ability of the later solvent.(8a, 9) GPC traces of TIPS fractions lack the low molecular tails apparent in pyridine fractions from sequential extraction, Figures 3 - 6. TIPS is isolated by precipitation from the total pyridine extract with excess toluene so that all toluene solubles are removed. However, during sequential extraction some small molecules are not extracted by toluene or THF because coal is not swollen enough for efficient mass transport and this material remains to be extracted by DMF or pyridine. Re-extraction of residue

R600 (Table 2) with pyridine produced 0.8% new extract and 97% recovery of residue, suggesting that little soluble material remains after sequential extraction.

GPC analyses of each soluble fraction, redissolved in pyridine, are plotted together as a Molecular Size Profile, Figures 3 - 6. The solid vertical bars represent the fraction of total extract soluble in the indicated solvent. Although the molecular mass scale cannot yet be used for quantitative analysis of these coal fractions, the changes in molecular size with extraction solvent, coal rank, and oxidation are apparent. Weathered coal gives lower yields in sequential extraction (Table 2), or single solvent extraction.(10) After a pyridine solution of MW 1530 TIPS from coal 450 (13.7% total soluble, 8.4% TIPS) was exposed to air for 4 days, 86% by weight remained pyridine soluble. This material had a MW of 1498 and produced no further precipitate upon additional air exposure. Pyridine extracts of weathered coals are less prone to oxidation induced precipitation, as if oxidation causes cross-linking which renders a portion of the coal insoluble, either within the coal matrix before extraction, or in solutions of extracts later.

ACKNOWLEDGEMENT

We thank the Illinois Coal Development for financial support, and Dr. Carl W. Kruse, Illinois state Geological Survey, and Dr. Karl Vorres, Argonne National Laboratory, for coal samples.

REFERENCES

1. Available from Aldrich Chemical Co., Milwaukee, WI.
2. Circular LM-IM-9, Spinco Division, Beckman Instruments, Palo Alto, 1982.
3. (a) Bellamy, L.J. "The Infra-red Spectra of Complex Molecules", 2nd ed., Wiley, New York, 1958, 179-191. (b) Silverstein, R.M.; Bassler, G.C.; Morrill, T.C. "Spectrometric Identification of Organic Compounds", 4th ed., Wiley, New York, 1981, 121-123.
4. Rhoads, C.A.; Senville, J.T.; Coleman, M.M.; Davis, A., Painter, P.C. Fuel 1983, 62, 1387.
5. (a) Cooke, N.E.; Fuller, O.M.; Gaikwad, R.P. ibid. 1986, 65, 1254. (b) Shepherd, R.A.; Kiefer, W.S.; Graham, W.R.M. ibid. 1986, 65, 1261.
6. (a) Collins, C.J.; Hagaman, E.W.; Jones, R.M.; Raaen, V.F. ibid. 1981, 60, 359. (b) Cooke, N.E., Gaikwad, R.P., ibid. 1984, 63, 1468. (c) Gethner, J.S. ACS Div. Fuel Chem., Preprints, 1986, 31(4), 103. (d) Erbatur, G.; Erbatur, O.; Davis, M.F.; Maciel, G.E. Fuel 1986, 65, 1265.
7. Glanville, J.O.; Wightman, J.P. ibid. 1980, 59, 557.
8. (a) Hombach, H.P. ibid. 1980, 59, 465. (b) Jones, M.B.; Argasinski, J.K. ibid. 1985, 64, 1547.
9. Green, T.K.; Kovac, J.; Larsen, J.W. ibid. 1984, 63, 935.
10. (a) Dryden, I.G.C. Chapter 6 in Lowry, H.H., ed.; "Chemistry of Coal Utilization", Suppl. Vol., John Wiley & Sons, New York, 1963, 232. (b) Liotta, R.; Brons, G.; Isaacs, J. Fuel 1983, 62, 781.

TABLE 1

ELEMENTAL ANALYSES (DAF) OF COALS STUDIED

COAL #	TYPE	FROM	%C	%H	%N	%S	%O(Diff)
0450	ILL 2	ISGS ^a	78.01	5.50	1.36	3.36	11.77
0500	ILL 5	ISGS	76.55	5.33	1.60	4.96	11.56
0501	OXID ^b	0500					
0600	ILL 6	ISGS	74.09	5.18	1.39	5.51	13.84
0700	ILL 6	ISGS	78.19	5.58	1.38	5.12	9.73
0701	OXID ^b	0700	76.55	5.45	1.39	4.99	11.59
0910	MVB1t ^c	APCS	86 ^d	5.3	1.9	2.8	4.0

a Illinois State Geological Survey

b Air oxidized, -100 mesh coal, room temperature, 6 months

c Upper Freeport, Agronne Premium Coal Sample # 1

d Approximate, final data not available from Argonne

TABLE 2

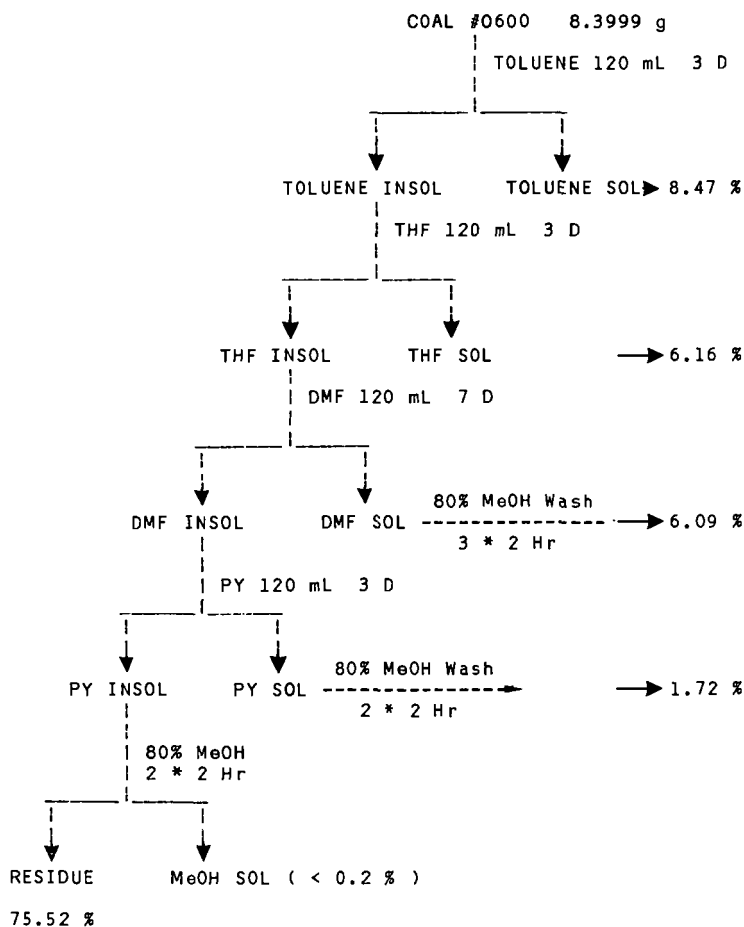
SEQUENTIAL SOXHLET EXTRACTION^a

COAL #	% TOL SOL	% THF SOL	% DMF SOL	% PY SOL	TOTAL % SOL	% RESID	% Mat Bal
0500	0.82	7.33	5.94	1.42	15.5	75.77	91.3
0501	3.57	3.72	4.23	2.18	13.7	86.16	99.9
0600	8.47	6.16	6.09	1.72	22.4	75.52	98.0
R600 ^b	0.18	0.01	0.43	22.17	22.8	74.85	97.6
0700	3.30	6.73	7.32	2.10	19.4	71.96	91.4
0701	6.54	5.69	4.70	1.81	18.7	72.39	91.4
0910	0.52	0.14	8.97	11.24	20.9	78.16	99.1

a Extraction order: Toluene, THF, DMF, Pyridine

b Extraction order: Pyridine, Toluene, THF, DMF

SCHEME
SEQUENTIAL SOXHLET EXTRACTION



TOTAL SOLUBLE: 22.44 %
TOTAL RECOVERED: 97.96 %

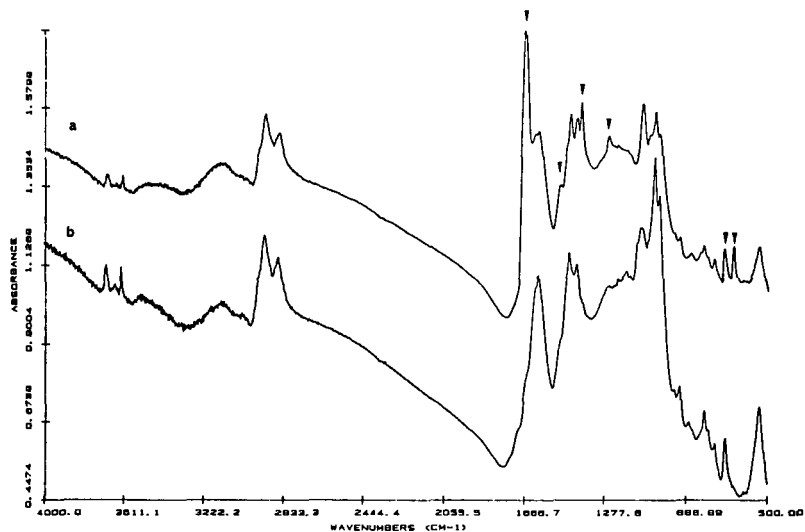


FIGURE 1. (a) FT-IR spectrum of residue from coal 0700 containing DMF and PY. ▲ = Solvent absorption bands. (b) Spectrum of same residue after 80% methanol/water wash and standard drying.

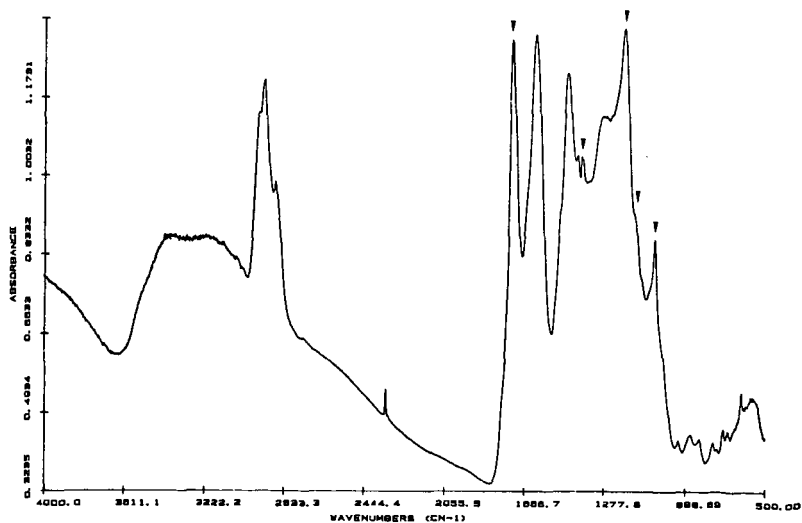


FIGURE 2. FT-IR spectrum of colloid isolated from Millipore filtration of THF extract from coal 0700. ▲ = Features discussed in text.

MOLECULAR SIZE PROFILE
GPC IN PYRIDINE
Coal 0600

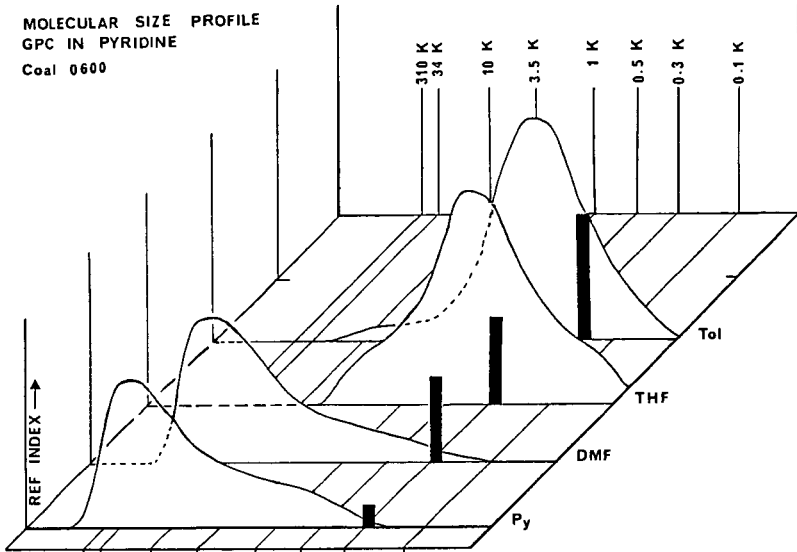


FIGURE 3. Combined GPC traces of sequential extracts from coal 0600 (Table 2). Concentration = 6.0 mg/mL in pyridine, flow rate 1.8 mL/min.

MOLECULAR SIZE PROFILE
GPC IN PYRIDINE
Coal 0910

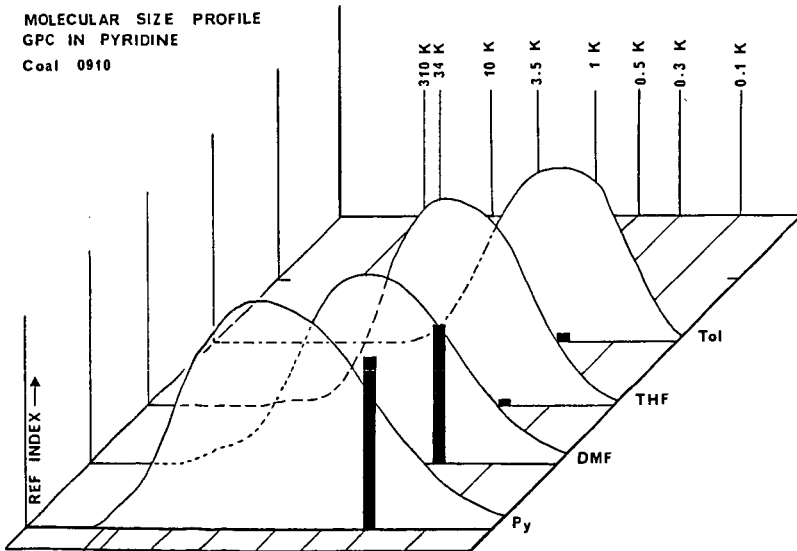


FIGURE 4. Combined GPC traces of sequential extracts from coal 0910 (Table 2). Concentration = 6.0 mg/mL in pyridine, flow rate 1.8 mL/min.

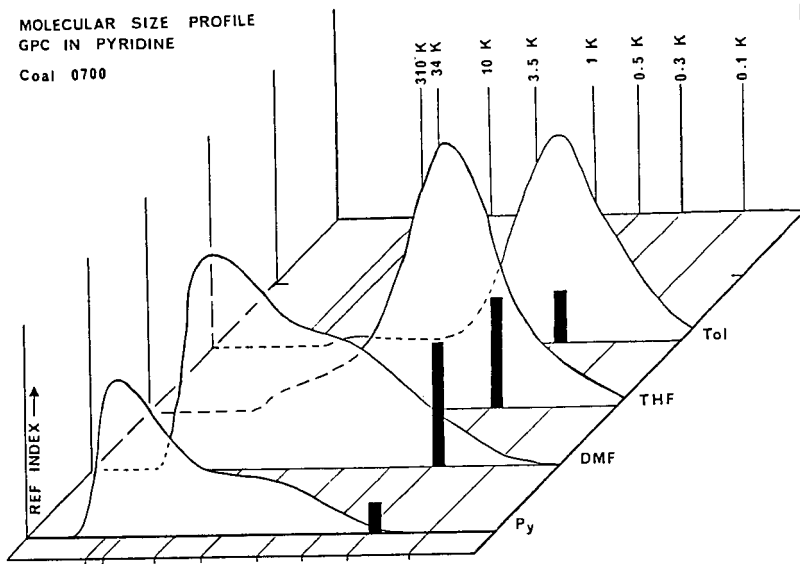


FIGURE 5. Combined GPC traces of sequential extracts from coal 0700 (Table 2). Concentration = 6.0 mg/mL in pyridine, flow rate 1.8 mL/min.

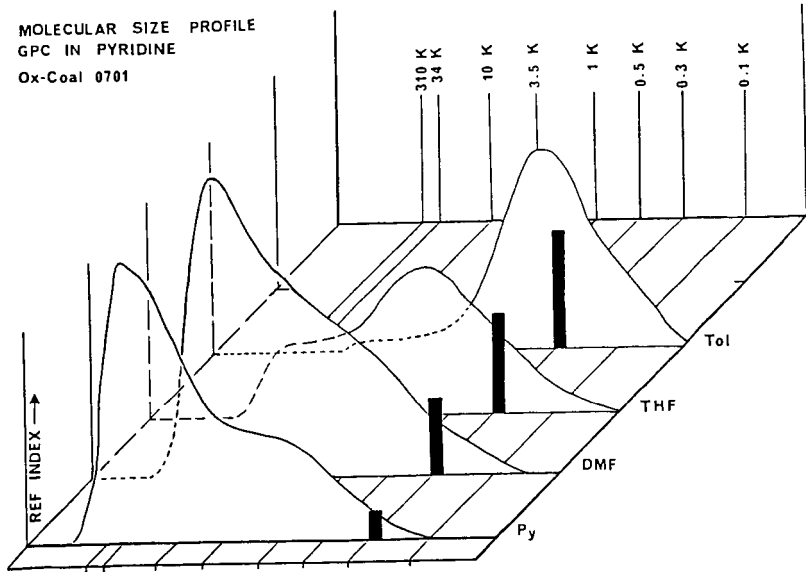


FIGURE 6. Combined GPC traces of sequential extracts from coal 0701 (Table 2). Concentration = 6.0 mg/mL in pyridine, flow rate 1.8 mL/min.

SECONDARY ION MASS SPECTROMETRY AND X-RAY
PHOTOELECTRON SPECTROSCOPY OF DERIVATIZED COAL SURFACES.

R.R. Martin, N.S. McIntyre, J.A. MacPhee, K.T. Aye.

Department of Chemistry, University of Western Ontario
London, Ontario, Canada. N6A 5B7

ABSTRACT

Secondary Ion Mass Spectrometry (SIMS) and X-ray Photoelectron Spectroscopy (XPS) have been used to study the low temperature oxidation of coal. ^{18}O has been used to trace the oxygen distribution on the coal surface. Several chemical derivatizations have been observed on the oxidized coal surface and the reactivity of specific regions have been monitored.

INTRODUCTION

The low temperature oxidation of coal leads both to loss of coking ability⁽¹⁾ and autoignition⁽²⁾ of coal stock piles. In this study we report the use of secondary ion mass spectrometry (SIMS) and X-ray photoelectron spectroscopy (XPS) in conjunction with $^{18}\text{O}_2$ oxidation to examine the oxygen distribution on a coal surface in relation to specific other elements. The use of both XPS and SIMS in coal studies have been described elsewhere.⁽³⁾

EXPERIMENTAL

The coal used in this study was a pyrite-rich fusinite supplied by the Canadian Center for Mineral and Energy Technology (CANMET). The coal was cut with a diamond saw, and polished on a silk wheel using diamond grit as abrasive and water as lubricant. The resulting coal surfaces were exposed to 0.1 atm of $^{18}\text{O}_2$ for 10 days at room temperature.

The SIMS measurements were made on a Cameca IMS 3 f using a Cs^+ primary beam rastered over a $(400 \mu\text{m})^2$ area. Ion images were collected from a central area $170 \mu\text{m}$ in diameter, these images were obtained at a mass resolution as high as one part in 3500, though for certain ions the secondary ion yield was insufficient to permit imaging. In most cases where SIMS images were taken mass spectral scans were also obtained.

XPS studies were also carried out on regions adjacent to those studied by SIMS using a Surface Science Laboratory Model SSX-100 spectrometer with monochromatized $\text{AlK}\alpha$ radiation with a spot size of approximately $150 \mu\text{m}$. The ^{18}O was used as an isotopic trace to distinguish between oxygen added to the coal as a result of this procedure and that already present.⁽⁴⁾ The pyrite-rich coal was selected because it provides remarkably well defined secondary ion images and pyrite is reported to play an important role in the self-heating of coal.⁽⁵⁾

RESULTS AND DISCUSSION

The assignment of ionic species to the secondary ion images obtained during high mass resolution imaging was achieved using two criteria. First the accompanying mass spectrum at a given nominal mass was analyzed to achieve a fit between the mass separation observed and that expected from the species assigned to the spectrum. Thus at mass 28 two peaks were observed separated by $.019 \pm .003$ daltons, only $^{28}\text{Si}^-$ and CO^- are likely to produce this pattern. In addition successive ion images may be used to eliminate some assignments, for example silicon molecular ions would not be expected in regions where silicon could not be detected. Finally, in one case at mass 30 high mass resolution was not used to distinguish between $^{30}\text{Si}^-$ and C^{18}O^- since the yield of C^{18}O^- was too low for effective imaging.

The ion images displayed in figure 1 are assigned to ions C_2^- , C_4^- , CO^- , S^- and CS^- . The images for C_2^- and C_4^- define the organic region of the coal surface while that of S^- outlines the pyrite region. The image for CO^- is confined entirely to the organic region and originates from a set of sources having a very small area. These represent oxidized areas on the coal surface and although the oxygen functional groups cannot be identified with certainty they may well be aldehydes or phenols.

The CS^- image is of particular interest since it is confined to the organic region of the coal. The XPS spectra from this area, figure 2, confirm the presence of organic sulfur. The suite of peaks associated with binding energies between 157 and 160 eV are assigned to iron sulfides while those between 163 and 165 eV are assigned to organic compounds probably dominated by sulfates. Thus the coal adjacent to the pyrite appears to have undergone a reaction which has tended to enrich the area in sulfur. It has been proposed elsewhere that pyrite oxidizes readily to form a series of hydrated ion sulfates and sulfuric acid.⁽⁶⁾ Since these reactions are exothermic⁽⁷⁾ the surrounding organic material would be exposed to sulfuric acid and simultaneously heated. Under these conditions sulfonation reactions would be expected. Accordingly we suggest that oxidation of pyrite is accompanied by sulfonation of the surrounding coal.

Figure 3 displays a series of oxygen-related images. The $^{16}\text{O}^-$ image which is coincident with OH^- is seen to be widely distributed in the coal, however there is oxygen enrichment in the organic region and in silicate regions identified in figure 4. A recurrent feature associated with silicate materials is identified by an arrow in figures 3 and 4. The persistence of oxygen-related species in this area (particularly $^{18}\text{O}^-$ and $^{18}\text{OH}^-$) provides evidence that the silicate serves as a catalyst during oxidation. The presence of $^{16}\text{O}^-$, $^{18}\text{O}^-$ and the molecular ions OH^- and $^{18}\text{OH}^-$ indicate that oxidation of the coal has taken place and that ^{18}O reacted with the coal surface under very mild conditions. The F^- image is diffuse within the organic region suggesting the presence of carbon monofluoride⁽⁴⁾ while other sources are clearly associated with the silicate material. The latter source represents fluoride replacement of OH^- in the mineral matter. The image obtained for H_2O indicates that traces of water are present in the sample.

Figure 4 serves to outline the silicate enriched regions as defined by the image at mass 28, which is a mixture of $^{28}\text{Si}^-$ and AlH^- since the mass resolution used cannot distinguish between these

species, by comparison with that obtained at mass 30⁻ (³⁰Si⁻ with traces of C¹⁸O⁻). A representative silicate mineral region is identified with an arrow in Figure 4(a). The images assigned to O₂⁻ and O₃⁻ also show some enhancement in the silicate region. The O₂⁻ originates from adsorbed oxygen while O₃⁻ may represent ozone on the coal surface.

It has been repeatedly suggested that the low temperature oxidation of coal proceeds by a free radical chain reaction(8). Minerals would be expected to act as catalysts in such reactions(5). Figure 3 shows the presence of ¹⁸O in molecular ions after mild oxidation while Figure 4 shows reactive oxygen species on the coal surface associated with mineral matter. These results would be expected if a free radical mechanism is involved in low temperature oxidation.

CONCLUSIONS

Detailed SIMS images can be obtained for ions differing in mass by as little as 1:3500.

The uptake of ¹⁸O and molecular ions containing ¹⁸O can be successfully studied using SIMS after exposure of coal surfaces to an ¹⁸O₂ atmosphere at room temperature.

The presence of organic sulfur in regions adjacent to pyrite probably result from sulfonation of the coal by the products of pyrite oxidation.

Molecular ions originating from oxidized regions of the coal surface are readily identified and reactive oxygen species have been imaged associated with mineral matter. These results support the suggestion that the low temperature oxidation of coal proceeds by a free radical chain mechanism.

REFERENCES

1. J. W. Larsen, D. Lee, T. Schmidt and A. Grint, *Fuel* (1986), 65, 595-6.
2. R.E. Jones and D.T.A. Townsend, *Nature* (1945), 155, 424-425.
3. N.S. McIntyre, R.R. Martin, W.J. Chauvin, C.G. Winder, J.R. Brown and J.A. MacPhee, *FUEL* (1985), 64, 1705-1712.
4. R.R. Martin, N.S. McIntyre and J.A. MacPhee, *Proceedings 1985 International Conference on Coal Science, Sydney, Australia*, 796-799.
5. R.G. Herman, G.W. Simmons, D.A. Cole, V. Kucicz and K. Klier, *FUEL* (1984), 63, 673-678.
6. F.E. Huggins, G.P. Huffman and M.C. Lin, *Int. Jour. Coal Geol.* (1983), 3, 157-182.
7. R.A. Robie, B.S. Hemingway and J.R. Fisher, *U.S. Geol. Survey Bull.* 1452, p. 456 (1978).
8. D.A. Cole, R.G. Herman, G.W. Simmons and K. Klier, *FUEL* (1985), 64, 303-6.



A

C_2^-

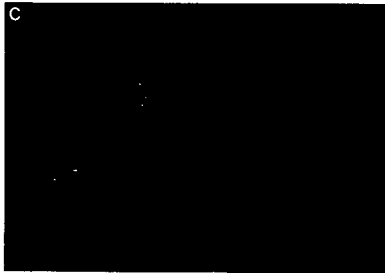
1/2 sec



B

C_4^-

1 sec



C

CO^-

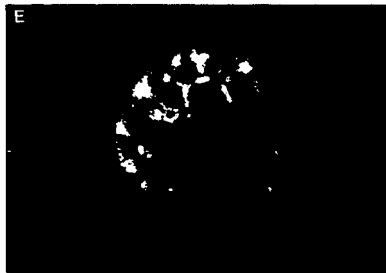
120 sec



D

S^-

1/2 sec



E

CS^-

30 sec

Fig. 1

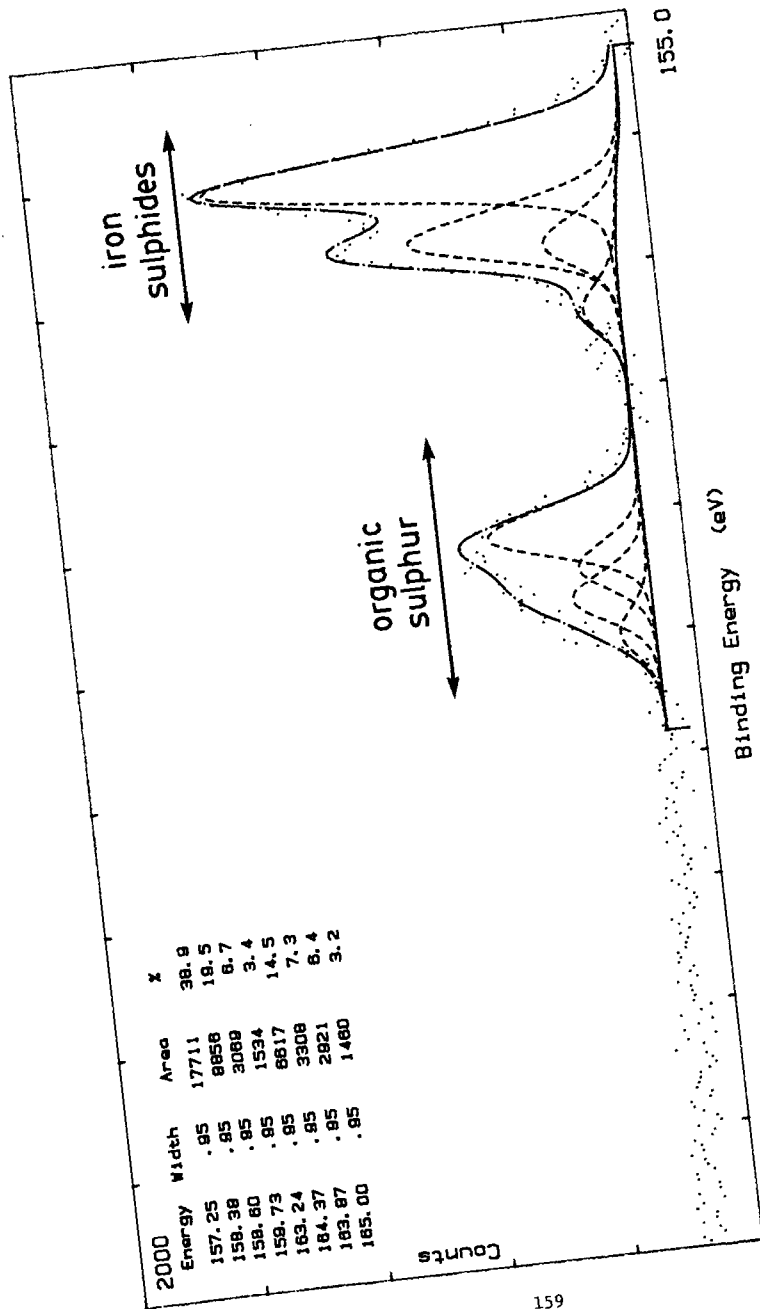
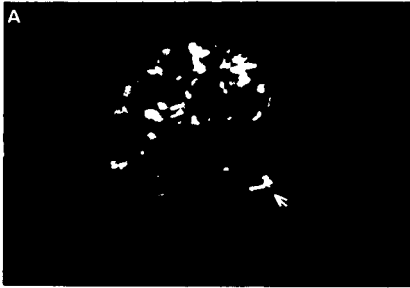
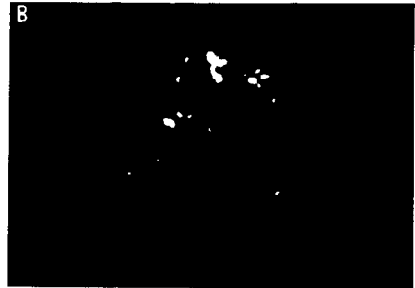


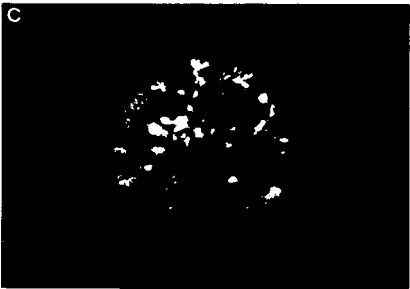
Figure 2
XPS SPECTRUM OF S_{2p} REGION



$^{16}\text{O}^-$ 1/2 sec



OH^- 2 sec



H_2O 60 sec



$^{18}\text{O}^-$ 30 sec



$^{18}\text{OH}^-$ 60 sec



F^- 60 sec

Fig. 3

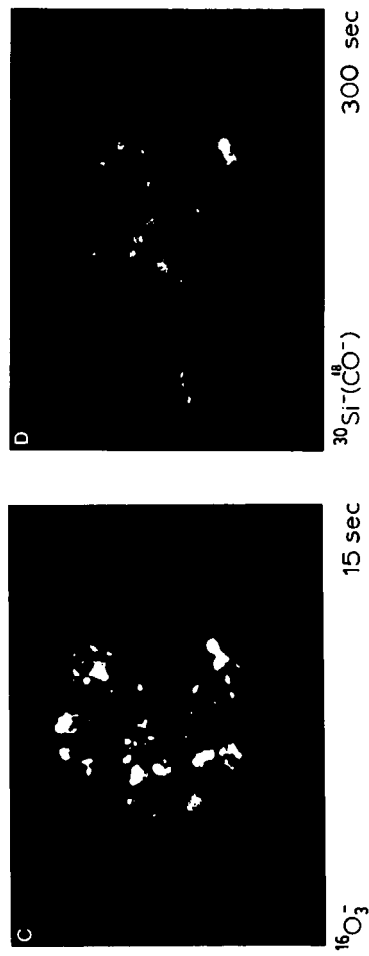
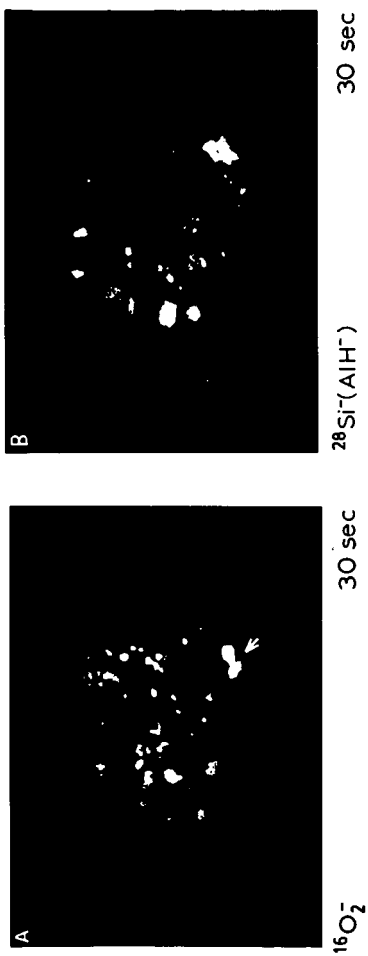


Fig. 4

SELF-HEATING OF COAL IN BARGES

J. T. Riley, J. W. Reasoner, S. M. Fatemi, and G. S. Yates

Department of Chemistry and Center for Coal Science
Western Kentucky University, Bowling Green, Kentucky 42101

I. INTRODUCTION

Self-heating, or spontaneous heating, is a process which results in an increase in temperature of a thermally-isolated mass of coal or other combustible material. This phenomenon is caused by the heat-generating chemical reactions between the oxidant (oxygen) and the fuel (coal). If the generated heat is removed or absorbed by the surrounding environment, then only low temperature oxidation will occur. However, if nothing is done to change the condition of the coal undergoing a self-heating process, spontaneous combustion will eventually occur.

Self-heating in coal has been observed for more than 100 years for many coals around the world. It is a problem that affects the mining, transportation, and storage of coal and contributes to the deterioration in its quality. Several comprehensive reviews have been written on the factors that may contribute to the self-heating in coal (1-8). These factors are numerous and include intrinsic properties such as rank, heat of wetting, porosity, exposed surface area, ash content, content of pyrites and other sulfur containing species, hardness, methane content, and thermal conductivity of the coal. Handling conditions that may contribute to coal self-heating include changes in moisture content of the surrounding environment, large variations in the temperature when the coal is shipped, and to the movement of air through the coal.

The purpose of this research was to examine the factors which may contribute to the self-heating of coal in barges. A data bank containing analytical data and barging information on 2283 barges was used to help identify the principal factors contributing to the self-heating of barged coal. Barging studies to examine coal handling and barging techniques designed to minimize the occurrence of self-heating were conducted.

II. EXPERIMENTAL

Two separate barging studies were carried out over a period of two summers. The studies took place on the Ohio and Mississippi rivers and involved 15 barges of coal in the first study and 10 barges in the second tow. The work performed and the number of researchers that could accompany the tows were restricted by the room available on the towboats, the safety considerations during tow work by the boat crew, and the availability of barges filled with a particular type of coal and loaded in a particular manner.

The coal studied in the barging experiments was steam coal (high volatile bituminous) loaded at four different river ports. The coal loaded at each port had been mined in the same general area and had been crushed, stockpiled, and handled by the same equipment. Consequently, the coal loaded at each port had the same general physical and chemical properties, and exhibited the same general behavior toward self-heating.

Two different loading schemes were used in the studies, single chute loading and loading with a "diffuser." The diffuser is a device added to a normal coal chute which splits the falling stream of coal into five streams. This loads the coal in a pattern of five rows of "cones" instead of a single row in the center of the barge. The diffuser was much more effective in preventing size segregation of the coal which would minimize the formation of channels for uneven air flow through the coal in the barge.

A second variable monitored during the study was the effect of compacting coal to minimize self-heating. Three methods of compacting coal in barges were studied. Two barges were lightly compacted using a "clam shell" bucket from a loading crane and this light compacting left voids in the ends of the barges. A second method studied did not compact the coal very much but simply leveled the tops of the cones of coal produced during loading. This method is often referred to as "trimming" and leaves large voids (3-10 ft.) in the ends of the barges. Five barges were prepared in this manner. The third method of compacting studied in this project was the most efficient method used. A small "Bobcat" front-end loader was hoisted into the barges and used to move the coal around to fill voids in the corners and sides of the barges. The weight of the coal in the loader bucket plus the weight of the loader itself compacted the coal under the rubber tires of the loader. Eight barges were compacted with the front-end loader. As an illustration of the difference in compacting, the coal in barges compacted with the front-end loader had a depth of about 13.5 ft., whereas the coal in "trimmed barges" had a depth of about 15.5 ft. All barges in a tow had approximately the same tonnage.

Daily temperature measurements of the coal in the barges were recorded in order to have a record of self-heating rates for different coals and at different positions in a barge. Care was taken that a representative temperature profile of the barges was obtained and recommendations for temperature measurements as presented in a report by the Coal Exporters Association/National Coal Association Task Force on Coal Handling, Storage and Transportation were used (9). Twenty-seven positions uniformly spaced down the sides and center of each barge were chosen for temperature measurements and temperatures were measured at depths of 3, 6, and 9 ft. at each position. The temperature probes used were constructed from 1/4 in. I.D. galvanized steel pipe and fitted with a metal tip machined to a point so that the probe could be pushed into the coal. Type J thermocouple wires were attached with epoxy cement at three 1/4 in. holes drilled at 1 in., 3 ft. and 6 ft. from the probe tip. The thermocouple wires were attached to an Atkins Model 39658J Digital Readout Meter with a three-position switch for reading the temperatures at the three depths. The probes were carefully calibrated before use and found to be accurate to within $\pm 1^{\circ}\text{F}$. After inserting the probes in the coal they were allowed to equilibrate for a minimum of 3 minutes before any temperature readings were made.

The movement of air through the coal in the barges loaded and compacted by different methods is closely related to the self-heating that occurs. To follow the movement of air through the coal a tracer gas, sulfur hexafluoride, was released at a depth of 10 ft. in some of the barges and its movement through the coal was monitored by measuring the concentration of SF_6 in gas samples collected at regular intervals. Bendix Model 44 Air Sampling Pumps were used to draw gas samples from the bottom of the barges through 1/4 in. I.D. steel pipes with holes drilled near the bottom end of the pipe. Gas samples were collected in 250 cc polypropylene gas collection bulbs and immediately analyzed using a gas chromatograph set up in the towboat. A Carle Model 6500 gas chromatograph with an 8 ft. x 1/8 in. activated alumina (80-200 mesh) column connected to a Hewlett-Packard Model 3390A Reporting Integrator was used for the analysis.

During the course of the project, 230 samples of coal being transported by barge to ports in the New Orleans area were obtained for analysis at the Western Kentucky University laboratory. Moisture, ash, volatile matter, carbon, hydrogen, nitrogen, sulfur and calorific values were determined using microcomputer-controlled instrumentation from LECO Corporation in St. Joseph, MI. Forms of sulfur, free-swelling index and Hardgrove grindabilities were determined using ASTM methods D 2492, D 720 and D 409, respectively. Fixed carbon and oxygen values were calculated by difference. Transportation histories of the barged coals were also obtained.

III. RESULTS AND DISCUSSION

The self-heating of coal is brought about through oxidation of coal surfaces, and the amount of air available to the coal is important. The air flow rate through the coal is a complex factor to consider since air both provides oxygen for oxidation of the coal and dissipates the heat generated by the oxidation process. Conditions which permit only a small amount of air to come into contact with the coal will keep oxidation at a minimum and little or no self-heating will occur. A very high flow rate of air provides sufficient oxygen for the oxidation process, but dissipates heat efficiently. In between these two limits is a state where the air flow is sufficient to promote oxidation of the coal surfaces but is not sufficient to dissipate the heat produced by the exothermic reaction. In this case the heat produced will raise the temperature of the coal and accelerate the rate of oxidation until, ultimately, ignition of the coal will occur (5,6,10,11).

A. Barge Loading and Compacting Methods

The techniques employed in loading barges with coal will affect the air flow rate through the coal. When coal is loaded from a single chute, the resulting conical piles tend to have the fines concentrated at the center of the cone with larger particles segregated around the surface at the base. Quite often at a point somewhere between the outer edges of the cone and the center the air flow rate is sufficient to initiate and support heating. The cone then acts as a "chimney" to draw air from around the base into the center to maintain the heating. The simple process of leveling the cones seals the coarser coal with the fines and restricts air flow through the coal. Compacting the leveled coal further limits its access to air by reducing interparticle voids. The reduction of these voids also results in an increase in thermal conductivity which helps dissipate any heat produced.

A comparison of the temperatures of coal in barges compacted by two different methods is given in Table 1. The barge number used in the table represents the order in which the barges were loaded. All the barges were loaded at the same port and with the same type of coal. The temperatures reported are those of the coal in the barges prior to unloading when the ambient temperature was 90°F. The average temperature is the average of 81 individual readings for each barge (27 positions and depths of 3, 6, and 9 ft.). At ports in the New Orleans area, the temperature of coal being exported has to be below 105°F before it can be loaded onto ocean-going vessels. As can be seen from the data there is a dramatic difference between the results obtained for the two methods of compacting coal, with nearly one-third of the temperature readings above 105°F for the lightly compacted coal. From these examples one can conclude that compacting coal in barges offers considerable protection against self-heating.

Table 2 shows temperatures of coal in barges loaded by two different methods. All the barges were loaded at the same port and with the same type of coal. The barge numbers again refer to the order of loading the barges and the average temperatures are the average of the 81 readings taken prior to unloading when the ambient temperature was 90°F. A comparison of the temperatures for the barges loaded by two different methods shows an average of 91.3°F for the barges loaded with the diffuser, whereas the barges loaded with the single chute have an average temperature of 95.2°F. The difference in average temperatures can be attributed to the fact that loading with the diffuser produces an even distribution of coal particles, whereas the single chute loading method yields a segregated mass of coal particles. The even distribution of particles yields a more uniform air flow through the coal which results in less self-heating.

The heating that took place in several of the barges was "triggered" by the occurrence of a heavy rain on the ninth day after the initial barges were loaded. On the morning following the rain a uniform layer of warm coal was noted in the barges

while making temperature and gas flow measurements. This layer was first apparent at a depth of about 6 inches, but later moved to a depth of 3 feet by the end of the day. It is believed that the layer of warm coal was caused by the water from the rain percolating down through the coal. This triggered self-heating in the coal, which was obvious by the higher temperature readings obtained on the days following the rain. It should be noted that the conditions for self-heating were already present and the rainfall simply initiated self-heating in the barges.

TABLE 1

Coal Temperatures in Barges Compacted by Different Methods

<u>Barge No.</u>	<u>Method of Loading and Compacting*</u>	<u>Days in Barge</u>	<u>Average Temp (°F)</u>	<u>Maximum Temp (°F)</u>	<u>Number of Temp Readings >105°F</u>
1	diffuser loaded and lightly compacted	11	105	133	23
2	diffuser loaded and lightly compacted	11	102	126	25
3	diffuser loaded and well compacted	11	92	115	1
4	diffuser loaded and well compacted	10	91	104	0
5	diffuser loaded and well compacted	10	91	102	0

 * Lightly compacted - with a clam shell bucket.
 Well compacted - with a Bobcat loader.

TABLE 2

Coal Temperatures in Barges Loaded by Different Methods

<u>Barge No.</u>	<u>Method of Loading*</u>	<u>Days in Barge</u>	<u>Average Temp (°F)</u>	<u>Maximum Temp (°F)</u>	<u>Number of Temp Readings >105°F</u>
3	diffuser loaded	11	92	115	1
4	diffuser loaded	10	91	104	0
5	diffuser loaded	10	91	102	0
6	single chute loaded	10	97	112	11
7	single chute loaded	9	97	111	12
8	single chute loaded	9	95	111	3
9	single chute loaded	9	97	119	9
10	single chute loaded	9	90	102	0

 *All barges were well compacted with a Bobcat loader.

B. Air Flow Studies

Sondreal and Ellman (12) studied air flow through piles of North Dakota lignite and assumed that air convection through the lignite was unidirectional and only due to pressure gradients induced by the wind. They also assumed that natural convection resulting from thermal gradients were negligible. In this work it was also assumed that air movement through barges was primarily due to pressure gradients induced by the apparent wind created by the moving barges and that natural convection was minimal. The raw data from the gas flow studies indicated there were definite flow patterns in the barges studied. However, the data represented concentrations taken at different times and at different distances away from the point of injection, and was too complicated to present and try to explain in raw form. A correction for the tracer gas flow rate was determined by calculating the percent reduction in SF_6 concentration at each point in the barges where multiple sampling was done. Two, and sometimes three, samples were withdrawn from each of the sampling positions down the middle of each barge. The percent reduction in SF_6 was then plotted against time intervals between sampling and the best fitting line was used to determine a correction factor for SF_6 flow rates at various time intervals. The raw data were then multiplied by the correction factors to produce a distribution pattern represented by the contour maps shown in Figures 1 and 2. The numbers used in each of the figures to represent the concentration of SF_6 are relative.

The contour maps shown in Figures 1 and 2 illustrate various air flow patterns in the barges. Barge 3 was loaded with the diffuser, whereas barge 6 was loaded from a single chute. The contour map for barge 3 shows a relatively even lateral flow of tracer gas, whereas the contour map for barge 6 shows an uneven lateral flow. The coal in barge 3 was more evenly dispersed and less segregated by particle size than the coal in barge 6. The uneven air flow in barge 6 resulted in an increase in the rate of self-heating in the coal as was illustrated in Table 2.

The movement of the tracer gas away from the point of injection in each of the barges presents an interesting pattern. The relative concentration of SF_6 decreased between the injection point and the stern (back) of each barge, while it increased between the injection point and the bow (front) of the barges. As previously mentioned, it was assumed that air movement through the coal in barges was primarily due to pressure gradients induced by the apparent wind created by the moving barges. The contour maps given in Figures 1 and 2 illustrate the horizontal movement of the tracer gas and support this assumption. Air flow through the coal would push the tracer gas rapidly away from the point of injection and toward the back of the barge. The rate of dissipation of the tracer gas depended on how well the coal was compacted in the barges.

Sulfur hexafluoride has a density approximately five times as great as that of air. Because of this, SF_6 will flow to, and accumulate in, areas where the air flow is minimal. The accumulation of SF_6 in the front of the barges indicates there is little air flow through the first 25 or so feet of each barge. There is strong evidence that shows the most frequent area of the barge in which self-heating begins is the first 25 feet of the barge. This has been observed during the examination of data from over 600 barges (8). The fact that SF_6 accumulated in the same section of the barge where self-heating begins is a very important observation. This indicates that self-heating in barges is likely to begin where there is a sufficient supply of air to provide enough oxygen for the slow oxidation of the coal, but not enough air to carry away the heat produced in this oxidation. More importantly, it is probably the uneven air flow throughout the barge that provides the conditions for the initiation of self-heating.

The data from the gas flow studies was used to determine the relative gas flow rate through the barges. The percent reduction in tracer gas was plotted against

the time interval between sampling for the points in the barges where multiple sampling was done. A linear regression of the data in each of these plots yielded slopes that are equal to the relative gas flow rates in each of the barges. Table 3 lists the relative gas flow rates obtained for the various loading and compacting methods used in this study.

TABLE 3
Relative Gas Flow Rates in Barges

<u>Loading Method</u>	<u>Compacting Method</u>	<u>Relative Gas Flow Rate</u>
Diffuser loaded	Well compacted with Bobcat loader	0.096
Single chute loaded	Well compacted with Bobcat loader	0.39
Diffuser loaded	Lightly compacted with clam shell bucket	0.66
Single chute loaded	Trimmed with small dozer	1.39

C. Chemical and Physical Properties of Barged Coals

A comparison of the mean values of the various chemical and physical properties of two types of coal studied in the barging experiments is given in Table 4. Five barges of coal were loaded at one river port and had a low potential for self-heating as is illustrated in the table. Ten barges were loaded at a different river port and had a relatively high potential for self-heating. A number of interesting differences between the two types of coal can be noted. The type of coal with the higher potential for self-heating exhibits a lower carbon content, a lower hydrogen content, and higher nitrogen, sulfur, and oxygen contents. The coal type with the higher self-heating potential has a higher sulfate sulfur content, a lower free-swelling index, and a lower heating value. These latter three properties are indicators that the coal has undergone "weathering" (13). What is not known about these particular barges of coal, however, is whether the apparent weathering of the coal is due to a long stockpile storage or to the inherent property of the coal to undergo weathering (oxidation) rapidly.

The computer-based data bank established as part of this project has made it possible to examine the behavior of coals during barging operations. In particular, information in the data bank has been used to determine the general characteristics of coal that undergoes self-heating and the average rate of self-heating during barging, the deterioration in the quality of barged coal, and the relative importance of various factors that contribute to self-heating in barged coal (8). Statistical analysis of the information in the data bank has been carried out using the SAS package developed by the SAS Institute, Inc., Cary, North Carolina.

Most of the barges of export coal included in the data bank have temperature measurements that were taken at the time the coal was unloaded from the barges. This information along with the extensive analytical data collected on samples of the barged coal makes it possible for one to compare the chemical and physical characteristics of coals that do, and do not, undergo self-heating during barging. For this particular comparison, it was arbitrarily decided to compare barges of coal with a maximum temperature reading less than 10^oF above ambient temperature (low

potential) with barges that had a maximum temperature reading 20°F or more above ambient temperature (high potential). With these guidelines the data bank was used to generate the last two columns of data listed in Table 4. These data compare very well with that obtained in the barging study. The coals with the higher potential for self-heating had lower carbon and hydrogen contents, lower free-swelling indexes, and lower heating values. These coals also had higher nitrogen, sulfur, oxygen, and sulfate sulfur contents. This information indicates that coals with characteristics of weathered coals have higher potentials for self-heating.

TABLE 4

Characteristics of Coals in Barging Study and Data Bank
With Low and High Potentials for Self-Heating

Parameter*	Barging Study**		Data Bank***	
	Low Potent.	High Potent.	Low Potent.	High Potent.
Moisture, as-received (%)	14.16	13.43	14.16	14.05
Ash, dry (%)	9.04	11.94	8.38	9.23
Volatile Matter (%)	39.49	39.13	41.96	41.55
Fixed Carbon (%)	60.45	60.72	58.05	58.48
Heating Value (Btu/lb)	14,650	14,309	14,582	14,562
Carbon (%)	81.65	80.24	81.09	80.27
Hydrogen (%)	5.41	5.31	5.43	5.26
Nitrogen (%)	1.70	1.82	1.69	1.73
Sulfur (%)	2.07	2.31	1.62	1.86
Oxygen (%)	9.17	10.32	9.18	9.54
Pyritic Sulfur (%)	1.57	1.48	1.12	1.14
Sulfate Sulfur (%)	0.03	0.16	0.14	0.22
Organic Sulfur (%)	0.45	0.66	0.95	0.67
H/C Atom Ratio	0.794	0.797	0.798	0.782
O/C Atom Ratio	0.082	0.095	0.084	0.091
Free-Swelling Index	3.3	1.7	2.38	1.88
Hardgrove Grindability	39.0	44.1	43.6	47.9
Average Barge Temp (°F)	87	96	74.5	84.9
Average Barge Temp (°F)	95	114	81.4	108

* All values are reported on a dry, ash-free basis unless otherwise noted and all temperatures refer to the temperature of the coal at the time of unloading.

** Barging Study -- a fifteen barge tow with five barges having a low potential for self-heating (maximum barge temperature less than 10°F above the ambient temperature) and ten barges having a high potential for self-heating (maximum temperature greater than 10°F above the ambient temperature).

*** Data Bank -- 127 barges with a low potential for self-heating (maximum barge temperature less than 10°F above the ambient temperature) and 100 barges with a high potential for self-heating (maximum barge temperature greater than 20°F above ambient temperature).

IV. CONCLUSIONS

In conclusion, there are several recommendations that can be made with regard to protecting coal from self-heating during barging. The method of loading coal in the barge is important, and a method that disperses the coal more evenly through the barge and minimizes segregation of the particles of coal will reduce the amount of self-heating. Leveling and thoroughly compacting the coal in the barge reduces

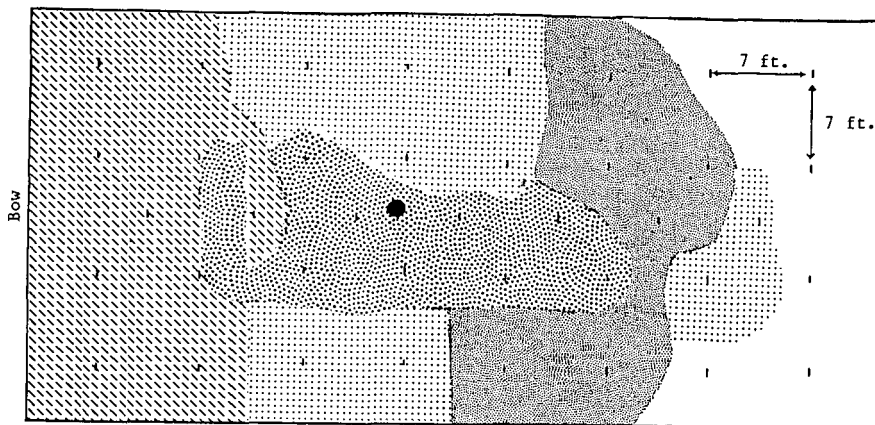
self-heating. Finally, coals with characteristics similar to those of weathered coals appear to undergo self-heating more readily than coals without these characteristics.

V. ACKNOWLEDGEMENTS

The authors are grateful to former students P. E. Pfannerstill, K. J. Thrasher and S. M. Williams for assisting in the collection of some of the data used in this paper. The financial support for the project received from the U.S. Department of Transportation under Contract No. DRRS 5683-C-00052 is gratefully acknowledged.

VI. REFERENCES

1. J. D. Davis and D. R. Reynolds, "Spontaneous Heating in Coal," U. S. Bureau of Mines Tech. Paper No. 409, (1928).
2. G. R. Yohe, "Oxidation of Coal," Illinois State Geol. Survey Rept. Invest. No. 207, (1958).
3. M. Guney, "Oxidation and Spontaneous Combustion of Coal: Review of Individual Factors," Coll. Guard., 217, 105-110, Jan. 26; 137-143, Feb. 2 (1969).
4. J. P. L. Bacharach, E. A. C. Chamberlain, D. A. Hall, S. B. Lord, and D. J. Steele, "A Review of Spontaneous Combustion Problems and Controls with Applications to U.S. Coal Mines," Final Technical Report to the U.S.D.O.E., Contract No. ET-77-C-01- 8965, (1978).
5. E. A. C. Chamberlain and D. A. Hall, "The Liability of Coals to Spontaneous Combustion," Coll. Guard., 221, No. 2, 65-72 (1973).
6. A. G. Kim, "Laboratory Studies on Spontaneous Heating of Coal: A Summary of Information in the Literature," U.S. Bureau of Mines Inf. Circ. No. 8756 (1977).
7. C. S. Daw, "Self-Heating of Coal and Char: A Literature Review," ORNL-TM 8273, June 1982.
8. J. T. Riley, J. W. Reasoner, N. L. Holy, S. M. Fatemi, G. S. Yates, D. D. Watson, P. E. Pfannerstill, A. Parvez, K. J. Thrasher, S. M. Williams, K. L. Diedrich, and T. B. Taylor, Jr., "Establishment of Data Bank on the Self-Heating of Coal", Final Technical Report to the U. S. Department of Transportation, Contract No. DRRS 5683-C-00052, July 1986.
9. ----, Draft Report of the Coal Exporters Association/National Coal Association Task Force on Coal Handling, Storage and Transportation, February 1983, pp. 15-16.
10. K. K. Feng, R. N. Chakravorty, and T. S. Cochrane "Spontaneous Combustion: A Coal Mining Hazard," Can. Min. Metl. Bull., 66, No. 738, pp. 75-84 (1973).
11. J. L. Elder, L. D. Schmidt, W. A. Steiner, and J. D. Davis, "Relative Spontaneous Heating Tendencies of Coals," U. S. Bureau of Mines Tech. Paper 681, (1945).
12. E. A. Sondreal and R. C. Ellman, Rep. Invest. U. S. Bureau of Mines No. 7887 (1974).
13. F. J. Beafore, K. E. Cawiezel, and C. T. Montgomery, J. Coal Quality, 3, 17 (1984).

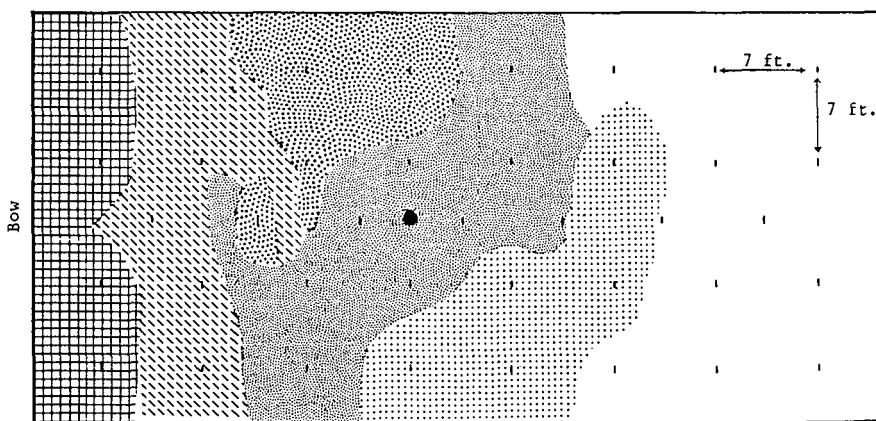


Relative Concentration of Tracer Gas

= 1-10
 = 10-20
 = 20-30
 = 30-130

(- marks indicate sampling points; ● indicates gas injection point)

Figure 1. Gas flow pattern in barge No. 3.



Relative Concentration of Tracer Gas

= 0-5
 = 5-15
 = 15-30
 = 30-50
 = 50-380

(- marks indicate sampling points; ● indicates gas injection point)

Figure 2. Gas flow pattern in barge No. 6.

AERIAL OXIDATION OF MACERAL ISOLATES FROM AN AUSTRALIAN BITUMINOUS COAL

A.G. Pandolfo^A, R.B. Johns^A, P.D. Nichols^{B,C} and D.C. White^{B,D}

- A. Department of Organic Chemistry, University of Melbourne, Parkville, Victoria, Australia 3052.
- B. Department of Biological Science, Florida State University, Tallahassee, Florida, U.S.A. 32306.
- C. Current Address: CSIRO Marine Laboratories, G.P.O. Box 1538, Hobart, Tasmania, Australia. 7001.
- D. Current Address: Oak Ridge National Laboratory, P.O. Box, Oak Ridge, TN, U.S.A., 37831

ABSTRACT

A comparative study of the relative reactivities of Run-of-the-Mine (ROM) Blair Athol coal and constituent maceral lithotypes, fusain and vitrain to laboratory oxidation conditions at 100°C is reported using a surface reflectance FTIR technique (DRIFT). The DRIFT spectra of pure maceral isolates established the aliphatic content to be in the order of exinite >> vitrinite > inertinite. The difference spectra of the maceral lithotypes fusain and vitrain show the ready loss of aliphatic groups in the former as an early oxidation step. Oxygen uptake by vitrain is initially slow compared with ROM and fusain coals. Carbonyl formation is a primary reaction in the earliest stages for all coal samples studied, and on more extended oxidation, leads to a range of oxygen functionalities including a shift of carbonyl absorptions to higher wavenumbers consistent with anhydride and lactone formation.

INTRODUCTION

Atmospheric oxidation or weathering of coal can result in the deterioration of many of its technologically important properties thereby significantly altering the utilization potential of coal. We are engaged in a longer term study of the chemistry of Blair Athol coal and the chemical effects of weathering has been one topic of major interest (1). Blair Athol coal from Queensland has an ASTM classification of high volatile bituminous C and is typical of many Gondwanaland coals in that it has a high inertinite maceral content. The porous nature, high moisture holding capacity, and very good steaming coal properties place Blair Athol towards one end of the range of Australian inertinite-rich coals.

The main seam of Blair Athol is best described as a durain coal but within the deposit samples of the maceral lithotypes fusain and vitrain occur, and this has allowed a chemical study to be undertaken of the effect of prolonged oxidation of each maceral lithotype and a comparison with Run-of-the-Mine coal (ROM) to be made. More recently we have been able to separate Blair Athol coal by the Density Gradient Separation technique (2,3) into high purity maceral isolates of exinite, vitrinite and inertinite. Their study, primarily by infrared spectroscopy, has further refined our understanding of the chemically reactive centres involved in coal oxidation and the relative reactivities of the macerals.

EXPERIMENTAL

The coal used was from the Blair Athol coal-field located in Queensland, Australia and was received as -40mm pieces in sealed containers. The naturally occurring maceral lithotypes were chosen with the assistance of the mine geologist and identification was based on their physical appearance (4). The 'pure' maceral isolates were obtained from a sample of ROM coal with the assistance of G.R. Dyrkacz and C.A.A. Bloomquist at the Argonne National Laboratories (U.S.A.) according to their published Density Gradient Centrifugation (DGC) procedure (2,3).

The naturally occurring maceral concentrates and a sample of ROM coal were oxidized at 100°C under a continuous flow of moist air (3 ml sec⁻¹) in a modified Kugel oven. A run was also performed under a nitrogen atmosphere. Samples were taken at regular intervals and stored in nitrogen flushed vials to prevent further oxidation before analysis.

Diffuse Reflectance FTIR (DRIFT) Spectra were obtained on a Nicolet 60SX FTIR equipped with a nitrogen cooled, high sensitivity mercury : cadmium : tellurium detector. Each sample resulted in a single sided interferogram of 4096 data points which provided a resolution of 4 cm⁻¹. 500 scans per sample were obtained.

RESULTS AND DISCUSSION

The naturally occurring maceral lithotypes were readily distinguished by their physical appearance. The vitrain sample was black, of very bright lustre and brittle. The fusain sample was black in colour and very soft and friable. Its physical structure appeared to be more porous and open and usually had a higher water content than the other samples investigated. The high proportion of this maceral lithotype in Blair Athol coal would appear to be the cause of the high water content of the 'as mined' coal (typically ~16%).

TABLE 1. Elemental and Petrographic Analyses of Blair Athol Coals

Elemental Analyses	C	H	N (DAF)	S	O*	Ash	H/C (atomic)	O/C
Run of Mine (ROM)	82.55	4.72	1.88	0.26	10.59	6.5	0.658	0.102
Vitrain	80.97	4.92	1.79	0.48	11.84	4.4	0.724	0.084
Fusain	80.27	4.06	1.78	1.30	12.59	9.4	0.602	0.118

* By difference

Petrographic Analyses

	Exinite	Vitrinite (wt %, mmf)	Inertinite
Run of the Mine	4.1	28.4	67.5
Vitrain	8.2	78.9	12.9
Fusain	3.1	15.7	81.2

Table 1 reports the elemental and petrographic analysis of the samples. Although these samples are petrographically and physically quite different, this is less obvious from their elemental analysis with the main difference being the hydrogen content of the samples. A variation in sulphur content is also seen.

Vitrain has the highest H/C value of the samples studied while fusain has a relatively low H/C value. The ROM and durain coal samples have similar H/C values and these lie between those for fusain and vitrain. These observations are strikingly reinforced by the DRIFT spectra of the C-H region (Fig. 1) which reveals that the aliphatic content of the maceral isolates is exinite >> vitrinite > inertinite.

Figure 1 reports for the first time DRIFT spectra of Gondwanaland coal maceral isolates of very high purity (98.5% and better). In addition to its high aliphatic component, the other distinguishing feature of the exinite fraction is the strong C=O absorption centred at ~1700 cm⁻¹ which has also been reported for Northern Hemisphere exinites (5,6). The broad 1100-1300 cm⁻¹ stretch which can be assigned to C-O type stretches together with the strong carbonyl peak and apparent lack of a

strong -OH band ($3200-3600\text{ cm}^{-1}$) suggest esters (especially alkyl esters in this case) may strongly contribute to the exinite fraction. The carbonyl absorption is much less marked in the spectra of the other two macerals. The DRIFT spectra suggest a strong aromatic contribution to both the vitrinite and inertinite. Pyrolysis-GC/MS also indicates that the vitrinite sample contains more phenolic material than either of the other two macerals. The unusually high, inherent water content of Blair Athol coal can be associated with the hydrophilic properties of these hydroxyl-containing residues as revealed by the release of the phenolic components on pyrolysis. Water is considered to be a factor in the weathering of coal.

Figure 2 gives further insights to the type of C-H bonding in the macerals, the changes in which are noticeable during coal oxidation. Fourier Self Deconvolution (FSD) has been used to enhance the resolution of the aliphatic region and give more specific structural information (7). The aliphatic symmetric and asymmetric bands resolve into asym. $-\text{CH}_2$ and asym. $-\text{CH}_3$ (2920 and 2960 cm^{-1} respectively) and sym. $-\text{CH}_2$ and sym. $-\text{CH}_3$ stretches (2853 and 2870 cm^{-1} respectively). The deconvoluted exinite spectra show extremely strong methylene stretches (2853 and 2920 cm^{-1}) relative to methyl stretches (2870 and 2960 cm^{-1}). This suggests a strong contribution of long chain aliphatic material to this maceral and is consistent with the release of $n\text{-C}_{10}$ to $n\text{-C}_{27}$ hydrocarbons by thermal distillation from ROM coal (8). By comparison, the deconvoluted vitrinite and inertinite spectra suggest a greater methyl contribution to their aliphatic component. The technique, however, was not successful in further improving the resolution of the carbonyl region due to complications with moisture variations.

Oxidation in a stock-pile is initially a surface phenomenon and we have used the DRIFT technique to observe sites of oxygen incorporation as revealed by IR. The oxidation profiles reported here are after oxidation at 100°C for convenience of study, although similar changes do occur at lower temperatures (i.e., 50°C) but observable only after extended periods of time.

Figure 3 shows the variation in atomic O/C ratio with time of oxidation for the natural maceral concentrates and the ROM coal. The ROM coal treated at 100°C but in nitrogen, showed only a small increase in O/C. Although a small amount of adventitious oxygen may have reacted with the coal, the increase in O/C is more likely due to the loss of volatile hydrocarbons through the thermal disruption of the coal (8). The ROM coal treated at 100°C in a constant air flow showed an increase in O/C value from 0.102 to 0.200 over a period of 20 days. The O/C increase is initially rapid but after 2 days the rate of increase slows. Although fusain has a higher initial O/C value (c.a., 0.118) it also shows a rapid initial increase. After 20 days the Fusain sample reached an O/C value of (0.248). The Vitrain sample, however, displayed a contrasting behaviour. From a relatively low O/C value of 0.084 it showed a slow initial increase in O/C over the first two days at 100°C , followed by a strong increase in O/C so that after 20 days it reaches an O/C value of 0.22.

It is evident that there is a difference in the mechanism or rate of oxygen reaction between the ROM coal and fusain sample when compared with the vitrain sample. This difference is undoubtedly due to the differences in the chemical composition of the coal maceral lithotypes and reflects the structural differences seen in the DRIFT spectra of the pure macerals (Fig. 1).

The structural changes occurring during the 100°C oxidation of the coal samples are seen in the DRIFT spectra of the $4000-800\text{ cm}^{-1}$ region (Fig. 4). The loss of aliphatic material indicated by the decrease in the aliphatic stretches ($2800-3000\text{ cm}^{-1}$) with oxidation is common to all the coal samples examined but is especially severe for the fusain sample which is 81% Inertinite. Fusain, although having little aliphatic material initially, is almost devoid of aliphatic material after 10 days oxidation.

Accompanying this decrease in aliphatic material is an increase in the C=O regions (centred at 1700 cm^{-1}). The formation of this peak begins early in all samples but for the fusain sample is resolved after 1 day of oxidation. Although the C=O peak is complex and consists of many overlapping bands it can be resolved into at least three major bands at 1840, 1770 and 1715 cm^{-1} . The 1840 cm^{-1} peak appears after prolonged oxidation and has been assigned to anhydrides (9). The appearance of this peak was not observed for the coal oxidized under nitrogen and hence is a genuine oxidation product. Careful examination of the spectra also reveals that the vitrain sample shows the greatest increase in the carbonyl region. This increase together with the greater aliphatic content of vitrain is consistent with benzylic sites as possible centres of oxidative attack. This is also supported by the observation that the pyrolytic yield of alkylated aromatics (including phenols) decreases more rapidly relative to their non-alkylated analogues as determined by Py-GC/MS.

The difference spectra (Fig. 4d) are useful in illustrating the changes in functionality consequent upon oxidation. The strong positive absorptions in the carbonyl region confirms earlier observations but further analysis reveals that the nature of the carbonyl groups formed changes in the latter stages of oxidation. For both the fusain and the vitrain samples a shift to higher wavenumber is seen for the carbonyl peaks in the latter stages of oxidation (i.e., 20-10 days). While fusain shows an early and continual loss of aliphatic material, vitrain shows little if any loss during the early stages (1-0 days). Fusain also displays a strong increase in the C-O region ($1100\text{-}1300\text{ cm}^{-1}$) in the latter stages of oxidation but which is not so significant as for the vitrain sample.

These observations are consistent with views that multiple pathways of oxidation are operative. The chemical nature of the coal and hence its maceral composition appears to influence the nature of the oxidative processes occurring. However, the resolving limits of IR spectroscopy allow us to observe only the broader effects. Even so the data suggest the insertion of oxygen into carbon centres that yield a variety of carbonyl containing structures. Some of these will be precursors for more complex products such as anhydrides. The data suggest that esters including lactones rather than carboxylic acid centres are formed. Small changes are also seen in the hydroxyl region. These changes are consistent with the initial formation of peroxides (10) which are known to show instability at 100°C and can be expected to lead to carbonyl as well as hydroxyl functionalities.

Figures 3 and 4 demonstrate clear differences of reactivity to oxidation between ROM coal and its constituent maceral lithotypes fusain and vitrain. The differences between ROM and fusain coals do not seem explicable in terms of Inertinite content only, suggesting that the physical properties of the fusain play a significant role. Since coal measures are by no means homogenous in their maceral composition, the data presented exemplify the predictive value of knowing relative chemical reactivities of constituent macerals, which could then be applied to minimizing handling problems where autooxidation can cause difficulties.

ACKNOWLEDGEMENTS

The authors thank Pacific Coal Pty. Ltd. for financial support. John Sangster (Pacific Coal) is thanked for providing the coal samples. G.R. Dyrkacz and C.A.A. Bloomquist (Argonne National Laboratories, Chicago, USA) are thanked for their assistance with the isolation of the pure maceral isolates.

REFERENCES

1. Pandolfo, A.G., Johns, R.B. and Buchanan, A.S., *Proc. Int. Cont. Sci.*, 479-482, Sydney, October 1985.

2. Dyrkacz, G.R., Bloomquist, C.A.A. and Horwitz, E.P., Separation Science and Technology, 16, 1571-1588, (1981).
3. Dyrkacz, G.R. and Horwitz, E.P., Fuel, 61, 3-12, (1982).
4. Stach, E., Mackowsky, M.-TH., Teichmuller, M., Taylor, G.H., Chandra, D. and Teichmuller, R., In Stach's Textbook of Coal Petrology., 3rd revised edition, Gebruder Borntraeger, Berlin, (1982).
5. Dyrkacz, G.R., Bloomquist, C.A.A. and Soloman, P.R., Fuel, 63, 536-542, (1984).
6. Allan, J., Ph.D. Thesis, University of Newcastle upon Tyne, 1975.
7. Wang, S-H. and Griffiths, P.K., Fuel, 64, 229-236, (1985).
8. Date, A.C. and Johns, R.B., Unpublished results.
9. Rhoads, C.A., Senftle, J.T., Coleman, M.M., Davis, A. and Painter, P.C., Fuel, 62, 1387-1392, (1983).
10. Jones, R.E. and Townsend, T.A., J. Chim. Phys., 47, 348-352, (1950).

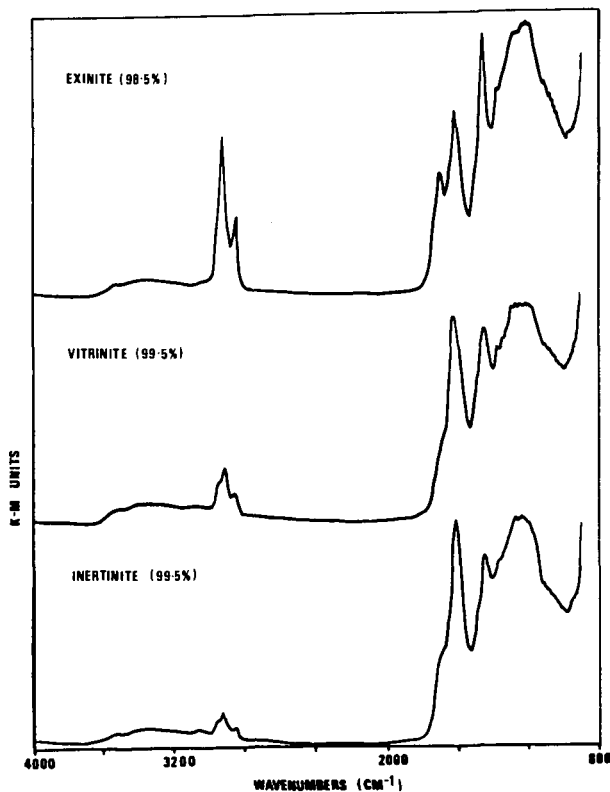


Figure 1. IR spectra (4000 - 800 cm⁻¹) of Blair Athol DGC pure maceral isolates.

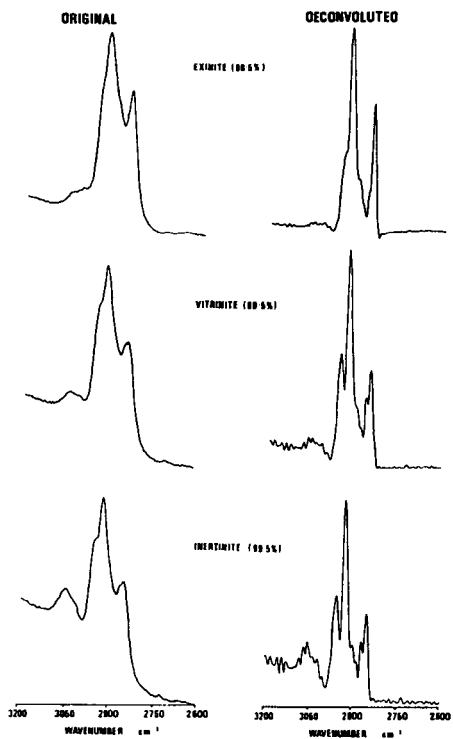


Figure 2. Original and deconvoluted DRIFT spectra (3200 - 2600 cm^{-1}) of the Blair Athol DGC pure mineral isolates.

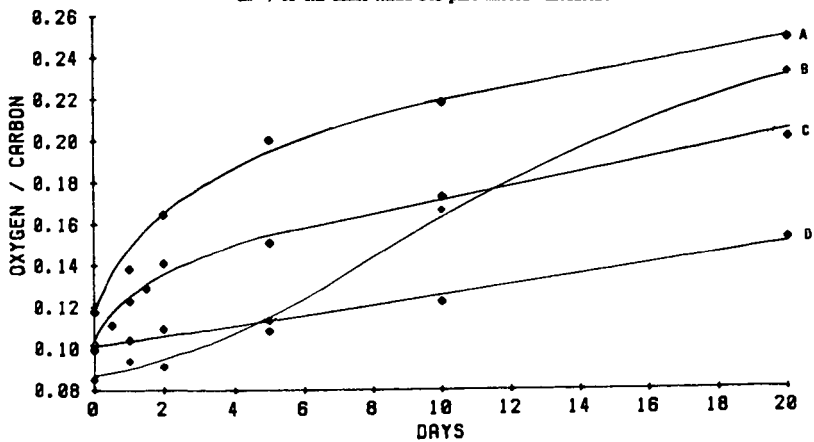


Figure 3. Variation in atomic O/C ratio with increased oxidation at 100 C.

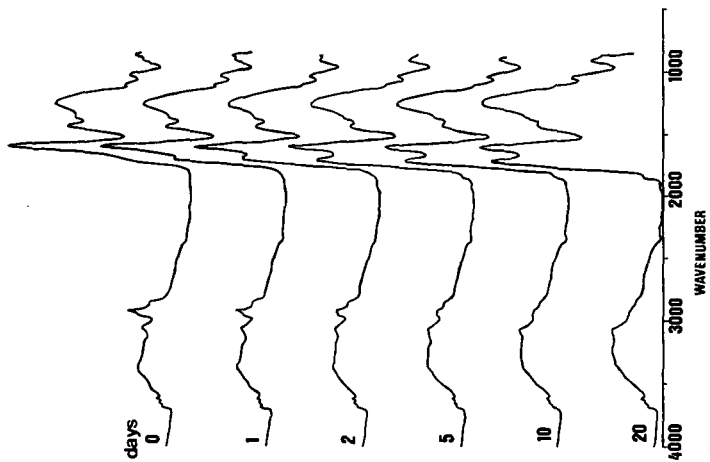


Figure 4(b). 4000 - 800 cm^{-1} DRIFT spectra of unoxidized (0 days) and progressively oxidized fusicin.

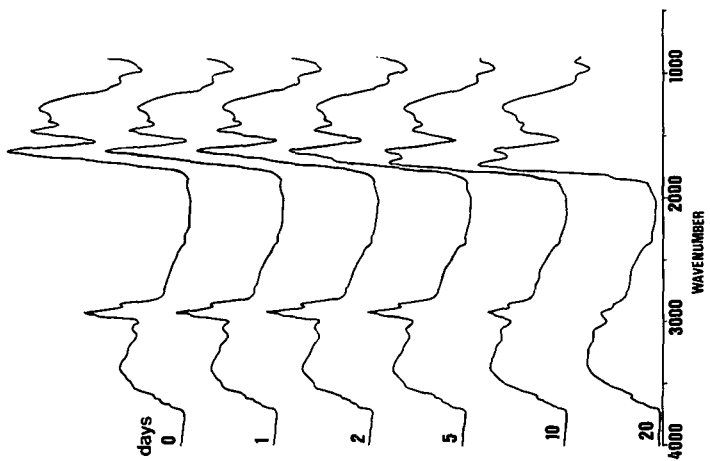


Figure 4(a). 4000 - 800 cm^{-1} DRIFT spectra of unoxidized (0 days) and progressively oxidized vitrain.

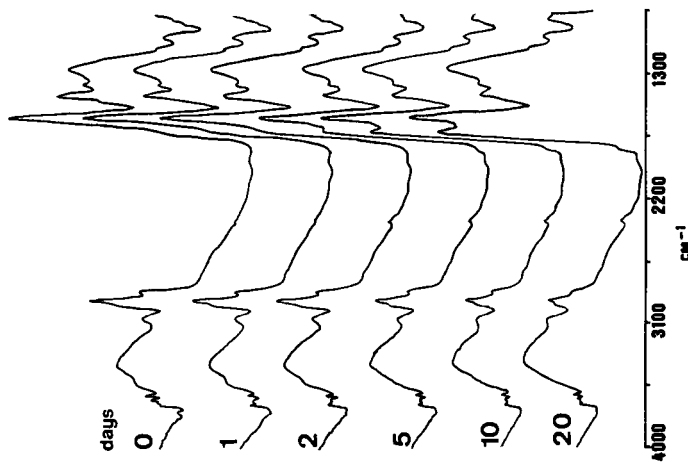


Figure 4(c). 4000 - 800 cm^{-1} DRIFT spectra of unoxidized (0 days) and progressively oxidized RCM coal

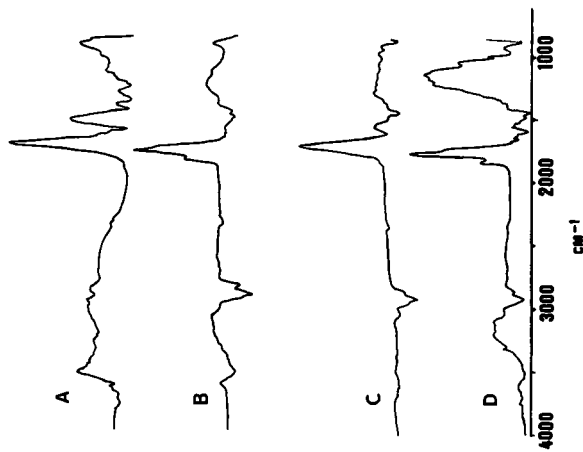


Figure 4(d). DRIFT subtraction spectra of: (A) oxidized(1 day) - unoxidized vitrain, (B) 20 day - 10 day oxidized vitrain, (C) oxidized(1 day) - unoxidized fusain, (D) 20 day - 10 day oxidized fusain.

THE MEASUREMENT OF WATER TIGHTLY BOUND BY LOW RANK COALS

E. J. Hippo, Southern Illinois University, Carbondale, Illinois
R. C. Neavel S. E. Smith, R. J. Lang, Exxon Research and Engineering
Company, Baytown, Texas
R. N. Miller, Air Products

Schafer¹ has suggested that low rank coals retain water after being nominally dried at 110°C. This paper discusses the results of direct determinations of water present in "dry" coals and the possible effects of tightly bound water on the measured physical, chemical, and conversion properties of coals.

A coal characterization program at the Baytown, Texas Labs of Exxon Research and Engineering Company employed a sample library of 66 samples ranging from lignites to low volatile bituminous coals.^{2,3} Apparent densities of the samples measured in polar organic probes (methanol, isopropanol, and methyl ethyl ketone) were much higher than densities determined in helium. These differences appeared to be related to coal rank and the polarity of the solvents. However, densities determined in water (more polar than the organic solvents) were within experimental error equal to density determinations in helium.

Franklin^{4,5} reported that the differences between densities determined in methanol and helium were proportional to the heat of wetting of methanol on coal and to the surface area of the coal. Walker, et. al.⁶ reported that a significant fraction of the surface area of low rank coals may be covered with carboxyl groups. Thus, apparent heat of wetting might reflect interactions of methanol and carboxyl groups. In addition, Schafer reported that dried coals decarboxylate under mild pyrolysis (175°C) to yield CO₂ and H₂O.¹ It is also known that small amounts of water can be incorporated into large excesses of methanol without apparent volume change.⁷ These observations lead us to formulate the following hypotheses: (1) water is bound tightly by low rank coals and is not removed by drying overnight in a vacuum; (2) the bound water is extracted by methanol refluxing, and (3) the bound water affects density measurements.

Experimental

Carboxyl group contents were determined for the library samples using a modification of Schafer's ion exchange.⁸ Samples of -325 M coal were washed with citric acid to remove metallic cations. Samples of 0.5 g were then refluxed in 0.5 N barium acetate at 50°C for 24 hrs under N₂. Solutions were back-titrated with BaOH to 8.5 pH.

To study the amount of tightly held water in dried coals, a ten-sample subset of the Exxon Coal Library was chosen on the basis of carboxyl group content. Aliquots of the raw and citric acid washed coals from the subset were dried overnight in a vacuum oven at 110°C. Vacuum was broken with N₂ and the samples transferred immediately into a glove box. After cooling, three grams of each sample were transferred to boiling flasks, 150 ml of methanol was added to the samples, and the mixtures refluxed for one hour. Prior to mixing, the methanol had been dried over 3A type molecular sieves and blank reflux tests were conducted. All transfers and subsequent refluxing were performed under nitrogen. Following reflux, the methanol extract was decanted. The residue was dried and weighed to determine the total weight extracted during refluxing. The density of the methanol extracts were determined at 30°C by pycnometry, and the water content in the methanol extract was determined by a Fisher Aquatest.⁹

In every case, the weight of the solid residue after refluxing and removal of methanol was within one percent of the starting weight of coal minus correction for the extracted "bound" water assayed by the Aquatest in the methanol.

Results and Discussion

As illustrated by Figure 1, one mole of water can be removed by CH₃OH refluxing of the "dried", raw* coal for each molar equivalent of carboxyl groups as determined by barium exchange of acid-washed coal. For "dried", acid washed coals, approximately one-half as many water molecules are held after drying as there are carboxyl groups. Approximately 0.2 milliequivalents of water per gram of coal is retained by the coals which contain very little or no carboxyl groups.

The results indicate that water is held by low rank coals even after drying overnight in a vacuum oven. Refluxing in excess methanol removes this water. Also, when some carboxyl groups are in a salt form, more water is held than when all the groups are in an acid form. Assuming that other typical coals contain carboxyl groups with similar proportions of cations exchanged to them, the amount of water held by raw coals can be approximated by the number of carboxyl groups present in the (acid washed) coal. The carboxyl groups present in coals can be estimated by the following equation derived from the Exxon library data base:

$$\text{COOH}_{\text{dmmf}} = 19.4 - 0.222 * C_{\text{dmmf}} - 0.0173 * \text{VIT}_{\text{VOL}} \quad (1)$$

where $\text{COOH}_{\text{dmmf}}$ = Carboxyl content (meq/g) (dry mineral free)
 C_{dmmf} = Carbon content of coal (%) (dry mineral free)
 VIT_{VOL} = Vitritine content (VOL. %, mineral-free)

The correlation coefficient squared (r^2) is 0.94, and the equation predicts COOH to within ± 0.1 meq/gram (dry mineral free coal basis).

Densities of the water-containing methanol solutions were determined by pycnometry. The densities of these solutions were proportional to the amount of bound water extracted; apparently no measurable volume change occurred when the water was incorporated into a large excess of methanol. Densities of extracts from methanol reflux measured at 30°C ranged from 0.783 g/ml to 0.789 g/ml with a mean of 0.786 g/ml for the 20 samples tested. Densities of the methanol blanks dried over 3A molecular sieves averaged 0.783 g/ml. Reproducibility of the density measurements was better than ± 0.0005 g/ml. The measured densities of the mixture, within experimental error, results from the addition of the water to the mixture without changing the volume of the mixture.

Water bound to the oven-dried coal would be extracted into the large volume of any polar liquid during density determinations; therefore, apparent densities measured in these polar liquids would be spuriously high. Water bound in the coal would be weighed, but its volume would not be measured. When the density of coal is determined in helium, water, n-hexane, or toluene, the bound water would be weighed and its volume would be measured. However, since the density of tightly held water is lower than the densities of coals (assuming that the

*Raw refers to state of the coal after preparation such as grinding and washing but prior to any chemical treatment such as acid washing.

density of the tightly held water is that of bulk water), the density of the solid material measured in these probes is lower than its true density. Also, since water will repel hydrophobic hexane and toluene, complete filling of the pore structure will not occur. Densities of the library coals determined in hexane and toluene are less than densities measured in helium.

Figure 2 demonstrates the effects of tightly bound water on the density of coals measured in methanol and in helium. In Figure 2, methanol densities are plotted as a function of helium densities. A parity line is included for reference. Apparent densities determined in methanol (squares) are based on the assumption that the density of the bulk methanol does not change during the density determination. The open circles represent corrected helium and methanol densities calculated from apparent densities, assuming that water is incorporated into bulk methanol without changing the volume of the bulk liquid, that the moles of tightly bound water present in the coal are equal to the moles of carboxyl groups in the coal, and that chemically held water has a density of bulk water. Correcting apparent densities for the tightly held water does not bring the corrected densities to the parity line, but differences between the corrected densities determined in the two media are much smaller.

Numerous explanations have been presented in the literature to account for differences in densities measured in various media. These are summarized as: (1) opening of pores by removal of various organic components causes methanol densities to be greater;^{10,11,13} (2) the differences in average molecular size of the probe causes differences in apparent densities;^{11,12} (3) Vander Waals contraction of methanol occurs on the coal surface during the density determination;^{4,5} (4) incorporation of solvent into the gel-like structure of coals occurs, causing an increase in density due to solvent-polymer interactions.¹² These factors can now be more satisfactorily applied because the differences which need to be explained range from 0.01 g/ml to 0.05 g/ml on the corrected basis instead of the 0.03 g/ml to 0.15 g/ml range for apparent densities where tightly held water is not taken into account.

In addition to the effects of tightly held water on apparent densities, the tightly held water may affect other physical properties. If polar functional groups project from the pore walls, significant interactions between the functional groups and polar probes by vapor adsorption could result in increases in the coal swelling through the disruption of intermolecular hydrogen bonding. Because bound water helps spread the charge density over a longer distance, its presence could enhance these interactions. Also, because pore volume calculated from equilibrium moisture volume is greater than pore volume calculated from particle and real densities, water swells the coals. Thus, the swelling volume attributed by some workers to "plastic swelling by solvent vapors" is, in part, due to disruption of secondary bonding^{14,15,16} that releases compression strain and creates larger pores. Second, if water is incorporated nonvolumetrically into the swelling solvent, solvent uptake on a weight percent basis will be affected because the water incorporated into the solvent leaves a void volume to be filled by the solvent. The weight gain is interpreted as a solvent-solid interaction instead of the water-solvent interaction. Third, hydrophobic solvents are repelled by the presence of water on the surface of the pores. Thus, the solvent is not incorporated into the bulk coal, which in the absence of bound water, the solvent might otherwise penetrate.

The presence of water might affect surface properties. For example, if solvent incorporates water into its bulk nonvolumetrically, a heat release would occur. Corrections for this heat release should be considered when studying the heat of wetting of solvents on coal surfaces. The presence of tightly held water may affect the contact angle between the coal and a wetting agent. Because particle densities and pore volumes are determined by mercury intrusion and calculated on the basis of contact angle, they could be in error.

Tightly held water is not measured in standard procedures that call for moisture determination by drying at 110°C for one hour. Therefore, any procedure that calls for correction of results based on determined moisture content does not adjust data properly. ASTM tests, such as the Btu content, volatile matter yields and elemental analyses are corrected for ASTM water only and are not corrected for the tightly held water which is present in the starting coal. In elemental analysis, water is weighed as part of the actual sample, then the sample is burned and the products of the combustion (water and CO₂) are trapped and measured. Tightly held water as well as ASTM moisture and water of combustion are also trapped. This procedure calls for an adjustment of the hydrogen content based on the ASTM water, but no adjustment is made for tightly held water. Therefore, the hydrogen in the tightly held water is assigned as organic hydrogen in the coal. The starting weight includes oxygen from the tightly held water which is incorporated in the calculations as oxygen by difference and assigned to the organic content of the coal.

Correcting the chemical analyses for tightly held water results in a change of as much as 0.5% in hydrogen content. The hydrogen to carbon ratio changes by as much as 0.075, and the oxygen to carbon ratio changes by as much as 0.03. The net result is that the relative positions of compositions of coals on a van Krevelen diagram change. These changes in relative position affect the concepts of coal metamorphism and average molecular structures.

The presence of tightly held water may affect chemical activity of the coal in three ways. First, water will react with certain reagents that react with coal structure. For example, water will hydrolyze Grignard reagents that would otherwise attack esters and ketones in the coals forming alcohols. It will also react with trifluoroacetic anhydride to form acetic acid during titrations for OH groups in the coals. Second, water will affect diffusion properties. For example, water bound to pore walls will restrict pore apertures and thus increase diffusional resistance of certain chemical reactions. Third, by being closely associated with the carboxyl groups, the water may effectively block reactions such as esterification.

Finally, quantitative results from analytical spectroscopic methods such as Fourier Transform Infrared Spectroscopy (FTIR) are calculated on the weight of the sample in the analyzed pellets. Because tightly bound water is present in varying amounts in each coal, each sample's spectrum should be corrected for that bound water. At present, standard techniques do not. Also, because the OH stretch of the bound water would absorb in the same regions of the spectrum as do acid functionalities, the acid (OH) content of the coal is overestimated by this technique.

Material and heat balances of conversion processes should account for tightly held water. For example, some water present in liquefaction products will be formed from bound water; therefore, heats of liquefaction should be adjusted accordingly. Also, the bound water may influence total yields and yield pattern in liquefaction, pyrolysis, and hydropyrolysis. Other processes such as grinding, dispersion of catalysts, cleaning, and coking may be affected by the presence of the tightly held water.

Conclusions

Coals dried by conventional techniques contain water that can be removed by polar organic solvents during refluxing. The incorporation of water into the solvents can lead to erroneous density determinations in polar organic solvents. The bound water is proportional to the carboxyl group content of the coal. Because lower rank coals contain more carboxyl groups than higher rank coals, the effects of bound water are more profound in lower rank coals. The presence of water on coals assumed to be dry could have far reaching significance in other areas of coal science such as solvent coal swelling, elemental analysis, coal classification, chemical activity, processing yields, and heat balances. We would recommend that such possible effects be kept in mind when treating data on presumably dry coals.

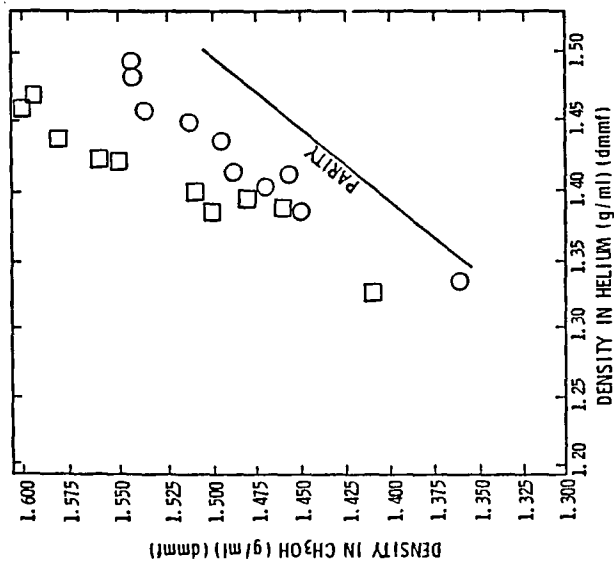
References

1. Schafer, H. N. S., Fuel, 59, 295-304, 1980.
2. Neavel, R. C., Smith, S. E., Hippo, E. J., and Miller, R. N., 179th Annual Meeting of ACS, Fuel Division Preprints, August 1980, 26, 3, pp. 246-257.
3. Neavel, R. C., Smith, S. E., Hippo, E. J., and Miller, R. N., Fuel, 65, p. 312, 1986.
4. Franklin, R. E., Trans. Faraday Soc., 1949, 45, pp. 274-286.
5. Lowery, H. H., ed., "Chemistry of Coal Utilization" Supplementary Volume, John Wiley and Sons, Inc., New York, NY, p. 108, 1963.
6. Morgan, M. E., Jenkins, R. G., and Walker, P. L., Jr., 179th Annual Meeting of ACS, Fuel Division Preprints, March 1980, 26, 1, pp. 219-223.
7. West, R. C., ed., Chemical Rubber Co. Handbook for Chemistry and Physics, 59th ed., 1978, D-284, CRC Press, Inc., West Palm Beach, Florida.
8. Schafer, H. N. S., Fuel, 49, p. 197, 1970.
9. Kolkhoff, I. M., and Belcher, C., Volumetric Analysis, Interscience, New York, NY, pp. 409-448, 1963.
10. Nelson, J. R., Ph.D. thesis, "Sorption of Organic Molecules in Carbons, Crosslinked Polymers and Coals of Various Ranks," The Pennsylvania State University, 1979.
11. Fossil Energy Report, FE-2286-32, "Preparation of a Coal Conversion System Technical Data Book," U. S. Dept. of Energy, Prepared by Institute of Gas Technology, IIT Center, 3424 S. State St., Chicago, February 1979.
12. Toda, Y., Fuel 51, 108-112, 1972.
13. Larsen, J. W., and Kovac, J., ACS Symposium Series Vol. 71, Washington, D. C., 1298
14. Van Krevelen, D. W., "Chemical Structure and Properties of Coal 28--Coal Constitution and Solvent Extraction," Fuel, 44, p. 229-242, 1965.
15. Sanada, Y., and Honda, H., Fuel, 45, p. 295, 1966.

RCN:cj
9/2/86

FIGURE 2

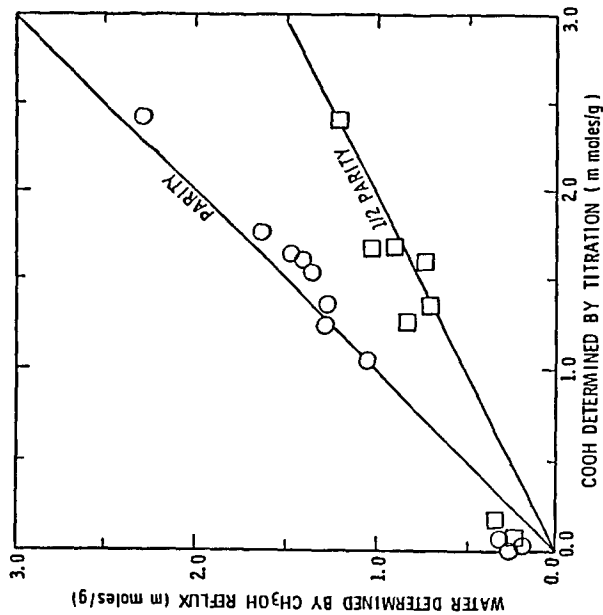
BOUND WATER EFFECT ON DENSITY



- Density Corrected for Bound Water Based on the Assumptions that:
 - Water Is Incorporated Into Bulk CH₃OH
 - Without Volume Change
 - Chemisorbed Water has Density of Bulk Water
- Density as Determined In Methanol

FIGURE 1

RELATIONSHIP BETWEEN ABSORBED WATER AND CARBOXYL GROUPS



- Water Determined on "Dry", Raw Coals
- Water Determined on "Dry", Acid Washed Coals

ENTHALPIES OF DESORPTION OF WATER FROM COAL SURFACES

J.E. Callanan, B.J. Filla, K.M. McDermott and S.A. Sullivan

Center for Chemical Engineering, National Bureau of Standards*
Boulder, CO 80303

Introduction

During our efforts to develop transferable techniques for the measurement of the heat capacity of coal and to develop a model that would facilitate the prediction of the thermal properties of coal, several series of measurements of the heat capacity of a single coal were made. Changes in thermal properties which appear to be related to weathering of the coal and to its inherent moisture content were observed. This paper deals with two facets of the interaction of moisture with coal surfaces, that are related to our study of these changes.

The first was the observation of significant qualitative and quantitative differences in the initial heat capacity scans as the coal under study became more oxidized (1,2). Particularly significant was the progressive development of an exotherm. As the projected heat balance of any process would be seriously affected by an unanticipated generation of heat, it is important to determine the magnitude of the enthalpy.

Second, our adaptation of a model which permits the prediction of the heat capacity of coal from parameters such as heating rate, ultimate analysis, and moisture content (3) requires a value for the heat of vaporization of water. Since the water interacted with the coal surface, it was not clear that the most suitable value was in fact an enthalpy of vaporization. We wished to determine the energy involved in removing water from the coal experimentally, whatever the nature of the process might be.

This paper describes the measurements and data reduction techniques used to evaluate the energy difference between initial and subsequent runs, a simple technique developed for heat of desorption measurements, and presents results obtained with both procedures.

Experimental

Materials

Two different coals were used for these studies. The first was a high-volatile bituminous coal (PSOC-854), obtained from the Coal Sample Bank at Pennsylvania State University. The second, a premium medium-volatile bituminous coal, was obtained from the Premium Coal Sample Bank at Argonne National Laboratories (4).

*Contribution of the National Bureau of Standards. Not subject to copyright.

Procedures - heat capacity measurements

Specimen preparation followed our established procedures (5). All preparation was done in a controlled atmosphere, either in a controlled-atmosphere chamber for the specimens sealed in nitrogen (6), or in a glove bag for specimens sealed in argon, helium and carbon monoxide. Representative fractions, obtained by riffing, were heated to 383 K in a stream of dry nitrogen and dried to constant weight. The specimens were pelletized before sealing. Pellet masses, accurate to 0.05 μg , varied from 5.33-21.53 mg. The temperatures are accurate to 0.1 K.

Heat capacity measurements were made with a scanning calorimeter at 5 K/min from 300-520 K. Calorimetry Conference sapphire was used as a standard (7). The running order for the measurements was empty, standard, coal 1, coal 1 repeat, standard, etc. The specimen mass was determined before the initial scan; following each scan of coal, the specimen was cooled and reweighed. The measurements, in air, made early in our development of recommended procedures, involved slightly different running procedures.

Data analysis - heat capacity and enthalpy

A fitting program was applied to the heat capacity data using algorithms developed in these laboratories. For each pair of fitted data, e.g., argon and repeat argon, the area between the curves was determined by numerical integration. This area corresponds to the enthalpy difference between the initial and repeat runs.

Procedures - enthalpy of desorption

The specimens used for the enthalpy of desorption measurements were equilibrated with water in atmospheres of the desired humidity, weighed and transferred quickly to the calorimeter. The calorimeter temperature was set initially a few degrees above the melting point of water. An enthalpic measurement technique was used (8,9). This technique for scanning calorimetric measurements of heat capacities and enthalpies measures the total enthalpy in a step change in temperature. Division by the temperature change gives the heat capacity at the midpoint of the temperature step. The temperature was raised rapidly to the desired final temperature and held constant for an hour; data were taken until the trace returned to the baseline. The repeat scan followed the initial scan immediately, without intermediate weighing. The mass loss, determined by weighing after the repeat run, was used to calculate the enthalpy. We had observed in other studies that mass losses rarely occurred in scans subsequent to the initial scan.

Data analysis - enthalpy of desorption

In the determination of the enthalpy using this procedure, the repeat scan, (for the dry coal) was used as the baseline in the determination of the heat input required by the moist coal (initial scan). The subtraction of the dry coal scan from that for the moist coal yielded a heat input versus time plot, from which the enthalpy of desorption could be determined. The enthalpy was obtained by integrating heat input versus time and dividing by the mass loss of the specimen. Fig. 1 represents a typical plot for the endothermic desorption of water from moist coal at temperatures around 400 K. At higher temperatures (400-500 K), the

coal exhibits the exotherm illustrated in Fig. 2.

Results

Enthalpy differences

The results presented for the enthalpy differences are based on studies on PSOC-854 made over a period of three years and on an initial study of the premium coal. Fig. 3 is a composite of the fitted heat capacity data from each of these studies. The A specimens were prepared and sealed in air; the B, C, and premium specimens were prepared and sealed in nitrogen. The exotherm is apparent in each of the PSOC-854 initial scans; it is not observed in the initial scan of the premium coal. The enthalpy difference between initial and repeat scans for each pair is given in Table 1.

A comparison of heat capacity data from specimens sealed in different atmospheres is given in Fig. 4. The heat capacity of the coal sealed in air is lower than the others. Values obtained in helium are highest. As the heat capacity of the specimens sealed in argon is similar to that for specimens sealed in carbon monoxide and nitrogen, the latter are omitted from Fig. 2. The enthalpy differences for the data obtained in various atmospheres are included in Table 1 also. As we were not aware of the exotherm in the initial studies (in air), the curves used for air were not obtained with the same running sequence as the other data: The scan used as the initial run was made approximately one year after the repeat run depicted. Thus the figure given in Table 1 for the enthalpy difference in air is influenced both by the varying oxidation levels of the specimens and by the effect of the different atmosphere. Because of the difficulty in comparing this with the other enthalpies, this figure is given in parentheses.

Heat of desorption

Representative data obtained using the methods described here for determining heats of desorption are presented in Table 2. The values are slightly higher than the isosteric heats of desorption reported by Allardice and Evans for Yallourn brown coals (10). The heat of vaporization of water as a real gas is 2.26 kJ/g at atmospheric pressure (11). The scatter in the data was less than 10 percent. A further study of repeated desorption and adsorption from the coal surface, not discussed in detail here, showed comparable precision. We have also applied the method described here to water-calcium sulfate and water-molecular sieve systems successfully.

References

1. MacDonald, R.A., Callanan, J.E., and Sullivan, S.A., *High Temperatures-High Pressures*, 17, 387 (1985).
2. Callanan, J.E., Sullivan, S.A., and MacDonald, R.A., *Int. J. Thermophys.*, 8, 133 (1987).
3. Merrick, D., *Fuel*, 62, 5534 (1983).
4. Callanan, J.E. and Sullivan, S.A., to be published.
5. Vorres, K., *Fuel Div. ACS Preprints*, 30 (4), 193 (1985).
6. Filla, B.J. and Callanan, J.E., *Rev. Sci. Instrum.*, 56, 592 (1985).

7. Ditmars, D.A., Ishihara, S., Chang, S.S., Bernstein, G., and Bernstein, G., and West, E.D., *J. Res. Nat. Bur. Stand. (U.S.)*, **87**, 159 (1982).
8. Mraw, S.C. in *Specific Heat of Solids (CINDAS, Purdue Univ., Lafayette, IN)*, to be published.
9. Callanan, J.E. and Sullivan, S.A., *Rev. Sci. Instrum.*, **57**, 2584 (1986)
10. Allardice, D.J. and Evans, D.G., *Fuel*, **50**, 236 (1971)
11. JANAF Thermochemical Tables: 3-31-1979.

TABLE 1 : $\Delta HI - \Delta HR$ VALUES FOR SEVERAL COALS

YEAR OF STUDY	SPECIMEN FIGURE REF.	ATMOSPHERE	$\Delta HI - \Delta HR$ (J/g K)
1983	A	AIR	(60)
1984	B	N ₂	18
1985	C	N ₂	34
1986	PREM	N ₂	6
1985	ARGON	AR	37
1985	HELIUM	HE	29

TABLE 2 : DSC COAL-MOISTURE DESORPTION DATA

RUN #	TEMP. RANGE (K)	SAMP.MASS (mg.)	% WT. LOSS	ENTHALPY (kJ/g)
CLW04	273-400	11.519	6.41	3.22
CLW05	273-400	10.952	6.15	3.32
CLW06	273-370	11.207	6.82	3.14
CLW07	273-370	14.304	6.01	2.79
CLW08	273-430	14.393	6.91	4.91
CLW09	273-430	11.508	6.21	4.30

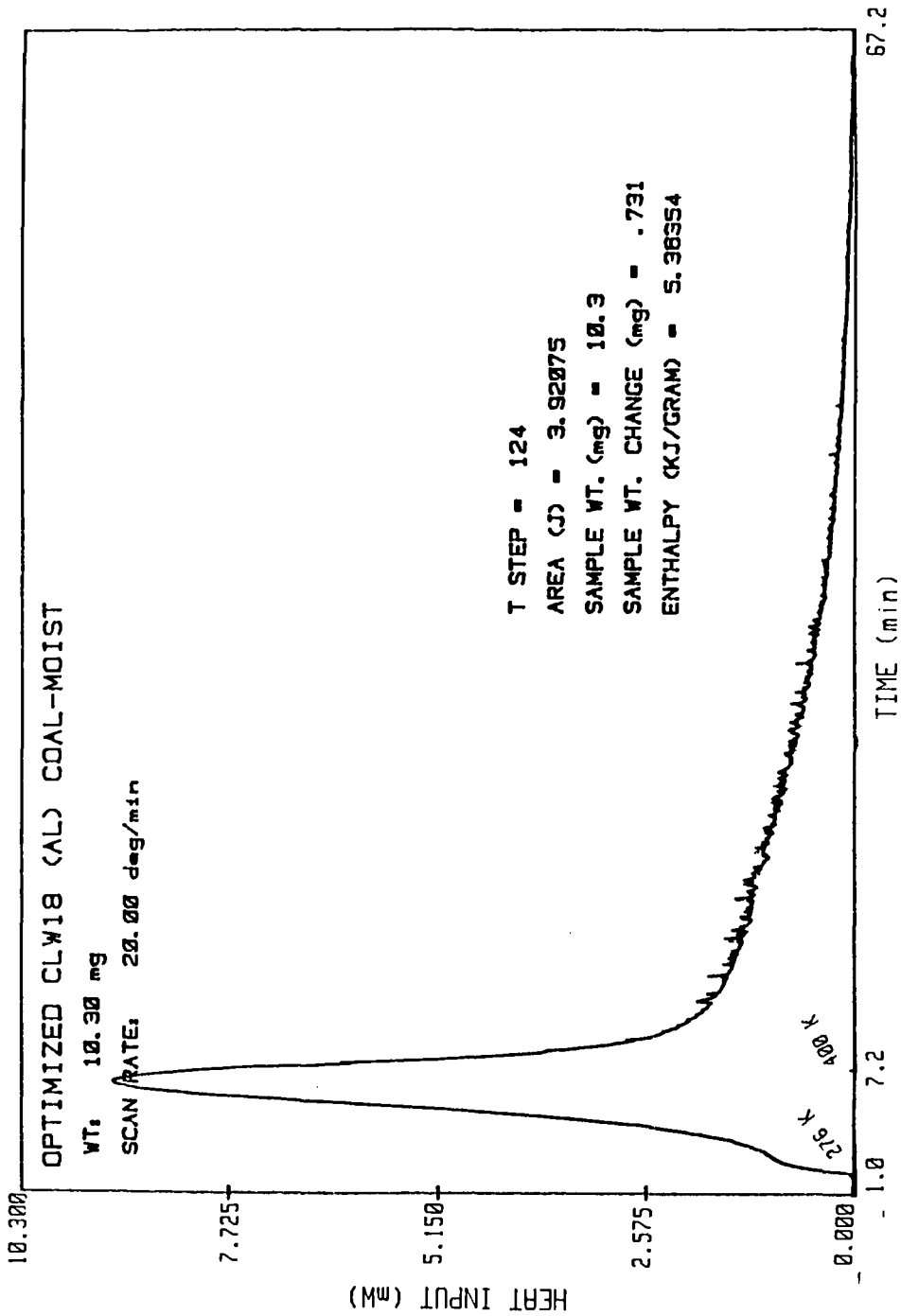
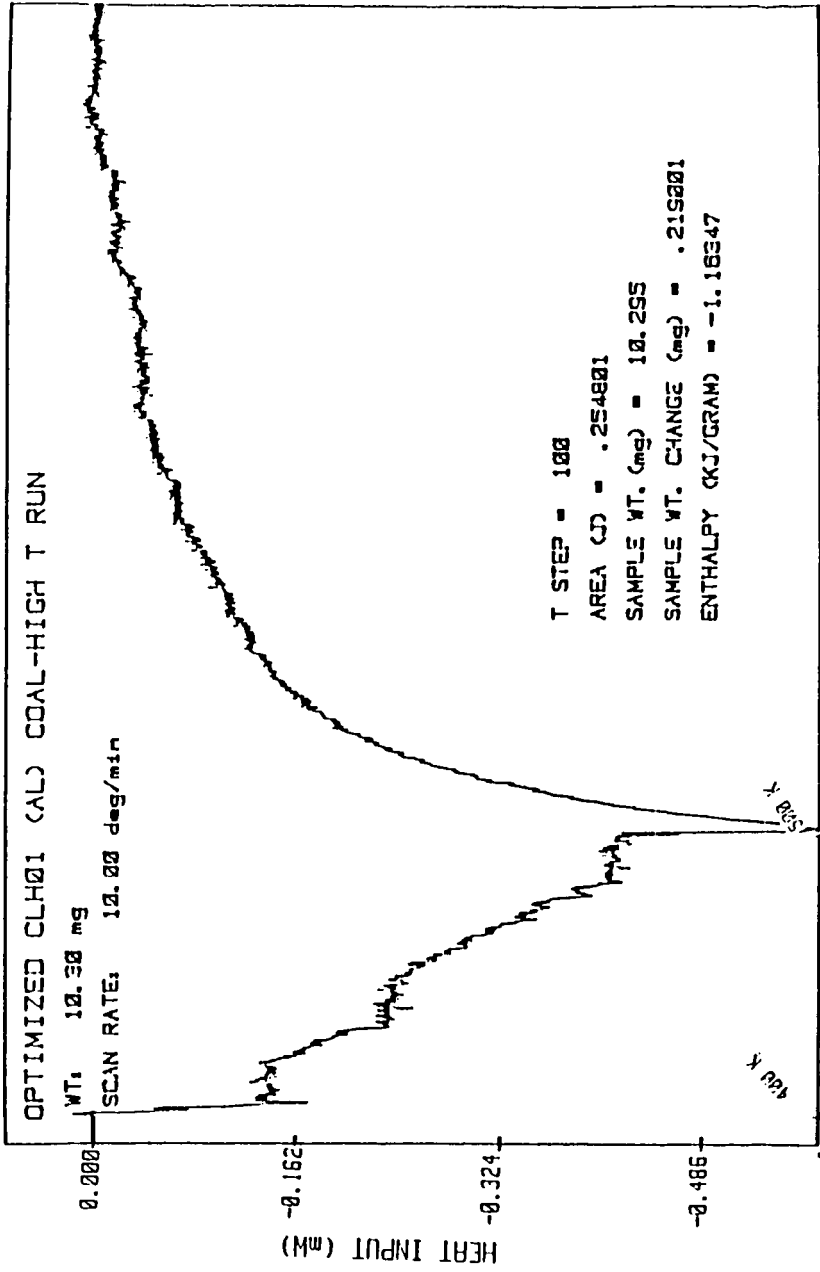


Fig. 1. Moisture desorption plot of PSOC-854 coal equilibrated in 70% relative humidity air at 295 K.



TIME (min)

1.0 11.0 41.0

Fig. 2. Moisture desorption exotherm of PSOC-854 coal after drying to constant weight at 400 K.

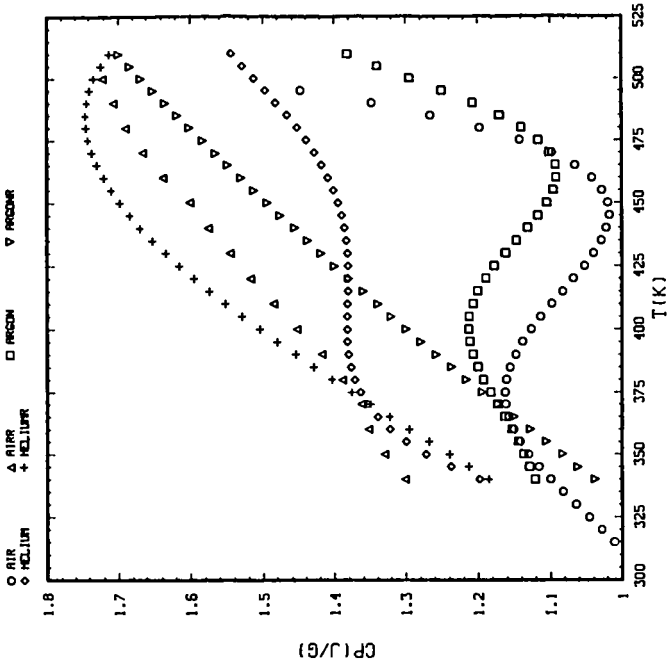


Fig. 4. Heat capacities of PSOC-854 in various atmospheres. The R after the designation of the gas denotes a repeat run.

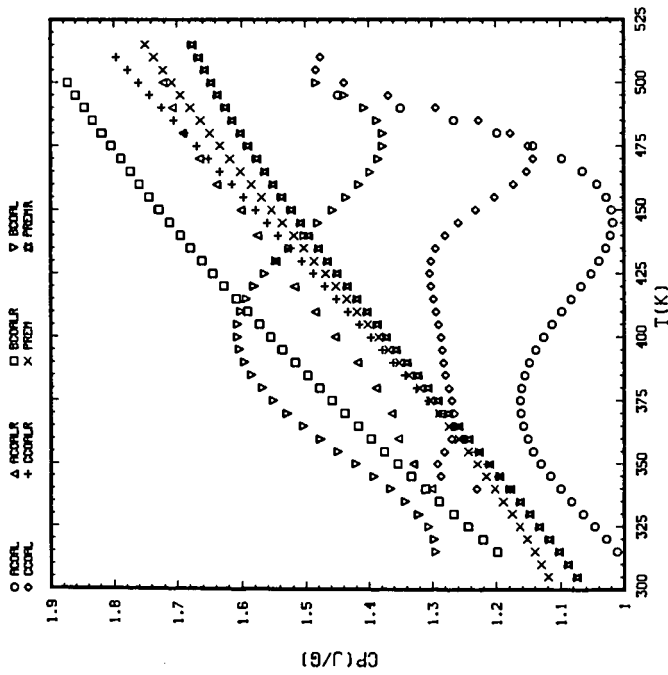


Fig. 3. Heat capacities of coals as a function of increased oxidation. PSOC-854: ACOAL, 1983; BCOAL, 1984; CCOAL, 1985. Prem, premium coal. The R after the designation of the gas in the legend denotes a repeat run.

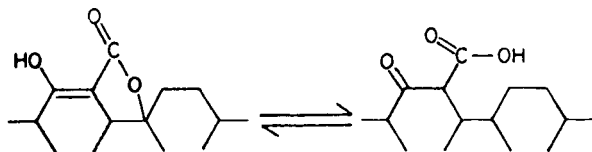
The Effect of Carbon Surface Oxides on the Enthalpy of Immersion in Water and the Adsorption of Water Vapour

Stuart S. Barton

Department of Chemistry and Chemical Engineering
Royal Military College of Canada
Kingston, Ontario, K7K 5L0

It has been known for a long time that carbon surfaces which have been exposed to even mild oxidation, become covered to a greater or lesser extent by chemically bonded oxide groups. Depending on the temperature at which the oxidation is carried out, the carbon surface can exhibit either acidic or basic characteristics. It is likely that the surface basicity developed on high temperature oxidation is related to unsaturated "centres" produced by the thermal removal of oxides. These oxide structures are thermally unstable and may be detected by the method exemplified by Fig. 1. In this figure the differential amount of CO₂ and CO desorbed per gram of Spheron 6 are shown as a function of temperature. The oxide structures which produce CO₂ are less stable than the structures which produce CO. Similar results have been obtained for other carbons.

Those oxides which are acidic can neutralize aqueous or ethanolic bases. In Fig. 2 is shown the decrease in the surface acidity of Spheron 6 with increasing thermal destruction of the surface oxides. It is apparent that acidic groups of different strengths are present. However, after treatment at 800°C it appears that all acidic surface oxide has been removed. The temperature interval over which the drop in acidity occurs is the same interval over which CO₂ is desorbed. When the CO evolution has reached a maximum, however, the acidity has almost disappeared. The CO producing oxide structures contribute very little to the surface acidity. The relationship between the basic uptake and the amount of CO₂ desorbed is shown in Fig. 3. The sodium ethoxide data fall on two intersecting straight lines. The initial line corresponds to the decomposition of the CO₂ producing oxide which is essentially complete at 600°C. This line has a slope of two indicating that the surface oxide being destroyed is dibasic. The second linear portion has a slope of one demonstrating that the less thermally stable oxide which decomposes around 250°C is monobasic. The acidic complex decomposing at 250° is not neutralized by aqueous OH⁻ ion whereas the 600°C desorbing species is neutralized by this base on a one to one ratio. Data of this type have been rationalized that the acid oxide group is a lactone or some similar functional group which is monobasic towards aqueous OH⁻ ion but can be opened into a dibasic structure by the stronger ethoxide ion. Such a structure was proposed by Garren and Weiss in 1957 i.e.



Treatment with specific chemical reagents can also provide information about the oxide structure. Diazomethane reacts quickly and smoothly with protonated sites which are carboxylate in nature to produce methyl esters. If the protonated site is phenolic then ether linkages will be formed. Since methyl esters are easily

hydrolysed while methyl ethers are resistant to hydrolysis, it is possible to discriminate between the two proton types. Fig. 4 shows data obtained with Spheron 6. It is seen that the methoxyl content can be decreased by hydrolysis and that at least two groups are being methylated. Treatment with diazomethane for up to twenty hours produces a constant methoxyl content. After this time methylation increases slowly and becomes constant again at about 120 hours. These results are consistent with the Garten and Weiss model which implies the existence of a tautomerization step which may be very slow and rate determining.

Carbon surfaces may also be probed for protonated species by treatment with ethereal Grignard reagent (methylmagnesium iodide). The gaseous hydrogen released can be measured.

All the chemical techniques outlined above were used to produce the data of Fig. 5. There is, initially, at low desorbing temperatures a considerable difference between the two methoxyl determinations (i.e. after 20 hours and 140 hours methylation) but this difference becomes smaller as degassing temperature is increased. The oxide structure which is decomposed around 250°C is apparently not methylated by diazomethane since no change in methoxyl content takes place over the range 200°-400°C. Also included in Fig. 5 are the variations of "active" hydrogen content measured by reaction with methylmagnesium iodide and the uptake of aqueous OH⁻ ion. The Grignard data fall on top of the 20 hr. reaction time results while the OH⁻ ion uptake data fall on top of the 140 hr. results. One must conclude that the slow step which retards the methylation reaction is absent during reaction with aqueous base.

A certain amount of information about the IR spectra of carbon surface oxides is also available. It has been shown in a study that a series of activated carbons, oxidized to different extents, gave IR spectra which were qualitatively similar (3 distinct bands in the 1800-1100 cm⁻¹ region). Peak areas could be quantitatively related to the amount of oxidation and, in particular, heat treatment at 1000°C produced a marked (although not complete) elimination of the spectral features.

These chemical studies and others like them, result in the conclusion that the acid surface oxides have a complex structure probably including carboxyl, phenolic and lactonic features. Surface oxides which desorb as CO are also present but do not contribute to the surface acidity.

Acidic or not, all these possible structures can contribute via hydrogen bonding and other hydration interactions to the energetics of the reaction of a carbon surface with liquid and vapour water. The measurement of the enthalpy of immersion is a convenient method for the investigation of the state of a carbon surface. Either commercial calorimeters or a "home-made" instrument may be used. Fig. 6 gives a schematic diagram of a simple, easily constructed but effective calorimeter based on an original design by Zettlemoyer. The temperature sensing thermistor is part of a Wheatstone bridge. The imbalance of the bridge as a function of the heat supplied by a calibration heater gives a measure of the heat capacity of the calorimeter and its contents. Samples of carbon are outgassed carefully in thin-walled glass bulbs which are sealed under vacuum. Three or more carbon samples are immersed in water (by breaking the submerged bulb) and the slope of the heat evolved vs mass of carbon gives the enthalpy of immersion ($h_i/J-g^{-1}$). This procedure automatically corrects for the "heat of breaking" i.e. the intercept on the heat axis. Typical data are shown in Fig. 7.

The change in h_i in water with outgassing temperature for graphite and Spheron 6 and given in Figs. 8,9. For both these substances h_i decreases with increasing temperature, after an initial slight increase due presumably to the removal of adsorbed water at the lower temperatures. On the other hand, h_i for

graphite in the organic liquid, benzene, stays reasonably constant as degassing temperature is increased (Fig. 10). It should be mentioned that the BET, N_2 areas of both of these adsorbents do not change appreciably with heating. Thus the h_i values obtained refers to a constant surface area. The relationship between h_i in water and the total amount of CO_2 and CO desorbed per gram (expressed as mmoles of oxygen) is shown for Spheron 6 and graphite in Figs. 11,12. The linear decrease indicates either that the energy of interaction between the two types of surface oxide (CO_2 producing and CO producing) are of the same magnitude or the CO producing site has a far stronger interaction. Probably it is the latter case which obtains.

Both graphite and Spheron 6 are not highly porous. Activated carbons, on the other hand are extremely porous. Fig. 13 shows the variation of h_i in water with outgassing temperature for the microporous carbon obtained by the vacuum pyrolysis of the polymer, polyvinylidene chloride (PVDC carbon). The surface oxide on this carbon had formed, after carbonization of the polymer, by storage in air for about six months. Fig. 14 gives the variation in h_i with total amount of oxygen thermally desorbed as CO_2 and CO. For PVDC carbon the relationship is not linear and a very large drop in h_i value takes place when the initial amounts of oxide are removed. It is obvious that unlike the case with the non-porous carbons, there is a source of interaction with water other than the surface oxides. This source must involve the pore structure. It is interesting to compare the rates of decrease of h_i with surface oxide removal, given in Table I. The second column of this table is simply the slope of the linear portions of the h_i vs oxygen removed curves of Figs. 11 and 12. For PVDC carbon linearity is not strictly followed and then only after most of the oxide has been removed.

TABLE I

	Slope $J\text{-mol}^{-1}$	h_i $J\text{-g}^{-1}$	Oxide mmol-g^{-1}	h_o $J\text{-g}^{-1}$	h_o $J\text{-g}^{-1}$	BET $\text{m}^2\text{-g}^{-1}$
Graphite	-10	13.0	0.569	5.7	7.3	160
Spheron 6	-9.2	11.6	0.703	6.5	5.1	120
PVDC carbon	----	50.2	1.45	21.7	28.5	---

For graphite and Spheron 6, where linearity is found, the slope gives the water-oxide interaction energy per mole of oxide site. For graphite and Spheron 6, the product of the slope and the oxygen desorbed at 1000°C gives the contribution to the overall h_i from oxide water interactions (h_o). These quantities when subtracted from the initial h_i values give the contribution from the "bare" carbon surface (h_c). Naturally, these latter are very close to the h_i of the 1000°C degassed samples and are proportional to the BET surface areas of the non-porous carbons. This simple analysis cannot be applied to the porous carbon where there appears to be some synergetic effect involving pore and oxide sites which contributes disproportionately to h_i . This behaviour may be explored by a different method in which h_i is measured for a series of PVDC carbon samples pre-covered with known amounts of water. The results of such a study are shown in Fig. 15. The slope of the curve is the net molar enthalpy of adsorption ($\overline{\Delta H}$). The data indicate that there are two distinct $\overline{\Delta H}$ values. Up to about 0.6 mmol-g^{-1} adsorption $\overline{\Delta H}$ is 24 kJ-mol^{-1} . Further adsorption proceeds with $\overline{\Delta H} = 1.7 \text{ kJ-mol}^{-1}$. At the point of the change from the high $\overline{\Delta H}$ to the low $\overline{\Delta H}$, the h_i value is 28.5 J-g^{-1} . This figure is very close to the h_i obtained with PVDC carbon degassed at 1000°C . This value then, represents the contribution from pore

filling and when it is subtracted from the initial h_i produces the contribution for water-oxide interactions (21.7 J-g^{-1}). A value for the energy of interaction of water per mole of oxide site for PVDC carbon may now be computed as $21.7/1.45 = 15 \text{ J-mole}^{-1}$. This larger value must reflect the synergetic effect referred to earlier.

The preceding analysis purports to show that it is possible to obtain from appropriate experiments the contribution to the overall interaction from oxide sites, bare open carbon surface and pore filling. Obviously much more work must be done before the validity of such an analysis can be established.

The dramatic changes in water vapour adsorption which can result from the presence of surface oxides is illustrated in Fig. 16. The figure shows the isotherms obtained after evacuation at 40°C of carbon cloth which had been progressively oxidized in 6M HNO_3 . The "as received" material produces a typical sigmoid (Type V) isotherm. The oxidized samples, on the other hand, show Type I or Langmuir behaviour. Values of h_i and $\Delta\bar{H}$ also increase greatly on oxidation. After evacuation at 400°C , when much of the oxide has been destroyed, the water vapour isotherms are all Type V.

If time permits application of immersional enthalpy measurement to complex solids such as coal will be examined.

BIBLIOGRAPHY

This discussion is based on the following articles:

- S.S. Barton and B.H. Harrison, CARBON 10, 245 (1972).
- S.S. Barton, B.H. Harrison and G.L. Boulton, CARBON 10, 395 (1972).
- S.S. Barton, B.H. Harrison and D. Gillespie, NATURE 235, 134 (1971).
- S.S. Barton and B.H. Harrison, CARBON 13, 47 (1975).
- S.S. Barton, B.H. Harrison and D. Gillespie, CARBON 16, 363 (1978).
- S.S. Barton, M.J.B. Evans and B.H. Harrison, J. COLL. INTERFACE SCI. 45, 542 (1973).
- S.S. Barton and J.E. Koresh, J. CHEM. SOC. FAR. TRANS. I 79, 1173 (1983).
- S.S. Barton, J.R. Dacey and M.J.B. Evans, COLL&POLYMER SCI. 260, 726 (1982).

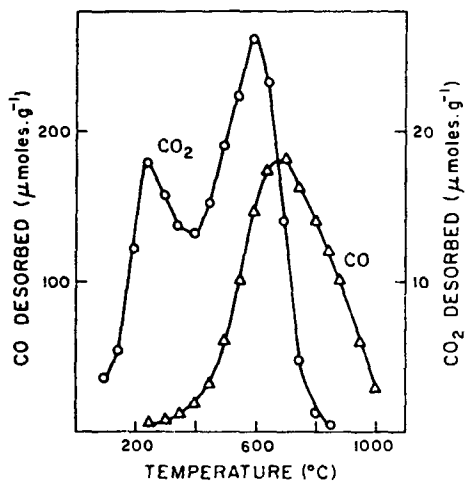


Fig. 1 Differential gas evolution curve.

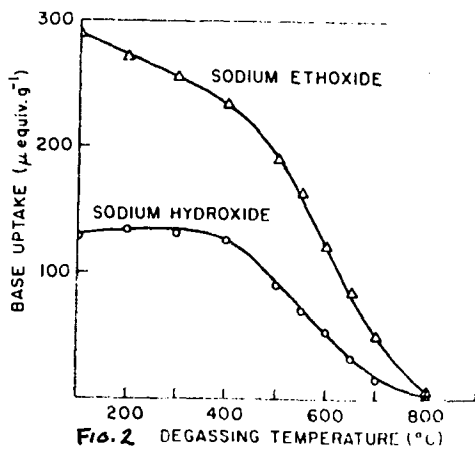


Fig. 2

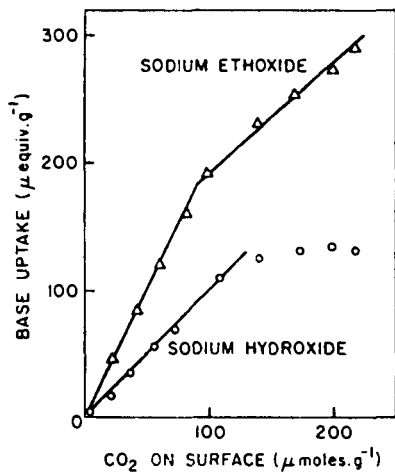


Fig. 4 Relation between base uptake and the oxides desorbing as CO_2 .

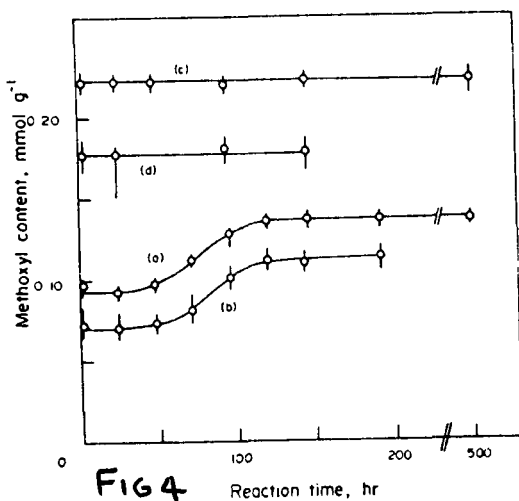


FIG 4

Reaction time, hr

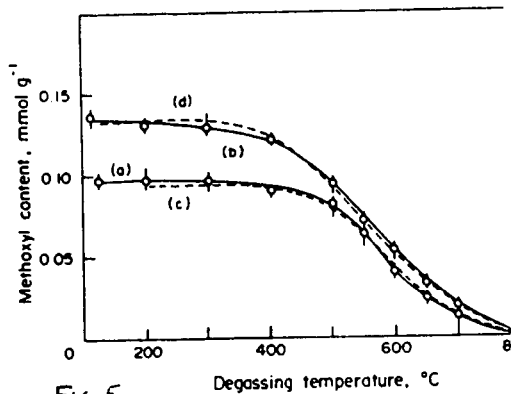


FIG. 5

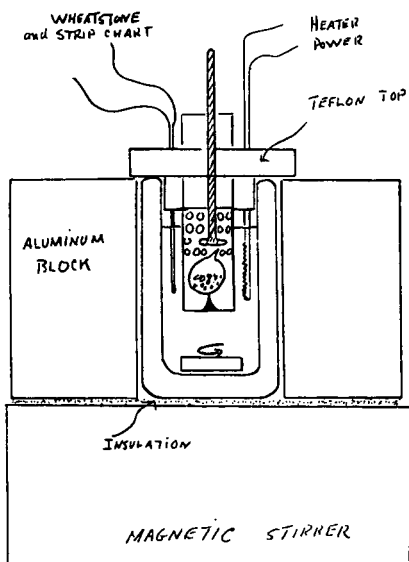


FIG 6

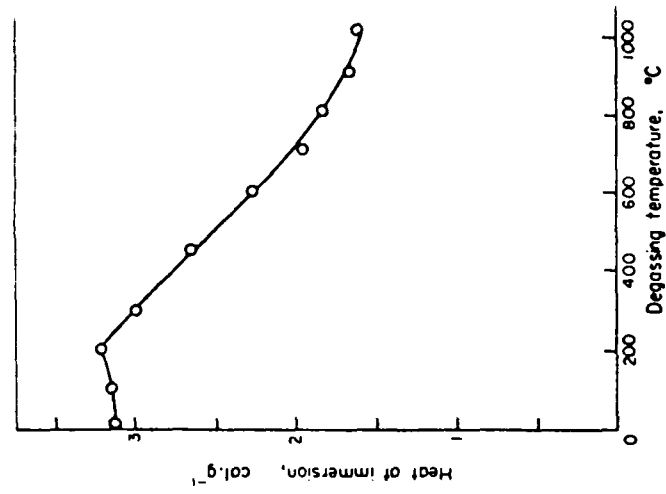


Fig. 8 Heat of immersion of graphite, degas temperatures up to 1000°C, in water.

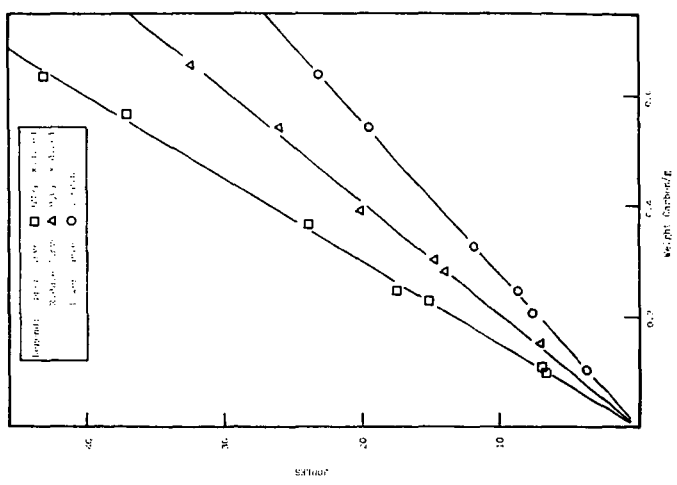


Fig. 7 Heat of immersion in water

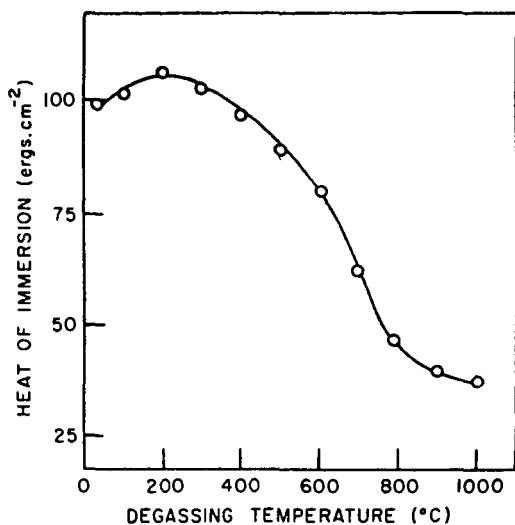


Fig. 9 Heat of immersion of Spheron 6, degassed at various temperatures, in water.

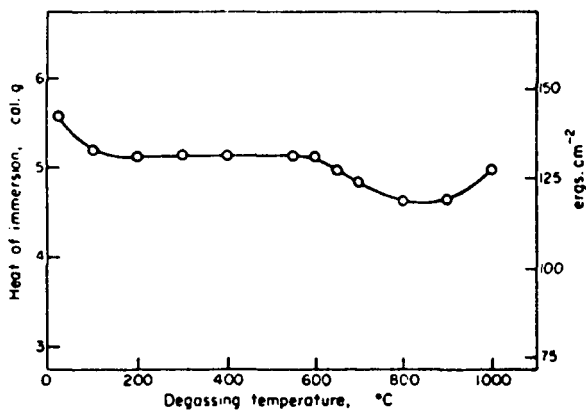


Fig. 10 Heat of immersion of graphite, degassed at temperatures up to 1000°C, in benzene.

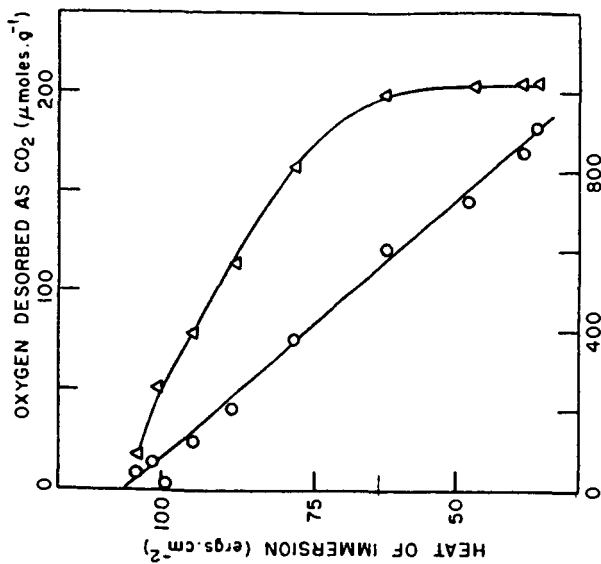


Fig. 11 Heat of immersion of Spheron 6 in water in relation to the amount of oxygen desorbed as CO₂ Δ, and to the total oxygen desorbed as CO and CO₂ ○.

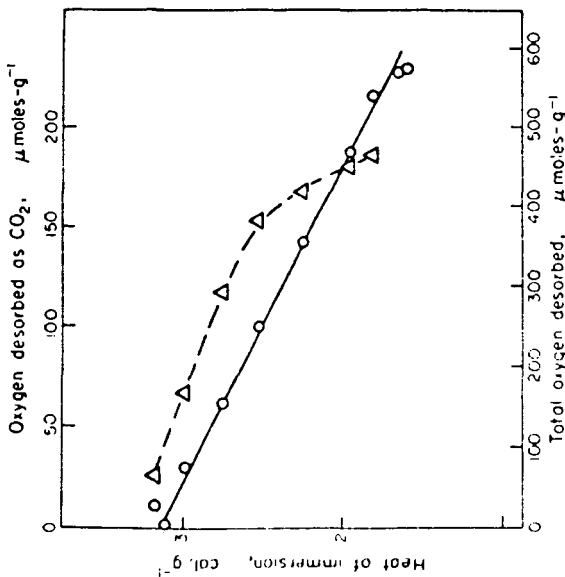


Fig. 12 Heat of immersion of graphite in water in relation to the amount of oxygen desorbed as CO₂ Δ, and to the total oxygen desorbed as CO and CO₂ ○.

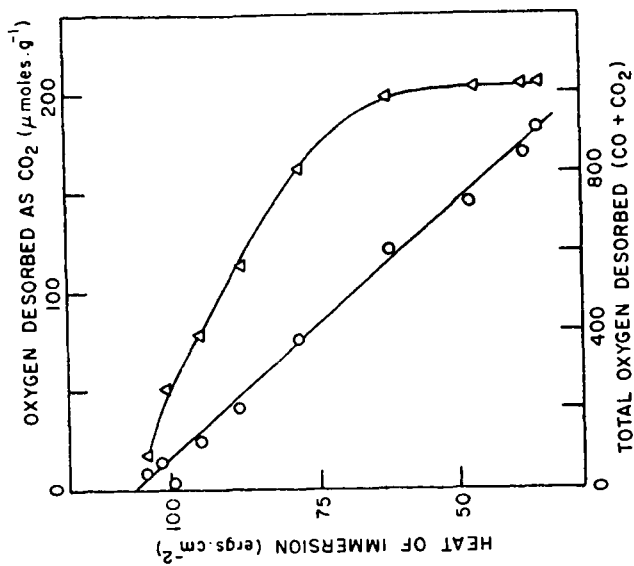


Fig. 13 Heat of immersion of Spheron 6 in water in relation to the amount of oxygen desorbed as CO₂, Δ, and to the total oxygen desorbed as CO and CO₂, O.

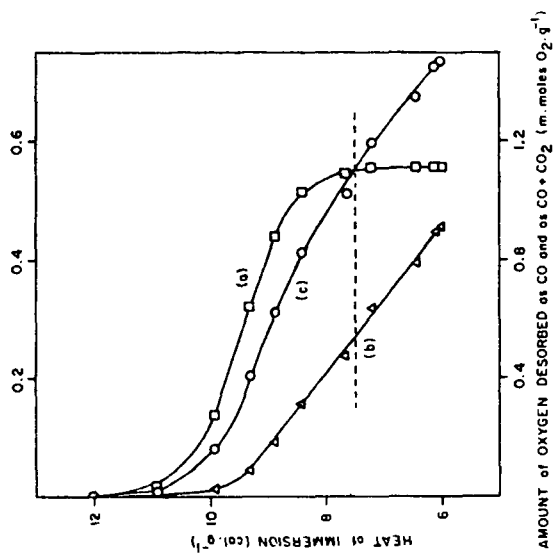


Fig. 14 Heat of immersion of PVDC carbon plotted as a function of (a) oxygen desorbed as CO₂, (b) oxygen desorbed as CO, (c) total oxygen (CO + CO₂).

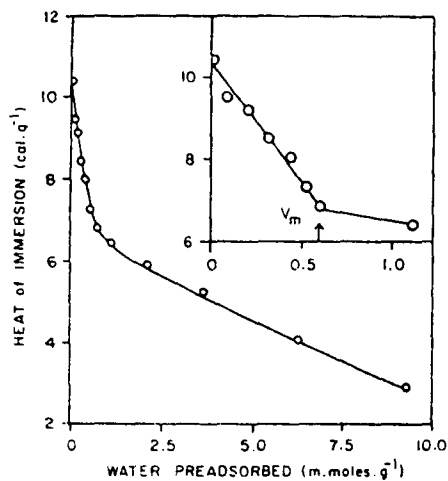


FIG. 15 Effect of preadsorbing water on the heat of immersion in water.

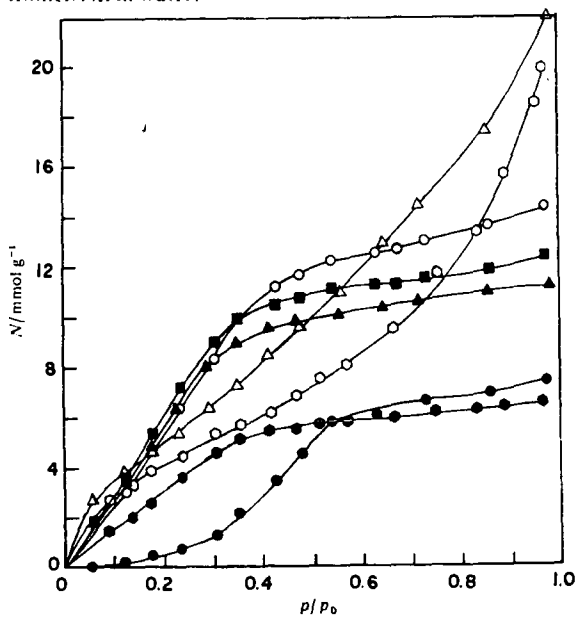


FIG. 16—Absolute water isotherms at 25 °C on the following air-activated carbons: ●, as received; ●, Ox-HNO₃-2; ▲, Ox-HNO₃-3; ■, Ox-HNO₃-4; ○, Ox-HNO₃-6; △, Ox-HNO₃-12; ○, Ox-HNO₃-16.

HEATS OF IMMERSION OF BITUMINOUS COALS IN LIQUIDS

J. P. Wightman, J. O. Glanville, J. B. Hollenhead, K. M. Phillips and K. N. Tisa

Chemistry Department, Virginia Tech, Blacksburg, VA 24061

INTRODUCTION

The interaction of liquids with solid surfaces may be studied by a variety of experimental methods including both thermodynamic and spectroscopic ones. Immersional calorimetry as a thermodynamic tool has proven particularly useful in probing this interaction. A dated but nonetheless excellent review of immersional calorimetry has been given by Zettlemyer (1). Although coal has a complex pore structure (2), a number of researchers have reported the heats of immersion of a variety of coals in a number of different liquids [3-13]. Indeed, Callanan has summarized [14] the case for additional studies of heats of immersion in a report describing measurement needs for coal. The objective of the present work was to assess the effects of wetting liquid chain length and coal surface oxidation on the heat of immersion of bituminous coals in both n-alkanes and n-alcohols and in water.

EXPERIMENTAL

Two bituminous coals were used in this study, Virginia-C and Pocahontas No. 3 obtained respectively from Buchanan County, Virginia and McDowell County, West Virginia. The coals were crushed and sieved to -325 mesh (<44 microns). The ash content of Virginia-C and Pocahontas No. 3 coals was 5.22 and 5.0%, respectively; the moisture content was 0.15 and 1.04%, resp. The ultimate analysis of the two coals is listed in Table I. The surface area of the Virginia-C and the Pocahontas No. 3 coal was 1.9 and 2.0 m²/g, respectively, as determined by low temperature gas adsorption. Some Pocahontas No. 3 coal was extracted with methanol in a Soxhlet apparatus for 24 hours.

Table I. Ultimate Analysis of Coals

Element	Weight Percent (MF basis)	
	Virginia-C	Pocahontas No. 3
Carbon	87.0	84.8
Oxygen (by difference)	6.9	8.9
Hydrogen	4.25	4.6
Nitrogen	0.97	0.97
Sulfur	0.64	0.61
Chlorine	0.20	0.08

Heats of immersion were determined in a Setaram Calvet MS 70 microcalorimeter using a previously reported procedure [11]. A known weight of coal (20-50 mg) outgassed at <10⁻⁴ torr for 2 hours at room temperature in a custom pyrex bulb was immersed in 5 ml of the wetting liquid. The precision of a typical heat of immersion was about 10%. A heat of empty bulb breaking correction was determined and applied.

Oxidation of the coal samples was achieved by heating the coal for varying time periods (10 - 1440 minutes) in a thermostatted forced air oven over a range of temperatures (110 - 320°C).

The XPS (α -ray photoelectron spectroscopy) spectra of the powdered coal samples were obtained using either a Kratos XSAM-800 electron spectrometer or a Perkin Elmer PHI 5300 electron spectrometer. Both spectrometers use a magnesium x-ray source (1254 eV) and a hemispherical analyzer. Coal powder was mounted on the sample probe with doublestick tape. The atomic fraction of each element was determined from the corrected area of the elemental photopeak.

RESULTS AND DISCUSSION

The heats of immersion of Virginia-C coal determined in a series of n-alcohols are listed in Table II. A decrease in the heat of immersion is noted as the carbon number of the alcohol increases. This decrease in the heat of immersion for coal is in contrast to the increase in the heat of immersion observed for graphitized carbon black [15]. This marked difference in behavior is due to differences in the structure of coal and carbon black. Larsen, et al. [16] have suggested that coal be treated as a cross-linked macromolecule. The swelling of coal by methanol is well known and this swelling phenomenon is typical of cross-linked polymers. Thus, the decreasing heat of immersion for coal undoubtedly reflects the inability of the larger alcohols to penetrate coal. Microcalorimetric measurements afford yet another measure of this diminished penetration by wetting liquids of increasing bulkiness. The time required for complete liberation of the heat of immersion can be followed conveniently in the microcalorimeter and is termed the immersion time. This time of immersion is short for methanol and n-dodecanol but is a maximum for n-butanol. The heats and times of immersion are consistent with a rapid and complete penetration of coal by methanol and a still rapid, but complete exclusion, of n-dodecanol by coal. Immersion in n-butanol gives intermediate heat and time results. The effect of outgassing temperature on heat of immersion is only modest. For example, the heat of immersion in methanol of Virginia-C coal outgassed at room temperature and at 120°C was 24 and 28 J/g, respectively.

Table II. Heats of Immersion of Coals in n-Alcohols and n-Alkanes

Liquid	Carbon No.	Heat of Immersion (J/g)	
		Virginia-C	Pocahontas No. 3
Methanol	1	24.	
n-Propanol	3	19.	
n-Butanol	4	15.	
n-Hexanol	6	4.6	
n-Dodecanol	12	4.6	
n-Octane	8		6.9
n-Nonane	9		5.5
n-Decane	10		5.1
n-Undecane	11		4.3
n-Dodecane	12		5.3
N-Tridecane	13		4.1
N-Tetradecane	14		3.7
N-Pentadecane	15		3.7
N-Hexadecane	16		3.7
n-Heptadecane	17		3.7
n-Octadecane	18		3.7
n-Nonadecane	19		3.2

The heats of immersion in water of Virginia-C coal heated for 24 hours at different temperatures are shown in Table III. There is nearly a fifty-fold increase in the heat of immersion for coal heated at 320°C compared to unheated coal. The change in the heat of immersion is modest until the coal is heated above 150°C. The surface composition of unheated coal and of coal heated to different temperatures can be determined by XPS analysis. The oxygen/carbon atomic ratios calculated from the XPS spectra of the unheated and heated coals are listed in Table III. The O/C ratio increases as the temperature to which the coal is heated increases. Indeed, the heat of immersion and XPS results are complementary, and the agreement reflects increasing numbers of surface polar (oxygen-containing) groups.

Table III. Heats of Immersion in Water and XPS Results for the Oxidation of Virginia-C Coal

<u>Oxidation Temperature (°C)</u>	<u>Heat of Immersion (J/g)</u>	<u>Surface [O/C] Ratio</u>
	2.5	0.053
110	3.0	0.065
150	4.5	0.087
175	9.0	0.11
210	23.5	0.16
225	34.0	0.18
250	59.0	0.22
300	75.0	0.27
320	99.0	0.28

The heats of immersion of Pocahontas No. 3 coal determined for a series of n-alkanes are listed in Table II. An initial decrease in the heat of immersion is noted as the carbon number of the alkane increases. Again, the exclusion of the longer alkane molecules by coal is demonstrated. The heats of immersion in water of Pocahontas No. 3 coal heated at 320°C for different times are shown in Table IV. An initial rapid increase in the heat of immersion with oxidation time is followed by a slower increase in the heat of immersion. For example, there is about a ten-fold increase in the heat of immersion for coal heated for only 2.5 hours compared to a two-fold increase over the next 20 hours. The oxygen/carbon ratios calculated from XPS spectra of the heated coals are listed in Table IV. The O/C ratio increases as the time of heating of the coal increases. Again, the heat of immersion and XPS results are quite complementary. Prior extraction of Pocahontas No. 3 coal by methanol has no significant effect on either the heat of immersion or the oxygen/carbon ratio.

SUMMARY

Differences in the heats of immersion of bituminous coals in a homologous series of n-alcohols and n-alkanes relate directly to the ability of these liquids to penetrate the coals. Heats of immersion of oxidized coals in water can be used to follow the extent of oxidation. Changes in the surface oxygen composition of oxidized coals determined by XPS parallel changes in the heats of immersion in water.

Table IV. Heats of Immersion in Water and XPS Results on the Oxidation of Pocahontas No. 3 Coal

Oxidation Time (min)	Heat of Immersion (J/g)	Surface [O/C] Ratio
0.0	3.6 *	0.071 *
0.0	3.8	0.086 *
10	28.	0.30
20	30.	0.33
30	41.	0.33
60	45.5	0.38
120	51.	0.38
180	52.	
300	69.	
360	75. *	0.46 *
600	75.5	
720	80. *	0.37 *
1080	84. •	0.43 *
1080	83.	
1440	88.	0.46
1440		0.43 *

• - value for methanol extracted coal

ACKNOWLEDGEMENTS

The authors thank Mr. T. F. Cromer and Mr. S. McCartney with help in the XPS analysis and Mr. A. Mollick for making the calorimetric bulbs. The authors acknowledge the financial support of the Mining and Mineral Resources and Research Institute and the Virginia Center for Coal and Energy Research.

REFERENCES

1. A. C. Zettlemoyer, in Chemistry and Physics of Interfaces, (S. Ross, ed.) American Chemical Soc., Washington, D.C., 1965, p 189.
2. O. P. Mahajan and P. L. Walker, Jr., in Analytical Methods for Coal and Coal Products, (C. Karr ed.) Vol. 1, Academic Press, New York, 1978 pp 125-162.
3. F. A. P. Maggs, Nature, **169**: 793 (1952).
4. D. W. van Krevelen, Coal, Elsevier, Amsterdam, 1961.
5. T. G. Gallcott, Fuel, **43**: 203 (1964).
6. H. Marsh, Fuel, **44**: 253, (1965).
7. J. W. Larsen and E. W. Kummerle, Fuel, **57**: 59 (1978).
8. S. M. Senkan and E. L. Fuller, Jr., Fuel, **58**: 729 (1979).
9. E. L. Fuller, Jr., J. Colloid Interf. Sci., **75**: 577 (1980).
10. J. O. Glanville and J. P. Wightman, Fuel, **59**: 557 (1980).
11. E. Widyan and J. P. Wightman, Colloids and Surfaces, **4**: 209 (1982).
12. J. O. Glanville, K. L. Newcomb and J. P. Wightman, Fuel, **65**: 485(1986).
13. J. O. Glanville, S. T. Hall, D. L. Messick, K. L. Newcomb, K. M. Phillips, F. Webster and J. P. Wightman, Fuel, **65**: 647(1986).
14. J. E. Callanan, NBSIR, Report 82-1666, Natl. Bureau of Standards, Boulder, CO (1982).
15. J. H. Clint, J. S. Clunie, J. F. Goodman, and J. R. Tate, Nature, **223**: 51 (1969).
16. J. W. Larsen, T. K. Green and I. Chiri, in Proc. International Conference on Coal Science, Pittsburgh, PA., 1983, pp 277-279.

CHARACTERIZATION OF COAL INTERFACIAL BEHAVIOR THROUGH FLOW MICROCALORIMETRY

D. W. Fuerstenau, G. C. Yang and S. Chander

Department of Materials Science and Mineral Engineering
University of California
Berkeley, CA 94720

ABSTRACT

To assess factors that affect the surface behavior of coals, flow microcalorimetry studies were carried out to measure the heat evolved when methanol is displaced by water. This heat appears to be a function of coal rank and coal oxidation. In general, oxidized coals evolve less heat, which is ascribed to the increase of polar sites and the preferential adsorption of methanol over water on the coal. However, coals having a high moisture content behave oppositely in that during the initial stages of oxidation the coal becomes more hydrophobic. These factors are delineated through flow calorimetry, functional group analysis, and wettability studies.

INTRODUCTION

Interfacial properties of coal are important in a number of coal processing and utilization technologies. Although several experimental methods such as electrokinetic potentials, adsorption, contact angle, etc., are available to assess interfacial behavior, each method measures a somewhat different aspect of interfacial behavior. In this investigation, flow microcalorimetry studies were carried out to study the nature of surface groups on the surface of coal. The flow calorimetry results have been compared with functional group analysis and wettability measurements.

Coal surfaces are postulated to consist of several oxygen containing functional groups, which include $-COOH$, $=CO$, $-OCH_3$ and $-OH$ (both alcoholic and phenolic) (1). Since these functional groups are expected to interact with water molecules, flow microcalorimetry has been used to measure the heat evolved when methanol, used as a carrier fluid, is displaced by water. Functional groups in coal samples were also determined by chemical analysis methods (2) and infrared spectroscopy (3).

Characterization of coal wettability by classical contact angle measurements requires careful sample selection to avoid cracks and other physical imperfections and a proper polishing procedure to avoid contamination. Furthermore, the large heterogeneity of coal may result in significant variation of measured contact angles from sample to sample. Therefore, in order to assess the wettability of fine coal particles and how it is influenced by coal rank and the degree of surface oxidation, the immersion time measurement technique has been employed (4,5).

Coal Samples:

The chemical analysis and surface areas of the four coal samples used in this investigation are given in Table 1. Four widely different samples were

Table 1 - Characteristics of Coal Samples

PROPERTY	COAL			
	BMC-A	BMC-B	GMC-B	DJM-SB
<u>Proximate Analysis</u>				
Moisture	3.56	2.31	2.67	27.65
Ash	5.06	5.99	8.22	6.26
Volatile	2.84	17.98	38.96	34.02
Fixed Carbon	88.54	73.72	50.15	32.07
Calorific Value (Btu/lb)	13,270	14,290	13,030	8,230
<u>Ultimate Analysis</u> (%, as-received)				
Moisture	3.56	2.31	2.67	27.65
Carbon	87.16	82.07	73.16	48.17
Hydrogen	1.45	4.19	4.98	3.56
Nitrogen	0.82	1.52	1.50	0.60
Chlorine	0.80	0.07	0.02	0.00
Sulfur	0.51	0.73	0.86	0.54
Ash	5.06	5.99	8.22	6.26
Oxygen (by diff.)	1.36	3.12	8.59	13.22
<u>Surface Area, m²/g</u> (as-received)				
Nitrogen (B.E.T. analysis)		7.50	3.60	2.90
Carbon dioxide (D-P analysis)	274.42	130.00	132.00	219.00
BMC-A: Pennsylvania Anthracite BMC-B: Pennsylvania Bituminous GMC-B: Geneva Mine Coal, Utah, Bituminous DJC-SB: Dave Johnston Coal, Wyoming, Subbituminous				

selected to determine the effect of coal rank and genesis on the interfacial characteristics. Dave Johnston coal is particularly high in moisture - a factor that markedly affects the interfacial behavior as shown later in this paper. As can be seen from the results in Table 1, there is a considerable difference between the surface areas obtained by nitrogen adsorption and those obtained by carbon dioxide adsorption. Since micropores are essentially inaccessible to nitrogen molecules at liquid nitrogen temperatures, the surface areas obtained by nitrogen may be taken as a measure of the external surface. On the other hand, carbon dioxide molecules can adsorb in the micropores with no activation energy needed at room temperature (6). The carbon dioxide surface areas, therefore, represent the total surface area.

RESULTS AND DISCUSSION

Immersion Time Measurements:

In a previous study (5), the technique of immersion time measurements was employed to characterize coals of different rank and origin. In this technique, a small mass of 150 x 200 mesh coal is placed on the surface of aqueous methanol solutions in a test tube and the time for the particles to sink into the liquid is measured. The time, referred to as the immersion time, is a measure of the relative wettability. The immersion times for the Pennsylvania bituminous coal are given as a function of methanol concentration in Figure 1. The nature of the immersion time - vs - methanol concentration plots is typical of the various coals investigated. The surface tension of the methanol solutions is also given in Figure 1. The concentration of methanol where wetting behavior changes abruptly from wetting (short immersion time) to non-wetting (long immersion time) is defined as the critical wetting concentration, CWC, and the surface tension corresponding to the CWC is defined as the critical surface tension of the coal.

The effect of surface oxidation on the critical surface tension of wetting of the various coals was determined by the above procedure and the results are plotted in Figure 2. For the "as-received" samples, a minimum is observed in the critical surface tension vs. the carbon content at about 80% carbon. These results are in general agreement with the contact angle measurements of Gutierrez-Rodriguez et al. (7). Brown (8) had also observed a similar variation of contact angle with carbon content, but the maximum in contact angle occurred at somewhat higher values of the carbon content. The effect of coal rank on immersion time can, therefore, be explained in terms of the variation of the hydrophobic sites (paraffinic and graphitic) and the hydrophilic sites (oxygen containing functional groups), as has been done to explain contact angle results (9). Except for the Dave Johnston coal, oxidation increases the critical surface tension of wetting, which is expected because oxidation is likely to increase the number of hydrophilic oxygen containing functional groups, thereby, increasing wettability of coals. The increase in oxygen functional groups is confirmed by the results given in Table 2. The concentration of oxygen functional groups was determined by chemical titration methods (2) and infrared spectroscopy (which gives only a relative measure. The critical surface tension of wetting of the "as-received" sample of Dave Johnston coal is greater than the same coal oxidized at 150°C. Although the results appear to be puzzling at first, they may be explained in terms of the higher moisture content of this coal. When the coal is heated to 150°C, the moisture content is decreased and the unfilled pore sites act as hydrophobic sites. In the "as-received" sample, the pores filled with water would behave as hydrophilic sites. At higher oxidation temperatures, this coal also becomes more hydrophilic as expected on the basis of the increase in oxygen-containing functional groups. The effect of high moisture content on coal is also observed in the flow microcalorimeter results, as discussed in a later section. Figure 2 also shows that the critical surface tension is lowered when an oxidized coal sample is washed with water, that is, the coal becomes more hydrophobic. This observation is in agreement with previously reported studies that soluble components are formed when coals oxidize (10). After the removal of water-soluble products from the oxidized surface, the coal becomes more hydrophobic. The increase in hydrophobicity of coal after the oxidation-washing treatment is greater for higher rank coals. In fact, the anthracite became considerably more hydrophobic than the "as-received" sample after such a treatment.

Table 2 - Concentration of Oxygen Functional Groups in Two Pennsylvania Coals by Titration and Infrared Spectroscopy

PRETREATMENT	WEIGHT % OXYGEN			$\left(\frac{I_{1690}}{I_{1600}}\right)$
	Carboxylic	Phenolic	Total	
<u>Anthracite (BMC-A)</u>				
None	0.023	0.029	0.052	---
Oxidized				
at 150°C in air	0.031	0.075	0.106	---
at 200°C in air	0.073	0.109	0.182	---
at 244°C in air	0.073	0.393	0.466	---
in 30% H ₂ O ₂	0.015	0.075	0.090	---
<u>Bituminous (BMC-B)</u>				
None	0.012	0.047	0.059	0.11
Oxidized				
at 100°C in air	---	---	---	0.13
at 150°C in air	0.016	0.065	0.081	0.71
at 200°C in air	0.100	1.905	2.005	0.91
at 244°C in air	5.074	6.185	11.259	1.00
in 30% H ₂ O ₂	0.024	0.156	0.180	---

Flow Microcalorimetric Measurements:

Calorimetry has been used in the past to study coal chemistry and to elucidate the structure of coal (11). Traditionally, calorimetric measurements involve heat of immersion measurements. Information about the application of flow calorimetry on coal chemistry is meager (12). In this investigation, an adiabatic flow microcalorimeter (Microscal Ltd., London) was used to measure the heat of displacement of a carrier fluid (methanol) by water. A water-methanol system was selected because the results could then be correlated with the wettability results. A known amount of aqueous methanol solution was injected into a bed of 150 x 200 mesh coal particles and the heat evolved was measured. The heat evolved increased linearly with the amount of water injected as shown in Figure 3 and is independent of the composition of the injected solution. The slope of the line is a measure of the heat evolved in units of millicalories per gram coal per microliter water. The heat evolved for the various coals and their pretreatment is given in Table 3. Except for Dave Johnston coal, the heat evolved is less when the coal is oxidized. At the start of the experiment, the strongly hydrophilic oxidized sites are already covered by water molecules and methanol as a carrier fluid does not displace them. Therefore, the contribution from strongly hydrophilic sites to the measured heat is nil. The heat of dissolution of soluble oxidation products could be endothermic, which would also contribute to an overall decrease in the amount of heat evolved. The calorimetric behavior of Dave Johnston, which also behaved differently in immersion time measurements, is different because of its high moisture content. When this coal is heated, the moisture is driven off, making the coal effectively more hydrophobic.

Table 3 - Heat Evolved in Millicalories/gul Water for Displacement of Methanol by Water in a Flow Microcalorimeter

PRETREATMENT PROCEDURE	COAL SAMPLE			
	BMC-A	BMC-B	GMC-B	DJC-SB
None	42	41	44	17
Oxidized at 200°C	33	15	23	48
Oxidized at 200°C and leached in H ₂ O	51	42	57	64

This is the reason for the evolution of more heat when this particular coal is oxidized. As postulated above, water soluble products form when coals oxidize. This is observed in the microcalorimetric results also. From the results summarized in Table 3, it is clear that more heat is evolved when the coal is oxidized at 200°C and is leached with water (the washed coal was dried in vacuum at 36°C prior to microcalorimetric measurements). The oxygen groups present on the surface of oxidized and washed coal contribute substantially to the heat evolved when water molecules displace methanol molecules, as shown in last row of Table 3.

SUMMARY

The immersion time measurement technique was used to determine the effect of coal rank and the degree of oxidation on the critical surface tension of wetting. Heat of displacement of methanol by water molecules, measured by flow calorimetry, generally correlates very well with the wetting measurements. The coal surface is considered to consist of hydrophobic sites (paraffinic and graphitic) and hydrophilic sites (oxygen functional groups). All oxygen functional groups are not similar, however. Methanol is able to displace water molecules from weakly hydrophilic groups, but not from the strongly hydrophilic groups. In addition, the state of filling of micropores strongly influences both the immersion time and heat measurements. Empty pores behave as hydrophobic sites (or patches), whereas pores filled with water as hydrophilic sites (or patches). The above model of coal surface can be used to explain the effect of coal rank and state of oxidation on the interfacial properties of various coals.

ACKNOWLEDGEMENT

The authors wish to acknowledge the Bethlehem Steel Corporation and the National Science Foundation for the support of this research.

REFERENCES

1. Ignasiak, B.S., Ignasiak, T.M., Berkowitz, N., Reviews in Analytical Chemistry, 2(3), 278, 1975..
2. Yang, G.C., Ph.D. Thesis, University of California, Berkeley, 1983.
3. Chander, S., unpublished results.
4. Walker, P.L., Jr., Peterson, E.E., Wright, C.C., Industrial and Engineering Chemistry, 44, 2389, 1952.

5. Fuerstenau, D.W., Yang, G.C., Laskowski, J., Coal Preparation, in press 1986.
6. Walker, P.L., Jr., and Patel, R.L., Fuel, 49, 91, 1970.
7. Gutierrez-Rodriguez, J.A., Purcell, P.J. Jr., Aplan, F.F., Colloids and Surfaces, 12, 1, 1984.
8. Brown, D.J., Coal Flotation, in Froth Flotation - 50th Anniversary Volume, Fuerstenau, D.W., ed., AIME, New York, 518, 1962.
9. Rosenbaum, J., and Fuerstenau, D.W., Int. J. Mineral Processing, 12, 313, 1984.
10. Maximov, B, Glebko, L.I., Geoderma, 11, 17, 1984.
11. Fuller, E.L., Jr., in 54th Colloid and Surface Science Symposium, Bethlehem, PA, CONF-7906117-119, 1979.
12. Anonymous, Characterization of Powdered Coal by Flow Microcalorimetry, FMC Application Notes No. 10, Microscal Ltd., London, England, 1980.

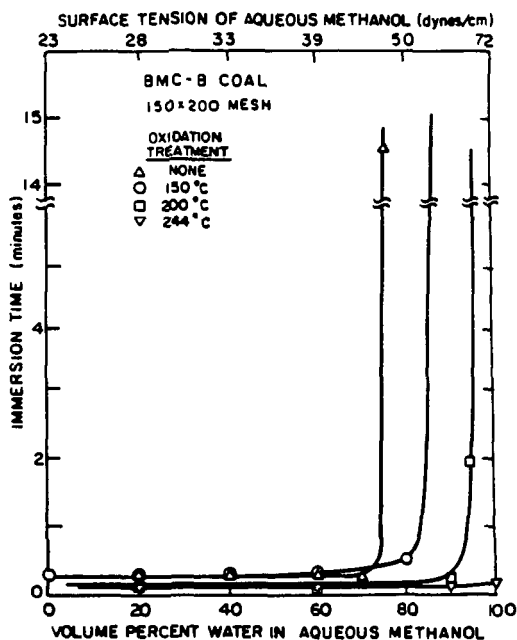


Fig. 1 - Representative immersion-time curves for Pennsylvania bituminous coal that had been oxidized in air at different temperatures along with the behavior of as-received coal.

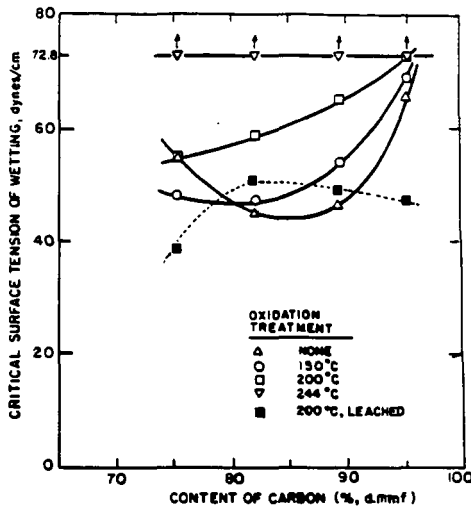


Fig. 2 - The critical surface tension of wetting as a function of coal rank and oxidation treatment.

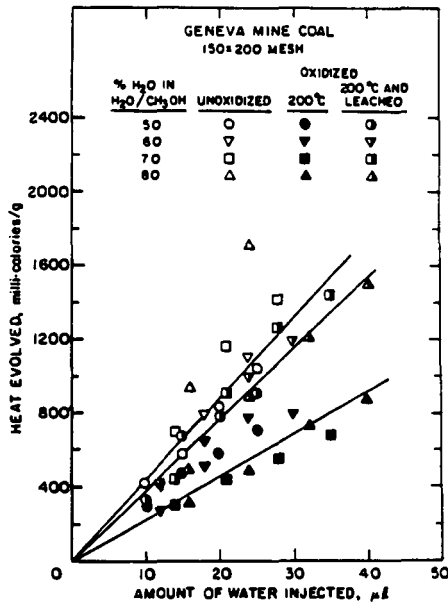
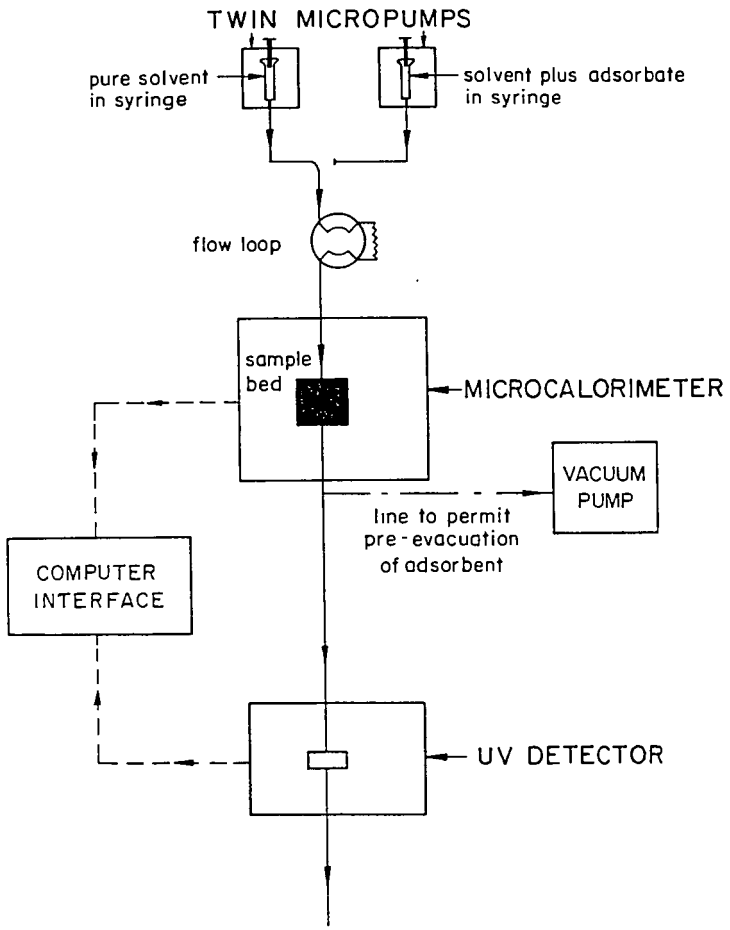
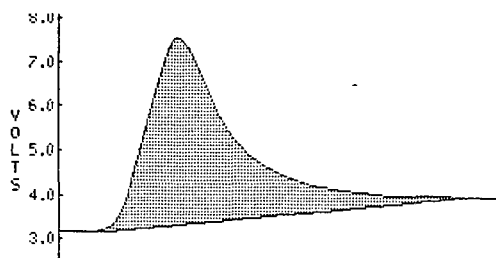


Fig. 3 - Heat of displacement of methanol by water on BMC-A coal as determined by a flow microcalorimeter.

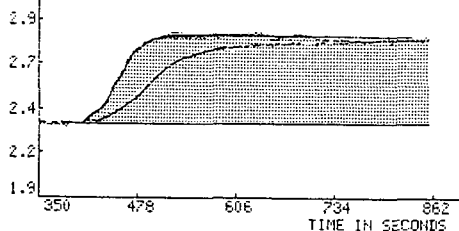


FLOW DIAGRAM

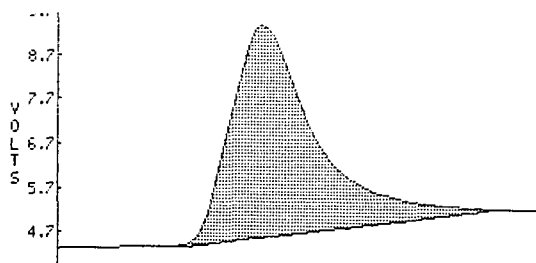
Figure 1. Diagrammatic sketch for lay-out of flow microcalorimeter with UV detector.



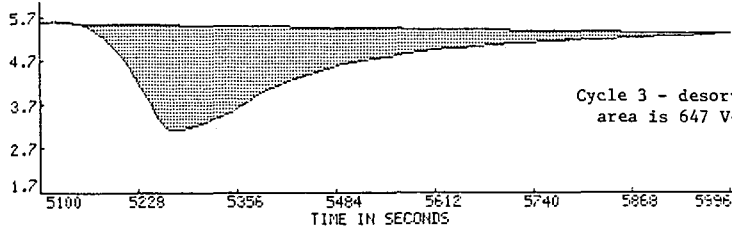
Cycle 2 - adsorption exotherm
area is 571 V-secs



Cycle 2 - UV absorption
Empty bed 201 V-sec
Coal bed 165 V-sec



Cycle 3 - adsorption exotherm
area is 596 V-sec



Cycle 3 - desorption endotherm
area is 647 V-sec

Figure 2. Flow microcalorimeter records of adsorption-desorption cycles for 25.4 mM 4-t-butylpyridine in iso-octane interacting with bed of heat-treated 170-230 mesh low-ash bituminous coal (PSOC #11).

chloroform and its shift upon complexation with bases (12).

The spectral shifts were determined with a Mattson FTIR spectrometer used in the transmission mode, operated to provide resolutions of one wave-number for OH and CD shifts, and about 0.3 wave-numbers for carbonyl shifts.

Surface Areas by Gas Adsorption

The specific surface areas of all coal samples were determined by nitrogen adsorption with the BET analysis, using the gas chromatography method with a Quantichrome Monosorb Surface Area Analyzer and the classical static equilibrium method with a Numinco-Orr Surface Area-Pore Volume Analyzer. The Numinco-Orr Analyzer was also used for adsorption studies with 2,2'-dimethylbutane and with carbon dioxide, both at 25 C. The adsorption data for dimethylbutane were analyzed with the BET method, and the carbon dioxide data were analyzed by both the BET and the Dubinin-Polanyi method (13).

Materials Used in this Investigation

Coal powders prepared from five different coal samples were investigated. Four came from the Pennsylvania State University coal bank, and we also tested a more recently mined bituminous coal from Bethlehem Steel Company (Van-131). The properties of these coals were as follows:

<u>Identification</u>	<u>Rank</u>	<u>% Carbon</u>	<u>% Moisture</u>	<u>% Ash</u>	<u>% Volatiles</u>
PSOC #11	Bituminous	81.62	1.50	2.04	35.62
PSOC #213	Bituminous	65.12	8.93	8.52	35.91
PSOC #870	Anthracite	89.52	3.84	2.46	2.93
PSOC #868	Anthracite	63.34	3.82	25.00	4.06
Van-131	Bituminous	80.4		5.00	39.60

The coals were obtained as coarse powders, were riffled to provide more uniform samples and were stored in the dark in argon-filled glass desiccators. They were subsequently ground to enhance the amount of surface available in the adsorption bed. Most of the grinding was done with a micro-mill from Technilab Instruments; the coal was micro-milled in air for two minutes in the water-cooled chamber. Other samples were ball-milled, and some Van-131 samples were γ -milled to much higher specific surface areas.

A major consideration in the selection of the carrier solvent and of the test acids and bases was their tendency to penetrate into the bulk region of the coal particles; we wished to sample only the surface region. This point will be discussed in more detail, but we have chosen to use iso-octane as carrier solvent and t-butylated acids and bases as "limited penetration" test probes for surface acidity and basicity. The iso-octane was Purified grade from Fisher, the pyridine and phenol were ACS Reagent grade from Fisher, and the t-butylated acid-base probes (4-t-butylphenol, 3,5-di-t-butylphenol, 2,6-di-t-butylphenol, 4-t-butylpyridine, 2,6-di-t-butylpyridine and 4-t-butylcyclohexanone) were all Aldrich Reagent grade. Some gas adsorption studies were made with 2,2'-dimethylbutane (98%) which we obtained from Aldrich Chemical Co.

Results and Discussion

Limited-Penetration Acid-Base Probes.

Pyridine is known to swell coal very considerably, but in studies of the equilibrium swelling of coal by pyridine and its derivatives, Larsen and co-workers found that the derivatives with side chains cause less swelling and that t-butyl derivatives cause the least swelling, about 10% of that observed with pyridine (1). Perhaps the most important effect of the t-butyl groups is on the rates of swelling; Aida, Squires and Hansen found that the t-butyl groups retarded the rates of penetration by a factor of a thousand or more (14).

An important consideration is the effect of t-butyl substitution on the strength of the acidity or basicity of a test molecule, so we investigated the heats of acid-base complexation of the candidate test acids and bases in a neutral organic solvent, using infrared spectral peak shifts measured in the presence of various excess concentrations of reactant. For example, the peak shift of 3,5-di-t-butylphenol was measured with a 17.5 mM solution in cyclohexane, and in the presence of a 3-fold, 10-fold and 30-fold excess of pyridine the spectral shift was -434 cm^{-1} in each case, showing none of the concentration-dependence reported by Drago and co-workers (4). The details of these measurements will be shown in the forthcoming publication. It was found that substitution of t-butyl groups in the 2-, 4-, or 3,5- positions do not affect the acid or base strength of phenol or pyridine appreciably, but in the 2,6- positions the t-butyl groups completely blocked any reactions of the phenol or pyridine sites.

In our flow microcalorimetry measurements the bed of powdered coal is exposed to test acid or base solutions for only about 5 to 10 minutes. In another few minutes pure solvent is pumped through the bed to desorb the adsorbed probe. If the probe is pyridine or phenol some of it tends to penetrate into the coal during the 5 to 10 minutes of exposure, but with t-butyl derivatives the degree of penetration is negligible. Table 1 illustrates this effect by comparing heats of adsorption and desorption in several successive adsorption-desorption cycles with phenol, pyridine, and their t-butyl derivatives adsorbing from iso-octane at 40 C onto low-ash anthracite (PSOC #870) and onto low-ash bituminous coal (Van-131) powders.

The penetration of pyridine into low-ash anthracite (PSOC #870) is illustrated in Figure 1. The heat of adsorption of pyridine was so excessive that the recorder went way off scale on the first adsorption cycle, and the subsequent heat of desorption was still quite large (+2130 Joules/kg); in the subsequent cycles only about half as much heat was evolved, with the heats of adsorption exceeding the heats of desorption by about 10%. On the same anthracite powder 4-t-butylpyridine is seen to desorb quantitatively, with an average heat of adsorption of -825 Joules/kg and an average heat of desorption of $+827\text{ Joules/kg}$.

The flow microcalorimetry results for phenol in Table 1 also shows much penetration into anthracite. The heats of adsorption are about double the heats of desorption, and the heats for the second adsorption-desorption cycle are much less than for the first cycle. The limited penetration of phenol with 3,5-di-t-butyl substitution is quite remarkable; the initial heat of adsorption (-237 Joules/kg) is exactly equal to the average of the five cycles, and the standard deviation for the five heats of adsorption and five heats of desorption is only 3.6%.

In Table 1 it is shown that 2,6-di-t-butylphenol has weak exothermic interactions (-4 to -6.6 kJoules/mole) with the surface of coal, even though FTIR studies showed that the phenolic group cannot interact with pyridine. Perhaps the weakly basic aromatic ring is the site of exothermic acid-base interaction with acid sites of coal.

The basic probes used in this study included two oxygen bases, ethylacetate and 4-t-butylcyclohexanone; their heats of acid-base interaction are -5.0 and -5.7 kcal/mole with phenol, as compared to the -8.1 kcal/mole for 4-t-butylpyridine. The 4-t-butylcyclohexanone performed well as a limited-penetration probe for acidic sites on Van-131 coal powders.

Statistical Significance of the Flow Microcalorimetric Measurements

The data in Table 1 illustrate the statistical significance of the flow microcalorimetric measurements. With the limited-penetration probes the heats of desorption are seen to be very close to the heats of adsorption; the average difference is only 2.7%. The standard deviations in the heats of adsorption and desorption (measured in Joules/kg) in repeat runs were found to be about 5% in all cases for the low-ash anthracite and about 15% in all cases for the low-ash bituminous coal.

The measurements of amounts adsorbed determined from the UV absorption were much less repeatable, and the molar heats of adsorption derived therefrom were also less repeatable. With the low-ash anthracite (PSOC #870) and with the low-ash

Table 1. Adsorption and Desorption of Acid-Base Probes on Low-Ash Coal Powders.

Coal	(m ² /g)	Acid-Base Probe	Cycle	Joules/kg		kJ/mole	
				mmoles/kg adsorbed	adsorbed desorbed		
PSOC #870	1.85	Phenol	1	37.2	-2438	+1295	-65.5
			2	27.8	-1808	+1100	-65.0
		3,5-di-t-Butylphenol	1	7.8	-232	+242	-29.9
			2	6.8	-238	+265	-35.2
			3	6.5	-237	+243	-36.5
			4	8.1	-242	+229	-30.0
			5	7.3	-236	+249	-32.2
		2,6-di-t-Butylphenol	1	16.9	-111,	+119	-6.6
			2	26.2	-112	+129	-4.3
			3	26.4	-135	+114	-5.1
			4	26.3	-123	+139	-4.7
			5	20.5	-91	+125	-4.5
		Pyridine	1		-????	+2130	
			2	34.6	-1477	+1375	-42.7
			3	38.1	-1392	+1270	-36.5
			4	37.0	-1432	+1242	-38.7
		4-t-Butylpyridine	1	37.4	-871	+863	-23.3
			2	28.7	-815	+864	-28.4
			3	27.0	-709	+817	-26.3
			4	31.1	-862	+782	-27.7
5	37.5		-868	+809	-23.1		
PSOC #11	1.81	3,5-di-t-Butylphenol	1	13.4	-391	+388	-29.2
			2	22.0	-481	+487	-21.9
			3	24.0	-570	+559	-23.8
			4	20.2	-617	+588	-30.5
		4-t-Butylpyridine	1	35.6	-893	+864	-25.1
			2	40.5	-1081	+1025	-26.7
			3	44.3	-1096	+1059	-24.7
			4	39.4	-1194	+1232	-20.3
			5	44.5	-1130	+1130	-25.4
Van-131	0.62	Pyridine	1		-536	+334	
			2		-668	+460	
			3		-572	+390	
	1.57	3,5-di-t-Butylphenol	1	12.1	-158	+184	-13.0
			2	9.9	-162	+155	-16.4
			3	4.2	-161	+162	-38
			4	4.7	-122	+127	-26
			5		-129	+128	
			6		-117	+105	
4-t-Butylphenol	1		-176	+221			
	2		-257	+258			
	3	15.4	-260	+259	-16.9		
	4	15.0	-250	+263	-16.7		

bituminous coal (PSOC #11) the standard deviations for repeat runs in the number of micromoles adsorbed per square meter varied from 10 to 20%, but with the Van-131 bituminous coal these deviations were much greater. In other flow microcalorimetric studies with this same instrument (15) we have achieved standard deviations between the heats of adsorption in successive repeat runs of about 2%, so we are encountering coal-related analytical difficulties in determining the concentration of the acid-base probes in the eluent. The UV flow detector is very sensitive to air bubbles, and as the solution flows through the calorimeter bed at 40 C, there is a tendency for bubble-formation; we have switched to 30 C, and this helps. There is also a tendency for small coal particles to be carried out of the bed and through the UV detector cell; we have introduced a micro-pore filter at the base of the bed, and this also helps. Nevertheless, there is a tendency for some aromatic components of coal to be leached out despite our use of iso-octane as a carrier liquid with of minimal solubility for aromatics. Perhaps a branched saturated hydrocarbon of higher molecular weight or some Freon-type solvent would give a cleaner eluent.

Differences in the Surface Properties of Coals

In the studies with low-ash coals, the heats of adsorption of limited-penetration acid-base probes are appreciably greater for the pyridine derivatives than for the phenol derivatives, and this is shown to result from higher surface concentrations of acidic surface sites in the three low-ash coals investigated, whether anthracite or bituminous coal.

Table 2. Heats of Adsorption of Test Probes on High-Ash Coal Powders

Coal	Milled	Acid-Base Probe	Cycle	mmoles/kg Joules/kg kJoules/mole			
				adsorbed	adsorbed	desorbed	
PSOC #213	no	3,5-di-t-Butylphenol	1	25.3	-536	+532	-23.1
			2	26.9	-649	+532	-24.1
			3	31.4	-649	+615	-20.7
	yes	"	1	36.6	-1351	+933	-37.9
			2	35.4	-1021	+874	-28.8
			3	29.8	-1067	+824	-35.8
			4	32.7	-1092	+1096	-33.4
	no	4-t-Butylpyridine	1	46.1	-1331	+636	-28.9
			2	35.6	-782	+619	-22.0
			3	43.3	-703	+678	-16.2
	yes	"	1	34.0	-1745	+1163	-51.5
			2	58.9	-1251	+1276	-21.3
3			60.3	-1318		-21.8	
PSOC #868	no	3,5-di-t-Butylphenol	1	41.8	-540	+389	-12.9
			2	43.6	-494	+406	-11.3
			3	45.7	-439	+439	-9.6
	yes	"	1	26.0	-916	+385	-35.2
			2	37.5	-607	+523	-16.2
			3	30.6	-619	+444	-20.3
	no	4-t-Butylpyridine	1	51.3	-2330	+1326	-45.6
			2	33.5	-602	+431	-18.0
			3	18.4	-436		-24.8
	yes	"	1	80.9	-1975	+594	-24.2
			2	53.1	-736	+590	-13.8
			3	71.9	-619	+540	-8.6

The presence of ash in the anthracite (PSOC #868) or bituminous coal (PSOC #213) made much difference in the heats of adsorption, especially in the repeatability of the heats of adsorption in a series of repetitive adsorption-desorption cycles. Table 2 shows trends indicating that the presence of ash caused stronger adsorption than desorption, especially in the first cycle, and that the heats of adsorption decreased in successive cycles. These findings suggest that the ash present in these powders binds the acid-base probes more strongly than the coal. In Table 2 results are compared for coal powders as received versus freshly micro-milled powders, and it appears that the molar heats of adsorption in the initial cycle are always higher with fresh-milled coal powders.

Surface Area Determination with Limited-Penetration Adsorbents

There has been some discussion in the literature (16) of discrepancies in specific areas determined by gas adsorption with nitrogen at liquid nitrogen temperatures versus carbon dioxide at 25 C. So much more carbon dioxide than nitrogen is picked up by the coal that it was proposed that hundreds of square meters per gram of surface is accessible to carbon dioxide but not to nitrogen. However, in modern studies it is becoming quite clear that carbon dioxide (like other small reactive organic molecules) dissolves into the coal, causing some swelling and allowing access to inner surfaces by a solution route. Carbon dioxide is a self-associated acid-base complex which readily dissolves into and swells any acidic or basic polymer. Coal is just one of the many polymers that picks up carbon dioxide vapors appreciably at one atmosphere and at room temperature. If one uses the Polanyi-Dubinin equation to elucidate the "specific surface areas" from such gas adsorption measurements the plots give very satisfying straight lines and high correlation coefficients, predicting over a hundred square meters of surface per gram for optically clear polymers such as polymethylmethacrylate.

The use of t-butyl derivatives to determine specific surface areas of coal powders has merit, for the t-butyl groups block penetration into the coal and no solution occurs. We have tried this approach with gas adsorption, using 2,2-dimethylbutane, which has a t-butyl group, and measured the adsorption of this vapor at 25 C, and calculated the specific surface areas with the BET method, using 0.40 nm² for the area per molecule. As can be seen in Table 3, the specific surface areas measured with 2,2-dimethylbutane agree quite well with those determined from nitrogen adsorption isotherms measured at -196 C. In Table 3 we compare specific surface areas for five lots of powdered Van-131 coal which were ground to various particle sizes. The specific surface areas determined from adsorption of nitrogen or 2,2-dimethylbutane increased upon grinding to smaller particle sizes, but the "areas" determined with carbon dioxide remained at about 100 m²/g. The specific surface area of the coarsest powder was measured to be 0.50-0.52 m²/g by nitrogen adsorption and 1.49 m²/g by 2,2-dimethylbutane. An intermediate powder was found to have 2.76-2.82 m²/g by nitrogen adsorption and 3.52 m²/g by 2,2-dimethylbutane adsorption, and the finest powder was found to have 14.0-20.5 m²/g by nitrogen adsorption and 14.7 m²/g by 2,2-dimethylbutane adsorption. It appears that the best agreement is found for the finer powders.

Specific surface areas were also estimated for the same Van-131 powders, using the amounts of adsorption determined in the flow microcalorimetric measurements with t-butyl derivatives of pyridine, phenol and cyclohexanone adsorbing from solution in iso-octane. The estimates shown in Table 3 were calculated from the assumption that the maximum surface concentrations attained in flow microcalorimetry correspond to tight-packed monolayers (4.1 micromoles/m²); however, the results with the finer powders suggest that the films are not tight-packed.

Table 3. Surface Areas (m²/g) Versus Particle Size of Ground Van-131 Coal

Coal Lot	Mesh Size	Adsorbent	Temp,C	Method	Analysis	m ² /g
Van-131C	50-100	Nitrogen	-196	Dynamic	BET	0.50
		Nitrogen	-196	Static	BET	0.52
		2,2-Dimethylbutane	25	Static	BET	1.49
		4-t-Butylphenol	40	Flow-Cal		3.8
		4-t-Butylcyclohexanone	40	Flow-Cal		2.8
		Carbon dioxide	25	Static	BET	88
		Carbon dioxide	25	Static	D-P	117
Van-131F	<325	Nitrogen	-196	Dynamic	BET	2.82
		Nitrogen	-196	Static	BET	2.76
		2,2-Dimethylbutane	25	Static	BET	3.52
		4-t-Butylcyclohexanone	40	Flow-Cal		1.9
		3,5-di-t-Butylphenol	40	Flow-Cal		2.2
		Carbon dioxide	25	Static	BET	56.6
		Carbon dioxide	25	Static	D-P	94.6
Van-131T	<<325	Nitrogen	-196	Dynamic	BET	14.0
		Nitrogen	-196	Static	BET	20.5
		2,2-Dimethylbutane	25	Static	BET	14.7
		4-t-Butylcyclohexanone	40	Flow-Cal		5.5
		4-t-Butylphenol	40	Flow-Cal		5.3
		3,5-di-t-Butylphenol	40	Flow-Cal		4.6
		Carbon dioxide	25	Static	BET	57.8
		Carbon dioxide	25	Static	D-P	99.8

References

- 1.- T.Green, J.Kovac, D.Erenner and J.W.Larsen, in Coal Structure, pp. 199-282 (Academic Press, 1982)
- 2.- N.A.Peppas and L.M.Lucht, Chem. Eng. Commun. 30, 291 (1984)
- 3.- J.E.Metcalf III, M.Kawahat and P.L.Walker, Jr., Fuel 42, 233 (1963)
- 4.- R.S.Drago, G.C.Vogel and T.E.Needham, J.Am.Chem.Soc. 93, 6014 (1971)
- 5.- R.S.Drago, L.B.Parr and C.S.Chamberlain, J.Am.Chem.Soc. 99, 3203 (1977)
- 6.- V.Gutmann, The Donor-Acceptor Approach to Molecular Interactions, Plenum Press, NY, 1978
- 7.- M.S.Nozaari and R.S.Drago, J.Am.Chem.Soc. 92, 7086 (1970)
- 8.- F.M.Fowkes, D.O.Tischler, J.A.Wolfe, L.A.Lannigan, C.M.Ademu-John and H.J.Halliwell, J.Polym.Sci., Polym.Chem.Ed. 22, 547 (1984)
- 9.- D.C.McCarthy and F.M.Fowkes, 40th Ann.Conf.Reinforced Plastics/Composites, Soc. Plastics Industry (Jan., 1985), Paper 17-D
- 10.- S.T.Joslin and F.M.Fowkes, IEC Product R&D 24, 369 (1985)
- 11.- R.S.Drago, W.O'Bryan and G.C.Vogel, J.Am.Chem.Soc. 92, 3924 (1970)
- 12.- H.F.Shurvell and J.T.Bulmer, Vibrational Spectra and Structure 6, 91. J.R.Durig, editor (Elsevier, Amsterdam, 1977)
- 13.- H.N.Dubin, Chem.Rev. 60, 235 (1960)
- 14.- T.Aida and T.G.Squires, Prepr. ACS Div. Fuel Chem. 30, 95 (1985)
- 15.- F.M.Fowkes, Y.C.Huang, E.A.Shah, M.J.Culp and T.B.Lloyd, submitted to Colloids and Surfaces
- 16.- P.J.Reucroft and K.B.Patel, Fuel 62, 279 (1983)

SURFACE STRUCTURE OF COALS STUDIED BY IODINE AND WATER ADSORPTION

N.M. Rodriguez and H. Marsh

Northern Carbon Research Laboratories, School of Chemistry,
University of Newcastle upon Tyne, Newcastle upon Tyne,
NE1 7RU, U.K.

1. Introduction

1.1 Iodine and carbon

The interaction of iodine with such carbonaceous materials as carbons and coals has been studied by adsorption both from the vapour phase (1-3) and from aqueous potassium iodide solution (1,3-6). Mechanisms of interactions have been studied using ESR (2,7) and related to the well-characterized formation of charge-transfer complexes of iodine with organic compounds (2). Thus, both classical physical adsorption theory and more specific chemical interactions have been proposed to model the adsorption of iodine by carbonaceous materials. Assessments of surface area and porosity in solid adsorbents are traditionally made from data of vapour phase adsorption (8). Although the technique is relatively elaborate, involving use of vacuum equipment, interpretation of a single component adsorbate is straight-forward. The alternative approach of adsorption from solution, a relatively simple experimental technique, is however much more difficult to interpret because of multi-component competitive adsorption processes (9). Adsorption of iodine from aqueous potassium iodide solution by carbons does however appear to be both relatively easy experimentally and to interpret. This study is concerned with the extension of the use of iodine as an adsorbate from carbons to coals. Kipling *et al.* (1) studied the adsorption of iodine, both from the vapour phase and organic solutions at 20°C on graphitized carbon blacks. Adsorption of iodine from organic solutions was solvent dependent and can be used to determine surface areas only under certain conditions mainly when solvent competition for the surface is minimized. Studies of the adsorption of iodine from aqueous potassium iodide solution on several porous carbons were carried out by Hill and Marsh (5). Iodine was not restricted to monolayer coverage and filling of meso-porosity occurred. The adsorption isotherm required the calculation of the concentration of free iodine (I_2) in equilibrium with the carbon surface. Surface area values were comparable to those from isotherms of nitrogen and carbon dioxide (5). Radioactive studies demonstrated that molecular iodine was physically adsorbed. Later, Juhola (3) using activated carbon reported similarly to Hill and Marsh (5). Meguro *et al.* (6) studied iodine adsorption on carbons from aqueous solution and concluded that iodine molecules were the only species adsorbed physically, in agreement with Hill and Marsh (5). Adsorption isotherms fitted the Langmuir equation over only part of the concentration range of free iodine whereas the Dubinin-Radushkevich (D-R) fitted the data much better over the whole range of concentration. Meguro *et al.* (6) therefore concluded that micropore filling rather than monolayer coverage occurred. To support this they showed that micropore volumes calculated from adsorption of carbon dioxide were in good agreement with values calculated from iodine adsorption using the D-R equation.

1.2 Iodine and coals

Although the interactions of iodine with carbons have been adequately studied, the literature of interactions with coals is scant. Aronson *et al.* (2) studied adsorption of iodine vapour on graphite, anthracite and bituminous coals at 70°C. Values of enthalpies of adsorption were in the range -44 to -60 kJ mol⁻¹, a value close to the enthalpies of complexing between model organic

compounds and iodine (10), indicating a relatively strong interaction when compared with, e.g. hydrogen bonding of -28 kJ mol^{-1} (11). Anthracite adsorbed more than the graphite from the vapour phase at equilibrium; the three bituminous coals and lignite all showed similar adsorption behaviour. The iodine/coal weight ratios had values of 2.5 (10 mmol g^{-1}) and 2.0 (8 mmol g^{-1}) for the three bituminous coals and lignite respectively. Such large extents of iodine adsorption by coals go far beyond extents of iodine adsorption by activated carbons and suggest a different form of iodine in equilibrium on coal surfaces.

It is established that iodine reacts reversibly with polynuclear aromatic hydrocarbons to form charge-transfer complexes in which several molecules of iodine are complexed with one hydrocarbon molecule (7,12). Aronson *et al.* (2) followed the reaction of iodine with polynuclear aromatic hydrocarbons from changes in vapour pressure and noted that the molecular ratio of iodine to hydrocarbon ranged from one to three. Perylene formed two complexes $\text{Pe}(\text{I}_2)_{1.5}$ and $\text{Pe}(\text{I}_2)_{2.9}$. Picene did not form a complex. Kim and Reiss (13) have studied adsorption of iodine vapour by films of polythiophene and shown it to be reversible, exhibiting Henry's law behaviour over a wide pressure range. They suggest that the number of iodine molecules adsorbed is comparable with the estimated number of thiophene monomer units in the polymer film.

1.3 Water vapour and coals

The interpretation of water vapour adsorption isotherms of coals is complex (14,15). Water within coal, prior to the initial degassing, can form part of the structure of coal, in particular the low rank coals. Here, their significant oxygen contents bond water to coal material. The initial outgassing of coals can cause structural changes resulting in shrinkage, the coal swelling on re-adsorption of water. Isotherms may not be reproducible. Extents of water adsorption can be as high as 80 wt% (45 mmol g^{-1}) far in excess of extents of adsorption of carbon dioxide at 195 or 273 K and resulting from volume filling and coal swelling. Water isotherms are usually of Type III BET classification but extents of adsorption are critically dependent upon the oxygen content of surfaces (8). Adsorption of water is relatively high for low rank coals (high oxygen content), passing through a minimum for the coking bituminous coals because of development of closed porosity and rising again for the anthracites of enhanced microporous content (15).

1.4 Macromolecular structure of coal

Although coal is extremely heterogeneous in composition (16) attempts have been made to treat the vitrinite components of coals in terms of a macromolecular structure (17-19). As coals increase in rank so carbon-oxygen cross-links are replaced by hydrogen bonding (coking coals) and carbon-carbon cross-links in anthracites, a minimum in cross-link density occurring at about 87 wt% of carbon (17). Aromaticity in coals increases progressively with rank. Oxidation of coal, in air, is thought to remove both hydrogen from the surface and to chemisorb oxygen (20), both effects contributing to the loss of plasticity of bituminous coals on heating. The thermolysis of the fusing bituminous coals brings about breakage of cross-links in the initial coal.

The objectives of this study in general terms are to advance an understanding of coal substance and in specific terms to examine (a) the adsorption of iodine both from the vapour phase and from aqueous potassium iodide solution from a rank range of fresh coals, (b) the behaviour of oxidised coals, (c) the behaviour of coals after thermolysis pyrolysis.

2. Experimental

2.1 Materials used

Eleven coals of a rank range were used and from these coals three were selected for further oxidation studies, i.e. Gedling (NCB rank 801), Cortonwood (501) and Cwm (301). Analyses of the coals are in Table 1. An activated carbon cloth, No. 005 manufactured by Charcoal Cloth Ltd., U.K. was used as a comparison (nitrogen BET surface area $1300 \text{ m}^2\text{g}^{-1}$, pore volume $\sim 0.45 \text{ cm}^3\text{g}^{-1}$).

2.2 Techniques used

Coals were oxidised in an air oven at 100° , 150° , 200° and 250°C for 1 and 2 days. Iodine and water were adsorbed by dry coals from the vapour phase (no air) at 25°C over a two-week period. The amount of iodine and water adsorbed were determined gravimetrically using the silica springs of a McBain-type equipment (8). The coals were degassed at 100°C prior to an adsorption run. In determinations of extents of adsorption of iodine from aqueous solution, 100 mg of each fresh, oxidised and pyrolyzed coal was sealed with 50 ml of aqueous solution of iodine and iodide (0.07 mol of I_2 plus 0.15 mol of KI l^{-1}) at 25°C in a flask, with occasional shaking. After four weeks an aliquot of the solution was taken and the iodine concentration determined with a standard solution of sodium thiosulphate (5). Samples of fresh and oxidised charcoal cloth were similarly treated and analysed after seven days. Extents of adsorption corresponded to an equilibrium relative concentration of 0.45.

Fresh and oxidised coals were kept in iodine (aqueous) solution (0.056 mol I_2 plus 0.15 mol KI per litre) for periods ranging from 1 to 28 days. Values of kinetic constants were determined from the variation of extents of iodine adsorption with time. To study the swelling of coals by water and iodine solution, ground fresh and oxidised coals (~ 100 mesh) were placed in a 3.5 mm (int. diam) pyrex glass tube and packed carefully according to the procedure used by Larsen (21). The height of the coal bed was measured (average of four measurements after rotating the tube) before and after addition of $\text{I}_2/\text{KI}/\text{H}_2\text{O}$ (0.056 mol I_2 , 0.15 mol KI per litre) solution. The swelling ratio, Q , was calculated as ($Q = V_f/V_i = H_f/H_i$) where V_f and V_i are the final and initial volumes of the coal bed and H_f and H_i the corresponding heights. To study the effects of pyrolysis of coals, fresh and oxidised coals were carbonized under flowing nitrogen in a horizontal furnace to 200° , 300° , 400° , 500° , 600° and 700°C with a heating rate of 3°C min^{-1} and a soak time of 0.5 h.

3. Results

3.1 Adsorption of iodine by fresh coals

Figure 1 shows the variation of iodine adsorption from aqueous solution as a function of coal rank for fresh coals with carbon contents lying between 80 wt% C and 95 wt% C. Iodine adsorption increased from $\sim 4 \text{ mmol g}^{-1}$ for coal with carbon content of 80 wt% to a maximum value of 6 mmol g^{-1} for coals of ~ 84 wt% carbon content (dmmf). Iodine adsorption then fell with increasing carbon content to $\sim 2.3 \text{ mmol g}^{-1}$ for a coal with a carbon content of 95 wt%.

3.2 Adsorption of iodine by oxidised coals

Figures 2-4 illustrate the isotherms for adsorption of iodine by fresh and oxidised coals at 25°C . In all the coals a decrease in the amount of iodine uptake with extents of oxidation was observed. Changes in the shape of the isotherms were also observed as oxidation progresses. The isotherms are Type I and II, (BET classification) (8). Extents of iodine uptake (mmol g^{-1}) can be converted to an equivalent surface area by assuming a cross-sectional area of an iodine molecule of 0.4 nm^2 (5). Figure 5 shows the

isotherms for the adsorption of iodine by fresh and oxidised charcoal cloth. An increase in the amount of iodine adsorbed with extents of oxidation was observed. The isotherms are Type 1. The maximum of iodine adsorption was at $C/C_0 > 0.4$ (C/C_0 = relative free iodine concentration (5); C_0 is taken as 1.2 mmol l^{-1}). Extents of iodine adsorption observed for coals were much higher than those for charcoal cloth at similar C/C_0 values. Figure 6 summarises the changes in iodine adsorption following oxidation at different temperatures and times for the three coals at constant C/C_0 value ($C/C_0 = 0.6$).

3.3 Adsorption of iodine by pyrolysed coals

The adsorption of iodine as a function of heat treatment temperature (HTT) for Cwm (301), Cortonwood (501) and Gedling (801) coals is illustrated in Figure 7. An initial increase in amounts of adsorbed iodine was observed at the lower values of HTT reaching a maximum at $\sim 400^\circ\text{C}$ and decreasing sharply thereafter to low values. The effect of preoxidation and heat treatment on adsorption of iodine for the three coals is illustrated in Figures 8-10. Little change was observed when coals were oxidised at 100°C compared with the non-oxidised samples, but a marked decrease was observed when the coals were oxidised at the higher temperature of 200°C .

4. Discussion

4.1 Adsorption of iodine by fresh coals

Figure 1 shows that for a rank range of fresh coals, there is a clear rank dependence of iodine adsorption from aqueous solution. A maximum in iodine uptake ($\sim 6 \text{ mmol g}^{-1}$) occurs at 84 wt% C dmmf. The minimum value ($\sim 2.3 \text{ mmol g}^{-1}$) was obtained for coals with 95 wt% C. The variation of surface properties as a function of coal rank has been studied previously (22-24). Carbon dioxide surface areas measured at 195 K (-78°C) and 273 K (0°C) varied from 110 to about $310 \text{ m}^2\text{g}^{-1}$ and fell within a broad band with the minimum at about 85 wt% carbon.

The results obtained in this present study of iodine adsorption as a function of coal rank do not relate to those of carbon dioxide surface areas. The coal rank series shows a maximum in adsorption of iodine at about 85 wt% carbon; with carbon dioxide a minimum is observed. Further, the equivalent surface areas of coals with 86 and 95 wt% C, based on iodine adsorption are 1400 and $530 \text{ m}^2\text{g}^{-1}$ respectively. These values are extremely high compared with the carbon dioxide surface areas. This indicates that the mechanism of adsorption by iodine and carbon dioxide must be different.

Although the temperature of adsorption of iodine is high enough (25°C) to eliminate activated diffusion effects restricting adsorption (22-24) the larger size of the iodine molecule would be expected to result in a decreased adsorption compared with carbon dioxide. This does not occur. However, the iodine adsorption from the vapour phase is much less than from aqueous iodide solution (Table 2) indicating a co-operative effect between the water and the iodine. With adsorption from the vapour phase, three interacting factors may control the ultimate extents of iodine adsorption. The higher internal porosity and larger pore sizes of the lower rank coals will promote adsorption; the increase in aromaticity of coals with increasing rank will promote increased adsorption with rank; overall, extents of adsorption will decrease as the strength of cross-links and cross-link density increase. For adsorption of iodine and water from the vapour phase, the higher internal porosity of the lower rank coal appears to dominate.

Extents of iodine adsorption are much higher from aqueous solution (Table 2, Figure 1). It is possible that the water when in the coal, is able to expand the macromolecular structure of the coal sufficiently to allow a considerably larger amount of iodine to be adsorbed, but the water is not significantly competitive for the surface. The swelling data of Table 3 indicate that the Gedling coal can respond most to the co-operative effects of the water and iodine agreeing with the highest uptake of iodine from the vapour phase. Thus, as the cross-link density of the coals decreases with increasing rank to about 85 wt% carbon and then increases, so the iodine adsorption will increase to decrease subsequently beyond the 85 wt% carbon level. Thus, Figure 1 is indicative of the cross-link density of the coals of the rank range.

Figures 2-4 shows the isotherms of the fresh coals and indicate a change in isotherm shape, almost Type II for Gedling coal and Type III for Cortonwood and Cwm coals of higher rank. This is indicative of a lower enthalpy of adsorption between the iodine adsorbate and the coal adsorbent for the latter two coals.

The charcoal cloth behaves differently from the coals. The surface areas calculated from iodine adsorption are commensurate with nitrogen areas, i.e. about $1300 \text{ m}^2 \text{ g}^{-1}$. Oxidation causes an increase in iodine adsorption unlike the coals. Possibly oxidation enhances pore volume and with the rigid carbon-carbon cross-linked structure already established, it cannot be enhanced further and hence iodine adsorption is not diminished. Carbons and coals respond differently to iodine adsorption.

4.2 Adsorption of iodine by oxidized coals

The effects of increasing duration and temperature of oxidation in air of the Gedling, Cortonwood and Cwm coals are to decrease extents of iodine adsorption from both the vapour and aqueous phases. For coals of maximum oxidation treatment (2d at 200°C) extents of iodine adsorption from the vapour phase are equivalent to about $25 \text{ m}^2 \text{ g}^{-1}$. For the same coals extents of water adsorption increase with severity of oxidation, as anticipated (14,15). For all three coals progressive oxidation promotes swelling of the coals by water alone and by the iodine-water system, probably to equal extents. The isotherms of Figures 2-4 shows that the Gedling oxidized coals retain the Type II isotherm shape of the parent coal, whereas the isotherms of the Cortonwood and Cwm coals change from Type III to Type II with progressive oxidation.

In interpreting these findings, the influence of coal oxidation on iodine adsorption from the vapour phase operates in possibly three ways. Chemisorbed oxygen reduces the effective pore diameters and restricts iodine penetration; chemisorbed oxygen cross-links the coal so preventing the iodine being accommodated by some relaxation of the cross-linked network; chemisorbed oxygen is electronegative and this could reduce electron availability for charge transfer complexing (2).

The adsorption of iodine from aqueous solution by oxidized coals is much less affected by the oxidation process than adsorption from the vapour phase. What is possibly happening here is that the water, by association with the chemisorbed oxygen, causes the coal to swell giving greater access to the iodine, and this effect enhances with progressive oxidation. Competition between adsorbed iodine and the water molecules becomes stronger and presumably the hydrogen bonding and clustering of water molecules (14,15) in the coal material prevents access of iodine to the macromolecular structure of coal and the balance is a diminished adsorption of iodine with increased oxidation at high relative concentrations of the isotherms (Figures 2-4). For the Cortonwood and Cwm coals, 230

the effects of oxidation are to enhance iodine adsorption at values of $C/C_0 < 0.2$. The Gedling coal, with its 9.4 wt% of oxygen has a Type II isotherm when fresh. Oxidation of the Cortonwood (5.9 wt% O) and Cwm (3.2 wt% O) coals changes these coal surfaces in a way comparable to the Gedling coal. The large extents of iodine adsorbed by the fresh coals, in the order of 6 mmol g^{-1} (equivalent surface area of $1,500 \text{ m}^2 \text{ g}^{-1}$ (25)) may also involve clustering of iodine molecules (7, 12). The presence of oxygen in the coal (either rank or oxidation related) creates sites of high adsorption potential which are covered at the lower values of relative concentration. Karsner and Perlmutter (26), in studies of coal drying and oxidation, report changes in the macro-molecular and microporosity of coals. Hence for the Cortonwood and Cwm coals the drying process associated with oxidation at e.g. 200°C could cause decreases in size of micro-porosity so enhancing the adsorption potential and shifting isotherm shape to a Type II. The studies of Oda *et al.* (27) on methanol and hexane densities of oxidised coals showed that coal density increased during the initial stages of oxidation. How this affects pore sizes remains to be clarified.

The variation of extent of iodine adsorption with time for fresh and oxidized Cortonwood and Cwm coals is illustrated in Table 4. The rate data approximate to first-order kinetics and what is clear is that rates of iodine adsorption decrease with severity of oxidation, more so for the Cortonwood coal. This suggests a diffusional limitation to adsorption with a possible pore narrowing as drying and oxidation proceed.

4.3 Adsorption of iodine by pyrolyzed coals

The findings of this aspect of the study (Figures 7-10) are that for the three fresh Gedling, Cortonwood and Cwm coals the effect of increasing heat treatment temperature (HTT) is to enhance iodine adsorption to a minimum of HTT of 400°C followed by a rapid decrease to 600°C (Figure 7). The chars (HTT 700°C) of Gedling and Cwm coals are able to adsorb iodine (equivalent to about $300 \text{ m}^2 \text{ g}^{-1}$) whereas the Cortonwood coke adsorbs no iodine.

The effects of oxidation for the Gedling coal (Figure 8) are to reduce the overall extent of iodine adsorption, to promote a minimum in adsorption at an HTT of 300°C but with still a maximum at 400°C and to decrease the HTT of closure of the porosity. This latter effect is very pronounced for the Cortonwood and Cwm coals (Figures 9,10). The rise in adsorption capacity with increasing HTT (Figure 8) is also found using nitrogen and carbon dioxide as adsorbates (28-30) but the magnitude of iodine adsorption (equivalent to $1750 \text{ m}^2 \text{ g}^{-1}$) must not be overlooked. The effect of pyrolysis could be to reduce, thermally, the cross-link density of coals and this allows greater access of iodine into the macromolecular system. Increasing HTT causes loss of volatile with considerable enhancement of cross-link density so reducing the ability of iodine to adsorb from an equivalent of 1750 to $300 \text{ m}^2 \text{ g}^{-1}$. The effect of oxidation of coals on their carbonization behaviour is to promote further the development of cross-links with increasing HTT (Figures 8-10). The evidence available from the water adsorption data is to suggest that oxygen cross-links are not formed during the oxidation process.

5. Conclusions

5.1 Adsorption of iodine by fresh coals

Adsorption of iodine by coals differs in mechanism from adsorption of nitrogen and carbon dioxide. Complexing of iodine with the molecular components of coal to the extent of an equivalent $1750 \text{ m}^2 \text{ g}^{-1}$ probably involves molecular clustering of iodine. Iodine adsorption by coals, at constant relative concentrations, is indicative of cross-link density of coals and is rank dependent. Extents of adsorption of iodine from the vapour phase are

significantly lower than from aqueous solution. The adsorption of iodine from the aqueous phase is dependent upon a co-operative effect with adsorbed water.

5.2 Adsorption of iodine by oxidized coals

Oxidation and associated drying of coal changes coal structure, removes hydrogen, introduced chemisorbed oxygen but probably does not create oxygen cross-links. Oxidation of coal reduces its capability for iodine adsorption from vapour and aqueous phases but water vapour adsorption is enhanced. Isotherm shape is changed and is indicative of structural change.

5.3 Adsorption of iodine by pyrolysed coals

Pyrolysis of fresh coals to 400°C enhances extents of iodine adsorption probably because of breakage of cross-links. Further pyrolysis severely enhances cross-link density. For all oxidised coals, in particular Cortonwood and Cwm heat treatment causes marked reductions in iodine adsorption, probably due to formation of oxygen cross-links.

Acknowledgements

The authors thank Miss B.A. Clow and Mrs. P.N. Wooster for assistance with the manuscript.

References

1. Kipling J.J., Sherwood J.N. and Shooter D.V., *Trans. Faraday Soc.*, 1964, 60, 401.
2. Aronson S., Schwebel A. and Sinensky G., *Carbon*, 1976, 14, 93.
3. Juhola A.J., *Carbon*, 1975, 13, 437.
4. Puri B.K. and Bansal R.C., *Carbon*, 1965, 3, 227.
5. Hill A. and Marsh H., *Carbon*, 1968, 6, 31.
6. Meguro T., Tonikari N. and Katanabe N., *Carbon* 1985, 23, 137.
7. Mulliken R.S. and Person W.E., "Molecular Complexes", John Wiley and Sons, N.Y., 1969.
8. Gregg S.J. and Sing K.S.W., "Adsorption, Surface Area and Porosity", 2nd Edition, Academic Press, London 1982.
9. Smisek M. and Cerny S., "Active Carbon", Elsevier, 1970, p. 135.
10. Aronson S., Sinensky G., Langsam Y. and Binder N., *J. Inorg. Nucl. Chem.*, 1976, 38, 407.
11. Pimentel G.C. and McClellan A.L. Ed. "The Chemical Bond", Linus Pauling, 1960.
12. Foster R., "Organic Charge Transfer Complexes", Academic Press, London, 1969.
13. Kim D. and Reiss H., *J. Phys. Chem.*, 1985, 89, 2728.
14. Allardice D.J., and Evans D.G., "Analytical Methods for Coal and Coal Products", Ed. Clarence Karr Jr., Academic Press, N.Y., 1978.
15. Mahajan O.P. and Walker P.L. Jr., *Fuel*, 1971, 50, 308.
16. "Coal Petrology", Ed. E. Stach *et al.* Gebruder Borntraeger, Berlin 1982.
17. Green T., Kovac J., Brenner D. and Larsen J.W., "Coal Structure" Ed. R.A. Meyers, Academic Press, N.Y., 1982, pp. 199-282.
18. Davidson R.M., *Coal Science*, Vol. I, Ed. M.L. Gorbaty, Academic Press, N.Y., 1982.
19. Given P.H., Marzec A., Barton W.A., Lynch L.J., and Gerstein B.C., *Fuel*, 1986, 65, 155.
20. Grint A., Marsh H. and Clarke K., *Fuel*, 1983, 62, 1355.
21. Larsen J.W., Personal Communication (1984).
22. Marsh H., *Fuel*, 1965, 44, 253.
23. Marsh H. and Siemieniowska T., 1965, 44, 355.
24. Mahajan O.P., "Coal Structure", Ed. R.A. Meyers, Academic Press, N.Y., 1982, pp. 51-86.

25. Sing K.S.W., Everett D.H., Paul R.A.W., Moscou L., Pierotti R.A., Rouquerol J. and Siemieniowska T., Pure and Applied Chem., 1985, 57, 603.
26. Karsner G.G. and Perlmutter D.D., Ind. Eng. Chem., Process Des. Dev. 1982 21(2)348-50 (ENG).
27. Oda H., Takeuchi M., and Yokokawa C., Fuel, 1981, 60, 390.
28. Toda Y., Fuel 1973, 52, 36.
29. Jenkins J.R., Nandi S.P. and Walker P.L. Jr., 1973, 52, 288.
30. Siemieniowska T., Tomkow K., Jankowska A. and Jasienko S., Fuel, 1985, 64, 481.

Table 1

Elemental Analyses of Coals (wt% dmmf)

Coal	%C	%H	%O	%N
Siemenowice	80.3	4.7	12.1	2.3
Gedling	81.6	5.2	9.4	1.7
Cresswell	82.3	4.6	10.1	1.8
Markham D.H.	82.3	5.7	7.9	1.5
Cortonwood	84.2	5.6	5.9	1.7
Manif. Lip	84.5	5.5	5.9	1.9
Horden	86.3	5.4	4.1	1.8
Cwm	90.0	5.0	3.2	1.6
Oakdale L.C.	91.7	4.8	2.0	1.6
Taft Merthyr	92.4	4.2	1.6	1.5
Cynheidre	95.2	2.9	0.9	1.0

Table 2

Adsorption of Iodine from Vapour and Solution and of Water Vapour

Coal Treatment Oxid. in days (d)	Adsorption of Iodine from Vapour $P/P_0 = 1.0$		Adsorption of Iodine from Solution $C/C_0 = 0.6$		Adsorption of Water Vapour $P/P_0 = 1.0$	
	mmol g^{-1}	$\text{cm}^3 \text{g}^{-1}$	mmol g^{-1}	$\text{cm}^3 \text{g}^{-1}$	mmol g^{-1}	$\text{cm}^3 \text{g}^{-1}$
<u>Cedling</u>						
Fresh	2.7	0.10	5.8	0.22	6.3	0.11
Oxid. 1d 100°C	2.5	0.10	5.6	0.21	7.0	0.13
2d 100°C	2.3	0.09	5.3	0.20	6.8	0.12
1d 150°C	1.1	0.04	5.0	0.19	7.3	0.13
1d 200°C	0.13	0.005	3.8	0.14	8.4	0.15
2d 200°C	0.09	0.003	3.6	0.14	8.2	0.15
<u>Coronwood</u>						
Fresh	1.4	0.05	6.8	0.26	6.6	0.014
oxid. 1d 100°C	1.2	0.04	6.7	0.25	1.1	0.020
2d 100°C	1.1	0.04	6.4	0.24	1.2	0.022
1d 150°C	0.7	0.03	6.2	0.23	2.1	0.038
1d 200°C	0.07	0.003	5.4	0.13	5.1	0.092
2d 200°C	0.06	0.003	3.5	0.13	6.4	0.115
<u>Canb</u>						
Fresh	1.5	0.06	4.6	0.17	0.8	0.014
Oxid. 1d 100°C	1.2	0.04	4.4	0.17	0.9	0.016
2d 100°C	1.2	0.04	3.9	0.15	1.0	0.018
1d 100°C	0.8	0.03	3.6	0.14	1.4	0.025
1d 200°C	0.16	0.006	3.3	0.13	3.2	0.058
2d 200°C	0.09	0.003	2.5	0.10	4.5	0.081
<u>Activated Charcoal</u>						
Fresh	-	-	3.8	0.15	-	-
Oxid.	-	-	4.3	0.19	-	-

Table 3

Swelling Ratio for Coals in Water and Iodine Aqueous Solution

Oxidation State	Coal: H ₂ O Q = Vf/Vi			Coal: I ₂ /I ₃ /H ₂ O Q = Vf/Vi		
	Gedling	Cortonwood	Cwm	Gedling	Cortonwood	Cwm
Fresh	1.00	1.00	1.00	1.06	1.00	1.00
Oxid. 1D 100°C	1.02	1.05	1.02	1.05	1.01	1.01
2D 100°C	1.04	1.07	1.02	1.09	1.00	1.02
1D 150°C	1.10	1.07	1.07	1.10	1.03	1.00
2D 150°C	1.14	1.07	1.03	1.12	1.03	1.02
1D 200°C	1.17	1.17	1.02	1.16	1.06	1.00
2D 200°C	1.25	1.17	1.03	1.17	1.15	1.09
1D 250°C	-	1.27	1.19	1.23	1.19	1.16
2D 250°C	-	1.31	1.17	1.20	1.23	1.16

Table 4

Kinetics of Adsorption of Iodine from
Solution

Oxidation State	-k values * x 10 ⁻³ days ⁻¹	
	Cortonwood	Cwm
Fresh	9.4	6.6
Oxid. 1D 100°C	8.1	6.6
Oxid. 2D 100°C	6.3	5.6
Oxid. 1D 150°C	6.3	5.8
Oxid. 2D 150°C	6.5	-
Oxid. 1D 200°C	3.8	3.5
Oxid. 2D 200°C	3.7	3.8

* 1st order kinetics in $\left\{ \frac{I_2}{I_2} \right\} = -kt$

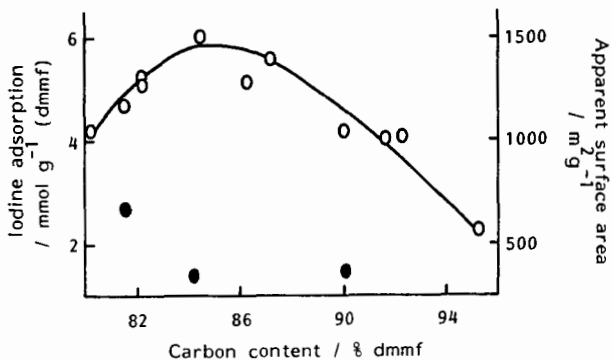
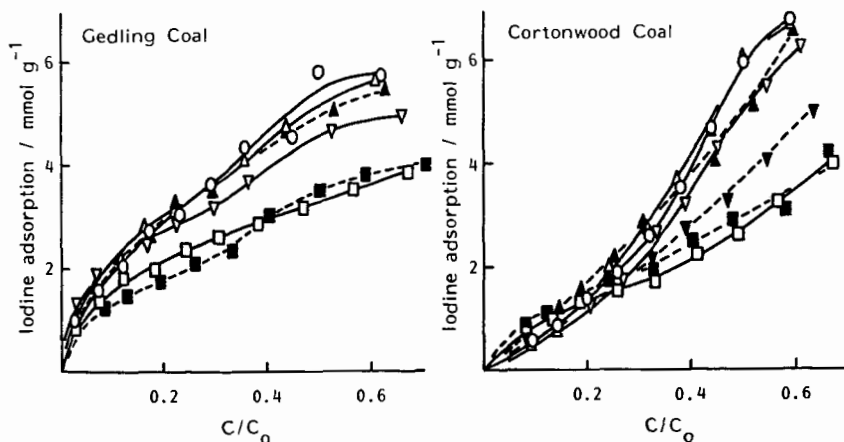


Figure 1. Variation of iodine adsorption with coal rank from vapour and aqueous phases ($I_3^-/I^-/H_2O$). ($t_{eq} = 28$ days).

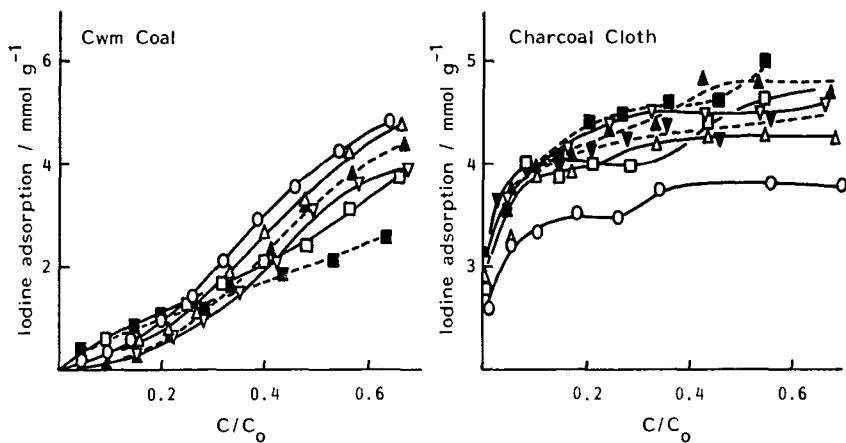
Iodine adsorbed from the vapour phase.

$1 \text{ mmol } I_2 = 250 \text{ m}^2 \text{ g}^{-1}$ of surface. $\sigma = 0.40 \text{ nm}^2$.



Figures 2 and 3. Variation of iodine adsorption from aqueous phase with iodine relative concentration for fresh and oxidized Gedling and Cortonwood coal ($T = 298 \text{ K}$; $t_{eq} = 28$ days).

○ Fresh; ▲ 1 day, 100°C ; ▲ 2 days, 100°C ; ▼ 1 day, 150°C ;
 ▼ 2 days, 150°C ; □ 1 day, 200°C ; ■ 2 days, 200°C



Figures 4 and 5. Variation of iodine adsorption from aqueous phase with iodine relative concentration for fresh and oxidized Cwm coal and activated charcoal cloth ($T = 298 \text{ K}$; $t_{\text{eq}} = 28 \text{ days}$ and 7 days respectively).

○ Fresh; Δ 1 day, 100°C; ▲ 2 days, 100°C; ▼ 1 day, 150°C;
 ▼ 2 days, 150°C; □ 1 day, 200°C; ■ 2 days, 200°C

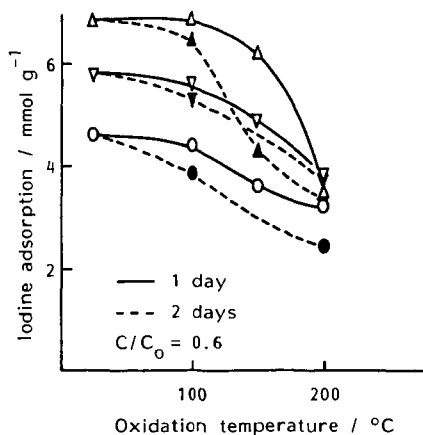


Figure 6. Variation of iodine adsorption from aqueous phase with oxidation temperature for three coals.

Δ Cortonwood Coal ▼ Gedling Coal ○ Cwm coal

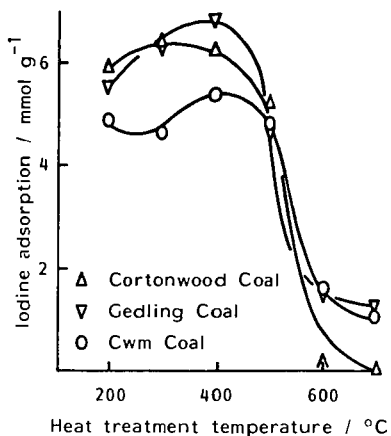


Figure 7. Variation of iodine adsorption from aqueous phase with heat treatment temperature for three fresh coals.

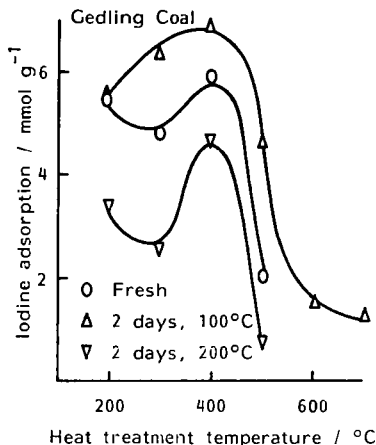
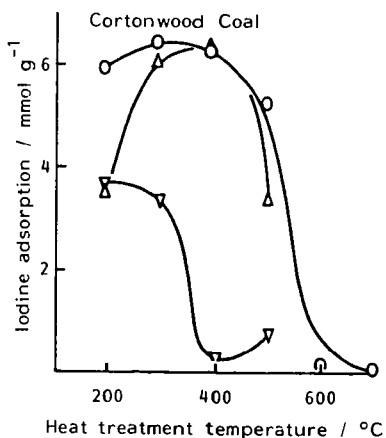
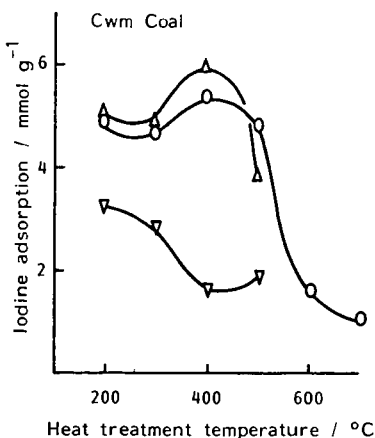


Figure 8. Variation of iodine adsorption from aqueous phase with heat treatment temperature for fresh and oxidized Gedling coal.



Figures 9 and 10. Variation of iodine adsorption from aqueous phase with heat treatment temperature for fresh and oxidized Cortonwood and Cwm coal.

○ Fresh; △ 2 days, 100°C; ▽ 2 days, 200°C



Porosity and Solvent-induced Pore Reconstruction in Coal as Determined by Neutron and Light Scattering Techniques

Jon S. Gethner

Corporate Research Laboratories
Exxon Research and Engineering Company
Annandale NJ 08801

Most naturally occurring coals are high surface area, microporous materials. Depending upon the rank of the coal, void volumes which range from as little as a few percent to as much as 50% are measured. Since the void dimensions extend to molecular size range, the corresponding surface areas are large (ranging to several hundred meters per cubic centimeter of solid). There are many consequences of the small void dimensions and large surface areas(1). The importance of porosity in determining internal mass transport characteristics of coals is widely accepted. Similarly, mass transport, and hence porosity, is assumed to be an important determinant of reactivity.

The explicit connection between mass transport through the void volume and reactivity has never been convincingly demonstrated. Recently, Suuberg has demonstrated that mass transport control can be used to alter the products in a coal pyrolysis reaction(2). Even this leaves unanswered many fundamental questions involving porosity and reactivity.

In this paper, we review some of the work carried out in this laboratory which was designed to "fingerprint" and semi-quantitatively characterize coal porosity and examine the effect of a variety of simple physical and solvent treatments on the coal. Commonly employed methods for porosity determination generally examine coal under specialized conditions and use specific solvents or gases(3). Such measurements do not directly permit one to answer the question of fundamental importance -- what is the void structure during the reaction or while a solvent is in contact with the coal.

We have employed a variety of non-intrusive optical techniques to examine the pore structure of coal both dry and in the presence of solvents. We discuss results from two--small-angle neutron scattering and visible light scattering. To date our experiments have been performed at ambient temperature. However, there is no fundamental limitation to extending these techniques to elevated temperature regimes. Indeed, since many common metals are nearly "transparent" to neutrons and visible light can be coupled into closed systems with fiber-optic techniques, the usual problems associated with in-situ measurements of coal

under technologically interesting conditions can be overcome.

Small-angle Neutron Scattering

Small angle scattering techniques have been applied to a large variety of structural studies of liquid and solid phase materials(4). The two radiation sources which have proven to be of importance for solid-state studies are x-rays and neutrons. We chose neutrons for two principal reasons: 1). The contrast, and hence the scattering efficiency, of included mineral matter with respect to organic components is small (by comparison to x-rays). Therefore, scattering due to mineral matter inclusions will not overwhelm the scattering due to the presence of voids. 2). The pore-to-carbon (or mineral) matrix contrast can be controlled by the addition of organic liquids containing hydrogen and deuterium atoms. Thus, the "visibility" of the voids can be controlled thereby allowing the scattering from the voids to be isolated from other sources of scattering (e.g. matrix structure, mineral inclusions). The wavelength of neutrons employed are generally in the 4 to 8 Angstrom range. This allows void structures in the range of about 2 to 40 nm to be examined and corresponds well with the micro pore and transitional pore regimes probed by nitrogen-BET and CO₂ adsorption-desorption measurements(3).

Light Scattering

Scattering studies employing visible light have several advantages as compared to those utilizing neutrons. The equipment needed is more readily available. Additionally, the size range probed is larger (ca. 50 nm to 2 micrometers) and is probably more important in determining the overall internal mass transport than is the micro and transitional pore volume. However, studies employing visible light have been impeded by the high optical density of coal. We have employed sub-micron thickness wafers of coal to overcome the latter and permit the direct measurement of the scattering and absorption strengths of coal which is immersed in a series of common organic solvents(7,8). The wavelength dependence of the absorption gives, in principal, information about the molecular components. The wavelength dependence of the scattering provides information about the sizes and shapes of the voids.

We have employed two different methods to perform these measurements. In early work, a microspectrophotometer operating in the near-UV to near-IR region of the spectrum was employed(8). This apparatus could not separate absorptivity changes from scattering changes. Hence data interpretation assumed that the absorptivity was unchanged upon solvent treatment. This assumption was confirmed in later work(9) in which a spectrometer was employed that was

capable of separately determining the scattering and absorptivity.

Void Volume Exhibits Adsorption Selectivity

We have carried out studies in which dried coal was exposed to water vapor(5,9), the vapor of various organic liquids(6,9), and slurried with water and several common organic liquids(7,9). In the case of exposure to aqueous media (either vapor or liquid), penetration into the void volume followed by condensation was found to be difficult. This was first noted in early neutron scattering experiments(5) in which D₂O vapor was found to incompletely fill the smallest voids of a broad void distribution. Subsequently we observed penetrability difficulties with some of the non-aqueous solvents used in the light(9) and later neutron scattering(7) experiments. One experimental consequence of the difficulty of aqueous penetration into dry coal is that extra care had to be taken to insure complete (aqueous) liquid penetration into the powdered coal slurries used both in later neutron scattering(7) as well as light scattering(9) work.

Reversible Deformation of Coal Thin-sections

In the case of sample preparation for light scattering, fascinating physical effects could be observed when the coal thin-sections were first placed under vacuum and then exposed to a moderate pressure (50 Torr < P < 760 Torr) of "non-wetting" liquids or vapors. Unlike particulate coal, a coal thin-section is easily deformed by "wrapping-up" on itself. Immersion in some vapors and liquids (esp. water) resulted in a non-penetrating "skin" on the thin-section surface. When the system pressure was increased (either by allowing access to air or controllably introducing a sub-atmospheric pressure of helium), the thin-section "collapsed". If this process was carried out in a controlled manner, the thin-section could be "rolled-up" in a spiral fashion upon application of system pressure and "unrolled" to its original shape and dimensions by removal of the higher system pressure. Our interpretation of this phenomena is that the non-wetting vapor or liquid skin prevents the system pressure from being equalized in the interior of the thin-section. The thin-section must then deform to relieve the resulting stress. The easiest physical transformation which will achieve the stress reduction is one which minimizes the "surface" area. In view of the geometry of the thin-section (0.5 micron thick by 1 mm by 1 mm) and the fact that cutting-induced fractures are present in the "plane" of the thin-section, the "rolling-up" of the thin-section is a reasonable method to relieve the induced stress. What is surprising is that the structural integrity in the "plane" of the thin-section is so great that the thin-section can be reversibly compressed into a microscopic area and returned

to its original shape. We were able to repeat such reversible cycles at least 4 to 6 times before any noticeable physical damage to the thin-sections were evident. Even then, the resulting damage appeared to be confined to tearing along previously weakened boundaries. These observations, though qualitative and empirical, are the most graphic demonstration that this author has even seen in support of coal being an internally crosslinked, gel-like material.

Void-size Distribution is Continuous

The void-size distribution was examined in dry coal as well as coal treated with liquids which are generally believed to have little or no effect on the internal pore structure (5,7,9). In our earliest neutron scattering work, power-law-like behavior was observed from coals both dry and exposed to the equilibrium vapor pressure of H_2O and D_2O (5). Such power-law behavior can arise from void or matrix structures having different geometrical properties, including fractal. Similar behavior has been reported by Bale and Schmidt and interpreted as arising from an internal surface fractal structure (10). In view of the limited range length scale range over which data is collected, the applicability of the fractal model as opposed to an unspecified broad and continuous distribution is questionable.

In subsequent neutron scattering work we confirmed the presence of near power-law behavior and continuous void-size distributions(7). The extension of scattering curves to probe larger length scales was achieved by observing the visible light scattering(9). Though the interaction of the radiation with the coal is different, the principal light scattering mechanism is that of pore-to-void contrast. Therefore, the light and neutron scattering curves can be "joined" in order to observe the scattering function over a wider length scale. From such a curve analysis, it is clear that the existence of a broad, continuous distribution of void-sizes is confirmed. Clear power-law behavior indicating fractal behavior is not observed. Comparisons with computer generated scattering curves for reasonable fractal structures indicates that exact adherence to a fractal model is unlikely(11). However, the near power-law behavior is evidence that a model incorporating an overall fractal structure with allowance for local deviations may be appropriate.

Micro Pores Are Unchanged by Non-swelling Solvents and Exhibit Penetrability Restrictions

Neutron scattering measurements of coal slurried in cyclohexane indicates that the micro and transitional pore distribution is unchanged from that in dried coal. Some

difficulty in filling of the smallest pores was observed. Differential scattering measurements can be used to obtain information about the unfilled voids. They were found to be modeled well by long, needle-like voids having a cross-sectional diameter of about 2 nm. Contrast matching techniques employing a series of cyclohexane/perdeutero-cyclohexane and H_2O/D_2O slurries indicate that the overall void surface is largely comprised of aliphatic and aliphatic carboxylic acid species. Therefore, the penetrability restrictions observed might indicate that intermolecular hydrogen-bonding interactions and a polar surface prevent complete penetration of the non-polar cyclohexane. This hypothesis contrasts with the usual restricted pore-entrance model. The polar-surface, hydrogen-bonding model implies that a large number of carboxylic acid dimers and multimers will be present on the surface of the void. Some confirmatory evidence that such species exist in large proportion is available from in-situ FT-i.r. experiments performed in this laboratory(12).

Transitional and Macro Pores Are Easily Deformed

The structural "rigidity" upon solvent saturation which is observed in the small void-size regime is not observed in the larger size regime probed by light scattering. Though broad continuous distributions were observed in coal immersed in each of 7 liquids, significant changes in the details of the distribution after liquid immersion were observed with all liquids(9). Surprisingly, even those liquids which result in little or no swelling (e.g. water, cyclohexane) show clear evidence for void-structure alterations. The void-structure alterations were accompanied, in all cases, by an increase of the total void-volume contributing to the light scattering. Though the size-range probed by light is broad, it does not encompass all sizes. Therefore, the mechanism for the volume increase is currently uncertain. One possibility is the "swelling" of voids which are smaller than the resolution limit of the light scattering measurement. Concomitant changes in the low-angle portion of the neutron scattering curves are ambiguous in this regard.

Light-transmission Losses Through Coal Result From Light Scattering

The origin of the high optical density of coal has long been the subject of study and debate(12). Our early work indicated that the overall light-transmission through coal can be substantially increased by immersion in liquid(8). This was subsequently confirmed in studies in which we simultaneously measured both the absorptivity and the light scattering through coal immersed in 7 different liquids(9). The liquids were chosen to cover a range of interaction

properties from non-swelling to highly-swelling and optical properties from low to high index of refraction.

In the mid-visible region of the spectrum, light scattering losses were found to account for over one half of the total light attenuation through coal. Additionally, negligible changes in the absorptivity were found upon immersion in the wide variety of solvents. The latter is not surprising since the molecular components leading to the absorptivity are unchanged. Significant contributions to the absorptivity due to aromatic-aromatic stacking interactions is unlikely in view of the observed insensitivity of the absorptivity to immersion in the variety of liquids chosen.

The large component due to light scattering and its significant wavelength dependence has important consequences on the interpretation of transmission and reflectivity data. Measurements made on coal undergoing any type of physical or chemical change will be accompanied by changes in pore geometry and possibly pore filling. Therefore, over most of the visible region of the spectrum, the dominant cause of light transmission changes will result from structural changes to the coal rather than chemical composition changes. Such transmission changes are frequently assumed to arise from absorptivity, hence molecular structure changes, and are interpreted in terms of chemical alteration to the coal. This cannot be correct. One example is the interpretation of color changes which occur when thin-sections having a thickness of several microns are treated with solvent or subject to reaction. By virtue of the strong wavelength dependence of the scattering, small changes in thickness or pore geometry will substantially alter the transmission losses, in this case. A color change can easily arise by altering the spectrum of the light transmitted through a coal thin-section or reflected from its surface.

While such light scattering effects have not been systematically dealt with in optical studies of coal, their quantification offers the possibility of preparing semi-transparent coal slurries in which the true changes to molecular absorption can be observed. In any such studies, it is critical that the wavelength dependence of the transmission and reflection spectrum be examined in order that the optical changes be properly assigned. A particularly interesting possibility is the measurement of internal network structure changes using polarized absorption and scattering measurements.

Summary

Neutron small-angle scattering and light scattering measurements of low and medium rank (sub-bituminous and bituminous) coals indicate that the void structure of coal

is best modeled as a continuous distribution of voids rather than a well defined discrete pore distribution. Solvent permeation studies indicate that the smallest voids are difficult to fill with a liquid when the liquid does not easily wet the surface. Solvent penetration into the void structure reduces the overall optical density of the coal with respect to the transmission of visible light. Analysis of the transmitted and diffusely scattered light indicates that the solvent partially index matches the void to the coal matrix with the resulting transmission increase. Analysis of the wavelength dependence shows that all imbibed liquids alter the internal pore and matrix geometries and generally results in an overall increase in the volume fraction of pores observed.

These observations imply that the pore structure is not a uniquely defined volume even at ambient temperature. Rather it is quite fluid and easily deformed upon application of mechanical stress. The light and neutron scattering from coal can be used to provide a fingerprint of the pore (and complimentary matrix) structure. Changes in the scattering can provide considerable detail about induced changes to the structure. Combined light scattering and absorption measurements, such as described herein, can be used to separate, uniquely, the chemical changes from the physical changes which occur during coal treatment and reactions.

Acknowledgement

The contributions of Drs. H. Kaiser and R.B. Stephens in aspects of the work were instrumental. Discussions with Drs. S.K. Sinha, C. Glinka and Prof. J.W. Larsen during various aspects of the work provided important perspective and understanding at many critical points. The technical assistance of G.W. Nalavany and G. Meyers made much of the work practical. Finally, the use of the small-angle neutron scattering spectrometers at the University of Missouri Research Reactor Facility and the National Bureau of Standards Reactor Facility is gratefully acknowledged.

References

1. a). D.W. vanKrevelen, Coal (Elsevier, Amsterdam, 1961).
b). R.C. Neavel, in Advances in Chemistry Series 192--Coal Structure, edited by M.L. Gorbaty and K. Ouchi (American Chemical Society, Washington, D.C., 1982), pp. 1-14.
c). H.H. Lowry, Editor, Chemistry of Coal Utilization--Supplementary Volume (Wiley, New York, 1963).
d). W.R. Grimes, in Coal Science--I, edited by M.L. Gorbaty, J.W. Larsen, and I. Wender (Academic, New York, 1982), pp. 21-42.
e). O.P. Mahajan in Coal Structure, edited by R.A.

- Meyers (Academic, New York, 1982), pp. 51-86
2. E. Suuberg, in Coal Conversion Chemistry, edited by R.H. Schlossberg (Plenum, New York, 1985).
 3. a) H. Gan, S.P. Nandi, and P.L. Walker, Jr., Fuel **51**, 272 (1971).
 b) O.P. Mahajan and P.L. Walker, Jr., in Analytical Methods for Coal and Coal Products, edited by C. Karr, Jr. (Academic, New York, 1978), Vol. I, pp. 125-162.
 4. a) J.S. Higgins and R.S. Stein, J. Appl. Cryst. **11**, 346-375 (1978).
 b) V. Gerold and G. Kostorz, J. Appl. Cryst. **11**, 376-404 (1978).
 c) H.B. Stuhmann and A. Miller, J. Appl. Cryst. **11**, 325-345 (1978).
 d) G. Kostorz in Treatise on Material Science and Technology **15**, edited by G. Kostorz (Academic, New York, 1979) pp. 287-289.
 5. H. Kaiser and J.S. Gethner in Proceedings of the 1983 International Conference on Coal Science (International Energy Agency, London, 1983) pp. 300-303.
 6. J.S. Gethner, unpublished data.
 7. J.S. Gethner, J. Appl. Phys. **59**, 1068-1085 (1986).
 8. J.S. Gethner, J. Chem. Soc., Faraday Trans. 1, **81**, 991-1001 (1985).
 9. R.B. Stephens and J.S. Gethner, Solvent-induced Reduction of the Light Scattering from the Pore Volume of Coal, submitted to Energy and Fuels.
 10. H.D. Bale and P.W. Schmidt, Phys. Rev. Lett. **53**, 596 (1984).
 11. J.S. Gethner, unpublished calculations.
 12. J.S. Gethner, Appl. Spectros., to be published (1987).
 13. H. Schmalzer and E. deRuiter, in Chemistry of Coal Utilization-Supplementary Volume, ed. H.H. Lowry (Wiley, New York, 1963)

Microstructural Variations of Three American Coals and Their High Temperature Chars

Wei De Jiang, In-Chul Lee and Ray Y. K. Yang

Department of Chemical Engineering
West Virginia University
Morgantown, WV 26506-6101

Microstructure of a North Dakota lignite, a Washington subbituminous and a New Mexico bituminous coal and their chars produced by devolatilization in nitrogen at 1000 to 1300°C was investigated in this work using the CO₂ adsorption method conducted at 25°C. For each coal and char, specific surface area, micropore volume, micropore surface area, mean equivalent radius of micropores and characteristic energy of adsorption, as well as micropore volume distribution, were determined and tabulated, and their variations with devolatilization temperature studied and interpreted. It was found that, overall, specific surface areas, micropore volumes and micropore surface areas of chars decreased monotonically as devolatilization temperature was raised from 1000 to 1300°C, although most of these values were much larger than that of their parent coals. The micropore volume distributions obtained were interpreted and found to provide an interesting insight into the microstructural variations of coals and chars.

Introduction

It is well known that coals and their chars possess a complex intraparticle pore structure, similar to the structure of a tree [1], with micropores (4-12Å) expanding gradually into mesopores (12-300Å) and eventually macropores (>300Å) [2]. For most coals and chars, surface areas and thus active sites for gasification are provided mainly by micropores, although mesopores and macropores are also needed to serve as feeder pores for transportation of reactant molecules to the micropores. Depending on the gasification condition and other factors, the intraparticle diffusional resistance caused by this complicate pore structure may become rate limiting. Hence the reactivity of coals and their chars during gasification is closely related to their microstructures.

Changes in surface areas of coals during devolatilization have been investigated by several research workers [3-5]. They observed that specific surface area increased with increasing devolatilization temperature, passed through a maximum at about 600-700°C and decreased thereafter. However, the heating rates involved were less than 20°C/min, which were too slow to be of practical use for commercial gasifiers, particularly the entrained flow type.

In the present work, specific surface area, micropore volume distribution and other microstructural parameters of three American coals of different rank and their chars were determined. The chars were prepared by devolatilization in a nitrogen atmosphere at 1000-1300°C. The heating rates involved were over 100°C/sec. The effects of devolatilization temperature on the microstructure of coals and chars were studied and the results reported and interpreted.

Experimental

Three coals obtained from the Penn State Coal Sample Bank were used in this work. They are lignite (PSOC-1423P) from North Dakota (Hagel seam), subbituminous coal (PSOC-240) from Washington (Big Dirty seam) and high volatile C bituminous coal (PSOC-309) from New Mexico (#8 seam). The proximate and ultimate analyses of these coals are given in Table I.

A thermogravimetric analyzer (TGA), developed by Sears et al. [6] and further improved by Peng et al. [7], was used to prepare chars at atmospheric pressure and four different devolatilization temperatures, viz., 1000 to 1300°C at intervals of 100°C. The particle size range used in this study was -70 + 100 U.S. mesh (average particle size 177.5 μm). Devolatilization was carried out in nitrogen environment at the desired temperature for one minute. The chars thus obtained are called "N₂ chars" to distinguish them from the "in-situ chars" [7] obtained by devolatilization in steam. Work associated with the in-situ chars will be reported elsewhere.

One of the unique features of this TGA is that the micromotor located inside the TGA is capable of lowering the sample from less than 1500°C to extreme high temperature (up to 1700°C) in less than 10 seconds. The heating rates of the coal particles were in the range of 100 to 1000°C/sec depending on the operating conditions and the samples used [6]. All the chars produced were immediately put into air-tight vials and stored in nitrogen environment. Experiments under various operating conditions were repeated several times to check reproducibility of data. In all the cases tested the experimental errors were within $\pm 10\%$, most being within $\pm 2\%$.

Microstructural properties of the three coals and their high temperature chars were determined by gravimetric adsorption method using CO₂ as an adsorbate. Char samples produced in the TGA were used without further classification by their particle sizes, although they were outgassed overnight at 110°C and 10⁻³ torr to remove moisture which might otherwise block entrances to some micropores.

The apparatus for measuring CO₂ adsorption gravimetrically consisted of a Cahn R-100 electronic microbalance, a mechanical vacuum pump, a U-tube manometer and two pressure detectors. For each series of adsorption runs, the system was maintained at 25°C and at preselected pressures ranging from 60-700 torr. At each CO₂ pressure, the weight-gain curve of the sample was continuously recorded in a strip-chart recorder until adsorption equilibrium was reached. For each run, the time required to reach equilibrium varied, depending on the type of coal involved. For the lignite and its chars, 8-10 hours were normally needed. On the other hand, it took about 24 hours for the subbituminous coal but only 2-3 hours for its chars to reach equilibrium. For the bituminous coal, the times needed were only 4-5 hours for coal but about 24 hours for chars.

Specific surface areas were determined by means of the Dubinin-Polanyi (D-P) equation [8-10]:

$$\ln W = \ln W_0 - D \ln^n(P/P_0) \quad (1)$$

where W is the weight of CO_2 adsorbed per unit weight of sample at pressure P . P_0 is the vapor pressure of CO_2 , whose value is 63.5 atm at 25°C [10], and the corresponding W is designated as W_0 . D and n are constants determined from experimental data. For most of the cases, n is equal to 2.0. The molecular cross-sectional area of CO_2 at 25°C was taken as $25.3 (\text{\AA})^2$ [10]. The relative pressure employed in all measurements was less than 0.015 to avoid capillary condensation [11]. Properties related to micropore, such as micropore surface area, mean micropore volume, mean equivalent radius of micropore and adsorption characteristic energy [12], as well as micropore volume distribution, were calculated by the Medek's method [12].

Results and Discussion

The data obtained from the gravimetric adsorption experiments for the three coals used in this work and their high temperature chars are presented as adsorption isotherms in Figures 1-3, and as linear plots of Equation (1) with $n = 2$ in Figures 4-6. All the data shown in Figures 4-6 fall on straight lines with correlation coefficients of each linear least squares fit greater than 0.99, thus reassuring the suitability of using the D-P equation for CO_2 adsorption on these coals and chars at 25°C and the choice of $n = 2$ [10,12].

The effect of devolatilization temperature on the intraparticle structure of coals and chars is vividly demonstrated by the equilibrium isotherms presented in Figures 1-3. For each coal, as the devolatilization temperature is raised from 1000°C to 1300°C , the amount of CO_2 adsorbed per gram of char decreases monotonically. Furthermore, with the exception of chars produced from the caking coal (PSOC-309, bituminous) at temperatures above 1200°C , all the other chars exhibit significantly higher capability to adsorb CO_2 than their parent coals.

Shown in Tables 2-4 are specific surface areas, micropore surface areas, micropore volumes and mean equivalent radii of micropores of coals and chars calculated from the data presented in Figures 1-6 using the methods mentioned in the previous section. For each char, extent of devolatilization expressed in terms of percentage of coal (DAF basis) devolatilized was also included in the tables. Micropore volume distributions of the three coals and their chars were also calculated and plotted in Figures 7-9. For convenience of comparison, some of the data given in Tables 2-4 are also plotted in Figure 10.

The plots in Figure 10 clearly illustrate that, for each coal, the specific surface area of the char obtained by devolatilization at 1000°C is larger than that of its parent coal; whereas the opposite is true for the mean equivalent radius of the micropores. This will be explained later. Furthermore, as the devolatilization temperature is raised from 1000°C to 1300°C , the overall trend for each coal appears to be that of a reduction in specific surface area and an enlargement of micropore size. The only exception is the reduction of pore size for chars prepared from the caking coal (PSOC-309 bituminous) at 1300°C . As expected, extent of devolatilization of each coal increases with increasing devolatilization temperature. The adsorption characteristic energy of micropores, on the other hand, shows little variation, being in the range of 9-13 KJ/g-mole for the chars and coals tested.

A close examination of the data on specific surface area, micropore volume and micropore surface area of chars reveals a striking similarity in their dependence on devolatilization temperature. This is true for all the three coals used in this work. This similarity is obviously related to our observation mentioned before on adsorption isotherm and extent of devolatilization.

Briefly speaking, coals are composed of aromatic and hydroaromatic layers terminated at their edges by various functional groups. Different functional groups are cross-linked to each other, causing poor alignment between layers and creating micropores of molecular dimensions. Some of them are closed, while most are open to mesopores and macropores, leading to a pore-tree structure. When coals are heated in an inert atmosphere, volatile matter is released, dead pores open up and the previously open pores enlarge in size, all leading to increased pore volume and surface area. Concurrent with these, some crosslinks between aromatic layers are broken, thus allowing them to align in a more orderly fashion and resulting in a loss of pore volume and surface area.

In general, at lower devolatilization temperature, the release of volatiles predominates; while at higher temperature, structure alignment becomes dominant, as the volatile release becomes small. Hence, it is expected that over a certain temperature range, the pore volume and surface area of coal chars will go through a maximum. The temperature at which the maximum occurs depends mainly on the parent coals [13]. As mentioned before, according to a number of studies conducted by several researchers [3-4] over a temperature range of 200 to 1200°C, the maximum usually falls around 600-700°C. Since the range of devolatilization temperature in this work is well above 600-700°C, our observation of decreasing specific surface area and micropore volume with increasing devolatilization temperature is thus consistent with those reported previously.

The changes in micropore volume distributions during the course of devolatilization should reflect the major changes in the porosity of coals and chars, because most of their pore volumes are contributed by micropores. Therefore, it is worthwhile to examine more closely the micropore volume distribution frequency curves presented in Figures 7-9. It is obvious that the area under each curve represents total micropore volume per gram of sample, whose dependence on devolatilization temperature, as mentioned before, is similar to that of specific surface area.

The significant increase in micropore volume from coal to char devolatilized at 1000°C is clearly demonstrated by comparing the corresponding distribution curves shown in Figures 7-9. For all the three coals involved, the curves for chars are much higher and wider, suggesting the creation of new micropores, the enlargement of open pores and the opening up of previously closed pores. Of particular interest are the extensions of the curves for the 1000°C chars beyond the lower limit of the curves for coals and their steep ascents in that region of extremely fine pores. The former implies the generation of new, extremely small micropores, and both together account for the reason why the 1000°C chars have smaller mean radii.

As devolatilization temperature increases from 1000 to 1300°C, the general trend is the reduction of the micropore volume of chars produced.

Although this holds for all the three coals involved, the behavior of the bituminous coal, a caking coal, is strikingly different from that of the other two coals, as mentioned before. While the micropore volume of the bituminous coal chars reduces rapidly down to a value well below that of the original coal, the values of the micropore volumes of the lignite and the subbituminous coal chars stay within the range of 0.12-0.17 cm³/g, which is well above that of their parent coals (see Tables 2-4). Furthermore, for the latter two coals, most of the reduction in micropore volume is due to the decrease in the number of micropores at the lower end of the distribution as shown clearly in Figures 7 and 8; whereas for the bituminous coal chars the reduction appears to be quite uniform across the whole range of micropores. The reason for this difference is worthy of further exploration.

As strong caking coal, such as the bituminous coal used in this work, is heated, it invariably passes through a softening stage. During that period, parts of the coal substance decompose and produce metastable fluid material which acts as a plasticizer and softens the mass. This unstable material, known as metaplast [14,15], primary tar or thermobitumen [16], consists of mainly heavy hydrocarbons with high viscosity and tends to seal up the micropores. The liberation of volatile matter against the sealing up leads to an initial expansion of micropores and thus an increase in the micropore volume of the resultant char (semicoke). As the temperature rises further, the semicoke, the thermobitumen and the primary volatile products start to decompose and/or polymerize. These secondary reactions eventually resolidify the plastic mass causing shrinkage of pores as well as pore blockage. The latter is due to the production of cracked carbon which deposits on the entrance of the pores. The higher the temperature, the more cracked carbon is produced and deposited uniformly throughout the whole range of the micropores, thus leading to a micropore volume smaller than that of its parent coal.

As for weak caking coal, such as the subbituminous coal used here, the plastic range is not very noticeable and the production of thermobitumen may not be significant. Hence the cracked carbon produced, though not sufficient to cover the whole range of micropores, does manage to deposit first on a portion of the finer micropores leading to a gradual reduction of the number of ultrafine micropores (see Figure 8), as pyrolysis temperature increases to 1300°C. As a result, the micropore volumes of chars decrease, but their mean equivalent radii of micropores increase. This is exactly what the data in Table 3 indicate.

In summary, the microstructural data of the three coals and their high temperature chars have been presented in this paper. In addition, the characteristics of the data have also been investigated, particularly with respect to their relation with the devolatilization temperature, and the meaning of the data interpreted.

Acknowledgements

This work was supported in part by the U.S. Department of Energy under contract No. DE-AC21-83MC20320. W. D. Jiang was on leave from the First Design Institute, Tianjin, China, during the period of this work.

References

1. Simons, G. A., *Combustion and Flame*, 26, 1 (1982).
2. Gan, H., S. P. Nandi and P. L. Walker, Jr., *Fuel*, 51, 272 (1972).
3. Toda, Y., M. Hatami, S. Toyoda, Y. Yoshida and H. Honda, *Carbon*, 8, 565 (1970).
4. Razouk, R. I., F. Z. Saleeb and A. M. Youssef, *Carbon*, 6, 325 (1968).
5. Chiche, P., H. Marsh and S. Pregermain, *Fuel*, 46, 341 (1967).
6. Sears, J. T., E. A. Maxfield and S. S. Tamhankar, *IEC Fund.*, 21, 474 (1982).
7. Peng, F. F., I. C. Lee and R. Y. K. Yang, *Proc. 3rd Pittsburgh Coal Conference*, 730-744 (1986).
8. Gregg, S. J. and K. S. W. Sing, "Adsorption, Surface Area and Porosity," 2nd Ed., Academic Press (1982).
9. Marsh, H. and T. Siemieniewska, *Fuel Lond.*, 44, 355 (1965).
10. Walker, P. L., Jr. and R. L. Patel, *Fuel Lond.*, 49, 91 (1970).
11. Johnson, J. L., "Kinetics of Coal Gasification," Wiley, 237-260,(1979).
12. Medek, J., *Fuel*, 56, 131 (1977).
13. Toda, Y., *Fuel*, 52, 99 (1977).
14. Fitzgerald, D., *Trans. Faraday Soc.*, 52, 362 (1956).
15. Chermin, H. A. G. and D. W. van Krevelen, *Fuel*, 36, 85 (1957).
16. Berkowitz, N., "An Introduction to Coal Technology," Academic Press, 152 (1979).

Table 1. Characteristics of Coals Used

	N.D. Lignite (PSOC-1423P)	Wash. Subbituminous (PSOC-240)	N.M. Bituminous (PSOC-309)
Proximate Analysis (wt%, as received)			
Moisture	29.53	18.21	10.09
Ash	5.75	18.39	18.32
Volatile Matter	31.76	32.00	33.80
Fixed Carbon	32.96	31.40	37.79
Ultimate Analysis (wt%, DAF)			
Carbon	69.80	72.59	77.08
Hydrogen	4.41	5.79	5.75
Nitrogen	1.35	1.41	1.70
Sulfur	1.14	1.30	1.02
Chlorine	0.00	0.01	0.00
Oxygen (diff.)	23.30	18.90	14.46

Table 2. Microstructural Parameters of Lignite (PSOC-1423P) and Its Chars

Sample	Coal	Char	Char	Char	Char
Devolatilization Temperature (°C)	NA	1000	1100	1200	1300
% Devolatilization (DAF basis)	NA	53.5	61.7	69.1	71.7
Specific Surface Area (m ² /g)	238	511	498	434	468
Micropore Surface Area (m ² /g)	223	496	462	399	421
Micropore Volume (x10 ² cm ³ /g)	7.7	16.6	16.2	14.1	15.2
Mean Equivalent Radius of Micropore (nm)	0.69	0.67	0.70	0.71	0.72
Adsorption Characteristic Energy (KJ/g-mole)	11.9	13.1	11.5	11.2	10.5

Table 3. Microstructural Parameters of Subbituminous Coal (PSOC-240) and Its Chars

Sample	Coal	Char	Char	Char	Char
Devolatilization Temperature (°C)	NA	1000	1100	1200	1300
% Devolatilization (DAF basis)	NA	58.3	60.4	65.6	69.3
Specific Surface Area (m ² /g)	198	499	472	451	382
Micropore Surface Area (m ² /g)	181	470	445	415	341
Micropore Volume (x10 ² cm ³ /g)	6.4	16.2	15.3	14.7	12.4
Mean Equi. Radius of Micropore (nm)	0.71	0.69	0.69	0.71	0.73
Adsorption Characteristic Energy (KJ/g-mole)	11.0	12.0	12.1	11.2	10.2

Table 4. Microstructural Parameters of Bituminous Coal (PSOC-309) and Its Chars

Sample	Coal	Char	Char	Char	Char
Devolatilization Temperature (°C)	NA	1000	1100	1200	1300
% Devolatilization (DAF basis)	NA	46.3	53.4	52.3	59.0
Specific Surface Area (m ² /g)	117	401	304	109	21
Micropore Surface Area (m ² /g)	106	373	272	95	19
Micropore Volume (x10 ² cm ³ /g)	3.8	13.0	9.9	3.6	0.7
Mean Equi. Radius of Micropore (nm)	0.72	0.70	0.73	0.75	0.69
Adsorption Characteristic Energy (KJ/g-mole)	10.7	11.6	10.3	9.4	12.0

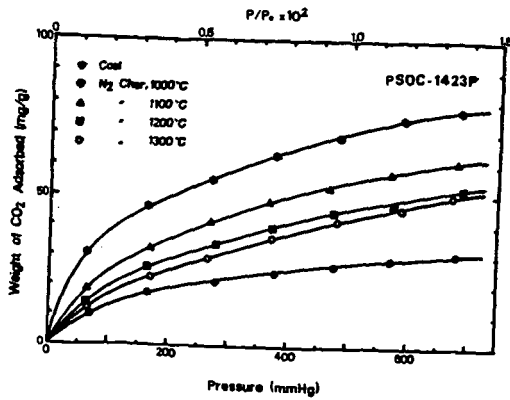


Figure 1. Isotherms of CO₂ Adsorption on Lignite (PSOC-1423P) and its chars at 25°C

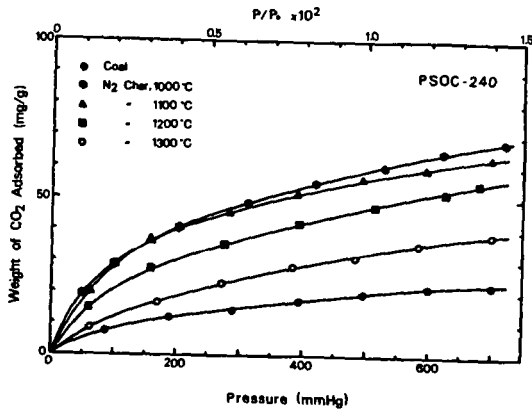


Figure 2. Isotherms of CO₂ Adsorption on Subbituminous coal (PSOC-240) and its Chars at 25°C

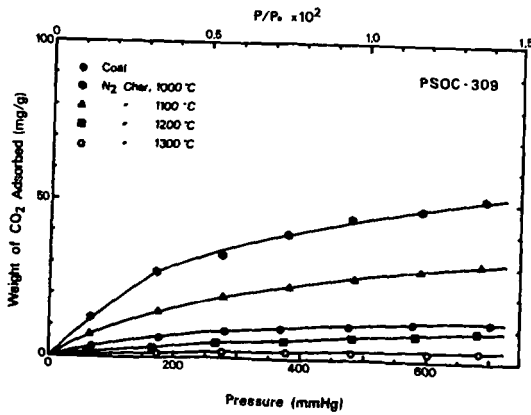


Figure 3. Isotherms of CO₂ Adsorption on Bituminous Coal (PSOC-309) and its Chars at 25°C

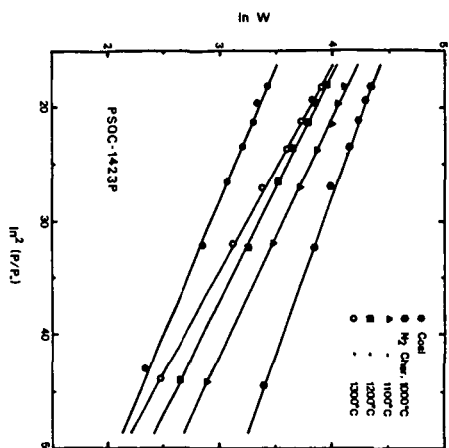


Figure 4. Linear Plots of the Isotherms from Figure 1 — Lignite

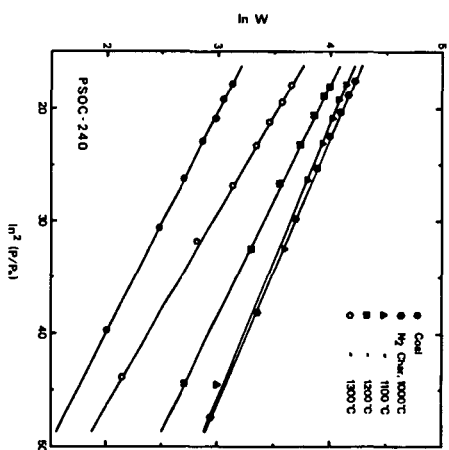


Figure 5. Linear Plots of the Isotherms from Figure 2 — Subbituminous Coal

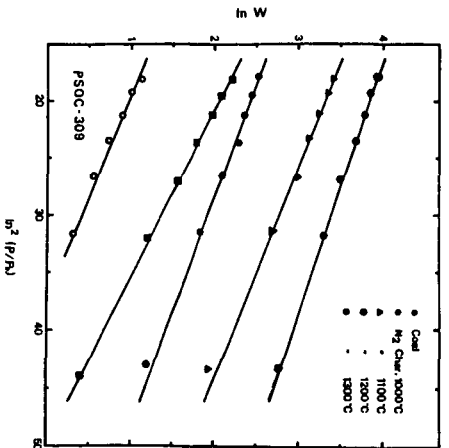


Figure 6. Linear Plots of the Isotherms from Figure 3 — Bituminous Coal

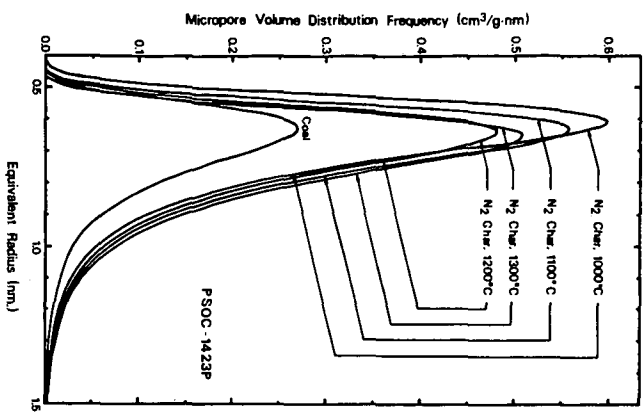


Figure 7. Micropore Volume Distributions of Lignite and Its Char.

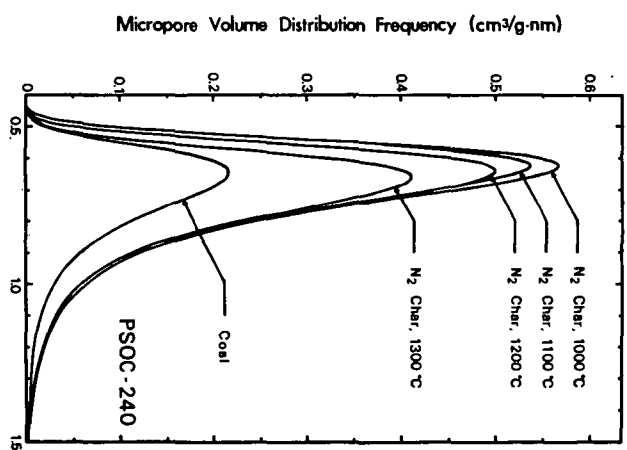


Figure 8. Micropore Volume Distributions of Substitutional Coal and Its Char.

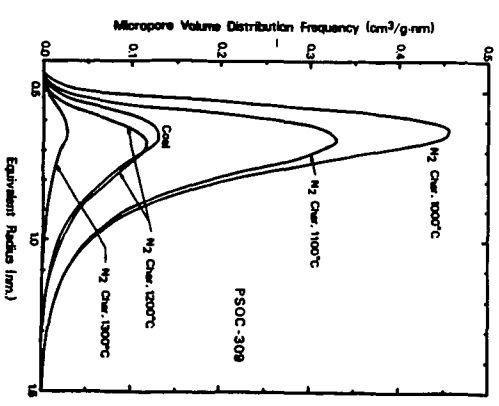


Figure 9. Micropore Volume Distributions of Substitutional Coal and Its Char.

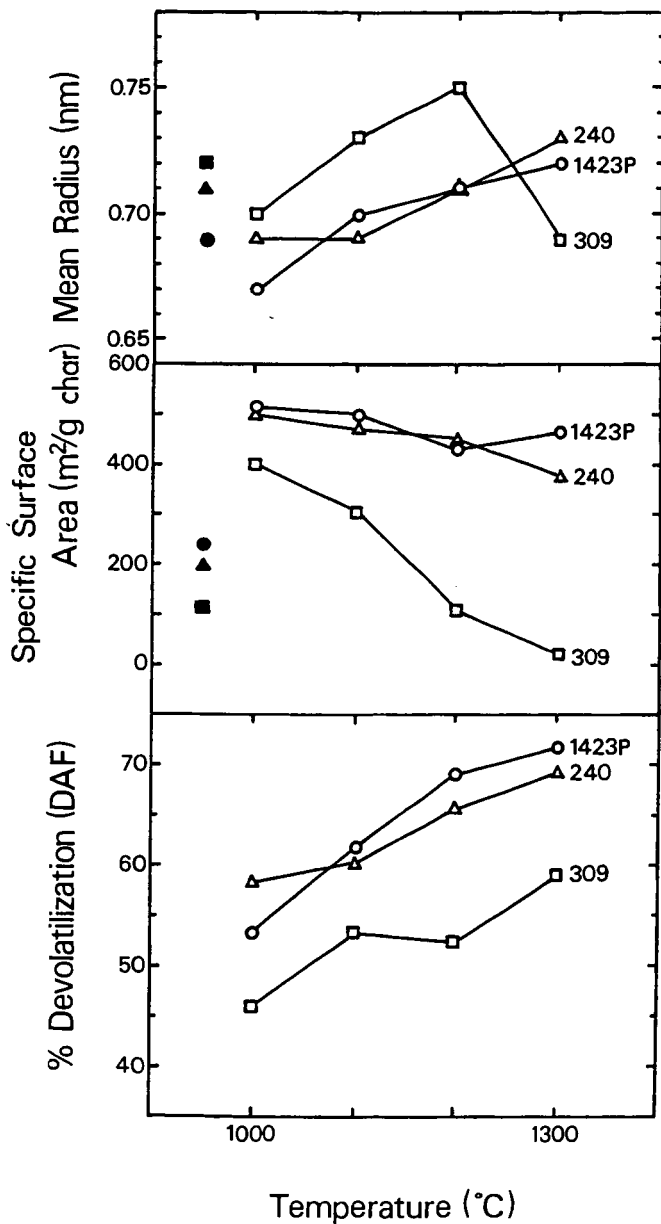


Figure 10. Effect of Devolatilization Temperature on the Microstructure of Coals and Chars (● Lignite; ○ Lignite Char; ▲ Subbituminous Coal; △ Subbituminous Coal Char; ■ Bituminous coal; □ Bituminous Coal Char)

Gas and Vapor Induced Coal Swelling

A. R. Sethuraman and P. J. Reucroft

Department of Metallurgical Engineering
and Materials Science
University of Kentucky
Lexington, KY 40506

Abstract

Dilatometric studies have been carried out on coal samples exposed to carbon dioxide at 5, 10 and 15 atmospheres and helium saturated with acetone vapor. Coals investigated included KCER 7463 (65.8% C), KCER 7122 (78.3% C) and KCER 7259 (83.8% C). Coal sample dimensions increased on exposure to both types of environment. Carbon dioxide induced swelling increased as the pressure increased. The swelling magnitude increased as the carbon content decreased, indicating that the macromolecular crosslink density in coal increases with increasing carbon content. The time to reach equilibrium swelling was shorter at higher CO₂ pressures. The swelling effect produced by acetone vapor was generally greater than that produced by CO₂ at 15 atmospheres. In the case of KCER 7259, the effect was reversed. It was estimated that the swelling effect can account for 20 to 50% of the surface area determined by CO₂ BET adsorption methods.

Introduction

Studies on the adsorption of organic vapors by coal (1) and the effect of CO₂ on coal swelling (2) have been carried out recently in order to clarify the role of adsorbate induced swelling in influencing coal surface areas determined by gas adsorption methods. BET surface areas determined by CO₂ adsorption are generally higher than N₂ surface areas (3-6). Dilatometric studies on coal samples exposed to CO₂ at 1 atmosphere showed that volume increases of up to 1.31% could be observed (2). It was concluded that swelling of this type could account for up to 14.5% of the CO₂ surface area.

The dilatometric results at 1 atmosphere indicated, however, that equilibrium swelling had not been reached at these CO₂ pressures, even at exposure times in excess of 240 hours. In the present investigation, the dilatometric studies have been extended to higher CO₂ pressures and studies have also been carried out on coals exposed to acetone vapor. The objective has been to evaluate the effect of gas pressure on the swelling behavior of typical coals, obtain a better estimate of the equilibrium parameters and compare the swelling effect of CO₂ with that of a typical organic vapor whose solubility parameter (7) is closer to that of coal (1).

Experimental

The dilatometer system and the experimental procedures have been described in previous publications. (2,8) The coals investigated included KCER 7259 (sample 1, 83.8% C), KCER 7122 (sample 2, 78.3% C) and KCER 7463 (sample 3, 65.8% C). The coal samples have been described previously in more detail (2). Samples were exposed to helium saturated with acetone vapor (at room temperature) in the acetone exposure experiments.

Results and Discussion

Acetone generally produced a greater swelling effect than CO₂. The KCER 7259 sample was an exception, however, in that CO₂ produced the greater swelling response. The swelling response of the coals to acetone vapor and CO₂ at several pressures is illustrated in Figures 1 to 3. Figure 4 compares the effect of acetone on these coals. In general the order of swelling was: KCER 7259 (sample 1) < KCER 7122 (sample 2) < KCER 7463 (sample 3). At constant pressure the response increased in magnitude as the carbon content decreased, in agreement with

previous results (2). The solubility parameter of acetone ($\delta = 9.6 \text{ cal}^{0.5}\text{cm}^{-1.5}$) is generally closer to that of coal (1) than the CO_2 value ($\delta = 6.2 \text{ cal}^{0.5}\text{cm}^{-1.5}$). Thus a greater swelling effect is expected with acetone. The results on KCER 7259 are, however, anomalous and not explained by these considerations. Table 1 summarizes the swelling response of the coal samples after 200 hours of exposure to acetone vapor.

Table 1 Comparison of Swelling Response of Coals after 200 hrs. of exposure to Acetone vapor

Sample	% C	Dimension Change	
		Specimen 1 microns	Specimen 2 microns
1	83.8	11.4	11.5
2	78.3	219.4	192.3
3	65.8	256.2	209.2

CO_2 induced swelling was investigated by exposing the coal samples to CO_2 at pressures of 5, 10 and 15 atmospheres. The results showed a dependence on the carbon content and pressure. The results are shown in Figures 1 to 3. The response increased with increase in CO_2 pressure but the ultimate response was still generally lower than the values obtained from swelling due to Acetone. This may be seen in two of the three samples. The response due to the highest pressure of CO_2 was greater than that obtained with Acetone vapor in the case of Sample 1. This result may possibly be due to CO_2 molecules creating new pores as the coal swells or the higher pressure of the gas may be modifying the crosslink structure in the coal. A more detailed discussion of the CO_2 -induced swelling results is presented elsewhere (9).

It is of interest to estimate the effect that this measured swelling (volume increase) may have on typical surface area values that have been reported for coals of these carbon contents. To facilitate this assessment it can be assumed initially that all the adsorbed molecules which are contained in the 'monolayer' are contributing volume to a swollen adsorbent-adsorbate system. Surface area values reported in the literature for coals of the same carbon content were employed. (5). The estimated swelling volume increases obtained in this way are compared with the measured volume increases in Tables 2-4.

The results in Table 2 indicate that the measured swelling may account for 13.8 to 24% of the reported surface area values. At higher pressures the swelling effect may account for higher fractions of the reported surface area values (Tables 3 and 4). It should be noted, however, that adsorption experiments to determine surface area are usually carried out at low pressures with an 'equilibrium' time of approximately 30 minutes whereas the swelling volumes were measured after more prolonged contact times. The estimated contributions of swelling to surface area at high pressures are thus more uncertain. There is also some uncertainty because the surface areas reported in the literature may not exactly represent the coal samples employed in the present study. In addition, because there is an inherent pore structure in coal, pore filling undoubtedly accounts for a large fraction of the adsorption and not all adsorbate contributes to swelling. The results indicate, however, that in low carbon content coals, the swelling of coal by CO_2 may account for a significant fraction of the measured BET surface area.

Table 2 Estimated contribution of swelling to CO₂ surface area
(pressure = 5 atm).

Sample	% C	CO ₂ surface area (m ² g ⁻¹)	Estimated ^b swelling vol (%)	Measured ^a swelling vol (%)
1	83.8	150	5.4	0.75(13.8)
2	78.3	150	5.4	1.24(22.9)
3	65.8	250	9.0	2.16(24.0)

^a Expressed as a percentage of estimated swelling in parenthesis

^b Estimated assuming that all the adsorbed molecules which are contained in the 'monolayer' are contributing volume to a swollen adsorbent - adsorbate system.

Table 3 Estimated contribution of swelling to CO₂ surface area
(pressure = 10 atm)

Sample	% C	CO ₂ surface area (m ² g ⁻¹)	Estimated ^b swelling vol (%)	Measured ^a swelling vol (%)
1	83.8	150	5.4	0.85(15.6)
2	78.3	150	5.4	2.23(41.3)
3	65.8	250	9.0	3.00(33.2)

^a Expressed as a percentage of estimated swelling in parenthesis

^b Estimated assuming that all the adsorbed molecules which are contained in the 'monolayer' are contributing volume to a swollen adsorbent- adsorbate system.

Table 4 Estimated contribution of swelling to CO₂ surface area
(pressure = 15 atm)

Sample	% C	CO ₂ surface area (m ² g ⁻¹)	Estimated ^b swelling vol (%)	Measured ^a swelling vol (%)
1	83.8	150	5.4	1.33(24.5)
2	78.3	150	5.4	3.11(57.6)
3	65.8	250	9.0	4.18(46.5)

^a Expressed as a percentage of estimated swelling in parenthesis

^b Estimated assuming that all the adsorbed molecules which are contained in the 'monolayer' are contributing volume to swollen adsorbent - adsorbate system.

The higher surface areas measured by carbon dioxide adsorption can also result from carbon dioxide dissolving in the coal, during the swelling process, and reaching inner pores which are inaccessible to nitrogen. By this process, the carbon dioxide has solution pathways through the coal to the inner pores that nitrogen cannot reach.

Summary and Conclusions

Significant swelling or volume increases ranging from 0.75 to 4.18% were observed in a range of coal samples when they were exposed to carbon dioxide at pressures up to 15 atmospheres. Increase in pressure produced an increase in swelling response and a decrease in the time required to reach maximum response. A lower carbon content correlates with a higher degree of swelling. The order of swelling was sample 1 (%C = 83.8) < sample 2 (%C = 78.3) < sample 3 (%C = 65.8).

Significant swelling response was observed when the samples were exposed to Acetone vapor. The values of the final swelling response were higher than the equilibrium response obtained by CO₂ swelling at 15 atm for samples 2 and 3. This is probably due to the fact that the solubility parameter of the coals is closer to that of the acetone vapor. The order of swelling was sample 1 < sample 2 < sample 3. A lower carbon content corresponded to a higher degree of swelling. Sample 1 showed anomalous behavior. The exposure to higher pressures of CO₂ produced a higher swelling response in comparison to the Acetone swelling. This could not be conclusively explained and further studies are required to understand the behavior.

CO₂-induced swelling may account for up to 50% of the reported CO₂ surface area values in lignite and subbituminous coals. In bituminous coals, swelling may account for about 20% of the surface area values. Thus, previously reported surface area values of these coals determined by CO₂ adsorption may be overestimated by 20 to 50%, depending on the coal.

References

1. P. J. Reucroft and K. B. Patel, *Fuel*, **62**, 279 (1983).
2. P. J. Reucroft and H. Patel, *Fuel*, **65**, 316 (1986).
3. O. P. Mahajan, *Powder Technology*, **40**, 1 (1984).
4. O. P. Mahajan, "Coal Porosity", in "Coal Structure", edited by R. A. Meyers, p. 51, Academic Press, New York, 1982.
5. O. P. Mahajan and P. L. Walker, Jr., "Porosity of Coal and Coal Products", in *Analytical Methods for Coal and Coal Products*, Vol. 1, edited by C. Karr, Jr., p. 125, Academic Press, New York, 1978.
6. O. P. Mahajan, "Adsorption and Pore Structure and Coal-Water Interactions", in "Sample Selection, Aging and Reactivity of Coal", edited by R. Klein and R. Wellek, John Wiley and Sons, New York, in press.
7. A. F. M. Barton, "Handbook of Solubility Parameters and Other Cohesion Parameters", CRC Press, Inc., 1983.
8. A. A. Sagues, *Rev. Sci. Instrum.*, **50**, 48 (1979).
9. P. J. Reucroft and A. R. Sethuraman, *Energy and Fuels*, in press.

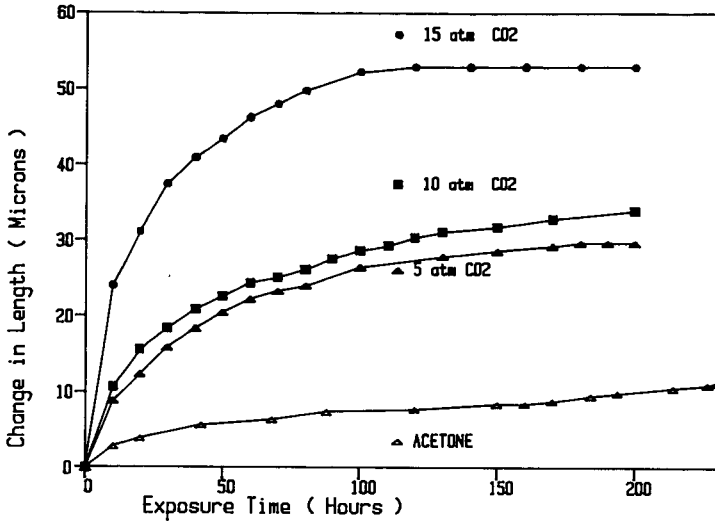


Fig. 1. Swelling response of KCER7259 samples on exposure to acetone vapor and varying pressures of CO₂.

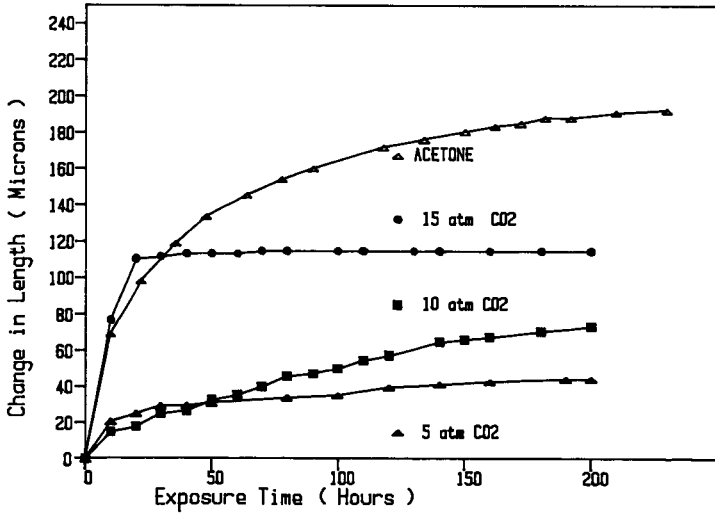


Fig. 2. Swelling response of KCER 7122 samples on exposure to acetone vapor and varying pressures of CO₂.

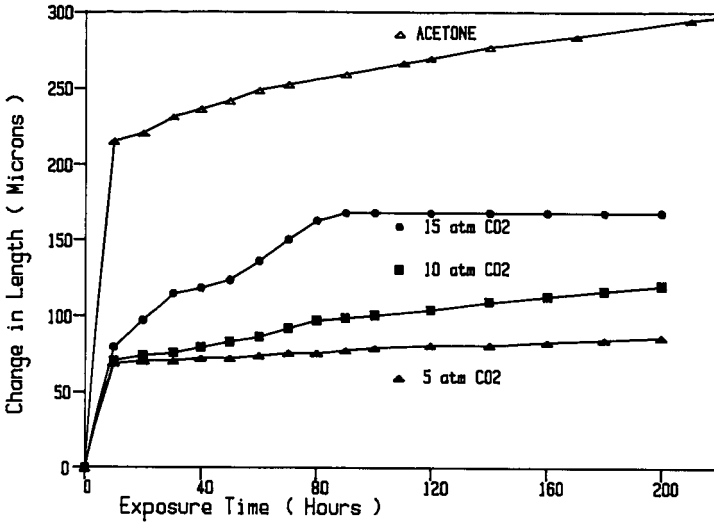


Fig. 3. Swelling response of KCER 7463 samples on exposure to acetone vapor and varying pressures of CO₂.

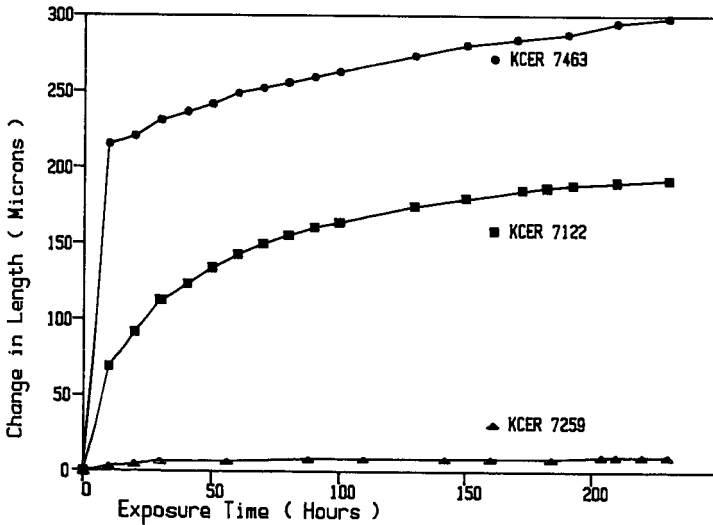


Fig. 4. Swelling response of three coal samples on exposure to acetone vapor.

INFLUENCE OF THE SUPERCRITICAL TOLUENE EXTRACTION OF BROWN COALS ON THE DEVELOPMENT OF POROSITY DURING CARBONIZATION AND STEAM GASIFICATION

Kazimierz Tomkow, Teresa Siemeniewska, Anrezej Albinak and Jan Kaczmarczyk
Institute of Chemistry and Technology of Petroleum and Coal, Technical
University of Wrocław, Gdanska 7/9, 50-344 Wrocław, Poland

INTRODUCTION

The supercritical gas extraction belongs to relatively new technologies of coal processing (1-7). In most cases the research was directed towards the yield of obtained extracts and their physico-chemical nature. Less attention was given to studies of the properties of the extract residues, which in this process are obtained in significant amounts and are usually utilized for combustion or gasification.

The work presented in this paper is focused on the extract residue, with the aim to obtain some information as to what extent the supercritical gas extraction of brown coals might modify their ability to develop a given capillary structure in the processes of carbonization and steam gasification.

EXPERIMENTAL

From Polish brown coal mines, five coals were chosen to represent samples with different content of humodetrinite. The petrographic and chemical analyses of these coals are presented in Table 1.

In a separate research project (8), supercritical gas extraction of these coals was carried out (toluene at 410°C and 13 MP; extract yields are given in Table 1), and the extracted residues were delivered to the authors of the present work for further investigations. Extracted residues from coals L, B, R, S, and T were designed as EL410, EB410, ER410, ES410 and ET410 respectively.

In order to obtain, from the initial brown coals (BC), such samples which would, as to their heat treatment temperature (HTT), correspond to the extract residues (EBC410), the BC samples were carbonized in an aluminum retort (5°C/min, atmosphere of pyrolytic gases) to HTT=410°C. After maintaining this temperature for 30 minutes, the obtained BC410 chars were cooled to room temperature in a stream of argon. The chars BC410 and EBC410 were further carbonized to HTT=900°C in a rotary furnace (5°C/min, Ar), maintaining this temperature also for 30 minutes and cooling the chars BC900 and EBC900 in argon. Results of proximate and ultimate analyses of the chars shows Table 2.

Gasification of the BC900 and EBC900 chars with water vapor was performed at 800°C in a thermogravimetric apparatus, to 50% burn-off of the organic substance of the chars; water vapor was generated in an electrically heated flask at constant water level, to ensure a flow rate of 30 dm³ h⁻¹ the diameter of the reactor tube being 40 mm.

On all the investigated carbonaceous samples, sorption measurements of benzene, carbon dioxide and water vapor at 25°C were carried out, using a gravimetric vacuum apparatus (McBain quartz springs).

RESULTS AND DISCUSSION

The influence of supercritical toluene extraction of brown coals on the course of their carbonization and gasification with water vapor (determined in a thermogravimetric apparatus) is shown in Figures 1 and 2 respectively.

As was to be expected, the yields of chars from extract residues are significantly greater than those obtained for the non-extracted coals (Figure 1). The plots in Figure 2 indicate that no definite influence of supercritical extraction of brown coals on the reactivity of their chars towards water vapor was found. This seems to be in accord with the results of Yuh and Wolf (4), concerning the catalytic effect of K_2CO_3 in the steam gasification of chars from a low rank coal and its supercritical toluene extract residues.

Figure 3 shows an example of sorption isotherms of benzene, carbon dioxide and water vapor (on chars from initial and extracted brown coal L); for respective chars from brown coals B, R, S and T, similar shapes of corresponding isotherms were found. In all cases the same characteristic trends could be noticed. Benzene sorption isotherms are characterized by a pronounced differentiation of shapes and amounts absorbed, depending on the HTT of the chars, their gasification and, in case of $HTT=410^\circ C$, on extraction. For the initial coals and the non-gasified chars, isotherms of type I are obtained, with low amounts adsorbed (although benzene adsorption on the EBC410 samples distinctly exceeds the adsorption on the chars BC410); a low-pressure hysteresis occurs in all cases. After partial gasification (activation) with water vapor, the phenomenon of low-pressure changes into type II, and the amounts adsorbed strongly increase. Contrary to what was observed with benzene isotherms, the adsorption of carbon dioxide is much less influenced by the kind of considered char. Water vapor isotherms, when passing from initial coals to chars with increasing HTT and further to activated chars, show - in the low-pressure region - a systematic decrease of amounts adsorbed; here no influence of extraction was noted.

Basing on benzene sorption data, the pore size distribution of mesopores was calculated (9,10), assuming a cylindrical shape of the pores (Figure 4). The resulting micropore volumes (in case of isotherms showing low-pressure hysteresis the adsorption branch of the hysteresis loop was considered) were in good agreement with the values of W_0 , calculated by means of the Dubinin-Radushkevich (DR) equation (11) - Table 3. In the benzene micropore volumes, super and ultramicropores were distinguished (12), estimating from the course of the isotherms, the regions of relative pressures corresponding to the primary and secondary process of adsorption: the amounts adsorbed at relative pressure of 0.01 were attributed to primary adsorption. The volumes of still narrower ultramicropores, indicated in the histograms shown in Figure 4, were estimated basing both on benzene and carbon dioxide adsorption isotherms, evaluated according to the DR equation. The volumes of ultramicropores accessible only for the CO_2 molecules, were calculated as the difference between the W_0 values from carbon dioxide and benzene adsorption.

In these calculations the density of the adsorbed carbon dioxide at $25^\circ C$ was taken as 1.038 g.cm^{-3} (11,13). Before the calculation of the W_0 values from the benzene and carbon dioxide adsorption isotherms the experimental isotherms (Figure 3) were corrected for adsorption in the mesopores, basing

on respective standard isotherms on non-porous carbonaceous materials (Spheron 6 and Vulcan 3).

Table 4 shows surface area values corresponding to benzene, carbon dioxide and water vapor adsorption. The cross-sectional areas of the molecules of these adsorbates were taken as 0.4375nm^2 , 0.185nm^2 and 0.106nm^2 correspondingly. The values of $S_{\text{BET},\text{C}_6\text{H}_6}$ were calculated from the benzene adsorption isotherms were calculated from the benzene adsorption isotherms according to the BET equation. The obtained surface areas were compared with the values of $S_{\text{p},\text{C}_6\text{H}_6}$, resulting from the amounts of benzene adsorbed at point B of the isotherms, and were found to be usually a little lower: the slope of the linear regression plot presented in Figure 5 is 0.89 ($r=0.996$).

Contrary to this, a very good accord is observed between the values of the surface areas $S_{\text{p},\text{C}_6\text{H}_6}$ and those calculated as follows: the values of micropore volumes $W_{\text{DR},\text{C}_6\text{H}_6}$, calculated from corrected (for mesoporosity) benzene isotherms, were expressed in surface area units, and to the obtained results: $S_{\text{DR},\text{C}_6\text{H}_6}$, the values of the surface areas of mesopores (S_{mes}) were added. The slope of the corresponding regression plot was now very close to unity (1.04), with r also equal 0.996. It seems possible that in case of benzene adsorption, the point a_m , resulting from application of the BET equation, corresponds mainly to the m volume filling of micropores (strongly enhanced heat of adsorption), and is not identical with the point B of the isotherm, where the amounts adsorbed might correspond not only to the volumetrically filled micropores, but also to the formation of a monolayer in the mesopores (this sum would correspond to a less enhanced heat of adsorption).

The surface areas S_{CO_2} were calculated as $S_{\text{wo,DR,CO}_2} + S_{\text{mes}}$. For initial brown coals these surface areas exceed significantly the respective values obtained on the basis of benzene adsorption, pointing to an important molecular sieve effect in these samples (this can also be seen from Table 3). This effect also strongly pronounced in the non-activated chars, seems to be to some extent still present even after their gasification to 50% burn-off.

The values of surface areas corresponding to adsorption of water vapor, were obtained, expressing in terms of surface areas the amounts of water adsorbed at $p/p_0 = 0.6$ (14). To gain some indication concerning the polarity of the surface of the investigated samples, the ratio $S_{\text{H}_2\text{O}}/S_{\text{CO}_2}$ was calculated; here S_{CO_2} and adsorption data were taken (as a parameter apt to described the total surface area accessible for the H_2O molecules), because of the mentioned molecular sieve effect for the benzene molecules.

For a clearer demonstration of the influence of supercritical extraction of brown coals on the parameters of their capillary structure formed during carbonization and steam activation, in Figures 6 and 7 the ratios of values of chosen parameters for chars from the extracted and non-extracted coals are presented.

CONCLUSIONS

The results obtained during this research, seem to furnish some indications concerning the kind of modifications, caused by supercritical toluene extraction of brown coals, in the course of development of their porosity

during carbonization and steam gasification.

The porous system of initial brown coals is composed mainly of very fine, benzene inaccessible, ultramicropores (V_{ult, CO_2}) - Figure 4a. The high oxygen content in these coals (Table 1) indicates a significant concentration of oxygen functional groups and explains a high ratio of S_{H_2O}/S_{CO_2} (Table 4).

In case of chars corresponding to $HTT=900^\circ C$, as well as in these chars after their steam gasification (to burn-off of 50%), the influence of coal extraction is very small: the ratios of all the considered parameters (Figures 6 b, c and 7 b, c) are very close to unity. This would mean that at $HTT=900^\circ C$ a very similar kind of porosity is being formed as the result of removal of the more volatile parts of the organic substance of coals, no matter if this was caused solely by the process of pyrolysis, or also by supercritical gas extraction (Figure 4 c, d).

However at a lower HTT ($410^\circ C$) as can be noted, that the supercritical gas extraction of the coals causes a distinctly greater development of the porosity than that which takes place on carbonization only (Figure 4 b). The extraction favors all the considered kinds of benzene accessible porosity, and this trend is the more pronounced, the narrower the pores. The highest ratios of pore volumes in the HTT $410^\circ C$ chars from extracted and non-extracted coals were obtained for the benzene accessible ultramicropores (V_{ult, CO_2}^{BC}) are below unity. These extremely small ultramicropores, which develop strongly on heating of the non-extracted coals to $410^\circ C$, partly disappear (compared with respective initial coals), when the process of supercritical toluene extraction is carried out. It is possible that these ultramicropores, present in the initial coals, might play the role of centres, facilitating the extraction process, in which benzene accessible ultra- and supermicropores are formed, at the expense of the pre-existing, only CO_2 accessible, ultramicropores.

This would perhaps also point to a special significance of the CO_2 surface area: a parameter able to detect in a carbonaceous material the presence of a very fine porous system (inaccessible for other adsorbates), the existence of which seems to facilitate the development of further porosity in thermochemical processes.

ACKNOWLEDGEMENTS

The authors wish to express their thanks to Dr. M. Stolarski, Dr. E. Sliwka, and Dr. J. Surygala from the Technical University of Wrocław for the samples of extract residues, and to Dr. J. Szwed-Lorenz from the Technical University of Wrocław for the results of the petrographical analyses of brown coals.

REFERENCES

1. Paul, P.F.M., and Wise, W.S. The Principle of Gas Extraction, Ed. Mills and Boon, London, 1971.
2. Bartte K.D., Martin, T.G., and Williams, D.F., Fuel, 54, 226 (1975).
3. Słomka, B., and Rutkowski, A. Fuel Process Tech., 5, 247 (1982).

4. Yuh, S.J., and Wolf, E.E. Fuel, 62, 738 (1938).
5. Amestica, L.A., and Wolf, E. E. Fuel, 63, 227 (1984).
6. Kershaw, J.R., Overbeek, J.M., and Bagnell, L.J., Fuel, 64, 1070 (1985).
7. Surygala, J., and Stolarski, M., Chemia Stosowana, in print.
8. Stolarski, M., Sliwka, E., and Surygala, J., unpublished results.
9. Pierce, C., J. Phys. Chem., 57, 149 (1953).
10. Kankare, J., and Jantti, O., Suomen Kemistilehti, 840, 51 (1967).
11. Dubinin, M.M., Chem. Rev., 60, 235 (1960).
12. Gregg, S.J., and Sing, K.S.W., "Adsorption, Surface Area and Porosity", Academic Press, London, 1982.
13. Tomkow, K., Siemieniowska, T., Baldyga, A., Guerin, H., Grillet, Y., and Francois, M., J. Chim. Phys., 71, 1062 (1974).
14. Dubinin, M.M., Carbon, 19, 321 (1981).

Table 1. The Characteristics of Polish brown coals

Symbol of brown coal:	L	B	R	S	T
Groups of macerals (vol. %, mineral matter free):					
- humotelinite	3.0	12.6	12.7	20.6	30.4
- humodetrinite	88.4	74.5	71.8	60.2	47.4
- humocollinite	1.5	1.4	6.5	16.9	10.5
- liptinite	5.7	10.6	5.8	1.0	10.9
- inertinite	1.4	0.9	3.2	1.3	0.8
Group components of the organic substance (% , daf):					
- bitumens	2.5	3.4	5.9	2.3	3.4
- humic acids (free)	55.9	22.3	65.1	18.8	14.7
- humic acids (total)	66.5	33.4	81.1	25.4	16.9
- residue	31.0	63.2	13.0	72.3	79.7
Yield of toluene extract (% , daf):	23.9	27.3	42.9	34.4	36.4
Proximate analysis:					
- total moisture (% , raf)	60.3	59.3	55.0	53.5	52.0
- ash (% , dry)	6.6	5.9	12.4	7.3	7.0
- volatile matter (% , daf)	55.0	56.1	62.1	55.2	58.1
Ultimate analysis (% , daf):					
- carbon	65.8	65.7	66.9	67.5	69.5
- hydrogen	5.7	6.1	5.9	5.2	5.8
- nitrogen	0.7	0.8	0.5	0.7	0.8
- (O + S) by diff.	27.8	27.4	26.7	26.6	23.9
Total sulfur (% , dry):	0.7	0.6	7.2	2.0	2.1

Table 2. Proximate and ultimate analyses of chars from initial and toluene extracted brown coals (%)

Symbol of initial brown coal	Chars from:									
	brown coals					extract residues				
	W ^a	A ^d	VM ^{daf}	C ^{daf}	H ^{daf}	W ^a	A ^d	VM ^{daf}	C ^{daf}	H ^{daf}
HTT=410°C										
L	1.5	7.5	37.1	70.5	4.5	3.2	9.0	30.3	76.7	4.0
B	2.6	7.0	37.2	71.5	4.6	1.5	8.4	28.4	75.7	4.3
R	1.8	16.7	31.9	79.0	4.5	2.3	19.8	33.8	79.3	4.3
S	1.7	8.6	32.1	75.1	4.3	2.0	9.7	30.5	77.4	4.1
T	2.6	8.1	34.5	74.2	4.7	1.7	10.4	24.5	78.9	4.1
HTT=900°C										
L	1.6	10.5	5.7	89.7	1.2	1.8	12.7	6.2	90.0	1.4
B	1.8	10.0	5.7	92.5	1.1	1.3	11.2	6.1	93.8	0.9
R	3.0	20.6	4.2	97.5	1.0	2.8	25.0	5.5	98.8	1.1
S	1.9	12.6	4.7	92.6	1.3	1.4	13.9	4.1	94.1	1.2
T	2.4	11.7	4.9	93.4	0.9	1.9	13.6	5.1	93.2	1.1

Table 3. Parameters W_0 ($\text{cm}^3 \cdot \text{g}^{-1}$) and B of the DR equation for benzene and carbon dioxide adsorption at 25°C

Symbol of initial brown coal	Adsorbate							
	C_6H_6		CO_2		C_6H_6		CO_2	
	W_0	$B \times 10^6$	W_0	$B \times 10^6$	W_0	$B \times 10^6$	W_0	$B \times 10^6$
	Brown coals				Extract residues			
L	0.006	4.05	0.086	3.59				
B	0.004	4.22	0.068	3.66				
R	0.006	6.50	0.066	3.01				
S	0.002	4.14	0.077	3.46				
T	0.003	5.57	0.061	3.46				
HTT=410°C								
L	0.021	4.39	0.128	3.97	0.081	1.35	0.144	3.38
B	0.017	3.12	0.115	3.63	0.089	2.53	0.176	3.70
R	0.017	3.49	0.111	3.80	0.076	1.60	0.149	3.59
S	0.016	4.22	0.122	3.54	0.100	2.11	0.152	3.50
T	0.017	2.95	0.093	3.54	0.104	2.49	0.140	3.59
HTT=900°C								
L	0.085	0.93	0.163	2.15	0.072	1.18	0.156	2.33
B	0.081	1.10	0.177	2.53	0.076	1.35	0.167	2.58
R	0.035	2.20	0.212	2.70	0.053	2.11	0.192	2.66
S	0.042	2.91	0.200	2.62	0.044	2.45	0.187	2.66
T	0.040	3.29	0.194	2.49	0.058	2.95	0.194	2.58
Chars HTT=900°C steam activated at 800°C (B0=50%)								
L	0.096	1.31	0.102	2.70	0.085	1.31	0.095	2.87
B	0.064	1.27	0.095	2.79	0.070	1.10	0.095	2.70
R	0.145	0.50	0.173	3.14	0.143	0.56	0.169	3.19
S	0.104	1.98	0.166	3.06	0.097	2.29	0.128	2.95
T	0.174	2.07	0.207	3.26	0.166	2.01	0.189	3.17

Table 4 Surface areas ($\text{m}^2 \cdot \text{g}^{-1}$) based on benzene, carbon dioxide and water vapor adsorption at 25°C

Symbol of initial brown coal	0.6				0.6			
	S_{BET}	S_{CO_2}	$S_{\text{H}_2\text{O}}$	S_{CO_2}	S_{BET}	S_{CO_2}	$S_{\text{H}_2\text{O}}$	S_{CO_2}
	Brown coals				Extract residues			
L	24	226	482	2.13				
R	21	179	458	2.56				
R	26	174	422	2.43				
S	21	202	436	2.15				
T	29	160	333	2.08				
HTT=410°C								
L	63	336	371	1.10	292	378	445	1.17
B	55	302	362	1.20	274	462	416	0.90
R	74	292	316	1.08	224	392	430	1.10
S	47	321	348	1.08	256	400	421	1.05
T	55	244	273	1.12	266	368	505	1.37
HTT=900°C								
L	216	428	385	0.90	211	410	357	0.87
B	211	465	389	0.84	192	439	338	0.77
R	108	557	479	0.86	161	505	466	0.92
S	108	526	396	0.75	132	492	380	0.77
T	84	510	419	0.82	148	510	413	0.81
Chars HTT=900°C steam activated at 800°C (B0=50%)								
L	458	500	158	0.32	424	452	139	0.31
B	390	455	135	0.30	387	453	131	0.29
R	482	577	405	0.70	501	584	311	0.53
S	477	669	237	0.35	432	554	198	0.36
T	516	661	351	0.53	469	613	334	0.54

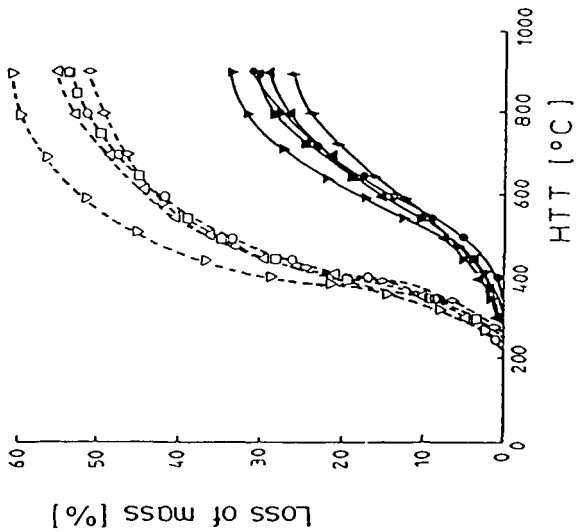


Figure 1 Influence of toluene extraction of brown coals on the course of carbonization $\circ L, \Delta B, \nabla R, \square S, \phi T; \bullet EL, \blacktriangle EB, \blacktriangledown ER, \blacksquare ES, \blacktriangleright ET$.

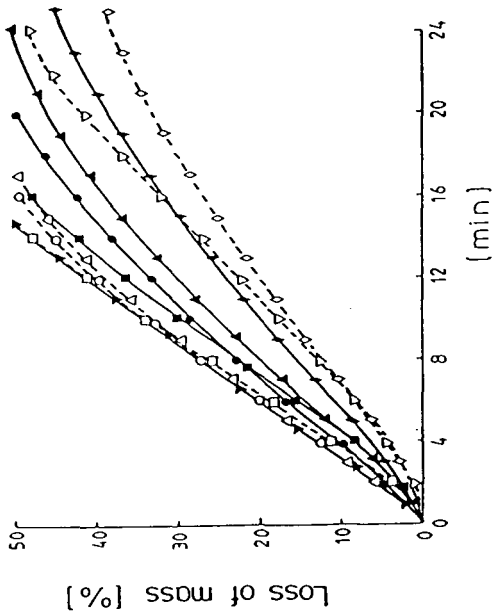


Figure 2 Steam gasification at 800°C of chars ($\text{HTT}=900^{\circ}\text{C}$) from initial $(\circ L, \Delta B, \nabla R, \square S, \phi T)$ and toluene extracted $(\bullet EL, \blacktriangle EB, \blacktriangledown ER, \blacksquare ES, \blacktriangleright ET)$ brown coals.

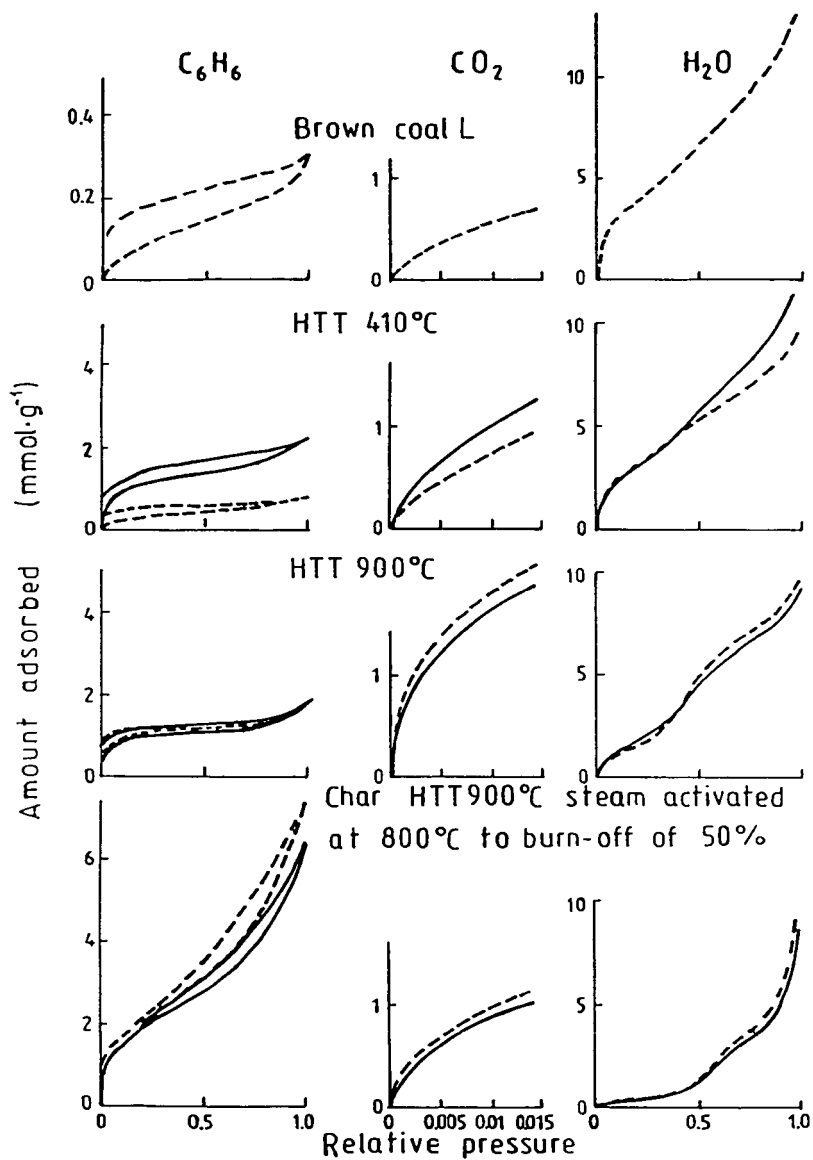


Figure 3 Isotherms (25°C) of C_6H_6 ad- and desorption, CO_2 adsorption and H_2O adsorption. --- sample from brown coal L; — sample from extract residue.

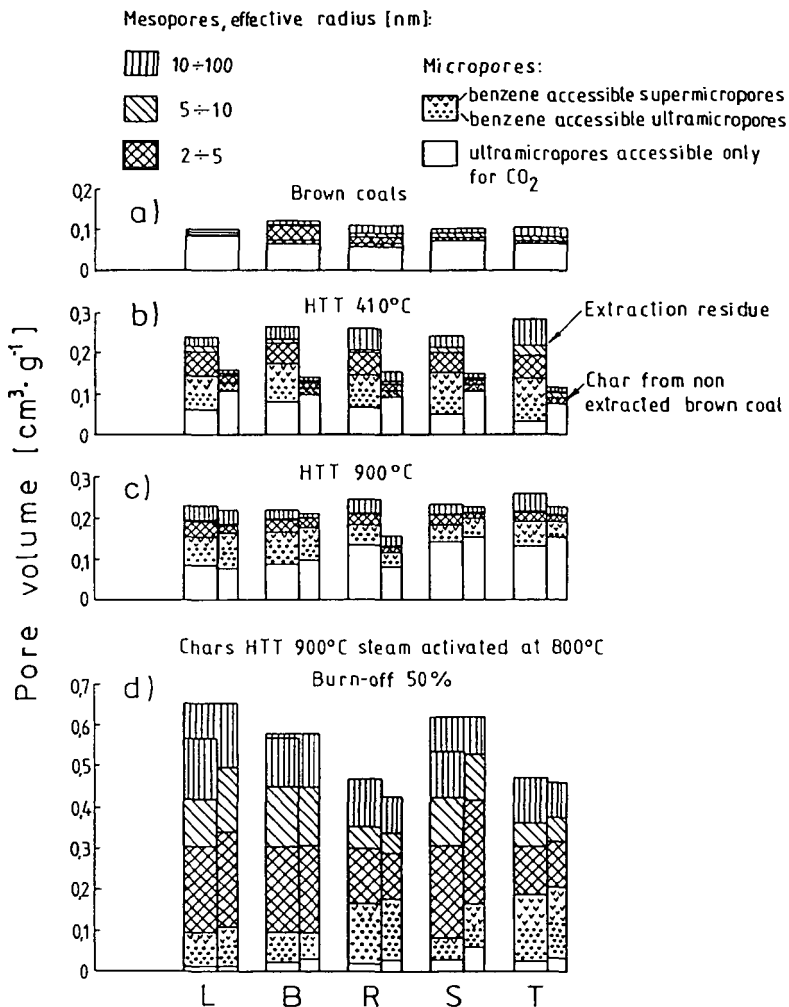


Figure 4 Influence of toluene extraction of brown coals on the pore size distribution in chars obtained on carbonization and steam activation.

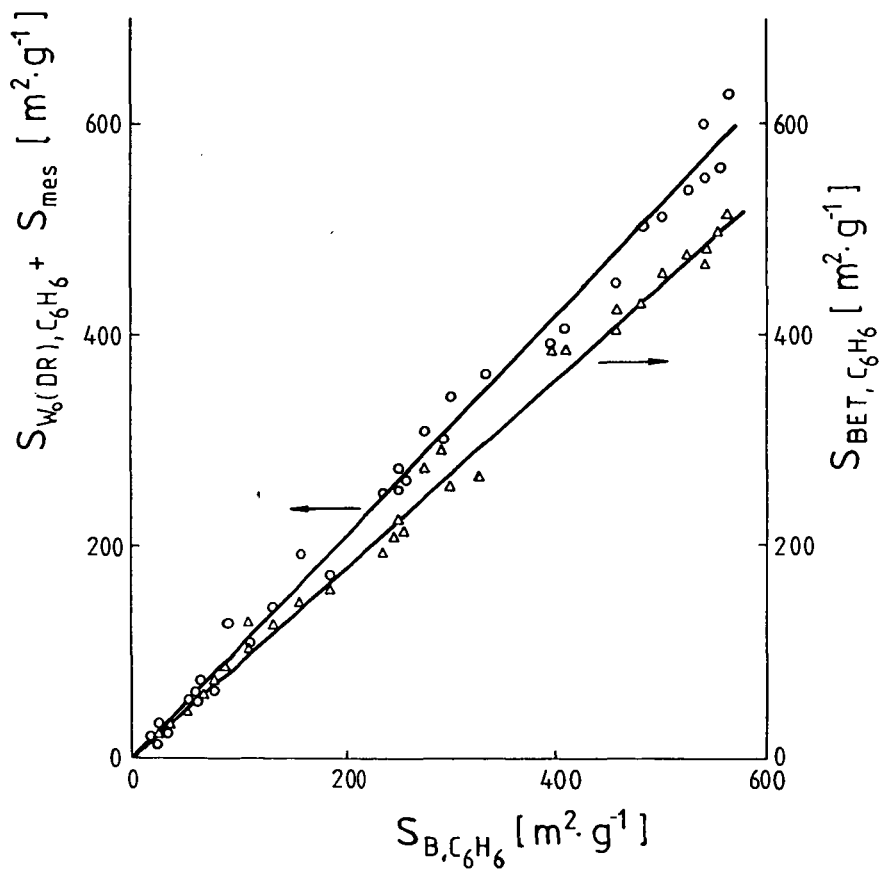


Figure 5 Relations between benzene surface areas of investigated carbonaceous samples estimated in different ways.

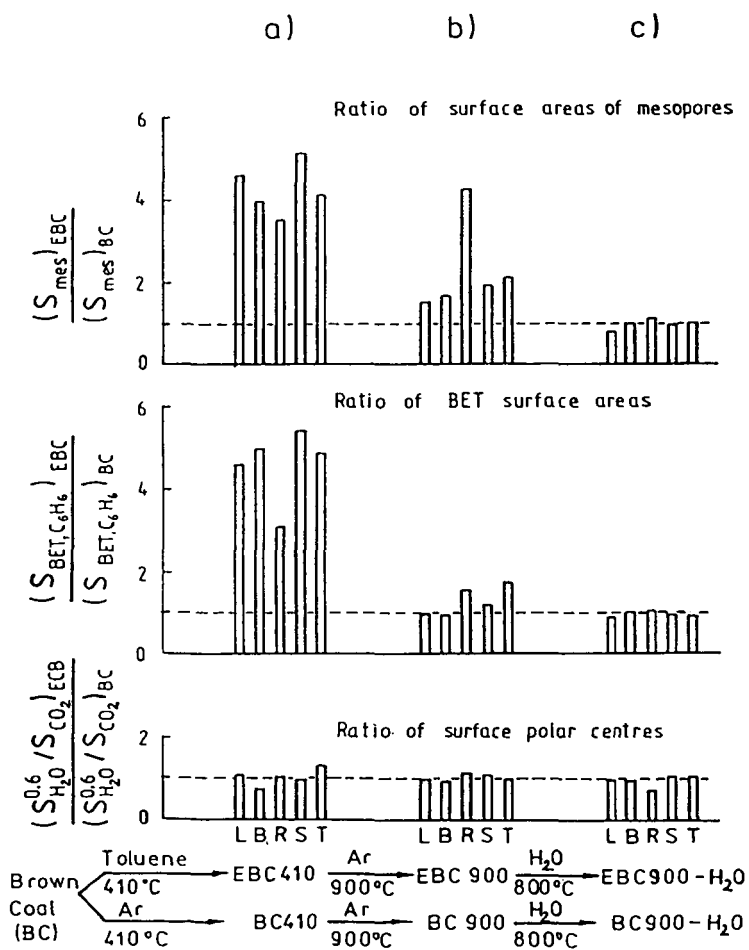


Figure 7 Influence of toluene extraction of brown coals on the development of surface area and surface polarity during carbonization and steam activation.

A TPD study on H₂O-gasified and O₂-chemisorbed coal chars

T. Kyotani, Z. G. Zhang, S. Hayashi and A. Tomita

Chemical Research Institute of Non-Aqueous Solutions.
Tohoku University, Sendai 980, Japan

INTRODUCTION

Steam gasification reaction of coal char is a very important reaction in both theoretical aspects and industrial applications. It is generally accepted that surface oxygen complexes on carbon substrate function as intermediate in gasification reaction and that such surface complexes are formed only at active sites (1, 2). Many investigators have studied oxygen chemisorption on a variety of carbons to estimate the amount of surface oxygen complexes (3-5). This amount is thought to correspond to the number of active sites or an active surface area. The reactivity of carbon was closely related to the active surface area on the carbon. However, the detailed feature of such surface complexes have not been well understood yet. Temperature-programmed desorption (TPD) technique is very useful in yielding information on surface oxygen complexes (6-8). By using TPD technique, this paper intends to clarify the nature of surface complexes on coal char after H₂O gasification or after O₂ chemisorption. In addition, the gasification reactivity was discussed in relation to TPD patterns of H₂O-gasified char or O₂-chemisorbed char. The effect of coal type and the mineral matter in coal on TPD pattern was also investigated.

EXPERIMENTAL

Materials

Five coals (16x32 mesh) varying in rank were used in this study. The ultimate and proximate analyses are presented in Table 1. The metal content of coals is given in Table 2. Some of the raw coals were demineralized by using a mixture of HCl and HF solutions. Ash content of the demineralized coal was: MW, 0.2; TH, 2.3; GV, 0.6 wt%(dry). The raw (Raw) and demineralized (Dem) coals were devolatilized in N₂ at 1100 K for 30 min in a small fluidized bed reactor as described in a previous paper (7).

Apparatus and procedure

Steam gasification, oxygen chemisorption and TPD were carried out in the same apparatus. A quartz basket containing about 50 mg of char was hung by a quartz spring in a quartz tube which was placed in a vertical furnace. The sample was heated to 1100 K under N₂ flow (40 ml(STP)/min) and then steam was introduced at the flow rate of 50 ml(STP)/min with diluent N₂ (10 ml(STP)/min). The weight change during gasification was followed by using a cathetometer. After the char conversion reached to 50 wt%(daf), the sample was cooled to 570 K in H₂O, followed by cooling to 420 K in N₂. This partially gasified char is referred to as G char in this paper. G char was outgassed to 0.1 Pa at 420 K and then subjected to TPD at a linear heating rate of 10 K/min up to 1100 K. A large portion of evolved gas was evacuated with a rotary pump and a slight portion of gas was introduced to a gas analysis system. The gases (CO₂, CO and H₂O) were analyzed with a quadrupole mass spectrometer. After TPD experiment of G char, the temperature was lowered to 420 K and oxygen at 0.1 MPa was admitted into the system for 1 h. This O₂-chemisorbed char is referred to as O char. O char was also subjected to TPD under the same conditions as above. The results are expressed per unit weight (daf). Although they are presented in arbitrary units, the peak intensity can be reasonably compared

with each other, because it was corrected by considering the pattern coefficient and the ionization efficiency of each gas.

RESULTS

The TPD patterns of Raw-G chars are shown in Fig. 1(a). MW Raw-G char yielded a sharp H₂O-peak at 590 K, a broad CO₂ desorption pattern in the range from 650 K to 1000 K and a sharp CO-peak at 1040 K. TH Raw-G char gave H₂O- and CO-peak at similar temperature ranges. YL Raw-G and WD Raw-G chars exhibited only a sharp CO-peak. It is noteworthy that all sharp CO-peaks from the above chars were observed in a similar temperature range. On the other hand, GV Raw-G char exhibited no clear peak and only a small amount of CO and H₂O was evolved over a wide range of temperature.

The TPD patterns of Raw-O chars (Fig 1(b)) are broad in comparison with those of Raw-G chars. All of Raw-O chars evolved CO₂ in the range from about 450 K to 1050 K. In addition to this CO₂ desorption, MW Raw-O gave a relatively sharp CO₂-peak at 770 K. With respect of ¹²CO, the desorption from Raw-O chars began at much lower temperature than that from Raw-G chars. The sharp CO-peak observed in Raw-G chars was not observed in Raw-O chars, but a small CO-peak appeared in YL and MW Raw-O chars.

In order to investigate the effect of mineral matter on the gas evolution, TPD were carried out with the chars prepared from the demineralized coals (Fig. 2). In the case of MW Dem-G char, the sharp peaks as observed in the Raw-G char completely disappeared as a result of the demineralization. A small amount of CO was evolved at a relatively high temperature. TH Dem-G char exhibited no sharp H₂O-peak, but the sharp CO-peak was still present in spite of the demineralization. The TPD pattern of GV Dem-G char was almost the same as that of GV Raw-G char. Generally the patterns of Dem-O chars resemble to those of Raw-O chars, that is, broad CO₂ and CO-desorptions were commonly observed in both chars. An exception was that the ¹²CO₂ peak at 770 K in MW Raw-O char was not observed in the pattern of MW Dem-O char.

Table 3 shows the gasification rate in steam at a char conversion of 50 % (daf) for Raw- and Dem-chars. The demineralization caused a considerable reduction in reactivity of MW char. This fact clearly shows that the mineral matter in MW coal was catalytically active in the gasification. On the other hand, the reactivity of TH char increased slightly and that of GV char was unchanged as a result of the demineralization.

DISCUSSION

Since many relatively sharp peaks disappeared from TPD pattern as a result of demineralization, these peaks must be closely associated with the presence of mineral matter in char. For MW Raw-G char we have shown that the interaction between finely-dispersed Ca and carbon is responsible for CO₂ peak and that the decomposition of Ca(OH)₂ is responsible for H₂O evolution(7). The dispersed Ca is derived from exchangeable Ca cation on carboxyl groups in MW coal. Although WD and TH coals have a large amount of Ca as indicated in Table 2, their Raw-G and Raw-O chars did not exhibit such a CO₂ peak. This suggests that there is little finely-dispersed Ca in WD and TH chars, because of a smaller amount of carboxyl groups in the coals than in brown coal like MW coal. Many Raw-G chars exhibited a sharp CO-peak at around 1040 K. It is not clear which inorganic species are responsible for the sharp CO-peaks, but the peaks may possibly be ascribed to the same kind of species (Fe and/or Na). Though TH Dem-G char exhibited the CO-peak, this may be due to incomplete demineralization. On the other hand, the broad CO desorption as

observed in GV Dem-G char is not due to the interaction with mineral matter. This desorption is associated with carbon substrate itself. Thus TPD pattern is appreciably influenced by mineral matter but the effect of coal type is not so significant.

The total amount of CO₂ and CO gas evolutions in TPD pattern of G char or O char was correlated with the gasification reactivity (Fig. 3). Although the amount of gas evolution from O char was slightly larger than that from G char, good correlations were found for both cases. The relationship between the gasification reactivity and TPD pattern may be postulated as follows. During steam gasification, water vapor chemisorbs at active site on carbon surface and surface oxygen complexes are formed. Catalytically active inorganic species such as finely-dispersed Ca may also have an ability to accept oxygen from H₂O, and this activated oxygen is transferred to neighboring carbon substrate to form surface complex. These oxygen complexes, whatever they are produced non-catalytically or catalytically, decompose and desorb gaseous products.



where C_f is an empty active site and C(O) is surface oxygen complex. In some cases, oxygen may be retained in the inorganic species and may react with carbon at the gasification temperature. When a partially gasified char is cooled in H₂O after gasification, the extent of Reaction 2 becomes smaller as the temperature decreases and all available active sites may be covered with surface oxygen complexes. When this sample, G char, is subjected to TPD, gases such as CO₂ and CO are evolved either by the decomposition of such complexes (Reaction 2) or by the solid-solid reaction between oxygen-containing inorganic species and carbon (the sharp CO peak in TPD pattern may be due to this reaction). Active sites become unoccupied after TPD of G char. When the sample after TPD was exposed to O₂ at 420 K, the empty active sites may be occupied again:



During the subsequent TPD of O char, Reaction 2 occurs again. Therefore, TPD patterns of both G char and O char essentially give the same information about active site on carbon surface, although the absolute amount of desorbed gas is somewhat different with each other. This is why good correlations were observed between the reactivity and the amount of desorbed gas either from G char or O char (Figure 3).

In order to check whether the chemisorption sites for O₂ and for H₂O are the same or not, one O₂-chemisorption experiment was carried out with MW char. After MW Raw-G char was prepared in H₂O, it was exposed to O₂ before TPD experiment. The TPD pattern of this sample was almost the same as that of G char. This fact suggests that all active sites on G char have already been covered with the oxygen from H₂O. Surface complexes characteristic for O char can not be produced on the G char anymore. In other words, the adsorption site for H₂O and O₂ may be the same. Nevertheless, the TPD patterns of G char are quite different from those of O char. This can be explained as follows. In G char, since H₂O chemisorbs at high temperature, only thermally stable surface complexes such as heterocyclic ether group can be formed. This mechanism was also proposed by Huttering and he pointed out that these ether groups function as intermediate in gasification reaction (8). On the other hand, when unoccupied active surface after TPD of G char is exposed to O₂ at temperature as low as 400 K, various kinds of surface complexes such as lactone, carbonyl, ether and others may be formed on the O char. Some of these

complexes may be decomposed at relatively low temperatures upon heating. Therefore, O char gave a broad CO₂-peak and the evolution of CO began at low temperature.

REFERENCES

1. Walker, P. L., Jr., Rusinko, F., Jr. and Austin, L. G., *Advan. Catalysis*, 11, 133 (1959).
2. Ergun, S. and Mentser, M. in "Chemistry and Physics of Carbon" (Ed. P. L. Walker, Jr.), Vol. 1, Marcel Dekker, New York, 1965, pp. 204-263.
3. Laine, N. R., Vastola, F. J. and Walker, P. L., Jr., *J. Phys. Chem.*, 67, 2030 (1963).
4. Chen, C.-J. and Back, M. H., *Carbon*, 17, 495 (1979).
5. Radovic, L. R., Walker, P. L., Jr. and Jenkins, R. G., *Fuel*, 62, 849 (1983).
6. Causton, P. and McEhane, B., *Fuel*, 64, 1447 (1985).
7. Kyotani, T., Karasawa, S. and Tomita, A., *Fuel*, 65, 1466 (1986).
8. Hermann, G. and Huttinger, J., *Fuel*, 65, 1410 (1986).

Table 1. Ultimate and proximate analyses for original coal

Coal	Code	Ultimate analysis (wt%, daf)					Proximate analysis (wt%)			
		C	H	N	S	O	Mois.	V.M.	Ash	F.C.
Morwell	MW	67.9	5.0	0.5	0.3	26.3	25.9	38.2	1.1	34.8
Yallourn	YL	66.1	5.3	0.6	0.3	27.7	14.3	47.3	0.8	37.6
Wandoan	WD	75.8	6.8	1.0	0.3	16.1	9.1	49.0	15.4	26.5
Taiheiyō	TH	77.0	6.3	1.5	0.3	14.9	5.8	46.5	10.8	36.9
Grose Valley	GV	81.7	5.1	1.4	0.4	11.4	3.4	29.7	16.6	50.3

Table 2. Metal content in original coal (wt%, dry)

Coal	Si	Al	Fe	Ca	Na	K
MW	0.04	0.01	0.10	0.30	0.05	0.00
YL	0.04	0.02	0.26	0.08	0.08	0.00
WD	4.21	3.24	0.20	0.60	0.12	0.16
TH	2.58	1.42	0.34	0.65	0.10	0.16
GV	4.97	3.27	0.46	0.01	0.02	0.11

Table 3. Reaction rate of char (h⁻¹)

Coal	Raw	Dem
MW	2.2	0.2
YL	1.3	n.d.
WD	1.6	n.d.
TH	1.0	1.7
GV	0.2	0.2

n.d., not determined

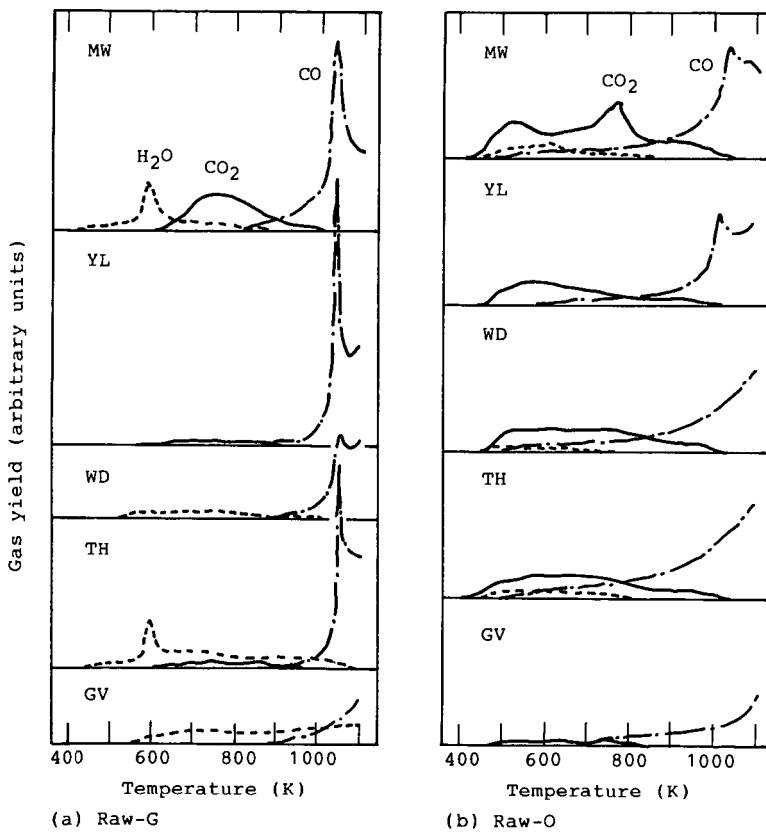


Figure 1. TPD patterns of raw coal chars.
 —, CO_2 ; - · - ·, CO ; - - - -, H_2O

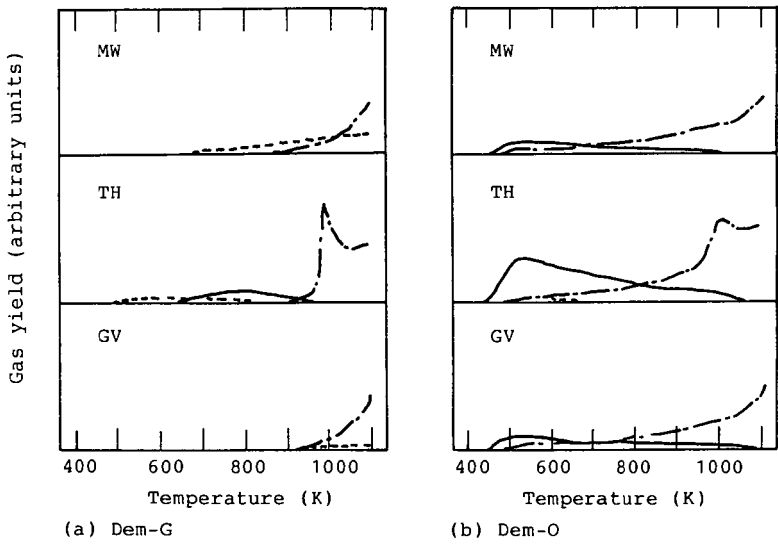


Figure 2. TPD patterns of demineralized coal chars.
 —, CO₂; - - -, CO; - · - ·, H₂O.

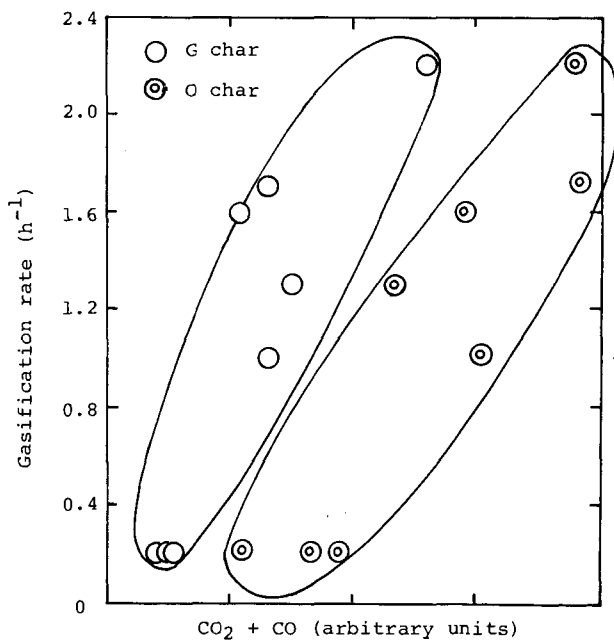


Figure 3. Correlation between the gasification rate and the amount of CO₂ and CO desorbed during TPD.

Kinetics of O₂-Chemisorption on Chars and its Relevance to Char Reactivity

Heinz-Jürgen Muhlen, Karl Heinrich van Heek, Harald Juntgen

Bergbau-Forschung GmbH, Franz-Fischer-Weg 61, 4300 Essen 13, F.R.G.

Abstract

O₂-chemisorption on char surfaces was investigated with special regard to the time-temperature-history of the material especially pyrolysis conditions (HTT: 700,800,900°C) and surface cleaning procedures in helium at elevated temperatures before chemisorption, the chemisorption temperature and the ambient O₂-pressure. The impact of the different parameters on the maximum amount of O₂ chemisorbed and the rates of chemisorption are discussed and the results are correlated to gasification rates in 40 bar steam determined at 750, 800 and 850°C and nonisothermally up to 950°C. Moreover the effect of combustion on O₂-chemisorption will be discussed.

Introduction

Chemisorption of oxygen on char surfaces to characterize char reactivity has been investigated intensively in the past (9,10,11). Most of the authors carried out the chemisorption at temperatures ranging between 20 and 200°C for an arbitrary chosen time, e.g. 23 hours, and they found fairly well correlations between the amount of oxygen chemisorbed and the reactivity as a function of e.g., the degree of burn-off measured in oxygen, as well as in steam, CO₂ and hydrogen (9,10,11). However, only little attention was paid to the impact of the chemisorption parameters applied as there are temperature, time allowed for chemisorption, preparation modality of the char or ambient O₂ pressure. Even less the kinetics of chemisorption were taken into consideration, whether it is controlled by chemical reaction or by diffusion. Although one cannot neglect the accessibility of active sites under the conditions applied for its determination, if one tries to correlate structural or chemical attributes of a material with reactivities.

The aim of the present work is therefore to contribute to the fundamental understanding of the processes involved during O₂-chemisorption and to improve this method for char characterization.

Experimental

For this study a thermogravimetric apparatus was employed which mainly consists of a balance (Sartorius model 4406) having a resolution of .001 mg. The sample is placed in the centre of an electrically heated steel tube and flushed continuously by pure helium during the cleaning and desorption period or by a mixture of helium and oxygen (79.1/20.9) during chemisorption.

The flow rates of the gases are adjusted by means of thermal mass flow controllers to .2 l/min (5,6)

To avoid weight errors induced by buoyancy of drag forces a special time-temperature-procedure was chosen which is illustrated in Fig. 1. At the beginning of each run the temperature is adjusted to a value equal to the chemisorption temperature T_s. After the weight signal became constant, i.e. after drying the temperature is increased up to the "cleaning temperature"

T_c . The duration of this period was chosen in such a way that there are only neglectable impacts on the char structure which otherwise could decrease the porosity (12) or the internal surface area (13), an effect which is well known as "thermal annealing". To which extent this thermal annealing can influence the reactivity can be seen from Fig. 10. Therefore we chose T_c 100°C lower than the heat treatment temperature (HTT), or if HTT was too low to assure that the surface can be cleaned properly, we took the value of HTT as T_c , and limited the time of cleaning to .5 hours. This could be done because the preparation of chars included 1 hour tempering after having reached HTT. Besides former experiments (1,2) have shown that an increase of pyrolysis time affects reactivity only slightly, if the residence time at HTT exceeds 1 hour.

After cleaning the temperature is lowered to T_s again and the gas flow is switched to the He/O₂-mixture which causes a small decrease in weight due to the higher gas-density of this mixture which causes a small decrease in weight due to the higher gas-density of this mixture compared to pure helium. O₂-chemisorption is then carried out for approximately 16 hours, after which the gas atmosphere is switched back to pure helium, the desorption performed at the same temperature used during cleaning. At the end of the experiment the temperature is decreased again to T_s . This procedure has the advantage, that the amount of oxygen taken up can be determined by both the difference between the periods C and E and the difference between starting and final weight signals in period D. Besides the difference B-F represents the carbon loss due to desorption and partial combustion and the difference F-G stands for the weight of carbon oxides desorbed during period E. Analysing these values one can determine which amount of the sample has been burnt, or if not any which composition (CO₂/CO) the desorption gas has had.

For the purpose of this investigation the char of a German bituminous coal "Westerholt" was ground to 100-315 microns and preoxidized in a fluidized bed under air for 24 hours at a temperature of 200°C in order to reduce the caking properties. Thereafter pyrolysis was carried out feeding the material into a preheated (700, 800 and 900°C) fluidized bed under argon. After a residence time of 1 hour the char was removed and stored. Proximate and ultimate analyses of the chars and the parent and preoxidized coal are given in Table 1.

To investigate the influence of the cleaning temperature on O₂-chemisorption the char prepared at 900°C was used after cleaning at temperatures ranging between 600 and 900°C. To investigate the temperature dependence of chemisorption the conditions were varied between 150 and 250°C for all chars. Lower and higher temperatures were not applied in order to avoid physisorption effects (8) and to keep the amount of char burned as small as possible. Moreover the partial pressure of oxygen was reduced in some experiments to determine the reaction order of chemisorption concerning oxygen.

RESULTS

Influence of cleaning temperature

In Fig. 2 the increase in weight as a function of time is shown for the different cleaning temperatures. It should be mentioned that the time for cleaning was such that as long as the weight signal needed to attain a

constant value. Therefore one would assume that after cleaning all active sites are available for the oxygen, however, Fig. 3 points out, that there still are occupied sites even after cleaning at 800°C. The total amount of O₂ taken up still raises, if T_s is increased from 800 to 900°C. This is shown in Fig. 2 which demonstrates further, that there exists a nearly linear relation between T_s and the amount chemisorbed during the first 16 hours. Also noteworthy is the fact that the shapes of all weigh curves seem to be identical, with the exception of the beginning.

Influence of chemisorption temperature

How chemisorption temperature influences the amount of oxygen taken up is shown in Fig. 4. For this series of experiments we fixed the cleaning temperature at 800°C for the 900°C char and at 700 for the 700 and 800°C chars. Starting with 150°C we varied T_s in intervals of 25°C up to 250°C. No higher temperatures were applied as during the chemisorption at 250°C almost 5% of the carbon has reacted and desorbed. Regarding the shapes of the weight curves can state that the sorption process is faster and that after 16 hours the slope of the curves has leveled off more the higher the temperature, indicating a more completed chemisorption. It can, however, not be deduced from these results whether or to which extent the equilibrium coverage with oxygen depends on temperature.

Influence of oxygen partial pressure

For the determination of the reaction order concerning oxygen, experiments were carried out using oxygen concentrations of 29.9, 10.5 and 5.3%. The results indicate that the reaction order is less than 1 as shown in Fig. 5 where the amount of oxygen taken up until the end of the run is plotted against the O₂-concentration of the He/O₂-mixture.

Discussion

Regarding the course of chemisorption, i.e. that the curve does not level off even after 16 hours at a temperature of 250°C, one can hardly imagine that all of the sites which are being covered after some hours or not yet after 16 hours are correlatable with reaction rates at temperatures twice as high than T_s.

Therefore we calculated the chemisorption rates on the basis of the weight curve and plot the logarithm of the rates as a function of time. As can be seen from Fig. 6, there is a fast reaction just at the beginning followed by a slower one indicated by the linear decrease of the graph after a time of 250 minutes. In order to determine the kinetics of these two reactions, i.e. to identify the processes involved, we tried to fit several kinetic models (3,4,8,9) and found that after approximately 20 minutes of chemisorption the weight curve can be described fairly well, assuming that diffusion is rate controlling. According to the study of Baumann, Klein and Juntgen (3,4) who have investigated the diffusion controlled chemisorption in the beginning as a square root law of time:

$$n(t) = n_{\infty} - \frac{12}{d} \sqrt{\frac{D_s \cdot t}{\pi}} \quad (1)$$

With:

$n(t)$ = O_2 -coverage at time t ; n_{∞} equilibrium coverage
 d = particle diameter; D_s = diffusion coefficient

and via an exponential function at the end of the sorption process.

$$1 - \frac{n(t)}{n_{\infty}} = \frac{6}{\pi^2} \exp \left[-4\pi^2 \frac{D_s \cdot t}{d^2} \right] \quad (2)$$

Both fitted the present data sufficiently which, however, is not significant enough. To confirm this assumption we plotted the logarithm of the rates concerned against temperature. In accordance we plotted the logarithm of the rates concerned against temperature. In accordance to theory the temperature dependence of the diffusion coefficient which in this case should be proportional to the rate can be described by:

$$D_s \sim T^{1.75} \quad (3)$$

Fig. 7 verifies this assumption. Since it is not correct to correlate chemical reactivities with amounts of oxygen taken up diffusion controlled, we focused our interest on the fast reaction subtracting the weight increase due to diffusion from the total increase in weight. One resulting weight curve is shown representatively in Fig. 8.

It is also interesting to examine the influence of cleaning temperature on chemisorption rate and to see whether it affects only the number of sites available or also their accessibility. For this purpose "diffusion coefficients" and diffusion corrected O_2 uptakes are compared in Table 2. Besides Fig. 9 shows the increase of the "diffusion coefficients" as a function of the amount of gases having evolved during the cleaning procedure. As can be seen from the picture this relation turned out to be fairly linear, whereas the "diffusion coefficients" seem to level off with increasing cleaning temperature. This means, that beyond a certain temperature a further increase in temperature only increases the number of sites available during chemically or diffusion controlled chemisorption.

Correlation with reactivities in steam

The reactivities of the chars under investigations were determined both isothermally and nonisothermally in 40 bar steam. A typical result is shown in Fig. 10 where the reaction rate

$$r_s = \frac{dX}{dt} (1-X)^{-2/3} \quad (4)$$

X = Degree of burn-off

is plotted as a function of burn-off for a gasification temperature of 750°C. The results depict that only in the beginning the reaction rates differ from each other and that after a certain time they narrow. An effect due to either thermal annealing of the char structure during gasification or the fact that in the beginning the unstable sites are gasified preferably and that already in the range of medium burn-off the structures of the different

chars became similar. These effects again point out how important it is to choose the correct cleaning time and temperature not to change the material under investigation.

For comparison we plotted therefore the first reaction rates versus the oxygen uptake during the fact chemisorption step as a function of cleaning temperature (s. Fig. 11). The relation seems to be linear in both cases for a cleaning temperature of 600 and 700°C. Both curves show similar slopes but different intercepts, as could be expected from the above mentioned. Next time it is planned to extend these correlations to a broader range of cleaning and chemisorption temperatures.

Conclusion

It could be shown that the O₂-chemisorption yield on chars produced from a German bituminous coal is affected to a large extent by diffusion processes and that its magnitude is influenced by the cleaning procedure which is absolutely necessary before chemisorption is carried out. Nevertheless the chars produced in different ways seem to behave similarly, i.e. whether they are cleaned at 600 or 700°C, the correlation with reaction rates depicts nearly the same slope. Therefore up to the time being only relative change in the reactivity of the chars originating from the same parent coal can be forecasted by chemisorption results, not the absolute magnitude of reactivity.

References

1. Chitsora Charles; Thesis GHS Essen, F.R.G. 1986.
2. Chitsora Ch., H.J. Muhler, K.H. van Heek, H. Juntgen; Proc. of the First Rolduc-Symposium 1986, to be published in Fuel Proc. Techn.
3. Baumann, H., J. Klein, H. Juntgen; Gluckauf Forschungshefte 39, 2, pp. 63-70, 1978.
4. Baumann, H., J. Klein, H. Juntgen; Gluckauf Forschungshefte 39, 2, pp. 105-113, 1978.
5. Muhlen, H.J., A. Sulimma; Process of the First Rolduc-Symposium 1986, To be published in Fuel Proc. Techn.
6. Muhlen H.J., A. Sulimma; Thermochimica Acta, 103, pp. 163-168, 1986.
7. Cheng, A., P. Harriott; Carbon Vol. 24, pp. 143-150, 1986.
8. Waters, B.J., R. G. Squires, N.M. Laurendeau; Carbon Vol. 24, No. 2, pp. 217-223, 1986.
9. Cypres, R., Ghodsi, H., Braekman, D.C., Planchon, D.; FUEL 64, pp. 45-55, 1985.
10. Laine N.R., Vastola F.J., Walker, P.L.; J. Phys. Chem. 67, p. 2030, 1963.
11. Causton, P., McNamey, B., FUEL 64, pp. 1447-1452, 1985.
12. Toda, Y.; FUEL 52, pp. 99-104, 1973.
13. Chiche, P., Durif, S., Pregerman, S.; J. of Chem. and Phys. 60, pp. 816-824, 1963.

	Original coal raw	Original coal ox.	Pyrolysis temperature [°C]		
			700	800	900
Proximate analysis					
Moisture %	2.1	3.3	0.6	0.4	0.2
Ash, df %	3.9	3.7	5.5	5.6	5.9
VM, daf %	37.4	34.6	4.1	3.6	1.5
Char %	62.2	63.2	89.8	92.8	95.0
Elemental analysis					
C, daf %	77.8	73.6	86.5	89.4	90.0
H, daf %	5.14	3.6	2.5	1.8	1.6
N, daf %	1.32	1.38	1.41	1.54	1.64
O, daf %	8.3	21.8	5.7	3.4	3.2
S, daf %	1.12	1.1	1.1	1.1	1.1

Tab. 1: Proximate and ultimate analysis of coal Westerholt and the concerning chars

Cleaning temperature °C	Slope in the $w(t) - \sqrt{t}$ -diagram	Diffusion corrected amount of O ₂ mg / 100 mg C	Total amount of O ₂ mg / 100 mg C
600	$9.65 \cdot 10^{-3}$	0.347	0.778
700	$1.73 \cdot 10^{-2}$	0.51	1.03
750	$2.73 \cdot 10^{-2}$	0.561	1.16
800	$3.94 \cdot 10^{-2}$	0.584	1.17
850	$3.86 \cdot 10^{-2}$	0.655	1.42
900	$3.67 \cdot 10^{-2}$	0.725	1.54

Tab. 2: Comparison of diffusion corrected and total O₂-uptake. Char Westerholt Chemisorption temperature 200 °C

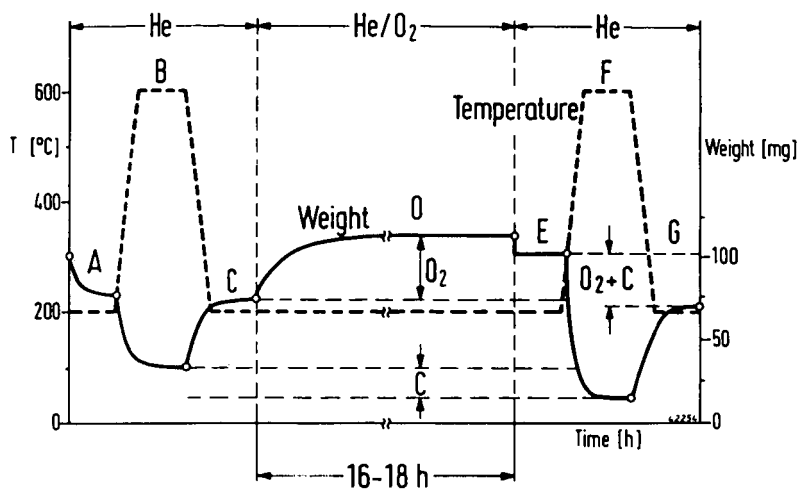


Fig. 1: Time-temperature-procedure for the determination of O_2 -chemisorption

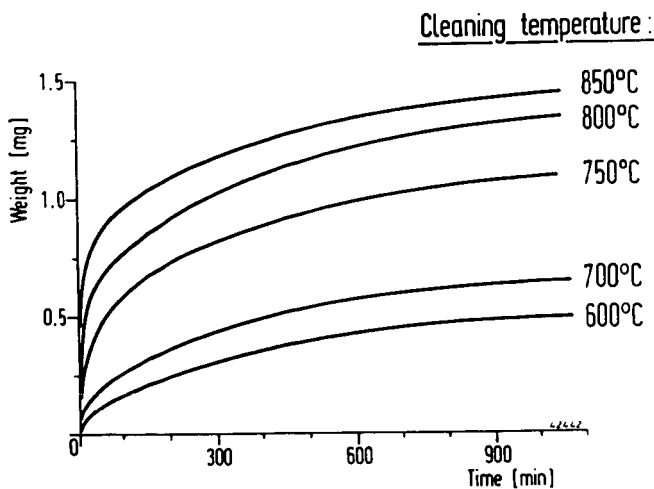


Fig. 2: Weight increase during O_2 -chemisorption on char Westerholt (HTT 900 °C) as a function of cleaning temperature

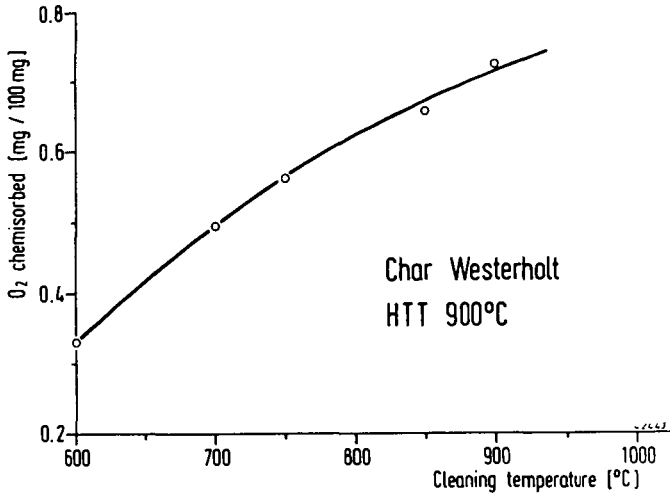


Fig. 3: Effect of cleaning temperature on the amount of O₂-chemisorption yield. Char Westerholt, HTT 900 °C, chemisorption temperature 200 °C

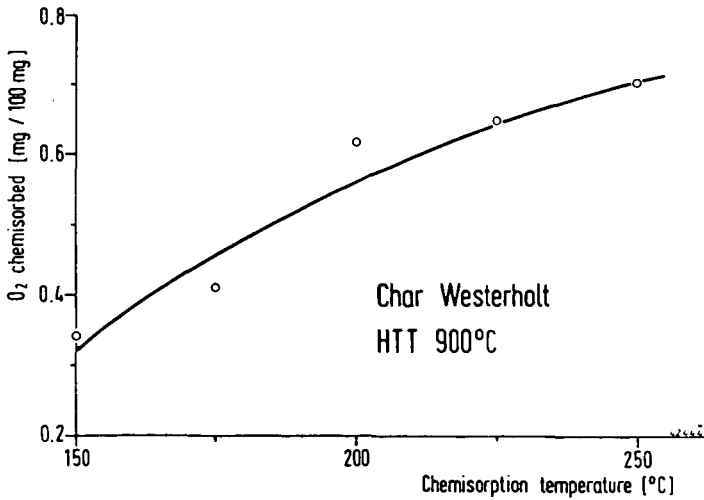


Fig. 4: Effect of chemisorption temperature on the amount of O₂ chemisorbed. Char Westerholt, HTT 900 °C, cleaning temperature 800 °C

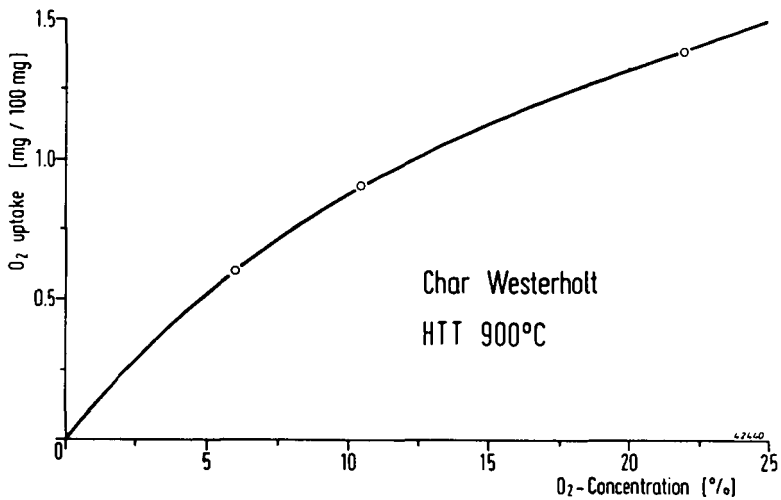


Fig. 5: Total O₂-uptake as a function of O₂-concentration. Char Westerholt, HTT 900°C, chemisorption temperature 200 °C

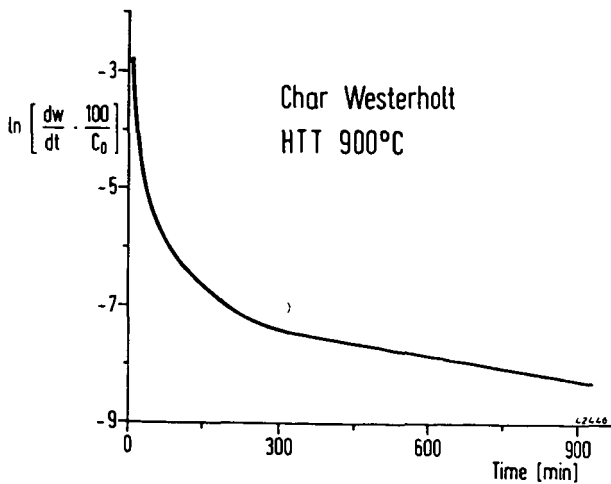


Fig. 6: Logarithm of weight increase with time during chemisorption at 200 °C. Char Westerholt, HTT 900 °C

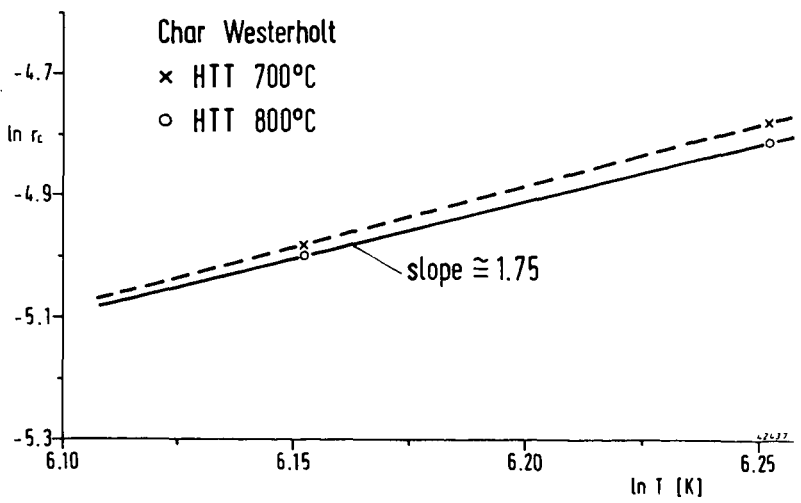
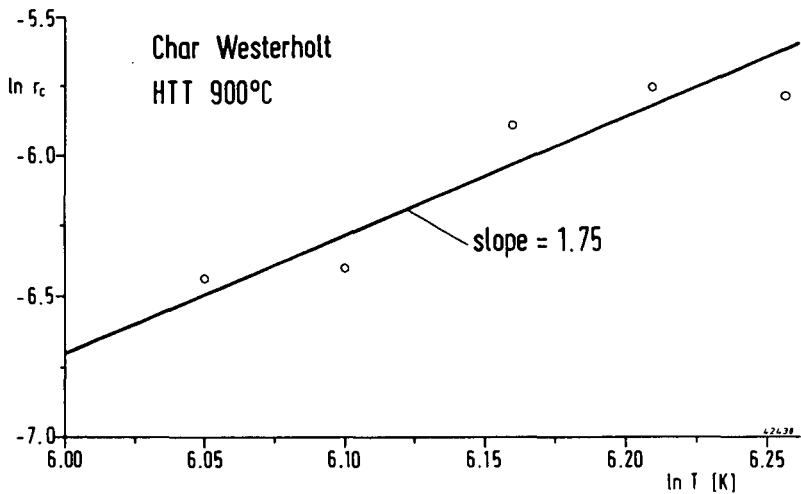


Fig. 7: Temperatur dependence of diffusion coefficients of chars prepared at a) 700, 800 °C; b) 900 °C

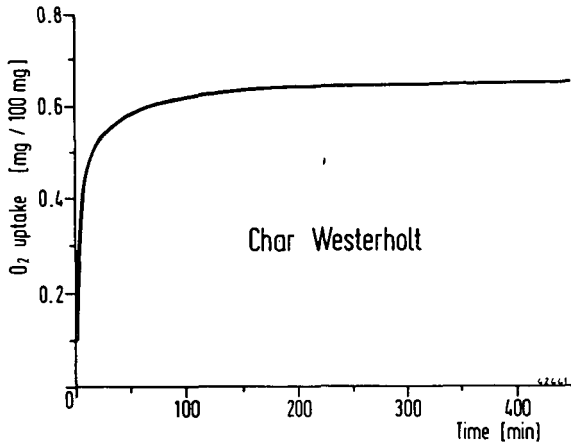


Fig. 8: Diffusion corrected weight increase during O₂-chemisorption on char Westerholt. Cleaning temperature 700 °C, chemisorption temperature 200 °C

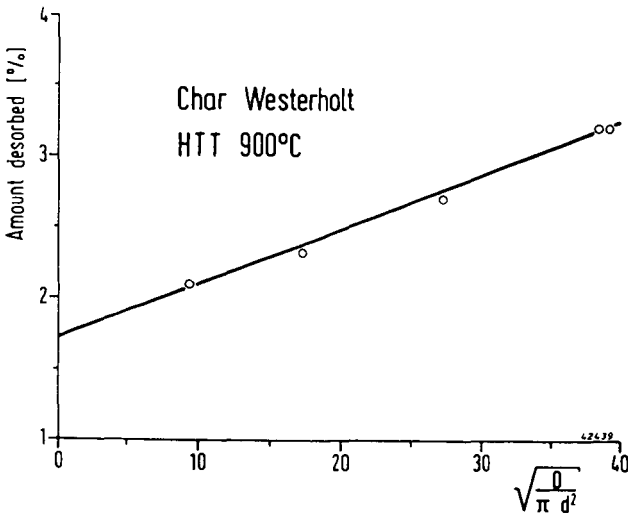


Fig. 9: Correlation between the slope of the $w(t) - \sqrt{t}$ - diagram and the extent of cleaning. Char Westerholt, HTT 900 °C

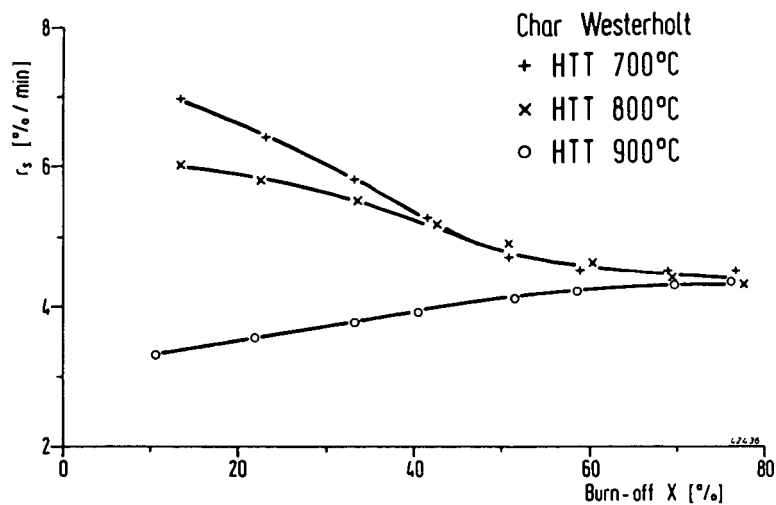


Fig. 10: Reaction rates of chars prepared at different HTT in 40 bar steam at 850 °C

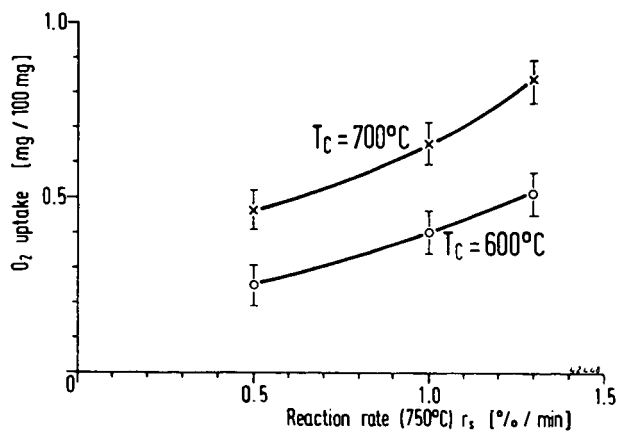


Fig. 11: Correlation of O_2 -uptake with initial reaction rates (750 °C) of chars prepared at 700, 800 and 900 °C. Cleaning temperatures 600 and 700 °C

Reactivity of Low-Temperature Chars: Significance of Char Active Surface Area as a Reactivity Parameter

M. Rashid Khan

U.S. Department of Energy
Morgantown Energy Technology Center
P.O. Box 880
Morgantown, West Virginia 26507-0880

ABSTRACT

Contemporary char reactivity studies have focused primarily on coal chars prepared at severe (high-temperature) conditions. In this study, the reactivity of chars prepared at mild (low-temperature) conditions has been addressed. A thermogravimetric analysis system (TGA) was used to determine the reactivity of chars in air or O₂ using isothermal or nonisothermal techniques. Coal chars were prepared in a TGA or in a slow heating rate organic devolatilization reactor (SHRODR) at a temperature range between 500° and 950°C. The chars prepared by mild pyrolysis of coal at 500°C are shown to be highly reactive. Comparison of reactivities of low- and high-temperature chars shows that the low-temperature chars exhibit higher reactivity than both the parent coals and the high-temperature chars. Correlation between isothermal reactivity results (e.g., time) and nonisothermal reactivity data (e.g., temperature) has been obtained. Hydrogen contents of chars correlate well with the reactivity of the chars. The study considers the significance of oxygen chemisorption capacity as a reactivity parameter.

INTRODUCTION

The Morgantown Energy Technology Center (METC) in-house results demonstrated that relatively high-quality liquids (low sulfur, high H/C) can be produced by low-temperature devolatilization of coal (1). The major product in a devolatilization process is char. Thus the utilization of the by-product chars by gasification/combustion should significantly improve the overall economics of a process that uses devolatilization. A literature review (2) suggests that previous studies of char reactivity were aimed solely at chars prepared at severe conditions (e.g., high temperatures). Consequently, there is a dearth of reactivity data on coal chars prepared at mild temperatures (e.g., 500°C). The volatile matter content of low-temperature chars, which can be appreciable, however, may favor reactivity of these chars. Literature data do not present a clear picture of the relationship between char hydrogen content or char volatile matter and the reactivity of char.

BACKGROUND

Coal chars are composed of pseudo-graphitic building blocks (3). In coal chars, particularly those prepared at low temperature, the carbon crystallites are small in size and poorly aligned because of crosslinking. The edge sites and various imperfections in the carbon structure (including singly-bonded "dangling" carbons) are thought to be the "active sites" during gas reactions.

The reactions of char with oxygen have generally been described (4,5) as governed by the following controlling processes: (a) mass transfer (by diffusion) of O₂ to reaction sites; (b) chemisorption of oxygen on the carbon surface, reaction of chemisorbed oxygen with carbon to form products, and desorption of products from the carbon surface, and; (c) mass transport of the gaseous products from the carbon surface. In the absence of mass transport limitations, the intrinsic char reactivity is controlled by (a) char active surface area, and (b) catalysis by impurities.

Laine, et al. (6) measured the kinetics of the C-O₂ reaction on graphitized carbon black using a combination of mass spectroscopy and oxygen chemisorption; the measurements showed clearly that gasification rates depend upon the fraction of active surface area (ASA) unoccupied by a stable oxygen complex. Hennig (7) developed an etch decorative technique to follow the enlargements of vacancies in the basal plane of graphite during reaction of carbon with oxygen; and established the importance of carbon active sites in determining the reactivity. Radovic et al. (8,9,10) extended the concept of active sites to lignitic chars prepared at various conditions and observed that the reactivity results can be normalized better when char ASA was considered.

As previously stated, the active sites are considered as imperfections in carbon crystallite edges or dislocations. The influences of hydrogen present on char surfaces, especially on those prepared at low temperatures, on reactivity or oxygen chemisorption are not well-known. For low-temperature chars, surface heteroatoms (mainly hydrogen) may play an important role in their reactivity by generating nascent sites (sites formed by devolatilization or gasification). ASA determination by oxygen chemisorption does not account for surface heteroatoms such as hydrogen. Suuberg, et al. (11), questioned the significance of oxygen chemisorption as a means to monitor ASA; and argued that the concept of active sites was too broad, since the reactive sites may be quite different in low-temperature chars from those in high-temperature graphitic carbons.

The effect of inherent inorganic constituents on char reactivity varies with coal rank. It is known that reactivity of chars prepared from lignites are markedly influenced by the inherently present well-dispersed metal cations. However, the reactivity of chars prepared from bituminous coals is not significantly influenced by the inorganic matter inherently present in chars, perhaps because of the discrete (lumped) nature of these minerals. Indeed, the reactivity of acid demineralized chars appeared to be slightly greater compared to the mineral-matter-containing chars (9). The effects of the demineralization process on the coal organic structures are not well known. It was shown (12) that commonly used demineralization procedures (13) markedly reduced the swelling of a plastic coal.

OBJECTIVES

The overall objectives of this study are the following: (a) quantify the reactivities of coal chars prepared at mild (low-temperature, 500°C) and severe (high-temperature, e.g., 950°C) conditions, (b) compare the reactivities of coals of various ranks with the corresponding low-temperature chars, (c) study the influence of char/coal hydrogen content on reactivities, (d) investigate the significance of oxygen chemisorption capacity as an index of char reactivity. Some preliminary results on each of these areas are presented.

EXPERIMENTAL

The coals were devolatilized either in a thermogravimetric analysis system (TGA) or in a slow heating rate organic devolatilization reactor (SHRODR), which allowed preparation of larger amounts of samples for characterization. In these units, chars were prepared at 20°C/min (TGA) or at 12.5°C/min (SHRODR). Descriptions of the TGA and SHRODR systems are available (1,14).

The analyses of coals and chars prepared at various conditions are presented in Tables 1A and 1B. As shown in Tables 1A and 1B, several high-volatile bituminous coals were used for devolatilization and reactivity studies. The Pittsburgh No. 8 coal pyridine extracted residue (subsequently water washed and vacuum dried at 200°C to remove pyridine) was also pyrolyzed at 500°C. In a TGA, the weight loss of a small amount of sample due to reaction is continuously monitored as a function of temperature. TGA has been shown to be useful for comparing reactivities of various feedstocks. To monitor the reactivity of the coal/char, isothermal and nonisothermal

reactivity techniques were used. The isothermal approach has been used to monitor char reactivity by others (8,10,15). Smith (4), Wagoner and Duzy (16), Wagoner and Winegartner (17) used derivative TGA profiles (DTA) for comparing relative reactivities of various coals, coal chars, or petroleum cokes under specified conditions.

TABLE 1A: Characterization Data for Raw Coals

	Pittsburgh No. 8 (hvAb)	Illinois No. 6 (hvCb)	Kentucky No. 8 (hvAb)
<u>Proximate</u> (As Received)			
Moisture	0.57	4.05	0.10
Ash	7.27	8.41	7.03
Volatile Matter	37.86	36.3	35.46
<u>Ultimate</u> (dry-ash-free basis, daf)			
C	83.75	69.3	86.35
H	5.46	4.75	5.41
N	1.56	1.32	1.53
S	2.15	3.2	1.21
O (By Difference)	7.08	10.26	5.50
H/C (atomic)	0.78	0.82	0.75
Heating Value (As Received) (Btu/lb)	13,976	12,523	14,256

TABLE 1B: Characterization Data for Chars

Sample/Preparation Condition	daf basis			
	C	H	N	H/C (Atomic)
Pit 8, TGA 500°C	79.7	3.02	1.67	0.45
Pit 8, SHRODR 500°C	84.4	3.05	2.15	0.43
Pit 8, TGA 650°C	83.8	1.98	2.12	0.28
Pit 8, TGA 750°C	86.0	1.20	1.77	0.17
Pit 8, TGA 950°C	90.4	0.52	1.64	0.07
Pit 8, Pyridine	79.82	2.65	2.79	0.40
Extracted residue 500°C				
Ill 6, SHRODR 500°C	89.2	3.06	2.57	0.41
Kentucky 8 SHRODR 500°C	91.14	1.66	1.81	0.22

In this study, the sample size used for a reactivity run was 2 mg or less. The gas flow rate for the reactants (O₂ or air) was 120 cc/min. The isothermal reactivities reported were independent of gas flow rate and, thus, the expressed rates are free from external mass transfer limitations. The char particle size was <74 μm. At these conditions, kinetically controlled reactivity results were obtained. The nonisothermal reactivity studies were performed at a heating rate of 100°C/min in air. In an attempt to measure the concentration of available carbon sites, oxygen chemisorption capacity of chars was determined. Chemisorption was carried out at ~200°C and 0.1 MPa O₂ for ~15 hours using the TGA.

RESULTS AND DISCUSSION

Isothermal Reactivity Results

The reactivity of char is generally expressed by the relationship, $R = -1/M_c \frac{dM_c}{dt}$. 1)

where dM_c/dt = instantaneous slope of burn-off curve

M_c = dry-ash-free (daf) basis char weight at time, t

In isothermal TGA studies, in the absence of catalysis, the rate is a function of concentration of reactants. Assuming the reactivity is first order for carbon (ASA), the char reactivity can be expressed by

$$\frac{dM_c}{dt} = -k M_c P_{O_2}^n \quad (\text{ASA}) \quad \begin{array}{l} P_{O_2} = \text{partial pressure of oxygen;} \\ n = \text{true reaction order} \\ \text{ASA} = \text{total active surface area} \end{array} \quad 2)$$

The intrinsic (in the absence of mass or heat transfer limitations) reaction rate constant k is given by, $k = A e^{-E/RT_p}$; where E = true activation energy, kJ/mole; T_p = particle temperature, K.

Equation 1 can be expressed in terms of fractional conversion, x :

$$M_c = M_i (1-x) \quad \text{or,} \quad x = \frac{(M_i - M_c)}{M_i} \quad 3)$$

$$R = \left(\frac{1}{1-x}\right) \frac{dx}{dt} = k P_{O_2}^n \quad (\text{ASA}) \quad 4)$$

where, M_i = initial daf char mass.

During a TGA run, T_p and P_{O_2} were held constant so that changes in the reactivity R with conversion could only be attributed to changes in ASA and k .

$$R = \left(\frac{1}{1-x}\right) \frac{dx}{dt} \propto k \quad (\text{ASA}) \quad 5)$$

The maximum rate of char reactivity (R_m , daf) widely used in literature (8,9,10,15), has been used as an index of char reactivity. Arrhenius relationships for the reactivity (R_m) of chars prepared at various peak devolatilization temperatures (PDT) are presented in Figure 1. The higher the PDT of the coals, the lower the reactivity of the resulting char; i.e., the highest R_m was noted for the char prepared at 500°C. This behavior is consistent with the trends available in the literature (10), although no data are reported for the low-temperature chars. The lower observed reactivity for the high-temperature chars are attributable to the loss of reactive sites and/or reactive functional groups (or hydrogen) on char surface at elevated temperatures.

The preliminary results show that the reactivity of low-temperature chars, like high-temperature chars, can be expressed by Arrhenius relationships. The activation energies of the low- and high-temperature chars are comparable. The observed activation energy of 130 kJ/mole is consistent with the literature results noted for various chars (10).

Significance of Oxygen Chemisorption Capacity as a Reactivity Parameter

The oxygen chemisorption data (e.g., percent O₂ uptake presented as m²/g, daf) were used to normalize the reactivity (at 400°C) results (Table 2) for chars prepared at low- and high-temperature conditions. For comparison, data on chars prepared at 500°C from various bituminous coals are also presented. Values for the active surface area, i.e., that surface area occupied by dissociatively chemisorbed oxygen atom (Table 2) were determined assuming a value of 0.08 nm² for the area occupied by each oxygen atom. The reactivity of different chars at 400°C showed variations by a factor of 13 (on g reacted/g initial material per h, basis). When the reactivity data are normalized on ASA basis (e.g., g/m²ASA.h), the variations in reactivity were reduced to a factor of 4. These findings are consistent with results reported by Radovic, et al. (8-10). These results provide credence that ASA as determined by oxygen chemisorption is a relevant reactivity parameter for low-, as well as high-temperature chars.

TABLE 2: Comparison Of Reactivities and Active Surface Areas For Various Chars

Sample/ Preparation Condition	ASA (at 200°C) (m ² /g)	Rm (400°C) (g/g/h,daf)	k, 400°C x 10 ³ (g/m ² ASA.h)
Pittsburgh No.8/TGA 500°C	253.5	3.3 (highest rate)	13.0
Pittsburgh No.8/TGA 650°C	150	1.2	8.0
Pittsburgh No.8/TGA 750°C	103	0.73	7.0
Pittsburgh No.8/TGA 950°C	70	0.26 (lowest rate)	3.7
Pittsburgh No.8 (Extracted)/TGA 500°C	251	3.2	12.7
Illinois No.6/SHRODR 500°C	157.5	1.26	8.0
Kentucky No.8/SHRODR 500°C	170.4	1.32	7.8
L. Kittanning/TGA 500°C (PSOC 1197; lvb)	158.7	1.14	7.2

Nonisothermal Reactivities

For dried char/coal samples (i.e., no moisture), the weight loss as a function of temperature is governed by the following events: (a) intrinsic gas solid reaction at low (10 percent) conversion, (b) at elevated temperature, the mass transfer of oxygen to the char limiting the intrinsic reactivity. However, with increased conversion and pore enlargement, the weight loss may shift between intrinsic reactivity limited to mass transport limited regions (4,5).

Nonisothermal reactivities of chars prepared at low- and high-temperatures were compared (Figure 2). As with the isothermal technique, the reactivity of the high-temperature chars were significantly lower than the low-temperature chars as was evident by a lower maximum rate of weight loss and increased temperature where the maximum rate peaked.

There are two primary schools of thought in the literature (5) on char oxidation mechanisms: (a) homogeneous combustion of volatiles formed during devolatilization is followed by slower heterogeneous oxidation of char, and (b) direct heterogeneous combustion of coal or char dominates. The results show that the latter mechanism prevails. For example, the mild pyrolysis chars (prepared at 500°C) demonstrated significant burn-off at 500°C, a temperature where little volatile matter is formed (Figures 2 and 3). The greater reactivity of the mild pyrolysis chars than that of the corresponding parent coals or the high-temperature chars can be attributed to

(a) easier accessibility of reactants into the chars structure compared to the parent coals, (b) the greater concentration of active surface area in the low-temperature chars as compared to the high-temperature chars, or (c) both.

Comparison of Reactivities of Coals and Chars

Nonisothermal reactivity measurements were performed in air to determine the reactivities of low- (500°C) and high-temperature (750°C) chars compared (Figure 3) to the parent coals. For the three high volatile bituminous coals (Pittsburgh No. 8, Illinois No. 6, and Kentucky No. 8), the maximum reaction rates of chars (prepared by pyrolysis at 500°C) were greater than the parent coals (Figures 3A, 3B, and 3C). By contrast, the maximum rates of weight losses for the char prepared from a low volatile coal (PSOC 1197, lower Kittanning seam coal, Pennsylvania) by pyrolysis at 500°C were lower than the corresponding parent coal (data not shown). It is suggested that highly agglomerated chars prepared from the HVA coals prevented diffusion of oxygen into the structure, and thus caused lower reactivity.

Reactivity of Preoxidized and Solvent Extracted Coals

It was hypothesized that preoxidized HVA bituminous coals, which do not become fluid, may demonstrate increased reactivity over untreated coals. A preoxidized (at 150°C for 6 days) Pittsburgh No. 8 coal was reacted nonisothermally in air. The maximum reaction rate for the preoxidized coal was greater than the untreated coal, but smaller than the char prepared at 500°C (Figure 3A and 4A). A comparison of nonisothermal (DTA) plots for the raw Illinois No. 6 and the preoxidized coal is presented in Figure 4B. It is interesting to note that the temperature of maximum rate of weight loss is shifted to elevated temperatures for the preoxidized coal. It is possible that upon preoxidation, some carbon sites for this coal are occupied by a stable oxygen complex which desorb at a higher temperature, causing an increase in the temperature of maximum burn-off rate. It is well-known that solvent extraction of bituminous coals destroys the plasticity of the residue during subsequent pyrolysis. To prevent coal swelling, the Pittsburgh coal was extracted with pyridine to remove materials that cause coal plasticity. The extracted coal also reacted nonisothermally in air. However, the maximum reactivity of the extracted residue was still lower than that of the char prepared at 500°C (Figure 4C). These results show that the char prepared at low temperature (500°C) is significantly more reactive than the preoxidized or solvent-extracted coal.

Correlations of Reactivity Results With the Char Hydrogen or H/C

Figures 5A and 5B correlate the reactivity (at 400°C) of the chars with the char H/C (atomic) or the hydrogen contents. The results show that the higher the char H/C (atomic) or hydrogen content, the greater the reactivity. The results suggest that the hydrogen rich portions of coal char are preferentially oxidized relative to carbon. Snow, et al. (18) studied the influence of hydrogen content on the oxidation of carbon blacks and observed that the higher the hydrogen content, the higher the reactivity (15,18). The significantly greater reactivity of the low-temperature chars compared to the high-temperature chars is attributable, at least in part, to the greater hydrogen contents of these chars. Hydrogen removal by oxidation leaves behind highly reactive "nascent" carbon sites (19). Walker, et al. (19,20) proved that removal of complexes from carbon surfaces enhanced the reactivity of carbons in carbon dioxide.

Correlations Between Isothermal and Nonisothermal Reactivity Data

Comparisons of the isothermal reactivity parameter (e.g., time for a given burn-off) with nonisothermal reactivity data (e.g., temperature for the same burn-off) have been made. Data in the Arrhenius forms are presented in Figures 6A (for 10-percent conversion, $T = 0.1$), 6B ($T = 0.3$), and 6C ($T = 0.4$). The activation energy (E_{act})

at low conversion ($T = 0.1$) is calculated to be ~ 130 kJ/mole, comparable to the isothermal case (Figure 1). At greater conversion ($T = 0.2$ to 0.4), the E_{act} reduced from 102 kJ/mole ($T = 0.3$) to 75 kJ/mole (at $T = 0.4$). This suggests that at low conversion, the weight loss is dominated by the intrinsic char oxygen reaction which has an $E_{act} \sim 130$ kJ/mole. At higher conversions (i.e., higher temperatures), however, the mass transfer of O_2 limits the weight loss. It is known that mass transfer process has a lower activation energy (4,5). Thus, at higher conversion ($T = 0.2$ to 0.4), the E_{act} is significantly reduced. The nonisothermal reactivity results (i.e., temperature) at low (10 weight percent) conversion can be correlated somewhat with the char active surface area (Figure 7), suggesting that active surface areas of these chars play an important role in determining the reactivity.

The influences of added inorganics on coal devolatilization and product yield/composition have been discussed (1,12,21). It was observed that addition of a hydrated dolomite [$Ca Mg (OH)_4$] at a low concentration (~ 5 weight percent) significantly reduced gaseous H_2S yield while the liquid quality was improved (i.e., reduced S content). A comprehensive study on the influence of various additives introduced prior to devolatilization on the reactivity is in progress. Figures 6A, 6B, and 6C presents some data (i.e., temperatures) derived from non-isothermal heating of a char prepared by co-pyrolysis of coal with dolomite.

There are several simplifications inherent in this study. The results presented in Table 2 (e.g., the absolute values of the reported ASA) should be interpreted with caution. As discussed previously, the ASA is a measure of available sites present on char surface. The analysis, in essence, demonstrates a trend that illustrates the principle of char reactivity. The actual reactivity mechanisms are complicated by the observations that (a) oxygen chemisorption capacity is a function of both the temperature and pressure of chemisorption, and (b) the measured oxygen uptake depends on whether it occurs in the presence or absence of concurrent gasification. A significant portion of sites on coal chars can be occupied by hydrogen, which may preferentially react with oxygen at low conversion, opening up new carbon active sites. However, the trends shown in Table 2, based on somewhat arbitrary conditions of chemisorption, illustrate the utility of oxygen chemisorption technique as an index of char reactivity.

SUMMARY AND CONCLUSIONS

(a) For char oxidation, the activation energy of 130 kJ/mole, comparable to literature data, was observed for both low- and high-temperature chars. This suggests that the chemistry of gas solid reactions follow comparable mechanisms for both low- and high-temperature chars. (b) The low-temperature chars prepared from various coals (at $500^\circ C$) appear to be more reactive (determined nonisothermally) than the parent coals. These low-temperature chars are also more reactive than the parent preoxidized coals or the solvent extracted residue. (c) The reactivity of various chars can be correlated with the H/C or char hydrogen contents. (d) The weight loss during nonisothermal reactivity at low conversion (10 percent) is limited by intrinsic gas-solid reactions. At elevated temperatures (or higher conversions), however, mass transfer limits the weight loss as is evident by lower activation energies for the process. (e) Finally, the char active surface area serves as a significant parameter for normalizing isothermal reactivity results. In addition, at low conversion, the non-isothermal reactivity parameter of chars can be correlated to the active surface area as determined by oxygen chemisorption.

ACKNOWLEDGEMENTS

The assistance of E. Newton and M. Rutherford, undergraduate student trainees at METC through Oak Ridge Associated Universities (ORAU) Program, who performed the TGA experiments, is acknowledged. J. Kovach and L. Headley made meaningful inputs in various aspects of this study.

REFERENCES

1. Khan, M. R., (1986) "Production of High-Quality Liquid Fuels From Coal by Mild Pyrolysis of Coal-Lime Mixtures," Fuel Science and Technology International, accepted for publication.
2. Khan, M. R., and Kurata (1985) "The Feasibility of Mild Gasification of Coal: Research Needs." DOE/METC-85/4019, (NTIS/DE85013625). Also, Khan, M. R. (1986), "Production of a High-Quality Liquid Fuel from Coal by Mild Pyrolysis of Coal-Lime Mixtures," DOE/METC-86/4060; NTIS-DE86006603.
3. Walker, P. L., Jr., and O. P. Mahajan "Analytical Methods for Coal and Coal Products" (C. Karr, Ed.), Vol. I, pp. 125 and 163. Academic Press, New York, 1978.
4. Smith, S. E., et al, Fuel 1981, 60, 459.
5. Essenhigh, R. H. in "Chemistry of Coal Utilization," 2nd Suppl. Vol. (Ed. M. A. Elliott), Wiley, New York, 1981, p. 1153.
6. Laine, N. R., F. J. Vastola, and P. L. Walker Jr. J. Phys. Chem. 1963, 67, 2030.
7. Hennig, G. R., "Chemistry and Physics of Carbon," Vol 2 (Ed. P. L. Walker, Jr.) Marcel Dekker, New York, 1965, p. 1.
8. Radovic, L. R., P. L. Walker Jr., and R. G. Jenkins, Fuel 1983, 62, 209.
9. Radovic, L. R., and X. Garcia, Fuel 1986, 65, 292.
10. Radovic, L. R., PhD Thesis, The Pennsylvania State University, 1982.
11. Suuberg, E. M., J. M. Calo, and M. Wojtowicz (1986), ACS Division of Fuel Chemistry Preprints, Vol 31, No. 3, pp. 186.
12. Khan, M. R., (1985) Ph.D. Thesis, The Pennsylvania State University.
13. Bishop, M., and D. L. Ward, Fuel 37, 191 (1958).
14. Khan, M. R. (1985), Proceedings, 5th Annual Gasification Contractors' Meeting, Morgantown, WV, June.
15. Jenkins, R. G., S. P. Nandi, and P. L. Walker Jr., Fuel 1973, 52, 288.
16. Wagoner, C. L., and A. F. Duzy, "Burning Profiles for Solid Fuels," paper presented at Winter Annual Meeting ASME, Pittsburgh, Pennsylvania, November 12-16, 1967.
17. Wagoner, C. L., and E. C. Winegartner, J. Engr. Power 1973, April 119.
18. Snow, C. W., D. R. Wallace, L. L. Lyon, and G. R. Crochen, Proceedings 4th Conference on Carbon, Pergamon Press, New York, 1960, p 79.
19. Phillips, R., F. J. Vastola, and P. L. Walker, Jr., Carbon 1970, 8, 197.
20. Walker, P. L., Jr., F. Rusinko Jr., and L. G. Austin, in "Advances in Catalysis," Vol. 11 (eds., D. D. Eley, P. W. Selwood, and P. B. Weisz), Academic Press, New York, 1959, p. 133.
21. Khan, M. R., (1986) Proceedings, 6th Annual Gasification Contractors' Meeting, Morgantown, West Virginia, June (1986).

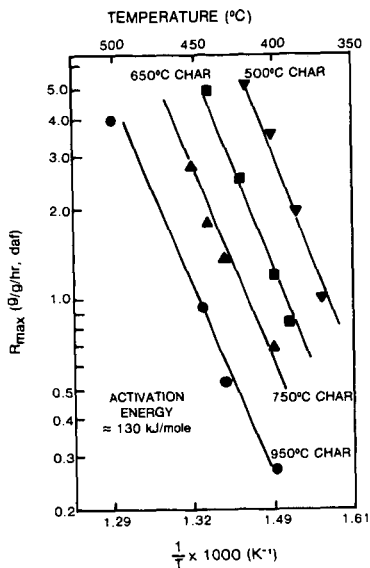


FIGURE 1. Arrhenius Relationships Between Chars (Prepared at Various Conditions) and Their Reactivities

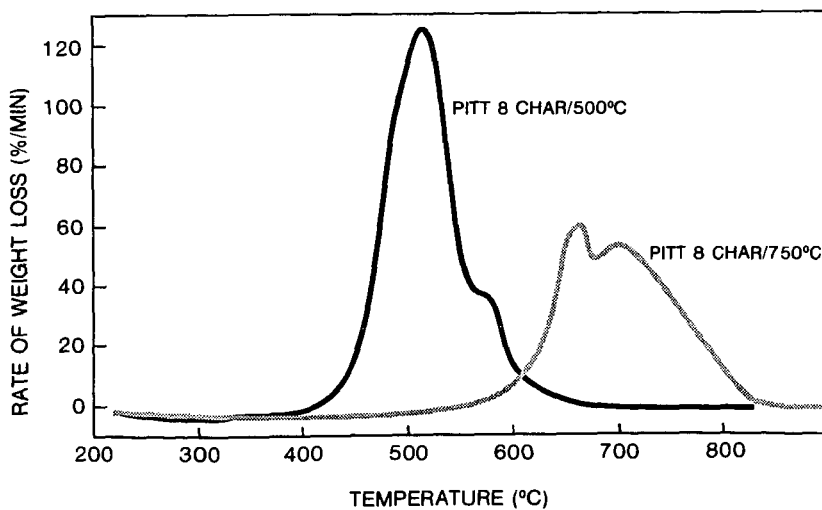


FIGURE 2. DTA Plots for Low- and High-Temperature Chars. (Air Flow Rate 120 cc/min)

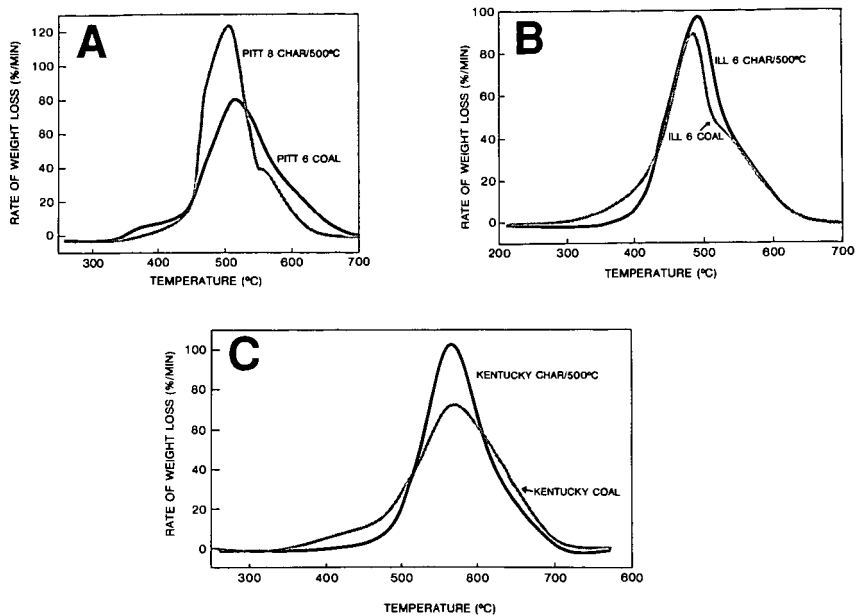


FIGURE 3. Comparison of DTA Curves for Coals with the Corresponding Low-Temperature Chars. (A) Pittsburgh No. 8, (B) Illinois No. 6, and (C) Kentucky No. 8. (Air Flowrate 120 cc/min)

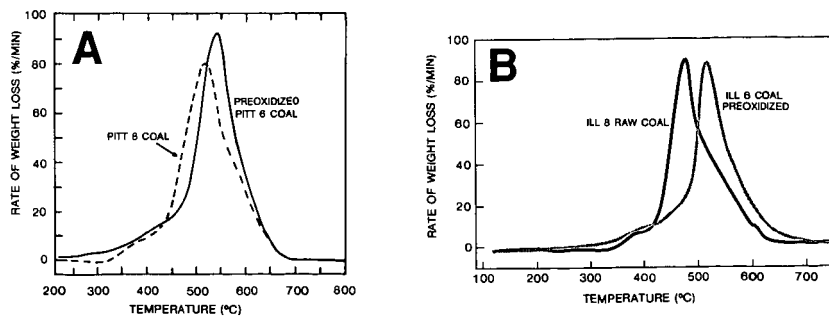


FIGURE 4. Comparison of DTA Curves for the Coals with the Corresponding Preoxidized Coals (A) Pittsburgh No. 8, (B) Illinois No. 6

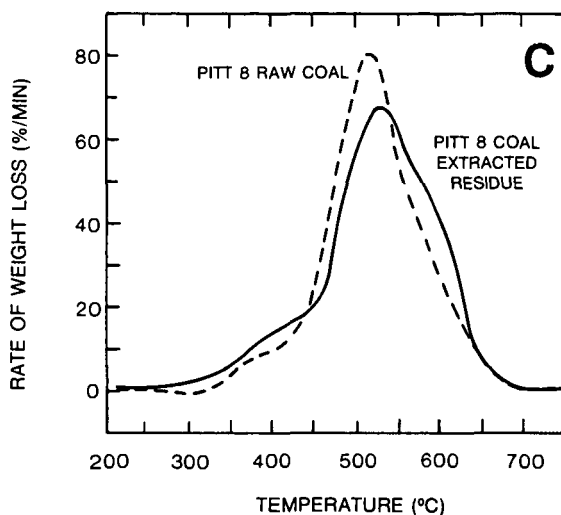


FIGURE 4. Comparison of DTA Curves for the Coals with the Corresponding Preoxidized Coals (C) Comparison of DTA Plots of Raw Pittsburgh No. 8 Coal with the Corresponding Pyridine Extracted Residue. (Air Flow Rate 120 cc/min)

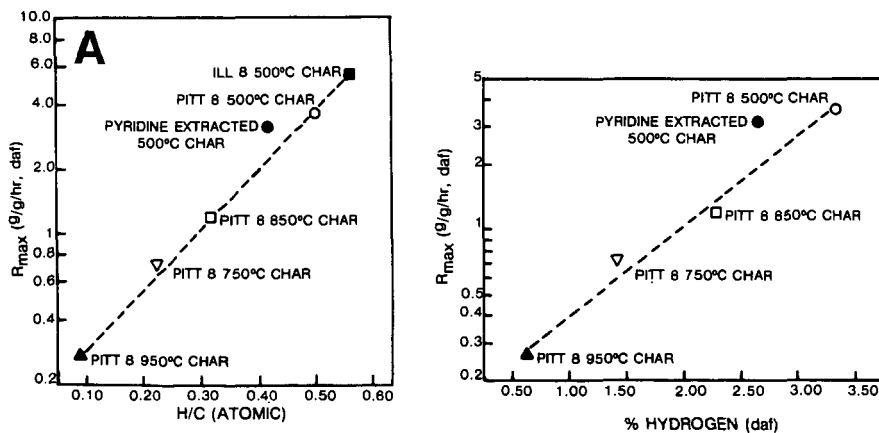


FIGURE 5. The Correlation Between Char Reactivity at 400°C (Isothermal) with (A) H/C (Atomic) or (B) Percent Hydrogen (daf) of the Chars

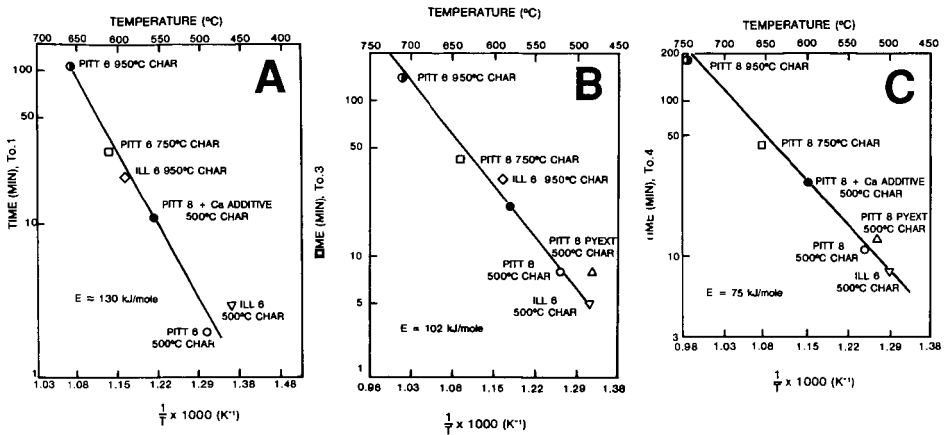


FIGURE 6. Correlation of Reactivity Results Obtained Using Isothermal (i.e., Time) and Nonisothermal (Temperature) Techniques at (A) 0.1 Conversion, (B) 0.3 Conversion, and (C) 0.4 Conversion. Isothermal experiments were performed at 400°C; nonisothermally, a heating rate of 100°C/min was utilized. To.1 signifies 10 percent conversion.

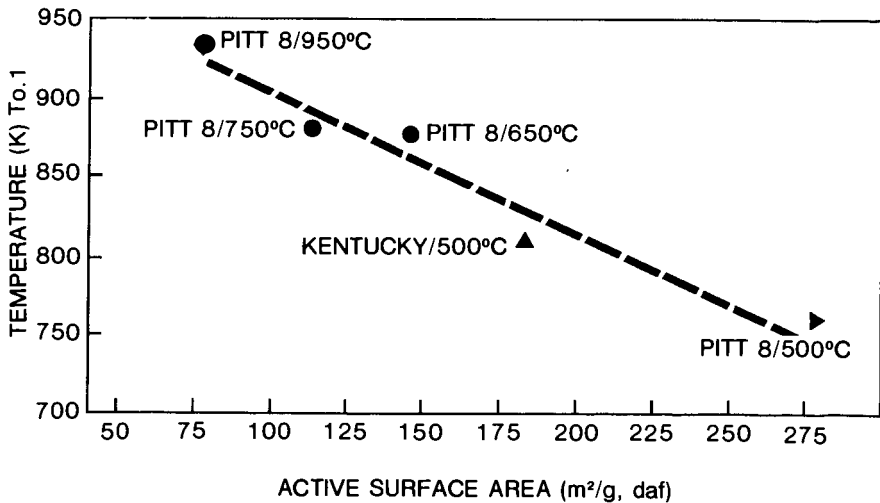


FIGURE 7. Correlation Between Nonisothermal Reactivity Parameter (i.e., Temperature) with the Char Active Surface Area as Determined by Oxygen Chemisorption. To.1 signifies temperature at which 10 percent conversion occurred when char was heated nonisothermally at 100°C/min in air.

EXAMINATION OF OXYGEN FUNCTIONAL GROUPS ON CARBONACEOUS SOLIDS BY
LINEAR TEMPERATURE DESORPTION TECHNIQUES

Yoshinobu Otake and Robert G. Jenkins

Fuel Science Program
The Pennsylvania State University
University Park, PA 16802

INTRODUCTION

It is important to understand the nature of carbon-oxygen complexes which exist on the surfaces of carbonaceous solids such as coal chars, activated carbons and carbon molecular sieves. The nature and concentration of the oxygen functional group will influence processes in which the carbon's surface is involved (1). As examples, wettability (2), adsorptive behavior (3,4), catalytic and electrical properties (5) are all affected by the chemical nature and extent of the oxygen-containing surface complex. In addition, oxygen chemisorption techniques have been used widely to estimate carbon "active site" concentration for various carbons and chars (6-9). These methods are used in attempts to correlate carbon reactivity with some fundamental property of the carbon. Of course, the surface complexes formed by this deliberate chemisorption of oxygen are the same as those produced by natural processes. Thus, a better understanding of carbon-oxygen complexes will be of value to practical and fundamental aspects of coal and carbon science and technology.

Highly porous carbonaceous solids, like coal chars, are mainly composed of relatively disordered carbon atoms. These materials, in general, demonstrate a high propensity for oxygen chemisorption because of large concentrations of edge carbon atoms. Once oxygen is chemisorbed onto these edge carbon atoms then carbon-oxygen complexes are formed. These surface functional groups can only be removed thermally as CO or CO₂. Complete thermal removal of the complexes requires temperatures of the order of 1250 K (6).

Direct analysis of the complexes has been performed (4) by a range of techniques. Unfortunately, many studies have produced conflicting results. This is probably a result of poorly defined carbons, poorly defined oxidation conditions and the use of widely different carbonaceous solids. In addition, it is understood that oxygen-carbon surface complexes do not behave necessarily in the same manner as do carbon-oxygen functionalities in simple organic compounds.

The principal purpose of this study was to examine oxygen complexes deliberately incorporated into a relatively pure, microporous carbon by using a Linear Temperature Programmed Desorption (LTPD) technique, in conjunction with chemical neutralization methods.

EXPERIMENTAL

Materials

A proprietary phenol-formaldehyde (PF) polymer was used to prepare the microporous char. The polymer was heated, in N₂, to 1275 at 10 K min⁻¹. The char was subsequently oxidized, to varying degrees, by (i) air oxidation performed in a fluidized bed over a range of reaction temperatures and times and (ii) treatment with concentrated HNO₃ solution for differing temperatures and oxidation times. Full details of these procedures (and others referred to in this paper) are given elsewhere (1).

Thermal Desorption Experiments

The LTPD experiments were generally carried out as follows. About 1 g of dried sample was heated in flowing N_2 at 5 K min^{-1} up to 1275 K. The evolved gases were continuously analyzed for CO_2 , CO, H_2 and H_2O vapor. Some experiments were performed in flowing H_2 , the procedure was identical to that using N_2 .

Selective Neutralization Technique

Small samples of char were immersed in separate solution of $NaHCO_3$, Na_2CO_3 , $NaOH$ and $Ba(OH)_2$. The amounts of acidic oxygen complexes neutralized by each solution were then calculated from titrations with HCl.

RESULTS AND DISCUSSION

Figures 1 and 2, respectively, present desorption profiles for the chars oxidized in HNO_3 (at 340 K, for 5 h) and in air (at 673 K for 3 h). As is to be expected, in both cases the principal gases evolved are CO and CO_2 . Essentially all the CO evolving complexes (CO-complex) and CO_2 evolving complexes (CO_2 -complex) are desorbed by 1275 K. It is important to note that each set of complexes (CO or CO_2 evolving) can be further divided into two categories depending on the temperature range of evolution. For example, in the case of the CO-complex, two evolution peaks are seen, one at about 900 K and one at 1100 K (Figures 1 and 2) for both samples. The CO_2 -complex on the HNO_3 treated char mainly appears at about 575 K (Figure 1), it then tails off with significant quantities of CO_2 being evolved up to 1000 K. On the other hand, the main CO_2 evolution for the air oxidized sample is around 900 K (Figure 2). This sample did evolve a small quantity of CO, in the lower temperature require (~ 550 K). For convenience sake we will refer to the four groups of complexes as lower and higher temperature, CO or CO_2 complexes. The main reasons for observing different evolution peaks for CO and CO_2 are that differing complexes will evolve the same gaseous species at various temperatures, and that the same oxygen complex may be formed at (and thus, desorbed from) energetically different carbon atoms in the zig-zag or armchair configuration.

It should be noted that the fraction of oxygen existing as CO_2 complexes on the samples is quite different for the HNO_3 and air oxidized samples. For example, in all cases, the HNO_3 oxidized chars at least 50% of the total oxygen is present as CO_2 -complex. However, for the air oxidized samples (ranging from 473 K for 1 h up to 783 K for 50 min) the oxygen present as CO_2 -complex varies from 25% to 50%. Obviously, the HNO_3 samples contain much more CO_2 -complex than do the air oxidized ones.

A direct correlation exists between total acidity (from NaOH neutralization) and the concentration of CO_2 -complex for both the HNO_3 and air oxidized chars (Figure 3). No such correlation can be found for the CO-complex on any oxidized char (1). As can be seen, the slopes of lines on Figure 3 are quite different. For the HNO_3 oxidized chars the slope is near to unity, whereas, for the air oxidized samples the slope is about two. From this, and other evidence from samples exchanged with sodium, it is suggested that the principal acidic CO_2 -complex from the HNO_3 oxidized chars is carboxylic acids. For the air oxidized chars, the main acidic CO_2 -complex is a carboxylic anhydride, which in aqueous solution (as in the neutralization experiments) forms two carboxylic acids for each anhydride hydrolyzed.

In an attempt to determine further the nature of the acidic functionalities ion-exchange experiments were performed with $Ba(OH)_2$. Boehm (10) observed that if two carboxylic acid surface groups were adjacent, then both could be neutralized by one $Ba(OH)_2$; if they are not near to each other, then one $Ba(OH)_2$ is required for neutralization of each carboxylic acid (the extra positive charge on the surface is balanced by OH^-). Thus, by comparing neutralization data from NaOH and $Ba(OH)_2$ one

can speculate on the relative distance between the acid groups. Such data for our samples are given in Table 1. For the HNO_3 chars, one observes an almost 1:1 relationship between the CO_2 complex and the moles of NaOH required for neutralization. The ratio for the number of moles of $\text{Ba}(\text{OH})_2$, needed for neutralization and CO_2 complex concentration is about 2:1. For the air oxidized chars, it is seen that the observations are very different. That is, the number of moles of NaOH and $\text{Ba}(\text{OH})_2$ needed for neutralization are very similar, and about twice the number of moles of the CO_2 complex.

TABLE 1
Neutralization Data for NaOH and $\text{Ba}(\text{OH})_2$ on Air and HNO_3 -Oxidized Chars

Sample	$-\text{CO}_2$ Complex mmol/g	Neutralization (mmol/g)	
		NaOH	$\text{Ba}(\text{OH})_2$
Air Char			
648 K, 3 h	0.4	0.8	0.9
698 K, 11 h	1.5	3.2	3.1
HNO_3 Char			
340 K, 0.1 h	0.6	0.6	1.3
340 K, 5 h	1.8	1.9	3.2

These data indicate that for these samples the acid groups are adjacent for the air chars and nonadjacent for the HNO_3 oxidized chars. This observation fits in with the suggestion of carboxylic anhydrides are the dominant CO_2 complex for the air oxidized samples because on hydrolysis the anhydride will yield two adjacent carboxylic acid groups.

Next we address the CO complexes by a series of LTPD runs made in 4.05% H_2 (balance N_2). The evolution of CO_2 was not influenced by the change to this gas mixture. The CO_2 profiles are almost identical to those obtained in N_2 . However, in this H_2 containing gas the LTPD profiles for the CO evolution are changed. For both the HNO_3 and air oxidized chars there is a dramatic loss of the higher temperature CO complex, but the lower temperature CO complex is little altered. In the case of the HNO_3 char, a second H_2O evolution peak appears at high temperatures, around 950 K (see Figure 4). For the air char, a H_2O peak is also observed at about 950 K. It should be noted that in all these runs the oxygen balance was remarkably good. That is, the total amount of 'oxygen' evolved is identical in both N_2 and H_2/N_2 gas mixtures. The only difference is in the distribution of species which indicates that the 'loss' of high temperature CO complex is quantitatively accounted for by the appearance of a new high temperature H_2O peak. Figure 4 also shows the consumption of H_2 during these experiments. The consumption of H_2 seems to parallel the evolution of the lower-temperature CO complex. A series of experiments was performed in which the lower temperature CO complex was systematically removed by heat treatment in N_2 , prior to LTPD in 4.05% H_2 . Figure 5 shows the results. There is an apparent direct relationship between H_2 consumption and CO complex decomposed.

Experiments were also carried out in pure H_2 at atmospheric pressure (Figure 6). The evolution of CO_2 was not influenced by H_2 , however, the evolution of CO is markedly reduced. There is a relatively large quantity of CH_4 produced. A run made with a clean char (heated to 1275 K prior to H_2 treatment) also produces some CH_4 (Figure 6) but it is also evident from this figure that the presence of some CO evolving complex enhances CH_4 evolution. Figure 7 is a plot of CH_4 evolved versus the amount of lower temperature CO complex that decomposes as CO (in H_2 , up to 1000 K). This figure does indicate that CH_4 production can be related to the lower-temperature CO complexes, irrespective of char type. The slope of this line

is the same as that (0.75) seen in Figure 5. These data suggest, strongly, that CH_4 evolution originates from the chemisorption of hydrogen on to carbon atoms made available by decomposition of CO complex. Ultimately the carbon-hydrogen complex decomposes to evolve CH_4 .

CONCLUSIONS

It has been shown that a combination of LTPD techniques, in different gaseous atmospheres, with selective neutralization techniques can yield very valuable information on carbon-oxygen surface complexes or chars. Specifically, it is concluded that, for these samples;

- The oxygen complexes can be conveniently divided into four groups comprised of lower and higher-temperature CO and CO_2 evolving complexes.

- CO_2 evolving complexes are mainly responsible for acidic nature of the chars studied.

- The principal CO_2 complexes can be characterized as (i) lower-temperature CO_2 complexes are nonadjacent carboxyl groups formed at dangling edge carbon atoms; (ii) higher-temperature CO_2 complexes are carboxylic anhydrides, which on hydrolysis form adjacent carboxyl groups.

- Thermal decomposition of the lower temperature CO evolving complex generates highly reactive dangling carbon atoms. These atoms can either chemisorb H_2 or produce CH_4 in the presence of H_2 .

REFERENCES

1. Otake, Y., Ph.D. Thesis, The Pennsylvania State University, University Park (1986).
2. Healey, F. H., Yu, F., and Chessick, J. J., *J. Chem.*, 59, 399 (1955).
3. Mahajan, O. P., Moreno-Castilla, C., and Walker, P. L., Jr., *Separation Sci. and Tech.*, 15, 1733 (1980).
4. Puri, B. R., in "Chemistry and Physics of Carbon," (Edited by P. L. Walker, Jr.), Vol. 6, p. 191, Marcel Dekker, New York (1970).
5. Coughlin, R. W., *Ind. Eng. Chem., Prod. Res. Develop.*, 8, 12 (1969).
6. Laine, N. R., Vastola, F. J., and Walker, P. L., Jr., *J. Phys. Chem.*, 67, 2030 (1963).
7. Radovic, L. R., Walker, P. L., Jr., and Jenkins, R. G., *Fuel*, 62, 849 (1983).
8. Suuberg, E. M., Calo, J. M., and Wojkovicz, M., *ACS Div. Fuel Chem. Prep.*, 31(3), 186 (1986).
9. Nayak, R. V., and Jenkins, R. G., *ACS Div. Fuel Chem. Prep.*, 29(2), 172 (1984).
10. Boehm, H. P., *Adv. Catalysis*, 16, 179 (1966).

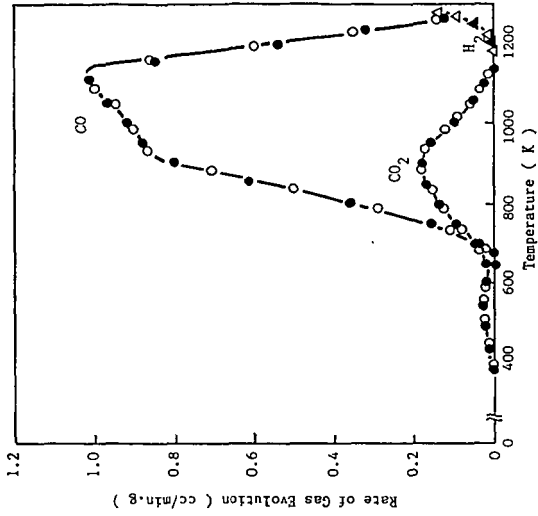


FIGURE 2. GAS EVOLUTION PROFILES FROM AIR CHAR (673 K, 5 H)

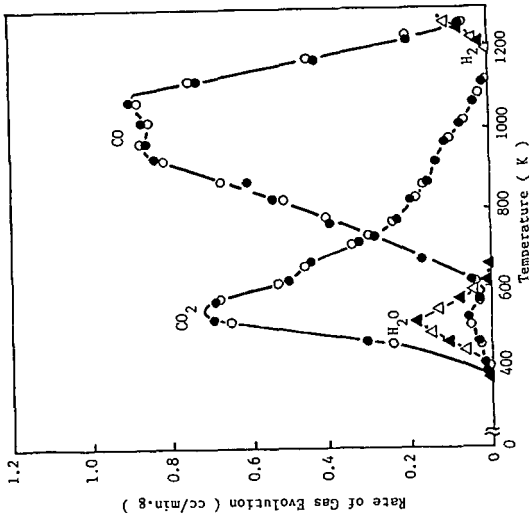


FIGURE 1. GAS EVOLUTION PROFILES FROM HNO₃ CHAR (340 K, 5 H)

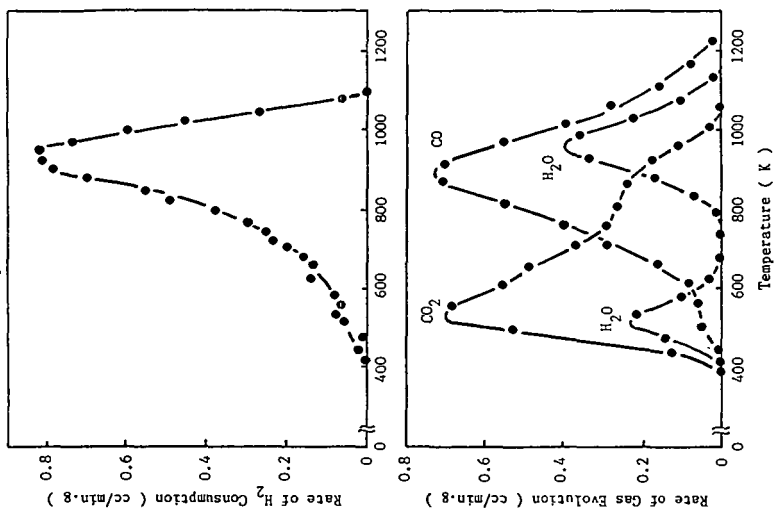


FIGURE 4. RATES OF GAS EVOLUTION AND H₂ CONSUMPTION ON HNO₃ CHAR (340 K, 5 H) DURING LTPD IN 4.05 Vol.% H₂

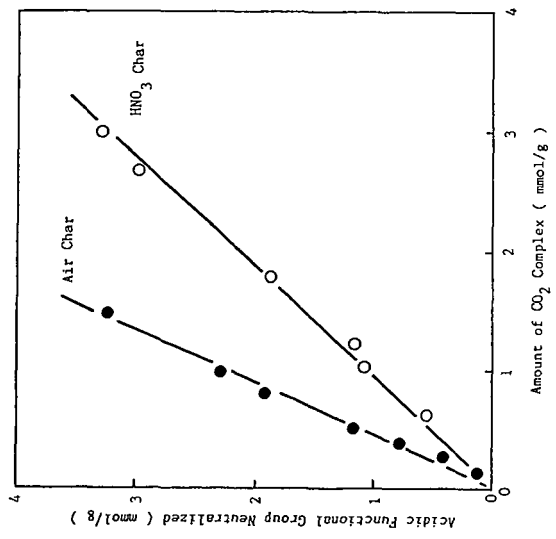


FIGURE 3. RELATIONSHIP BETWEEN TOTAL ACIDITIES MEASURED BY NaOH AND SITE CONCENTRATIONS OF CO₂ COMPLEXES PRESENT ON HNO₃ CHARs AND AIR CHARs

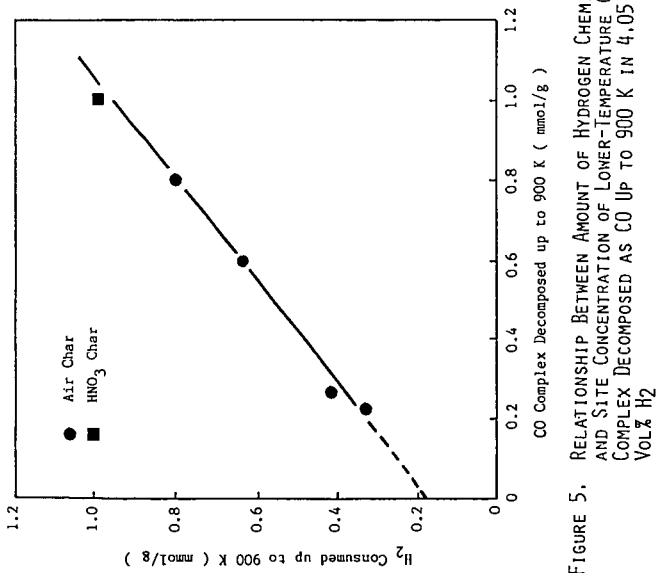


FIGURE 5. RELATIONSHIP BETWEEN AMOUNT OF HYDROGEN CHEMISORBED AND SITE CONCENTRATION OF LOWER-TEMPERATURE CO COMPLEX DECOMPOSED AS CO UP TO 900 K IN 4.05 VOL% H₂

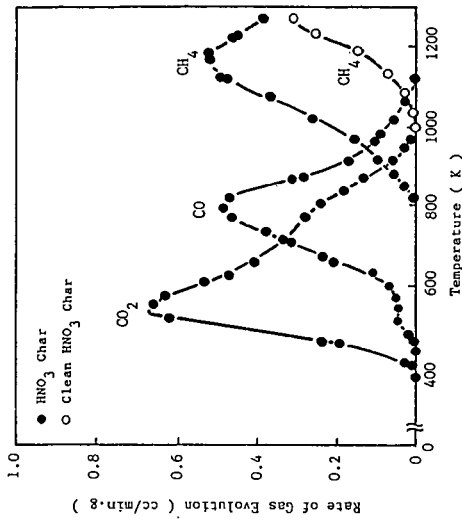


FIGURE 6. RATES OF GAS EVOLUTION FROM HNO₃ CHAR (340 K, 5 H) DURING LTPD IN ATMOSPHERIC PRESSURE H₂

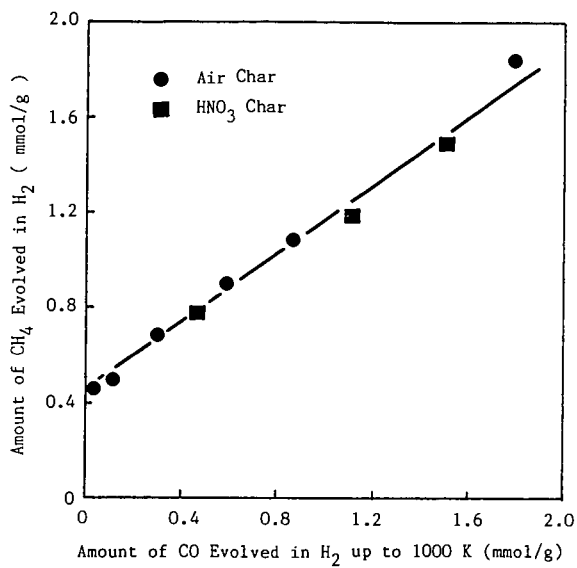


FIGURE 7. RELATIONSHIP BETWEEN AMOUNT OF CH₄ EVOLVED AND SITE CONCENTRATION OF LOWER-TEMPERATURE CO COMPLEXES DECOMPOSED AS CO UP TO 1000 K IN ATMOSPHERIC PRESSURE H₂

SURFACE CHARACTERIZATION OF O₂ AND CO₂ ADSORPTION ON CLEAN AND OXIDIZED GLASSY CARBON SURFACES

S. R. Kelemen and H. Freund

Exxon Research and Engineering Company
Route 22 East, Annandale, NJ 08801

Abstract

ESCA was used to characterize glassy carbon surfaces following exposure to O₂ and CO₂. Temperature-programmed Reaction Spectroscopy (TPRS) was used to monitor subsequent decomposition chemistry. The ability of O₂ and CO₂ to undergo dissociative chemisorption depends on the extent of prior oxidation. On initially clean surfaces, CO₂ and O₂ oxidation produced similar species characterized by a 531.0 (eV) O(1s) peak and a 285.8 (eV) C(1s) peak in the difference spectrum. The species decomposed above 700°C to produce gaseous CO. Additional exposure to CO₂ up to 700°C did not increase the oxygen surface coverage. O₂ generated additional oxygen with a 531.5 (eV) O(1s) and a 285.8 (eV) C(1s) peak in the difference spectrum. This oxygen species is associated with the production of CO near 600°C. O₂ is distinguished in its ability to dissociate on partially oxidized surfaces. The 285.8 (eV) C(1s) peak could not be interpreted in a straightforward way in terms of a carbonyl functionality. HNO₃ oxidation of glassy carbon was studied as a reference and favors the formation of carboxylic acid groups characterized by a 288.4 (eV) C(1s) peak and O(1s) peaks at 531.2 and 532.7 (eV).

Introduction

ESCA has been used to characterize the surfaces of a wide variety of different carbons which include glassy carbon(1-3), graphite(4,5) and carbon fibers.(6-11) Information has been gathered about the degree of surface oxidation and type of oxygen complexes formed after various oxidative treatments.(1-3, 5-11) The degree of oxidation can be monitored by the O(1s) intensity. In general a distinction about the kind of surface oxide is made based on the C(1s) emission which occurs at higher binding energies from the main (1s) line. Extensive ESCA studies of organic molecules and polymeric materials(12-16) have demonstrated that the magnitude of the C(1s) peak shift to higher binding energy is related to the number of carbon oxygen bonds and in the range of 1.5 eV ± 0.4 per bond. The result is significant because common functionalities can be grouped according to their C(1s) shift. The guidance from these simple additivity rules have been employed in the interpretation of results from carbon surfaces. For example ~1.5 eV shifts are associated with alcohols and ethers, ~3.0 eV shifts with carbonyl groups, ~4.5 eV shifts with acids and esters.(1-3, 6-16)

The O(1s) peak also contains functional group information. In esters singly and doubly bonded oxygen is separated by ~1.3 eV with the singly bonded oxygen at higher binding energies.(13-16) A distinction between carbonyl oxygen at 531.6 eV and ether oxygen at 533.1 eV was recently made on carbon fiber surfaces.(10)

We have previously used AES in a comparative study of the O₂ and CO₂ oxidation of glassy carbon surfaces.(17) As expected O₂ has a much higher reactivity. This was associated with a more facile gaseous dissociation step at high oxygen coverages which generated lower energy CO formation sites. The available ESCA results suggested that CO₂ and O₂ produced similar oxygen functionalities at 300°C having a 532 eV binding energy with the absence of carboxylic-like C(1s) features. These results are consistent with a carbonyl-type functionality, however, a definitive identification based on the C(1s) peak was not made. The object of the present work is to obtain high resolution C(1s) and O(1s) spectra produced under previously defined chemical conditions. The spectra should lead to functional group identification. This information coupled with TPRS results and previous kinetic data(18) will provide a good basis for further fundamental mechanistic work and interpretation of carbon oxidation and gasification processes.

Experimental

The glassy carbon starting material was obtained as plates from Atomergic Chemetals. Samples were made in the form of powders and chips. Both powders and chips were used in TPRS experiments while chips were used exclusively in ESCA experiments. 60-80 mesh powders were produced by grinding and sieving glassy carbon plates. Powders were found to have 5 m²/g specific surface area based on Kr chemisorption measurements. The powders were outgassed to 900°C prior to oxidation. O₂ and CO₂ oxidation were done in a Dupont model 951 thermogravimetric analyzer. 50 mg of material was normal sample size. The glassy carbon chips were cut from plates with a diamond saw to 1 cm x 1 cm x 1 mm dimensions. The chips were successively polished with Buehler Carbimet silicon carbide paper up to 600 grit number. The samples were further polished with Buehler Alumina paste down to 0.05 micron size.

The chips were washed with deionized water and then outgassed to ~1300°C in UHV prior to use. The specific surface area of the chips were 0.3 m²/gram based on Kr chemisorption measurements. Oxidative treatments could be given to samples in the TGA apparatus as with powdered samples. The chips were especially suited for use in a atmospheric pressure/UHV sample introduction system. Samples could be given reactive treatment up to 700°C in 1 atm gas and returned into a UHV apparatus for surface analysis without exposure to air. Glassy carbon chips as well as powdered samples which received oxidative treatments in the TGA apparatus and which were cooled to room temperature in the reactant gas mixture, could be transferred in atmosphere to respective holders for TPRS experimentation. Brief exposure to air at room temperature did not alter reactivity patterns observed in subsequent TPRS experiments. Nitric acid oxidation was accomplished by boiling the samples in HNO₃ under reflux conditions.

The TPRS apparatus used with powdered samples was specially constructed as an appendage to a UHV spectroscopy chamber which housed an EAI and an Extranuclear quadrupole mass spectrometer. The EAI unit had dual mass scanning capability during a TPRS experiment while the Extranuclear Spectrometer, interfaced to a PDP 11 data acquisition system, provided the capability to follow up to eleven masses during a TPRS experiment. The TPRS unit had a base pressure of 5×10^{-10} Torr pumped separately by a Balzers 300 l/s turbomolecular pump. 5-10 mg samples were accommodated in a ceramic vessel 9mm long x 3 mm diameter. A chromel-alumel thermocouple was inserted into the sample bed. The sample holder was resistively heated by tantalum elements and the sample temperature was controlled by a Micristar controller. The volume of the TPRS apparatus was approximately 100 cc.

ESCA Spectra were obtained from a Vacuum Generators ESCALAB equipped with a 150 degree Spherical Sector Analyser. The base pressure in the analysis chamber was less than 1×10^{-10} torr. Non-monochromatic Mg K α radiation was the excitation source. The x-ray source was operated at 300w (20ma, 15 kV). Glassy carbon and graphite samples did not experience charging problems during data acquisition. The work function of freshly cleaned Union Carbide XYA Monochromator Graphite was 4.2 eV and the carbon (1s) binding energy with respect to the vacuum level was 284.4 eV. The work function of Glassy carbon was also 4.2 eV. The binding energy of the C(1s) peak of clean Glassy carbon was 284.5 eV with respect to the vacuum level. Oxidation of Glassy by O $_2$ at 700°C increased the work function of the sample to 4.4 eV. The increase was smaller for milder oxidations while HNO $_3$ oxidation increased the value to 4.5 eV. The slight binding energy corrections due to the increase in work function upon oxidation, < 0.3 eV, were not made to the oxidized spectra. All N(E) spectra were obtained at 0.9 eV resolution. The signal from the C(1s) peak of graphite corresponded to 35,000 counts/sec. Typical counting times yielded spectra with 10 6 maximum counts. Data acquisition was by means of VGS 2000 software package using multi scan averaging.

Results

Following HNO $_3$ oxidation, glassy carbon samples were temperature programmed and the gaseous evolution recorded as a function of temperature. Figure 1 shows the results at two different heating rates. The gaseous production patterns shift to higher temperatures with increased heating rate. It was not possible to derive detailed energetics of the decomposition processes from the variation of the peak maximum with heating rate(19, 20) because of the extremely broad features from overlapping peaks. Nevertheless the evolution patterns are sufficiently distinct so as to be interpreted on a chemical basis. H $_2$ O is a major product below 200°C. CO $_2$ and CH $_4$ dominate the profile between 200 to 400°C. CO production increases over this interval while H $_2$ O declines to background levels. Above 500°C there is a fall off of CO $_2$ and CH $_4$ as CO becomes the major product.

ESCA was used to characterize the initial state of HNO $_3$ oxidized glassy carbon surfaces and as a function of heating in UHV. The heating schedule was approximately 1 degree per sec. to a maximum temperature then cooled in UHV for analysis. The C(1s) ESCA results are shown in Figure 2 in

the form of a difference spectrum. The spectrum of a "clean"(21) glassy carbon sample outgassed at 1300°C in UHV was used as the reference spectrum for subtraction from each oxidized spectrum. The y axis scales are different in each spectrum so as to highlight the relative changes. The absolute magnitude of the changes relative to the reference spectrum decreases with decreasing degrees of oxidation. The 600°C sample contains approximately 1/4 the oxygen as the 100°C case and the 600°C difference spectrum is on a four times more sensitive scale relative to the 100°C case. The magnitude of the change is clearly evident from the actual spectra, not shown. The large negative going peak in each spectrum is a result of decreased emission from the parent C(1s) signal upon oxidation. The positive going features are a result of oxidation and represent modified carbon forms. The 100°C spectrum has one prominent peak at 288.5 eV. The peak occurs 4.1 eV shifted from the parent carbon (1s) line. In additivity terms the peak can be related to carbon atoms triply coordinated to oxygen, as in the case of an acid functionality. The total amount of hydrogen produced as H₂O and CH₄ in TPRS experiments relative to the total oxygen produced as CO, CO₂, and H₂O is consistent with the 288.5 eV peak in the 100°C spectrum being primarily due to acid functionalities. There is another major peak at 285.2 eV which is shifted by 0.7 eV. The magnitude of the shift is consistent with it being a β peak, i.e., a shift of the carbon atom adjacent to the acid carbon.(22)

There is also a broad decrease in emission, representing a 50% absolute decrease centered at 290.5 (eV). We have observed a broad peak centered at this energy with clean glassy carbon samples. As in other aromatic systems the peak is due to π to π* transitions.(23) UPS studies of glassy carbon(21) show substantial valance band emission within 2 (eV) of the Fermi level. This emission is derived from the π bonding structure and is associated with unsaturated carbon valencies. Upon oxidation this emission decreases. In the case of HNO₃ oxidation the emission within 4 eV is lost and the UPS valance band spectrum resembles that from insulating structure. It is not surprising that π to π* emission intensity would decrease upon oxidation although we do not know what changes occur in the unoccupied states.

Between 100-525°C, during the stage of major CO₂ evolution, the 285.2 eV peak and the 288.5 eV peak simultaneously decline. There is an absolute 80% decline evident in the 288.5 eV peak from the N(E) spectra. The coupled decline further supports the contention that the 285.2 eV represents a β peak. At 600°C a peak near 286.0 eV becomes the major component and the subsequent gaseous evolution is mainly to CO. Note also the retention of a proportionate decline in the π to π* intensity.

The initial oxygen (1s) spectrum is broad (FWHM 3.5 eV) and can be resolved into two peaks of equal intensity at 531.2 and 532.7 eV. Two peaks are anticipated for an acid structure with the doubly bonded oxygen at lower binding energy. As the sample is heated in stages the O(1s) incremental difference spectra between 100 to 300°C show a slight nonuniform decline in intensity toward the low binding energy side and H₂O is an important product. H₂O formation may result from acid decomposition and formation of lactone structures. Between 300° to 525°C there is a uniform decline in O(1s) intensity and CO₂ and CH₄ are major products. The O(1s) behavior indicates that the initial O(1s) spectrum may be composed of several different acid functionalities with individual two-peaked structures. Above 600°C the O(1s) signal can be resolved into two peaks at 531.0 eV and 533.2 eV. The 531.0 eV

peak declines at higher temperatures and there is CO evolution. The 533.2 eV peak corresponds to stable ring ether.

Clean glassy Carbon samples were oxidized in O₂ and CO₂ and characterized with ESCA and TPRS. Figure 3 show the O(1s) signal on the same intensity scale. Each sample was oxidized for 300 sec under specified conditions and cooled in the reactant gas. Negligible burn-off occurred below 300°C. The 700°C oxidations in O₂ and CO₂ corresponded to 20% and <0.1% burn-off respectively. The amount of surface oxidation that could be achieved with O₂ increased with temperature. A 531.0 eV peak is generated at 150°C with a shoulder at higher binding energies. The O(1s) intensity increases at 300°C and 700°C as higher binding peak components begin to contribute. In contrast there is a limited amount of oxidation with CO₂ and similar levels are achieved at 300°C and 700°C. This is consistent with previous AES studies.(17) Two main components occur at 531.0 eV and 533.0 eV. The 531.0 eV peak decreases with concomitant CO evolution upon heating above 700°C.(17) The 533.0 eV peak represents very strongly bound oxygen with small residuals stable at 1300°C (see Figure 6). The 533.0 eV peak is associated with ring ethers.

It is tempting to interpret the 531.0 eV O(1s) peak produced by CO₂ and O₂ with doubly coordinated oxygen as in a carbonyl functionality. Indeed we had previously taken an unresolved 532 eV peak as evidence for a carbonyl functionality. Current carbon (1s) difference spectra in Figure 4 seem to belie the presence of a simple carbonyl functionality. From simple additivity arguments we would expect a carbonyl oxygen to shift carbon by approximately 3.0 eV. There is little intensity in this region. The main carbon (1s) difference features look very similar for O₂ and CO₂. The large negative going peak represents lost parent C(1s) intensity upon oxidation. The main positive peak occurs at 285.8, shifted 1.3 eV from the main line. This would represent carbon singly coordinated to oxygen based on additivity reasoning. In the case of 700°C CO₂ and 300°C O₂ oxidation there is a decrease in emission centered near 290.5 eV reflective of lost π to π^* intensity. In the case of 700°C O₂ oxidation a small positive peak occurs at 288.7 eV along with added emission near 291 eV. The 288.7 eV can be rationalized by the presence of carbon triply coordinated to oxygen. Acidic properties have been reported following O₂ oxidation of carbon which have been supported with spectroscopic evidence.(28) It should be recognized the enormous amount of material on the atomic scale which must be removed to achieve 20% burn-off. The exact nature of the residual carbon may be different. We have observed UPS features from glassy carbon which tended more toward graphite after 1300°C cleaning following severe oxidation; specifically the appearance of a Γ_{3u} final state peak of graphite.(25) The fine luster of a polished surface was gone; the surface was dull and pitted. The selective oxidation of less refractory carbonaceous components in glassy carbon could change the π to π^* intensity contributions and account for the broad 291 eV peak. The other possibility is the presence of carbonate structures, however, this interpretation is less likely as the added emission at 291 eV persists upon heating to high temperature where carbonates should decompose.

As observed in previous systems(26), O₂ oxidation and quench procedures results in both CO and CO₂ evolution in subsequent TPRS experiments. Figure 5 shows the results with glassy carbon as well as for CO₂ oxidation. CO₂ oxidation produces surface species which only yield CO. O₂ generates

surface species which produce CO at much lower temperatures. This behavior has been detailed in previous work.(17) The small 288.7 eV C(1s) peak decreases along with the 285.8 eV peak concomitant with CO₂ and CO evolution between 400-600°C. Above 600°C CO is produced and the 285.8 eV peak decreases. A distinction between the species generated at high oxygen coverages with O₂, which produces CO near 600°C, and the species generated at low oxygen coverages with either O₂ or CO₂, which produces CO above 700°C cannot be made based on C(1s) spectra.

The O(1s) spectra, shown in Figure 6, produced a clear indication of a distinct electronic configuration at high oxygen coverages. A glassy carbon sample was heated for 300 sec in 1 atm O₂ at 700°C, cooled in the reactant gas and then incrementally heated in UHV. The initial oxygen spectrum at 100°C was previously described. The O(1s) signal decreases at each temperature interval. Previous AES results(17) mapped the oxygen stability profile at high oxygen coverages. We expect a step decrease in signal between 450-600°C. The O(1s) difference spectra shows a selective decrease in O(1s) signal over this interval characterized by a 531.5 eV peak (FWHM of 1.7 eV). At 600°C the O(1s) signal is a two-peaked structure and can be resolved into 531.0 eV and 533.0 eV components. A 531.0 eV peak can be produced by low temperature O₂ and CO₂ oxidation and yields CO between 700 and 900°C. The 533.0 eV peak represents oxygen more strongly bound, probably ring ether. A small peak remains after 1300°C heating. Similar structures remain above 900°C on potassium catalyzed glassy carbon surface following potassium loss. The relative amount of this type of oxygen depends on the prior sample treatment.(27) It is a minor component following 150°C O₂ oxidation as these conditions are not harsh enough to generate substantial oxygen incorporation into the ring structure. The relative amount of oxygen stable above 900°C tends to increase with increasing severity of prior oxidation. It is a significant component following O₂ oxidation at 700°C and HNO₃ oxidation of glassy carbon. The ability of O₂ and CO₂ to dissociatively adsorb on glassy carbon depends on the amount of oxygen already present. It is likely that this kind of very stable oxygen will also modify the ability of O₂ and CO₂ to dissociate on proximate carbon sites.

Discussion

The ability of O₂ and CO₂ to dissociatively adsorb on glassy carbon is dependent on the degree of surface oxidation. Similar kinds of species are produced by CO₂ and O₂ up to moderate oxygen coverages. O₂ is distinguished by its ability to dissociate on partially oxidized surfaces. It is apparently this property which enables O₂ chemisorption to be a useful surface area probe in gasification systems.(29) The nature of the CO₂ and O₂ dissociation products is a more complicated question. C(1s) deconvolution schemes based on the simple additivity relationship have been used in the interpretation of oxidized carbon surfaces (1-3, 6-16). In the study of carbon fiber surfaces Takahagi and Ishitani (7) use a 2.4 eV shifted peak for carbonyl groups. Proctor and Sherwood (8) use a 3.0 eV shifted peak; nevertheless, the same authors present evidence that carbonyl functional groups on extended aromatic ring systems may have smaller shifts than those found for similar functionalities in polymers. They suggest that the C(1s) shifts in extended aromatic carbonaceous systems are modified due to the presence of π -interactions. Kozlowski and Sherwood (9) have electrochemically oxidized

carbon fiber surfaces in nitric acid and show a distinct C(1s) peak shifted 2.1 eV and assigned to carbonyl type oxides. This is in addition to ester-type groups shifted ~4.0 eV. In later work (10) these authors suggest the 2.1 eV shifted peak is a result of a keto-enol type structure. In general, it is believed that the C(1s) position, for a carbonyl-like group on a carbon surface, does not depart significantly from the simple additivity relationship of ~3.0 eV. While a ~3.0 eV shifted peak has been used to represent a carbonyl-like species, only in one study has a spectrum been presented which shows this as the dominant surface species.(1) In this study glassy carbon was oxidized in an O₂ RF plasma. CO₂ and H₂O RF plasmas were ineffective in the production of carbonyl-type functionalities.(1) IR photothermal beam deflection spectroscopy has been used to study the O₂ oxidation of high temperature chars (28). Evidence of ether-like species appeared as a band centered near 1300 cm⁻¹. The presence of a band corresponding to carbonyl-like species was absent.

The presence of carboxylic acid functionalities following HNO₃ oxidation is supported by TPRS and ESCA results. The C(1s) peak at 288.5 eV could be interpreted in terms of simple additivity behavior. Extensive TPRS and thermal stability (17) studies of O₂ and CO₂ oxidation have defined conditions where species are produced which yield CO upon decomposition. The C(1s) peak at 285.8 eV in difference curves decreases concomitant with CO evolution. We cannot interpret this peak as a carbonyl functionality on the basis of the widely accepted additivity behavior of the C(1s) "shift" with carbon bond coordination. Either the chemical shift for this particular system is significantly different than in polymeric systems or a different species is involved in carbon oxidation. Within the framework of the additivity rules the 285.8 eV peak, shifted by ~1.3 eV, is consistent with carbon singly bonded to oxygen. We would expect this peak for ring ethers, however, it is not likely that this species is responsible for low temperature CO formation. The peak is also consistent with phenolic groups but subsequent O₂ and CO₂ oxidation chemistry which yields virtually no hydrogen containing products would necessitate that hydrogen would remain on the surface and thus participate in a quasi catalytic manner.

The carbon-carbon bonding situation on the glassy carbon surface may depart from a simple two dimensional picture. LEED results from the clean edge surface of graphite were not representative of bulk lattice terminations and suggested substantial surface reconstruction (30). The well ordered C (2 x 2/3) LEED pattern from the edge graphite surface was lost and only a diffuse background scattering was observed upon surface oxidation with O₂(31). The pattern was regenerated by heating above 800°C in vacuum. Similar kinds of perturbations away from two dimensional organic chemistry analogues may also occur with glassy carbon. The carbon (1s) peak shifted by ~1.3 (eV) may be a consequence of a surface ether-like species. It is currently not possible to distinguish whether a breakdown in additivity behavior or novel bonding configurations is responsible for the C(1s) spectrum of these systems. Future work using HREELS is under way to help clarify this dilemma by providing surface vibrational information.

References

1. C. W. Miller, D. H. Harweik, T. Kuwana, *Recent Advances in Analytic Spectroscopy*, Pergamon Press, Oxford, England (1982) pp. 233-247.
2. C. W. Miller, D. H. Harweik and T. Kuwana, *Anal. Chem.* (1981) 52, 2319.
3. G. N. Kamaw, W. S. Willis and J. F. Rusling, *Anal. Chem.* (1985) 57, 545.
4. R. Schlägl and H. P. Boehm, *Carbon* (1983) 21, 345.
5. S. Evans and J. M. Thomas, *Proc. R. Soc. London A* (1977) 353, 103.
6. A. Ishitani, *Carbon* (1981) 19, 269.
7. T. Takahagi and A. Ishitani, *Carbon* (1984) 22, 43.
8. A. Proctor and P. M. A. Sherwood, *J. Electron Spec. and Relat. Phenom.* (1982) 27, 39.
9. C. Kozlowski and P. M. A. Sherwood, *J. Chem. Soc., Faraday Trans.* (1984) 80, 2099.
10. C. Kozlowski and P. M. A. Sherwood, *J. Chem. Soc., Faraday Trans. 1* (1985) 81, 2745.
11. C. Kozlowski and P. M. A. Sherwood, *Carbon* (1986) 24, 357.
12. D. T. Clark and H. R. Thomas, *J. Polym. Chem. Ed.* (1976) 14, 1671.
13. D. T. Clark, *Adv. Polym. Sci.* (1977) 24, 125.
14. D. T. Clark, *J. Polym. Sci., Polym. Chem. Ed.* (1978) 16, 791.
15. D. T. Clark, B. J. Cromarty and A. Dilks, *J. Polym. Sci., Polym. Chem. Ed.*, (1978) 16, 3173.
16. D. T. Clark and A. Dilks, *J. Polym. Sci., Polym. Chem. Ed.* (1979) 17, 957.
17. S. R. Kelemen and H. Freund, *Carbon* (1985) 23, 723.
18. H. Freund, *Fuel* (1985) 64, 657.
19. P. A. Redhead, *Vacuum* (1962), 12, 203.
20. J. L. Falconer and J. A. Schwary, *Catal. Rev. Sci. Eng.* (1983) 25, 141.
21. S. R. Kelemen, H. Freund and C. A. Mims, *J. Vac. Sci. Technol.* (1984) A2, 987.
22. B. J. Lindberg, *J. Electron Spectrosc. Relat. Phenom.* (1974) 5, 149.
23. D. T. Clark in: *Handbook of X-Ray and Ultraviolet Photoelectron Spectroscopy* (Heyden London, 1978).

24. S. R. Kelemen and C. A. Mims, Surface Science (1983) 133, 71.
25. P. M. Williams in: Handbook of X-Ray and Ultraviolet Photoelectron Spectroscopy (Heyden London, 1978).
26. N. R. Laine, F. J. Vastola and P. L. Walker, Jr., J. Phys. Chem. (1963) 67, 2030.
27. S. R. Kelemen, C. A. Mims and H. Freund, Journal of Catalysis (1986) 97, 228.
28. C. Mortina and M. J. D. Low, Langmuir (1985) 1, 320 and references therein.
29. L. R. Radovic, P. L. Walker and R. J. Jenkins, Fuel (1983) 62, 191.
30. S. R. Kelemen and C. A. Mims, Surface Science (1984) 136, L35.
31. S. R. Kelemen, unpublished results.

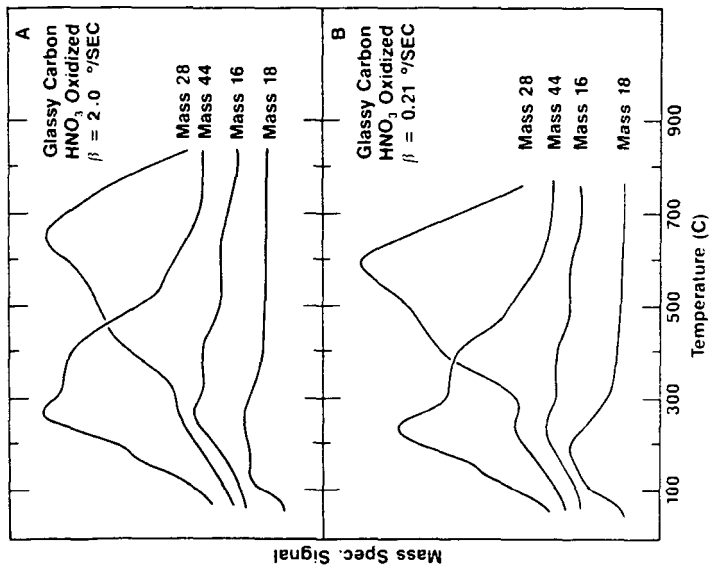


Fig. 1

TPRS after HNO₃ oxidation and subsequent heating in UHV.

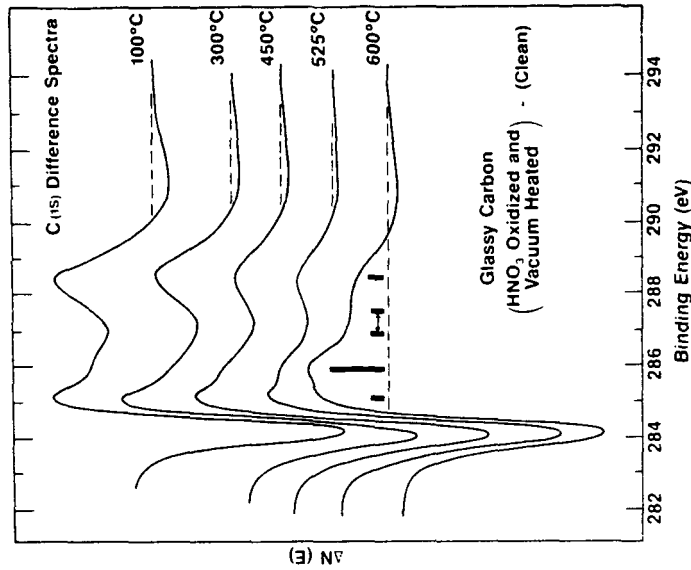


Fig. 2

C(1s) difference spectrum following HNO₃ oxidation and subsequent heating in UHV.

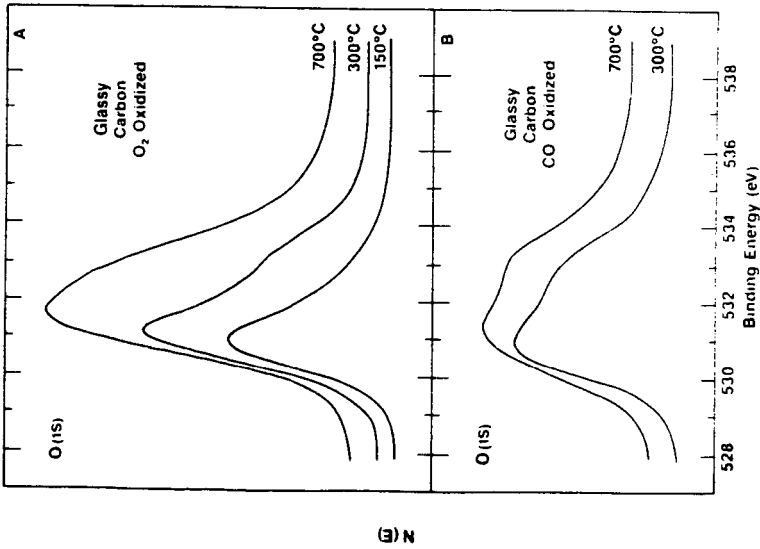


Fig. 3

- A) O(1s) spectrum for glassy carbon samples oxidized at different temperatures with O₂.
- B) O(1s) spectrum followed different CO₂ oxidations.

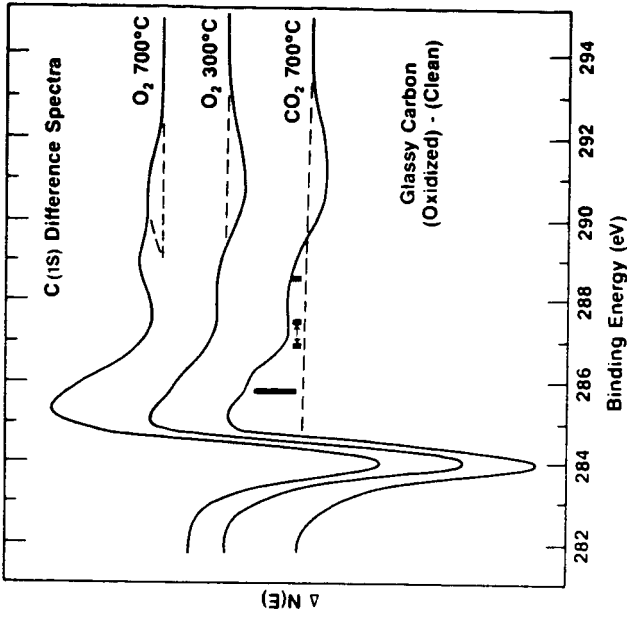


Fig. 4

- C(1s) difference spectrum following O₂ and CO₂ oxidations.

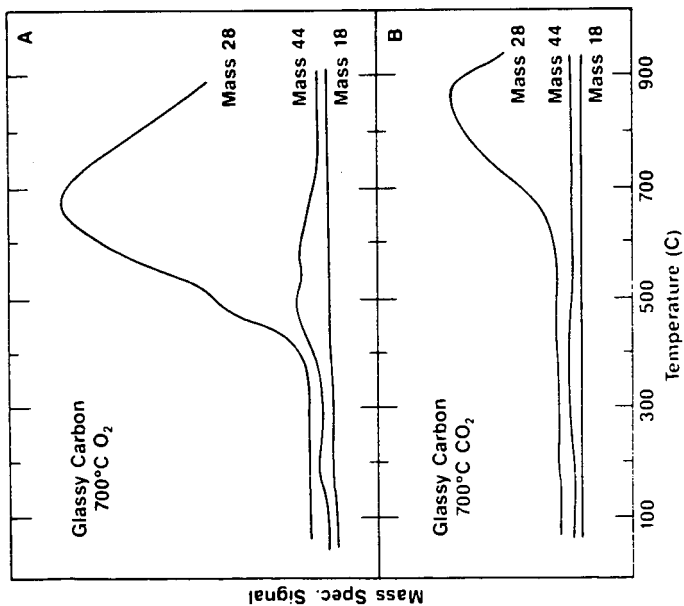


Fig. 5

- A) TPRS following 700°C O₂ oxidation.
 B) TPRS following 700°C CO₂ oxidation. The heating rate was 1.0 degrees per sec. in both experiments.

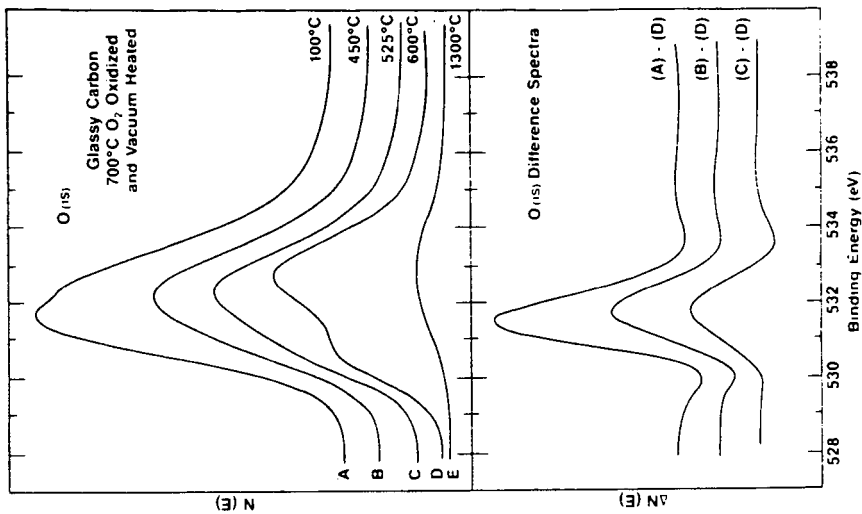


Fig. 6

- A) O(1s) spectrum following O₂ oxidation at 700°C and after heating in UHV to the indicated temperatures.

EFFECT OF WEATHERING ON THE GASIFICATION OF ANTHRACITE

Peter L. Rozelle and Alan W. Scaroni

Fuel Science Program
The Pennsylvania State University
Combustion Laboratory
University Park, PA 16802

Background

Recent developments in electric power generation in the northeastern United States have cast a favorable light on anthracite as a power plant fuel. Although it has not received much attention in the literature, anthracite has been used continuously to generate power for over a century. The recent attention being paid to anthracite is largely due to investments being made in anthracite-fired cogeneration plants. (1) This paper presents some of the development work being done to put one such plant into commercial operation. The objective of the investigation was to specify fuel and operating parameters to allow cheap low-grade anthracite reclaimed from refuse to be fired in fixed-bed Wellman Galusha gas producers designed for premium anthracite.

The Pennsylvania anthracite deposits underlay approximately 480 square miles of the eastern part of the Commonwealth of Pennsylvania (see Figure 1). Table I shows variations in the H, O and N concentrations of 46 samples taken from the four major anthracite fields (2) (Northern, Eastern Middle, Western Middle, Southern). Some of the variations listed in Table I were caused by weathering of the coal. This paper reports on how the weathering of anthracite refuse can affect the gasification performance of the fuel derived from it.

Anthracite refuse is the legacy of a century and a half of coal mining in eastern Pennsylvania. It is a mixture of preparation plant refuse, noncarbonaceous mine refuse, wood, cinders, and discarded equipment such as mine cars and boattice cloth. There is low grade coal in these deposits, which can be expediently reclaimed to provide a relatively inexpensive solid fuel. Anthracite refuse has been stored above ground in a broken state and as such its chemical constitution is subject to change due to exposure to the elements. The weathering process can oxidize the organic fraction of coal as well as associated minerals.

Oxidation of lower rank coals due to weathering is a well known phenomenon, but little has been written about anthracite weathering. The organic fraction of the coal is known to lose calorific value upon exposure to the elements. For above ground deposits 5-10 years old, this can be up to 100-200 Btu/lb, while 40-year-old deposits have lost as much as 500 Btu/lb. (3) Refuse-derived anthracite is known to have a high volatile matter content compared to freshly-mined coal, this being due to its high mineral-derived water and chemisorbed oxygen contents.

The pyrite contained in anthracite, which can represent as much as 5% of the coal's mineral matter, is also subject to weathering. Pyrite in refuse banks can be oxidized to iron sulfate and sulfuric acid (4), the latter contributing to groundwater pollution. This is also of interest to fixed-bed gasification, since pyrite is the principal source of iron (in reduced form) in the gasifier bed, which is known to cause severe bed agglomeration and can lead to expensive gasifier downtime.

The focus of this paper is the weathering of the organic fraction of refuse-derived anthracite. While the effect of long-term ambient temperature oxidation of anthracite has not been widely studied, short-term low-temperature (100-350 C) oxidation has been the subject

of investigations (5). The aim of the work was to use mine gas composition to chart the path of underground mine fires, and data have been generated on the effect of low temperature oxidation on the volatile matter content and composition of anthracite. The normal volatile matter of freshly-mined anthracite contains predominantly hydrogen. Table II shows average volatile matter compositions for 46 anthracite samples. The bulk of the volatiles are evolved above 735 C for heating rates between 2 and 16 C/min. CO and H₂ are the principal species liberated above this temperature while CO₂ and CH₄ evolution occurs at lower temperatures.

A fixed-bed Wellmann-Galusha gasifier can be divided into distinct zones along its vertical axis. Upwards from the bottom they are the cinder, burn, gasification, devolatilization, and drying zones (see Figure 2). Devolatilization is the second last process which impacts the composition of the producer gas before it leaves the gasifier. As such, any change in volatile matter quality and/or evolution temperature will affect producer gas quality. Preoxidation, such as that induced by weathering, has been shown by the Bureau of Mines (5) to dramatically affect the content and composition of anthracite volatile matter and lower the evolution temperatures of CO and CO₂. In that work coals were oxidized for relatively short times (generally less than 100 hours) in dry air at temperatures ranging from 100 to 350 C. Increases in oxygen content at lower temperatures, such as 2.2 to 4.1% wt O₂ (dry) in 91 hours at 200 C, correspond to the range of weathering-induced oxidation which although taking place at a lower temperature, occurs over decades rather than hours and as such could produce similar alterations to the volatile matter.

Oxygen interacting with anthracite during low-temperature oxidation was found to produce gaseous products, such as H₂O and CO₂, and to be "fixed" on the coals. The quantity of adsorbed oxygen was found to linearly increase the volatile matter content. Distillation tests on the oxidized coal showed that preoxidation lowered the H₂ and CH₄ yields by 30-50%, while producing order of magnitude increases in CO and CO₂ evolution. It also radically increased the amount of CO being liberated in the 500-900 C range. (5) This is of importance to gasifier operation since the lower the temperature at which a gaseous species is liberated, the closer it is to the gas offtake and this increases its chances of passing out of the gasifier unreacted.

Experimental

Two freshly-mined and four refuse-derived anthracites were sampled for this work (Table III). One sample from other work, sample IIIa, was included since freshly-mined coal from this location is unavailable. Samples Ia and IIa were produced in preparation plants. Sample IIIa was laboratory-prepared. In each case corresponding refuse-derived samples were prepared in an attempt to match the organic fractions as closely as possible. Specific gravity and particle size were the parameters varied to achieve this. Table III lists the specific preparation data on the samples.

Table IV shows the approximate ages of the refuse-derived fuels and Table V gives the ultimate analyses of the fuels. As expected, the data indicate a higher degree of oxidation for refuse-derived fuels than the corresponding freshly-mined coals. While Table V shows a general trend toward higher oxygen contents for refuse-derived coals, a corresponding increase in volatile matter is only present for Sample IIb. Since this fuel, which came from the oldest refuse deposit, indicated the possibility of an increased CO percentage in its volatile matter, it was chosen for full-scale gasification testing. Sample Ia, a freshly-mined low grade coal, was also fired in the Wellman-Galusha gas producers.

Results

Full-scale gasification data for two samples (Ia and IIIb) are provided in Table VI, along with published results from two other tests conducted by the Bureau of Mines in the 1950's (6,7). These runs were all conducted in a 10 foot diameter air-blown Wellman-Galusha gas producer. Runs 1 and 2 were conducted in gas producers without bed agitators while 3 and 4 were conducted in the current gas producer, which employs a bed agitator. Run 1 was conducted using freshly-mined premium anthracite and as such can be considered the baseline run for normal operation. Runs 2 and 3 were conducted with low-grade freshly-mined coal and run 4 was conducted with low-grade coal reclaimed from refuse. The higher oxygen and volatile matter contents of sample IIIb suggest a high potential yield of CO, and this is reflected in the increase in CO percentage in the producer gas, apparently at the expense of hydrogen. These data are consistent with the previous work on the effect of oxidation on the volatile matter content and composition (5). The results indicate that up to 10% increase in the producer gas calorific value can be achieved by firing refuse-derived anthracite rather than freshly-mined product. Comparisons of the the oxygen and volatile matter contents of refuse-derived and freshly-mined coal from the same location can serve as a measure of the potential to produce this effect. An increase in the (dry-ash-free) oxygen and volatile matter contents indicates a potential increase in the CO content of the producer gas and a corresponding increase in its calorific value.

Summary

Dry-ash-free oxygen contents of several anthracites were compared with published data to determine the extent of oxidation experienced by fuel derived from anthracite refuse. These have been compared to published data on the effect of preoxidation on the composition of the volatile matter in order to predict the effect of weathering on producer gas composition. Full scale gasification data from Wellman-Galusha gasifiers show that a refuse-derived anthracite, which was the oldest and most oxidized fuel, produced a gas enriched in CO. The data imply that refuse-derived anthracites can produce a higher calorific value product gas than freshly-mined coals of similar quality.

References

1. Anon, *Coal and Syntfuels Technology*, 28 October, 1985, pp 2-3.
2. Anon., "Physical and Chemical Properties of Pennsylvania Anthracite," Anthracite Institute, Wilkes-Barre, Pa., 1945, 26 PP.
3. Sisler, J. D., T. Fraser, and D. C. Ashmead, Anthracite Culm and Silt, PA Bureau of Publication, Bull. M-12, 1928, 268 pp.
4. McCartney, J. C., and R. H. Whaite, Pennsylvania Anthracite Refuse, A Survey of Solid Waste from Mining and Preparation, Bu Mines Inf. Circ. 8409, 1969, 77 pp.
5. Scott, G. S., G. W. Jones, and H. M. Cooper, "The Effect of Oxidation on the Volatile Matter of Anthracite and its Significance in Mine Fire Investigations," Bureau of Mines Report of Inv. 3398, May 1938, 8 pp.
6. Eckerd, J. W., J.D. Clendenin, and W.S. Sanner, and R. E. Morgan, "Gasification of Bone Anthracite," Bureau of Mines Rept. of Inv. 5594, 1960, 24 pp..
7. Teure, R. F. J. D. Clendenin, and W. S. Sanner, "Anthracite Gas Producer Tests at a Brick Plant," Bu Mines Rept. of Inv. 5556, 1960, 25 pp.
8. Bracy, G. A., and H. H. Griffiths, Properties of Anthracite from the Bottom Ross Bed, Bu Mines Rept. of Inv. 7086, 1968, 29 pp.
9. Reproduced from Wellman Engineering Company brochure.

Table I*. H, O and N Concentrations for Samples from Different Anthracite Fields

Field	No. of Samples	Range of Concentration, wt% dry		
		H	O	N
Northern	22	2.0-3.1	1.1-3.2	0.6-1.1
Eastern Middle	6	1.7-2.0	1.2-1.9	0.6-0.9
Western Middle	6	1.2-2.9	0.9-2.0	0.6-1.0
Southern	12	1.8-3.1	1.1-2.4	0.6-1.2

*From Reference 2

Table II. Average Volatile Matter Composition for Samples from Different Anthracite Fields

Field	No. of Samples	Average Volatile Matter Composition, %vol (dry)					
		CO ₂	O ₂	H ₂	N ₂	CO	CH ₄
Northern	22	1.8	1.0	85.2	1.8	4.1	6.0
Eastern Middle	6	1.9	2.6	81.1	6.9	5.5	1.9
Western Middle	6	1.8	3.3	78.8	7.4	4.5	4.1
Southern	12	2.1	1.2	83.3	3.8	4.0	5.6

TABLE III. SAMPLES USED AND PREPARATION METHOD

Sample	Location	Particle Size Range, mm	Preparation Method
Ia (freshly-mined)	Eastern	14 x 4.7	Prep. Plant, 1.90 float
Ib (refuse-derived)	Middle Field	12.7 x 6.4	Laboratory, 1.90 float
IIa (freshly-mined)	Southern	4.7 x 2.4	Prep. Plant, 1.70 float
IIb (refuse-derived)	Field	4.7 x 1.2	Laboratory, 1.70 float
IIIa* (freshly-mined)	Northern	75 x 0.5	Laboratory, 1.70 float
IIIb (refuse-derived)	Field	50 x 0.5	Prep. Plant, 1.70 float
IVb (refuse-derived)	Western Middle Field	9.5 x 3.2	Laboratory, 1.70 float

*From Reference 8

TABLE IV. ESTIMATED AGE OF REFUSE-DERIVED COALS

Sample	Estimated Age, Yrs
Ib	> 50
IIb	> 40
IIIb	40-80
IVb	> 30

TABLE V. VOLATILE MATTER CONTENT AND ULTIMATE ANALYSIS OF FUELS

SAMPLE	VM	S	C (wt% daf)	H	O	N
Ia	7.8	0.56	95.6	1.47	1.67	0.70
Ib	6.5	0.61	92.8	1.97	3.75	0.87
IIa	6.4	0.93	94.9	1.76	1.78	0.83
IIb	7.3	0.63	93.6	1.59	3.23	0.95
IIIa*	4.4	0.60	94.0	2.30	2.00	1.00
IIIb	8.7	1.27	90.9	1.99	3.87	0.95
IVb	8.6	0.62	93.0	2.12	3.20	0.96

*from Reference 8

TABLE VI. WELLMAN-GALUSHA PRODUCER GAS COMPOSITIONS FROM PAST AND PRESENT WORK USING ANTHRACITE COAL

Run	Coal Type	Ash Approx. %wt	Dry Producer Gas (% vol)*				CO ₂	Net CV Btu/ft ³	Ref
			H ₂	N ₂	CO	CH ₄			
1	Freshly-Mined	10	18.1	47.6	27.2	1.0	5.9	145	7
2	Freshly-Mined** Middling	30-45	15.8	51.9	22.6	0.8	8.5	123	6
3	Sample Ia	25-30	17.8	47.3	28.3	0.5	6.0	145	this work
4	Sample IIb	30-40	15.4	45.0	31.4	0.3	4.2	147	this work
	Gasifier Conditions		-16.3	-47.6	-34.1	-0.4	-4.0	-159	

Coal feed rate, tons/hr

1. 1.0 - 2.5
2. 1.0 - 2.5
3. 1.0 - 1.5
4. 1.0 - 1.5

Saturation Temp. °F

- 147
- 170
- 150-160
- 150-160

*Ranges given for 6 gas samples taken over a 6 hr period

**0.4% O₂ in gas

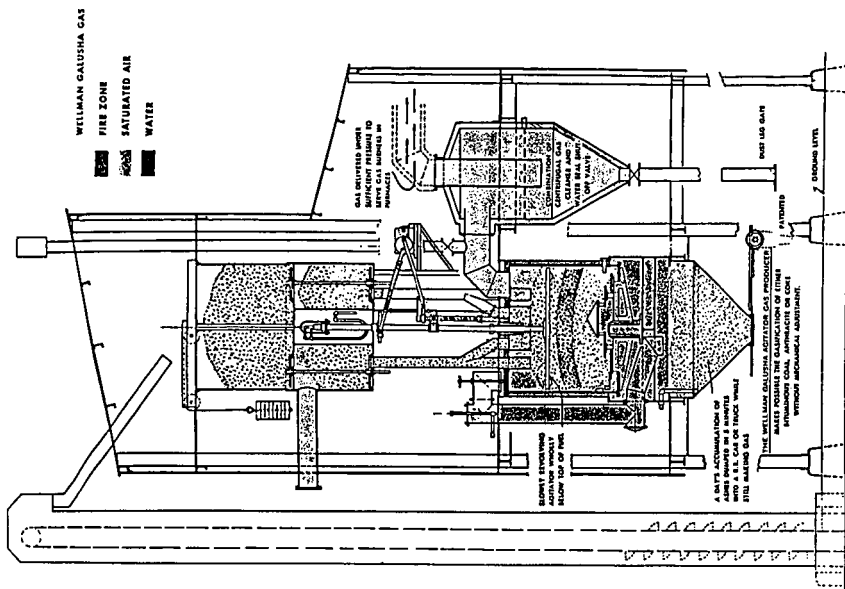


Figure 2. Wellman Galusha Gasifier (9)

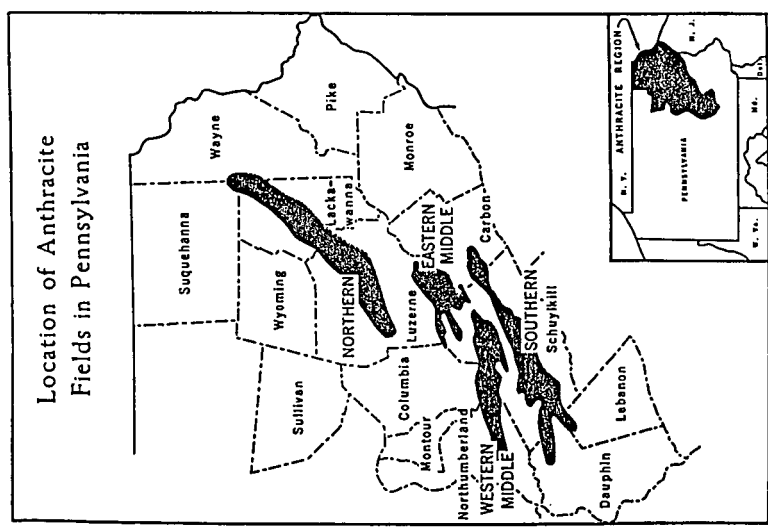


Figure 1. Location of Anthracite Fields of Pennsylvania

IN SITU ACETYLATION STUDY OF A SUBBITUMINOUS COAL BY DIFFUSE REFLECTANCE
INFRARED FOURIER TRANSFORM (DRIFT) SPECTROSCOPY

N. R. Smyrl and E. L. Fuller, Jr.

Plant Laboratory
Oak Ridge Y-12 Plant*
Martin Marietta Energy Systems, Inc.
Oak Ridge, Tennessee 37831

ABSTRACT

Diffuse reflectance infrared Fourier transform (DRIFT) spectroscopy has been utilized to monitor the in situ acetylation of a powdered subbituminous coal at the Oak Ridge Y-12 Plant. The acetylation reaction was carried out by the adsorption of acetic anhydride onto the powdered coal from the gas phase with subsequent heating above 100°C required to initiate the reaction. This technique can be used to gain insight into the hydroxyl (O-H) content of the specific coal sample under study by simultaneously observing the disappearance of infrared absorptions due to various types of O-H functional groups and the appearance of absorptions due to carbonyl functional groups resulting from reaction with the anhydride. This entire study can be carried out on a single sample without any intervening sample handling or the introduction of extraneous parameters that could alter the results.

INTRODUCTION

The determination of hydroxyl functional groups in coal by infrared (IR) and Fourier transform infrared (FTIR) methods has been previously attempted. One of these approaches (1-3) involves direct measurement of the intensity of the broad O-H band in the spectrum of coal centered at ~ 3400 cm^{-1} , while a second technique relies on the measurement of band intensities due to products derived from chemical reaction with the various O-H groups, such as by acetylation (4-6). Both methods utilized standard transmission techniques using potassium bromide (KBr) pellets. Although the direct-measurement approach has been used with some apparent success, this method suffers potential interference from moisture (whether it be in a latent form within the coal or from KBr or other sources in the pellet-preparation step). The acetylation approach has also been used with a certain degree of success but can suffer potential problems related to uncertainty in the extent and completeness of reaction and in the handling and pellet-preparation steps subsequent to the chemical-reaction step. This appeared to be an area where in situ diffuse reflectance (DR) measurements could incorporate the best aspects of both methods and have the potential of yielding more accurate and more detailed information without introducing unknown factors due to sample manipulations.

*Operated for the U.S. Department of Energy by Martin Marietta Energy Systems, Inc., under contract DE-AC05-84OR21400.

The first work to demonstrate the analytical significance of the infrared DR technique as applied to coal was a report by Fuller et al., (7) and subsequent studies (8-10) in our laboratory have further proven the value of this technique. The DR method, however, has really not received widespread use and acceptance in relation to coal work, probably because the quantitative correlation of band intensities with concentration is not as straightforward as it is with transmission spectroscopy. There is one property of coal that makes it ideally suited for DR measurements, which is not a well-known fact. Coal forms its own dispersion medium and can be directly examined in the neat form without dilution in another dispersion matrix.

Perhaps the single strongest point associated with the DR sampling method is the ability to perform in situ reaction studies. This ability, when coupled with the aforementioned property of coal, makes the DR method a very powerful technique for the study of coal. We have previously demonstrated the usefulness of DR in situ measurements in the study of coal oxidation (8-10) and other heterogeneous reactions involving inorganic materials (10-12). In this particular report, we present some preliminary results of in situ acetylation studies of a subbituminous coal by DR.

EXPERIMENTAL

A 30-mg sample of a powdered subbituminous coal from the Wyodak Mine in Wyodak, Wyoming, was placed on a gold-plated, 304 stainless sample pedestal within the DR cell [thoroughly described in a previous report (11)]. This cell can be used in applications involving ultra-high-vacuum and/or flowing-gas conditions at varying temperatures (-77° to 800°C). The cell is used in conjunction with a Harrick Model DRA-SID DR accessory designed for adaptation to a Digilab Model FTS-15 side-focus FTIR spectrometer.

The coal sample used in this study was obtained directly from a freshly opened mine face and stored under argon to minimize oxidation until the experimental work was initiated. A similar technique has been described in a recent article (13) for maintaining coal samples from various sections of the country as known quality reference standards.

The DR sample cell was first evacuated to ~20 mtorr for 40 h. Previous studies for this particular sample (8,9) have shown that these conditions are adequate for removing the most loosely bound "bed moisture" associated with this coal sample. The sample was then exposed under dynamic flowing conditions to argon/acetic anhydride vapors by bubbling dry argon through a reservoir of the anhydride at room temperature (RT). The temperature of the sample was then raised from RT to 450°C in roughly 100-degree intervals. A final deuteration experiment using D₂O was carried out on the sample, which contained some residual O-H groups that could not be forced to react or that were inaccessible to the anhydride. Spectra were scanned periodically throughout this sequence of events.

All spectra were obtained on a Digilab Model FTS-15C FTIR spectrometer at a resolution of 2 cm⁻¹ using a triglycine sulfate (TGS) pyroelectric bolometer detector. The merits for use of the TGS detector versus a mercury cadmium telluride (MCT) are discussed in Ref. 10 for the DR reaction studies of coal and other materials at elevated temperatures. The benefit of greater sensitivity derived by using an MCT detector can largely be over-

ridden by its nonlinear response and the saturation effects encountered as the temperature of the sample is increased. For most of the experiment, 100 scans proved adequate to produce spectra with a satisfactory signal-to-noise (S/N) ratio and yet short enough in duration to kinetically follow the reaction. Some scans of longer duration were also obtained for production of high-quality spectra for use as subtraction standards. All reflectance spectra recorded in this paper are plotted in the absorption format $[-\log(R_s/R_o)]$. (See the appendix in Ref. 11 for a discussion of the merits of various plotting formats.)

RESULTS, DISCUSSIONS, AND CONCLUSIONS

Figure 1 represents the DR spectra of the sample of Wyodak powdered coal in the C-H and O-H stretching regions before and after evacuation to 23 mtorr at 25°C. Refer to Table 1 for correlation of the spectrum numbers appearing in Fig. 1 and with those appearing in subsequent figures to the corresponding experimental conditions. These spectra show that the loosely bound "bed moisture" can essentially be totally removed under these evacuation conditions. Comparison of Curves 7 and 3 reveals some distinct features in the O-H stretching region at 3625, 3540, 3390, and 3290 cm^{-1} that were not observable prior to evacuation. Previous work involving this sample (8,9) has shown that further heat treatment under vacuum causes little or no change in the spectrum depicted by Curve 7. This spectrum was chosen as a vacuum reference state to which all subsequent spectra will be compared.

Curve 15 in Fig. 2 represents the spectrum of an equilibration state resulting from exposure of the coal sample to a flowing argon/acetic anhydride mixture at 25°C for 2.25 h. The difference spectrum (Curve 15 - Curve 7) very clearly shows bands that are present in the exposed state that are not present in the reference vacuum state.

For simplification of the subsequent discussion, all difference spectra using Curve 7 as the reference state for the subtraction are referred to merely by the corresponding spectral or sequence number. All difference spectra are also direct 1:1 subtractions with no scaling. Curve 15 was presumed to represent an equilibration state because very little if any change could be noted from the two previous spectra (see Fig. 3).

Bands are observed to grow at 900, 1000, 1130, 1375, 1760, and 1825 cm^{-1} in Fig. 3 and maximize in intensity in Curve 15. These bands can be attributed to acetic anhydride physically adsorbed onto the powdered coal surface. A band at 1730 cm^{-1} also appears immediately, as noted on Curve 10, that remains at a near-constant intensity through Curve 15. This band may possibly be due to some residual adsorbed acetic acid. A quantity of moisture is also adsorbed in this sequence, as noted by the growth of a broad feature in the O-H stretching region.

Curves 16 and 21 represent the first spectra obtained after the sample had been heated to 100° and 200°C, respectively. Each step up in temperature was taken only after the reaction had reached a state of equilibration, with no further reaction appearing to occur at the given lower temperature. The bands due to the adsorbed anhydride and moisture diminish until they are barely observable in Curve 21. Also, a band starts to grow at 1770 cm^{-1} in Curve 16 that is hard to distinguish from the 1760 cm^{-1} band of the

Table 1. Diffuse reflectance spectra sequence: Wyodak coal acetylation

Spectrum number	Sample conditions	Temp. (°C)	Time conditions changed	Time spectral collection complete	Day
1	Air (1 atm)	25	-	3:00 p.m.	0
2	Ar purge	25	-	3:10 p.m.	0
3	Ar purge	25	-	3:20 p.m.	0
4	Ar purge	25	-	3:35 p.m.	0
5	Vacuum (30 mtorr)	25	-	3:55 p.m.	0
6	Vacuum (23 mtorr)	25	-	4:50 p.m.	0
7 ^a	Vacuum (23 mtorr)	25	-	8:00 a.m.	1
8	Ar purge	25	-	9:25 a.m.	1
9	Ar/acetic anhydride	25	9:45 a.m.	9:53 a.m.	1
10	Ar/acetic anhydride	25	-	10:10 a.m.	1
11	Ar/acetic anhydride	25	-	10:25 a.m.	1
12	Ar/acetic anhydride	25	-	10:45 a.m.	1
13	Ar/acetic anhydride	25	-	11:20 a.m.	1
14	Ar/acetic anhydride	25	-	11:30 a.m.	1
15	Ar/acetic anhydride	25	-	12:00 a.m.	1
16	Ar/acetic anhydride	100	12:08 p.m.	12:15 p.m.	1
17	Ar/acetic anhydride	100	-	12:30 p.m.	1
18	Ar/acetic anhydride	100	-	12:45 p.m.	1
19	Ar/acetic anhydride	100	-	12:55 p.m.	1
20	Ar/acetic anhydride	200	1:00 p.m.	1:05 p.m.	1
21	Ar/acetic anhydride	200	-	1:25 p.m.	1
22	Ar/acetic anhydride	200	-	1:50 p.m.	1
23	Ar/acetic anhydride	300	2:10 p.m.	2:20 p.m.	1
24	Ar/acetic anhydride	300	-	3:15 p.m.	1
25	Ar/acetic anhydride	300	-	3:55 p.m.	1
26	Ar/acetic anhydride	300	-	4:30 p.m.	1
27	Ar/acetic anhydride	300	-	5:05 p.m.	1
28	Ar/acetic anhydride	300	-	9:35 p.m.	1
29	Ar/acetic anhydride	428	9:40 p.m.	9:45 p.m.	1
30 ^b	Ar/acetic anhydride	428	-	10:05 p.m.	1
31 ^b	Ar purge	300	10:07 p.m.	7:30 a.m.	2
32	Ar purge	300	-	7:45 a.m.	2
33	Ar/acetic anhydride	450	8:00 a.m.	10:20 a.m.	2
34	Ar purge	100	10:25 a.m.	11:00 a.m.	2
35	Deuterium oxide flow	100	11:20 a.m.	11:25 a.m.	2
36	Deuterium oxide flow	100	-	11:33 a.m.	2
37	Deuterium oxide flow	100	-	11:40 a.m.	2
38	Deuterium oxide flow	100	-	11:55 a.m.	2
39	Deuterium oxide flow	100	-	12:23 p.m.	2
40	Deuterium oxide flow	100	-	1:00 p.m.	2
41	Deuterium oxide flow	80	1:02 p.m.	1:10 p.m.	2
42	Deuterium oxide flow	65	-	1:25 p.m.	2
43	Deuterium oxide flow	50	-	1:40 p.m.	2
44	Deuterium oxide flow	34	-	1:55 p.m.	2
45	Vacuum (30 mtorr)	30	1:57 p.m.	2:10 p.m.	2
46	Vacuum (23 mtorr)	28	-	2:30 p.m.	2

^a20,000 scans; ^b10,000 scans

anhydride at the expansion shown in the figure. This band stands out essentially by itself in Curve 21 and really appears at 1770 cm^{-1} , as denoted in Fig. 4. The temperature of the sample was raised again to 300°C , with Curve 23 being the first spectrum to be collected after this step. This spectrum was also the first to be corrected for window background due to condensation of a volatile acetylation product that was discovered on the cell windows after the experiment had been completed. The spectrum due to the window background appears in the upper curve of Fig. 5, along with the difference spectra before and after correction for Curve 31 presented as a typical example. The proper amount of scaling for this correction was determined by nulling out the intensity of the C-H stretching bands in the difference spectrum as depicted in the lower curve in Fig. 5. The C-H stretching bands could be utilized in this way since the acetylation reaction is expected to alter this portion of the spectrum little if any. All spectra including and subsequent to Curve 23 have been similarly corrected for this background, since the higher temperatures readily facilitated volatilization of the product onto the zinc selenide windows.

The 1770 and 1200 cm^{-1} bands, along with some weaker features, are observed to continually grow in Fig. 4 until Curve 28 where the temperature was again raised to 428°C . These bands can be attributed to acetylated esters of the various O-H functional groups in the coal. In this same sequence of spectra, a broad negative band can also be observed to grow in the 3600 to 3000 cm^{-1} region, which can be attributed to the corresponding loss of O-H groups. A weak band appears at 2150 cm^{-1} (starting with Curve 24) that is apparently due to formation of gas-phase carbon monoxide. This band appears only when the temperature is 300°C or above and when the anhydride reactant mixture is present. A good explanation for the observation of this species has not presently been formulated. The sample had essentially reached the final state of acetylation, as noted in Curve 30. At this point exposure to acetic anhydride was terminated and the sample temperature was reduced to 300°C . The difference spectrum representing the final acetylated state is shown in Curve 31. A raw spectrum of this state appears in Curve 33 of Fig. 6, which shows that some residual O-H bands at 3550 and 3440 cm^{-1} remain--indicating either a lack of reactivity for these remaining O-H groups or, more likely, an inaccessibility due to steric effects. The position and relative sharpness of these O-H bands indicate that hydrogen bonding effects have been reduced considerably for these residual O-H groups, which supports the latter contention that the groups are isolated and difficult to access by the relatively large acetic anhydride molecule.

In an effort to gain more information about the residual O-H groups, the hydrogen atoms on these groups were then allowed the opportunity to exchange with deuterium by exposure to flowing D_2O as the sample was cooled from 100°C to near RT. Curve 46 in Fig. 6 represents the raw spectrum of the final deuterated state of the acetylated Wyodak powdered coal sample. Essentially all of the remaining O-H groups experience exchange, with the exception of those due to the inherent mineral bands--as noted by the loss of intensity in the O-H stretching region and the appearance of a band in the 2600 cm^{-1} region due to O-D stretching. The difference spectra for the deuteration sequence, again referenced to Curve 7, are displayed in Fig. 7. Deuteration was essentially complete by the time Curve 40 was collected, as noted by a lack of further increase in the intensity of the positive 2620

cm^{-1} O-D band or that of the negative O-H feature. An interesting observation that can be noted from Fig. 7 is the reappearance of adsorbed acetic anhydride on the powdered coal surface, as indicated by the growth of bands at 1825 and 1130 cm^{-1} with a decrease in temperature. This readsorption must result from residual acetic anhydride in the vacuum system and is easily removed by evacuation, as indicated in Curve 46.

Although the present acetylation work represents only a preliminary, qualitative study, it reveals an additional, potentially powerful technique for probing the structure of coal with regard to hydroxyl functional groups. This technique appears to provide complimentary information to previous liquid-solid acetylation work (4,5) by permitting O-H groups which are either relatively inaccessible to reaction with acetic anhydride from the gas phase or are less reactive under these conditions to be sorted from the total hydroxyl content. Another area where our results appear to differ somewhat from previous acetylation studies involves the relative amounts of phenolic- versus alkyl-type acetyl esters that are formed in reaction with similar subbituminous coals. Examination of the carbonyl region of the difference spectrum of the final acetylated state (Curve 31 of Fig. 4) shows essentially a single band centered at 1770 cm^{-1} with no apparent asymmetry observed on the low-frequency side that would indicate the presence of other bands. The 1770 cm^{-1} band has been attributed to phenolic acetyl esters, while bands at 1740 and 1670 cm^{-1} have been assigned to alkyl and amide acetyl esters (4). Presuming the assignments are correct, our data can be interpreted in either of two ways, one being that the coal sample we studied contains only phenolic type O-H groups with essentially none of the alkyl type. The other interpretation, which is probably the least plausible, would be that only the phenolic groups reacted in the acetylation--leaving the alkyl O-H groups unreacted. Further work should be done in this area to clarify this discrepancy. The acetylation technique in combination with deuteration appears to be an excellent method for revealing information with regard to hydroxyl-containing mineral matter. Considerably more work needs to be done in determining the quantitative potential of in situ DR technique. It is quite clear, however, that such a technique applied to acetylation, and possibly to other types of derivative reactions, can yield new and potentially enlightening information with regard to the structure of coal.

REFERENCES

1. Y. Osawa and J. W. Shih, Fuel, 50, p. 53 (1971).
2. P. R. Solomon, D. G. Hamblen, and R. M. Carangelo, "Applications of Fourier Transform IR Spectroscopy in Fuel Science," p. 77 in Coal and Coal Products: Analytical Characterization Techniques, 205, ed. E. L. Fuller, Jr., Am. Chem. Soc. Symp. Ser., 1982.
3. P. R. Solomon and R. M. Carangelo, Fuel, 61, p. 663 (1982).
4. P. C. Painter et al., Applied Spectrosc., 35, p. 475 (1981).
5. P. Painter, M. Starsinic, and M. Coleman, "Determination of Functional Groups in Coal by Fourier Transform Interferometry," p. 169 in Fourier Transform Infrared Spectroscopy, 4, eds. J. R. Ferraro and L. J. Basile, Academic Press: New York, 1982.

6. P. C. Painter et al., "Fourier Transform IR Spectroscopy: Application to the Quantitative Determination of Functional Groups in Coal," p. 47 in Coal and Coal Products: Analytical Characterization Techniques, 205, ed. E. L. Fuller, Jr., Am. Chem. Soc. Symp. Ser., 1982.
7. M. P. Fuller et al., Fuel, 61, p. 529 (1982).
8. N. R. Smyrl and E. L. Fuller, Jr., "Chemistry and Structure of Coals: Diffuse Reflectance IR Fourier Transform (DRIFT) Spectroscopy of Air Oxidation," p. 133 in Coal and Coal Products: Analytical Characterization Techniques, 205, ed. E. L. Fuller, Jr., Am. Chem. Soc. Symp. Ser., 1982.
9. E. L. Fuller, Jr., and N. R. Smyrl, Fuel, 64, p. 1143 (1985).
10. E. L. Fuller, Jr., N. R. Smyrl, and R. L. Howell, "Chemistry and Structure of Fuels: Reaction Monitoring with Diffuse Reflectance Infrared Spectroscopy" p. 215 in Chemical, Biological and Industrial Applications of Infrared Spectroscopy, ed. J. R. Durig, John Wiley and Sons: New York, 1985.
11. N. R. Smyrl, E. L. Fuller, Jr., and G. L. Powell, Appl. Spectrosc., 37, p. 38 (1983).
12. E. L. Fuller, Jr., N. R. Smyrl, J. B. Condon, and M. H. Eager, J. Nucl. Mater., 120, p. 174 (1984).
13. J. Haggin, Chem. and Eng. News, 64, p. 28 (1986).

VACUUM DEHYDRATION: WYODAK POWDER (D-1)

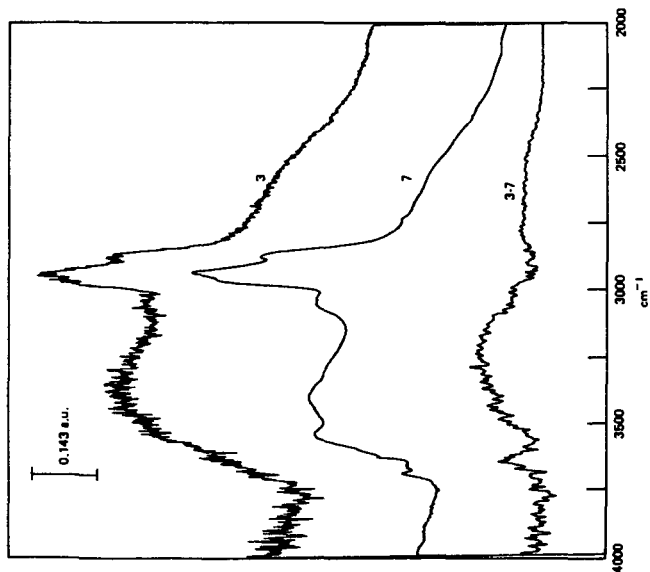


Fig. 1. Diffuse reflectance spectra of Wyodak coal: Curve 3 is the spectrum under argon purge at 25°C for 100 scans, Curve 7 is the spectrum under vacuum at 23 mtorr at 25°C for 10,000 scans, and Curve 3-7 is the difference spectrum.

ACETIC ANHYDRIDE ON WYODAK POWDER (D-1) AT 25°C

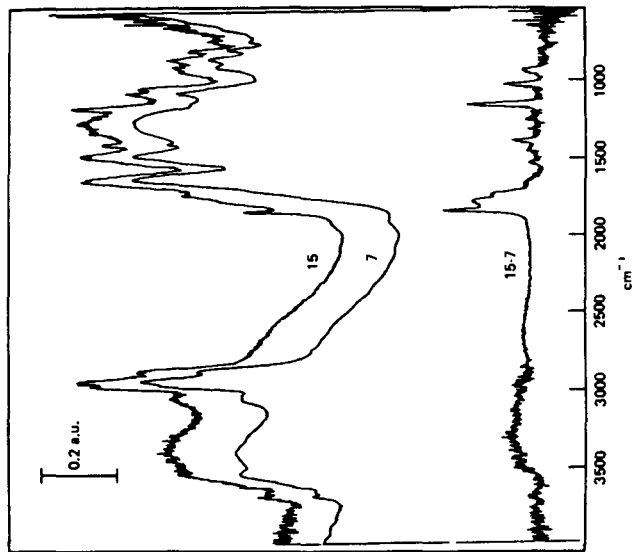


Fig. 2. Diffuse reflectance spectra of Wyodak coal: Curve 15 is the spectrum of Wyodak coal exposed to a flowing argon/acetic anhydride mixture for 2.25 h at 25°C, Curve 7 is reference state spectrum under vacuum at 20 mtorr at 25°C, and Curve 15-7 is the difference spectrum.

ACETIC ANHYDRIDE ON WYODAK POWDER (D-1) 100°C AND 200°C

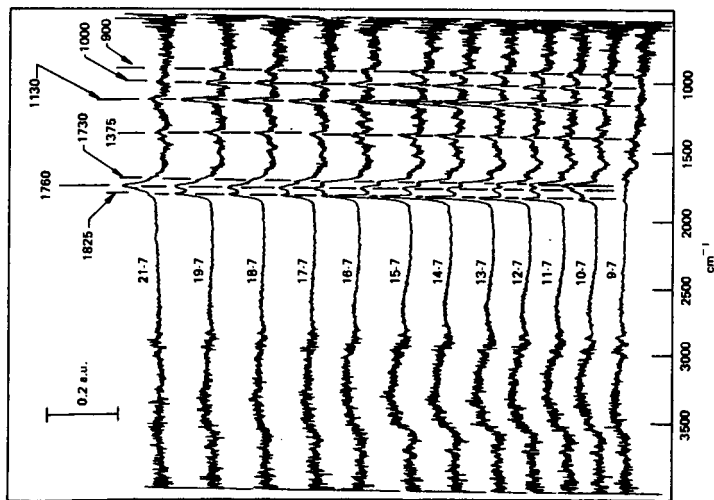


Fig. 3. Difference spectra for acetic anhydride reaction with Wyodak coal at 25°, 100°, and 200°C. (See Table 1 for correlation of spectral numbers.)

ACETIC ANHYDRIDE ON WYODAK POWDER (D-1) AT 200, 300, 428 AND 450°C

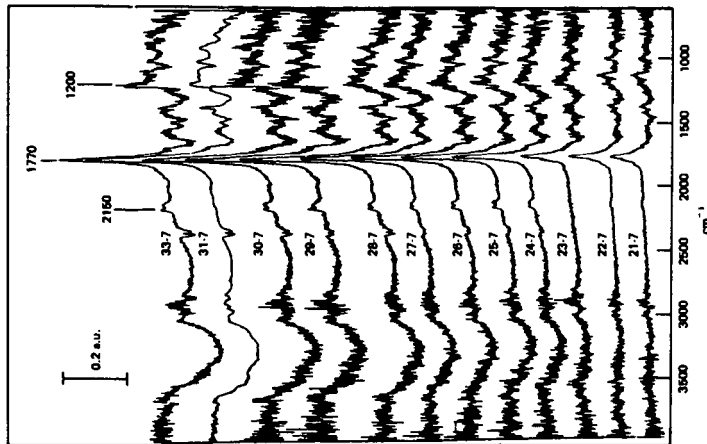


Fig. 4. Difference spectra for acetic anhydride reaction with Wyodak coal at 200°, 300°, 428°, and 450°C. (See Table 1 for correlation of spectral numbers. All spectra starting with no. 23 have been corrected for window background. See Fig. 5 for details concerning this correction.)

D₂O EXCHANGE WYODAK POWDER (D-1)

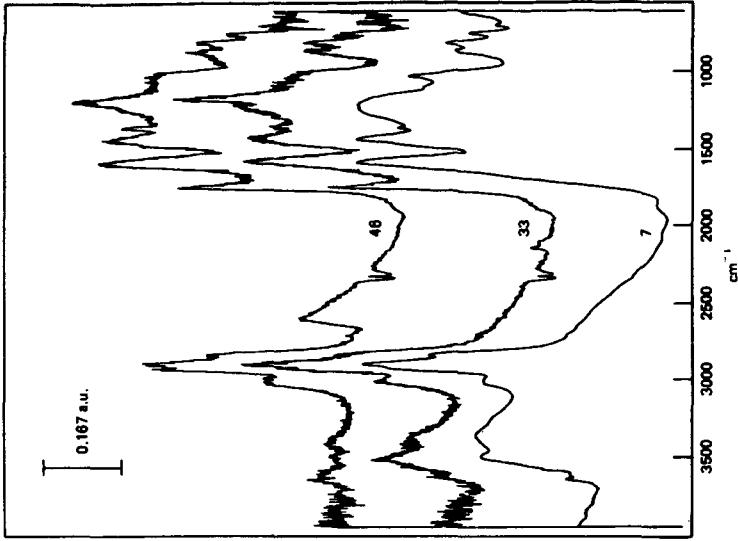


Fig. 6. Diffuse reflectance spectra of Wyodak coal: Curve 46 is the spectrum following deuterium oxide exchange of final acetylated state at 23 mtorr at 28°C, Curve 33 is the spectrum of the final acetylated state, and Curve 7 is the spectrum of the vacuum reference state.

CONDENSATE CORRECTION WYODAK POWDER (D-1)

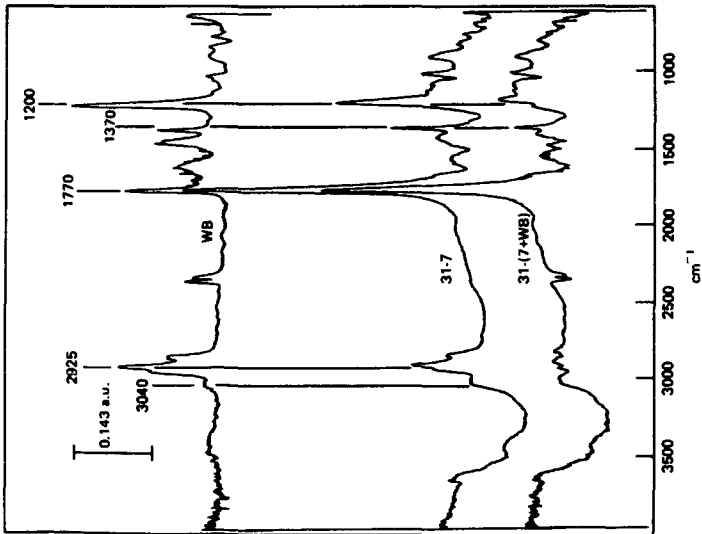


Fig. 5. Window background correction: "WB" is window background of DR cell after completion of the acetylation and deuterium oxide exchange reactions, Curve 31-7 is the difference spectrum of the acetylation reaction at 428°C for 25 min and the vacuum reference state, and Curve 31-(7+WB) is difference spectrum with window background removed.

PROGRESSIVE D₂O EXCHANGE: WYODAK POWDER (D-1)

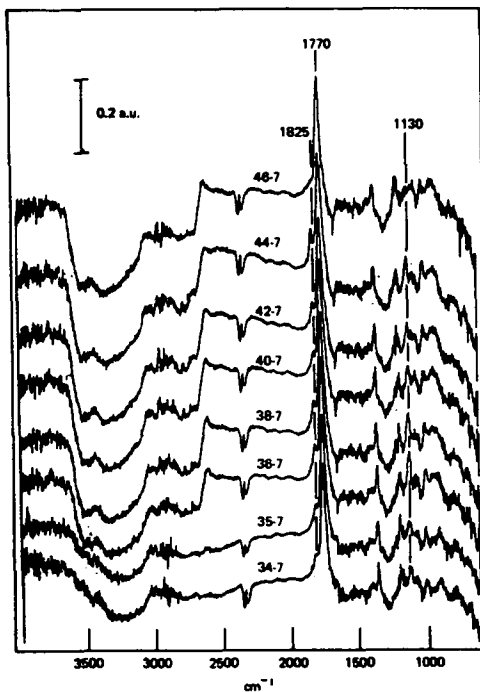


Fig. 7. Difference spectra for the deuterium oxide exchange reaction of Wyodak coal after acetylation. (See Table 1 for correlation of spectral numbers. All spectra have been corrected for window background.)

THE ELECTROPHORETIC MOBILITY DISTRIBUTION IN AQUEOUS DISPERSIONS OF BITUMINOUS COAL AND RESIDUAL HYDROCARBON MATERIALS

R.E. Marganski* and R.L. Rowell

Department of Chemistry
University of Massachusetts
Amherst, MA 01003

INTRODUCTION

The effect of mineral content on the electrokinetics of coal is very pronounced and contributes to a more hydrophilic surface that contains a substantial quantity of bound water. Mineral composition is known to vary markedly from coal to coal as does water content. Dewatering is an important aspect of coal preparation (1). In addition, there is evidence that the native mineral residue in coal plays an important catalytic role in direct hydro-liquifaction.

All of the above can be related to the electrophoretic behavior of the coal surface which in turn depends on the surface functional groups present. Even though intrinsic heterogeneity in coal produces no single and universal structure, enough similarity exists in those functionalities to predict the surface charging mechanisms. Previous explanation for surface charging on coal, based on oxide-like hydration and dissociation, fail to explain the positive charge at low pH so that the surface functionalities involved must include more than simple oxide groups.

These ideas were extended to the surface chemistry of residual hydrocarbon materials, the unconverted vacuum bottoms (uvb), obtained in petroleum refining. The uvb products are an unknown material that may have an asphaltene character, but the test is not conclusive. A significant result of this work was the finding that the electrophoretic properties of the uvb products resemble bituminous coal.

Coal fines and uvb products have not been commercially successful materials in the past. Recent efforts in coal-oil and coal-water systems, utilizing pulverized coal, have been promising. A similar role may be foreseen for the uvb products in slurry form.

In this paper, we report the full electrophoretic mobility distribution for several bituminous coals and a friable uvb sample as a function of pH in aqueous media. A discussion of the main structural features that effect electrophoresis is presented. The key parameters include determination of heteroatoms, carbon framework, mineral matter and physical structure, especially pores.

EXPERIMENTAL

Materials

The bituminous coal samples were kindly supplied by the Atlantic Research Corporation of Alexandria, Virginia, USA, and were studied along with a reference sample obtained from the General Motors Corporation that had been extensively studied in earlier work (2-5). All samples have been ground in the dry state and then sieved, as designated in Table 1. The ash content was determined by the University of Massachusetts Microanalysis Laboratory at 1000°C in oxygen and also reported in Table 1. The coal was stored in closed containers until used.

*Presently at E.I. Dupont de Nemours & Co., P.O. Box 430, Pass Christian, MS 39571.

The Chyoda sample, an unconverted vacuum bottoms residue, was obtained from Japan and supplied by KSE, Inc. of Amherst, Massachusetts. The initial condition was 0.5 centimeter friable black lumps. Samples were ground by hand in a mortar and pestle and then sieved dry, 100% -200 mesh. An elemental analysis was determined at the University Microanalysis Laboratory and is reported in Table 2. The percentages are in quantitative agreement with the elemental analysis generally found in these materials (7).

The water was distilled a second time from the in-house supply in a Corning AG-1b all Pyrex still. Certified ACS grade NaOH and HCl were obtained from Fisher Chemical Company.

Sample Preparation

A stock slurry was made by adding one gram of powder to 20 ml of twice distilled water. This was then mixed continuously on a stirring plate at medium speed for 48 hours at room temperature (23-25°C). The Chyoda sample was stirred for 72 hours at the same temperature.

Clean polyethylene containers (Nalgene LPE) were partly filled with 50 ml of distilled water and the pH adjusted to a preliminary value using KOH or HCl respectively. Ten drops of the stock coal slurry were then added to the bottles containing the water of known pH, giving a volumetric dilution factor of approximately 1/200.

The samples were then stirred on a stirring plate for 3 minutes at fast speed and then allowed to settle overnight at 30°C. After equilibration, the pH of the supernatant was taken, the mixture stirred at medium speed for two minutes, and the mobility then measured.

Microelectrophoresis

Electrophoretic mobility was measured with a Pen Kem 3000 automated electrokinetics analyzer (8). The instrument has a silica sample chamber with permanently bonded palladium electrodes. Particles are illuminated with a 2mW He-Ne laser and their image is projected onto the surface of a rotating radial grating. Electrophoretic movement causes a frequency shift in the light transmitted through the grating as compared to a reference detector. A fast Fourier transform analyzer computes the frequency spectrum from the individual contributions of the light scattered from many particles in order to obtain a representation of the electrophoretic mobility distribution. Focusing at the stationary layer is under automatic control. Measurements were made at both front and back stationary layers, under computer control, and the results averaged to ensure maximum accuracy.

RESULTS

In Figure 1 we show the distribution of the electrophoretic mobility for GM coal C8 at selected pH over the range studied. The pronounced features, multiple peaks and variation in peak breadth, were also observed in the other coal samples. In Figure 2 we show the dependence of the electrophoretic mobility distribution on pH for the Chyoda uvb C27 sample. The general features, multiple peaks and variation in peak breadth are shown by the Chyoda sample as well.

The average mobility as computed by the Pen Kem 3000 is shown as a function of pH shift from the isoelectric point (iep) for all four samples in Figure 3. The iep's for the coals were 6.0, 6.2, and 6.4, somewhat lower than 6.8, the iep of the Chyoda uvb sample. The curves reflect the specific nature of each sample within a similar overall envelope and a trend that shows extrema in mobility at low and high pH.

DISCUSSION

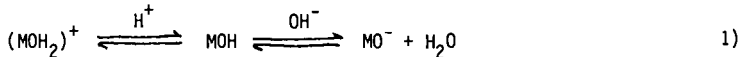
Multimodal Distribution

GM coal had a multimodal distribution, shown in Figure 1, which suggested the presence of a major second component such as a mineral oxide. The effect of polydispersity in size, although a complicating factor, cannot explain the wide differences in electrophoretic mobility of the individual peaks. For example, at a pH of 6.65, the emd peaks occurred at a mobility of -2.2, -0.9, -0.4 and +0.1 ($\mu\text{m/s})/(\text{V/cm})$ respectively. The differences observed here are far larger than the 50 percent mobility variation expected between the Hückel and Smoluchowski limits at a given zeta potential. In addition, since there is a continuous distribution in size as verified in photomicrographs, separate peaks would not be expected to occur. It is interesting to note that the individual peaks appeared to be reproducible over a wide pH range and individual peaks widened away from the iep in a similar manner to the other coals studied in this work. Statistical variation in sampling plus a small amount of flocculation near the iep could have had some effect on the emd.

AMPHOTERIC BEHAVIOR

The hydrogen and hydroxyl ions were found to cause amphoteric behavior in all samples measured as shown in Figures 1-3. This observation is in agreement with the conclusions of Fuerstenau et. al. (9), who observed amphoteric behavior in both native and demineralized coal samples.

Amphoteric behavior is caused by dissociation of a single surface group,



where M represents a metal ion, or, in the case where there are two distinct functional groups present, one that accepts a proton to become positively charged and one that dissociates and leaves a negative site. The zwitterionic surface is common in biological systems where the two groups responsible are usually the carboxylic and the amino groups.

The change in zeta potential (derivable from the mobility) with pH, $d\zeta/d\text{pH}$, at the isoelectric point (iep) gives an indication of how closely H^+ and OH^- can be considered potential determining ions. It is assumed here that the surface potential is close to the potential at the surface of shear, near the iep. Addition of acid or base will alter the chemistry of the solid, creating irreversible effects, which causes deviation from the ideal Nernstian behavior of 59.2 mv/pH unit at 25°C (10).

Smith (11-13) has shown that deviations from the ideal Nernst equation become important when the fraction of sites ionized at the point of zero charge is small. Under these conditions the Nernstian slope is reduced by a factor equal to $\ln(\theta_+/ \theta_-)$, where θ is the fraction of sites of given charge that are ionized at the iep. The iep is then characteristic of an absence of charge rather than an equal number of positively and negatively charged sites.

All coals measured in this work had slopes roughly one half of the Nernstian value. The simple oxide, alpha alumina, reported elsewhere (14), had a slope similar to the coal samples. The uvb had a much lower slope, indicating that a small amount of charge was present at the iep. This suggests that the surface charging on coals used here behaved more like an oxide than a hydrophilic carbon. Fuerstenau (9) has demonstrated the importance of using low ash coal in order to avoid measuring an oxide rather than a coal surface. It is interesting to note the significant rise in mobility at the extremes of pH for the uvb sample. This can be interpreted as ionization of heteroatoms at high and low pH values, leaving little or no ionization at the iep. Zwitterionic surfaces such as these were shown to be expected to depart markedly from Nernstian behavior as discussed by Hunter (15).

The interpretation of the dependence of the breadth of the distribution on pH has been given in an earlier paper (16). Increased ionization at larger pH shift from the iep produces a wider spectrum in the electrophoretic mobility distribution.

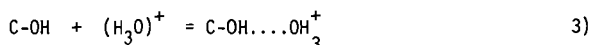
Several authors have proposed that the principal charge bearing groups on demineralized coal were oxygen functionalities such as aromatic alcohols (phenolic) and carboxylic acids (9,17). If these groups were alone responsible for surface charge on coal, hydrolysis in water would cause the donation of protons to water, the weaker Brönsted acid, creating only negative charge. Amphoteric behavior would not be observed. This is predicted by the theoretical work of Healy and White (18).

Attempts to explain the positive surface of coal by the following charging mechanism (19),



are based on the unsupported hypothesis that the adsorbed proton bears the positive charge. The origin of this concept lies in the attempt to compare the charging mechanism on coal to the metal oxides such as AlO. Protonation of a metallic hydroxide, MOH, produces a coordinated water molecule which gives an unbalanced and positive formal charge to the metal ion as, M:OH. The hydrogen atoms of water do not bear the charge. This is supported by the fact that charge on a hydrated metal ion in solution resides on the ion and not on any protons of the coordinated water molecules (20). Carbon, which is unable to coordinate water molecules, cannot give rise to positive charge in this manner.

We propose an alternative mechanism giving a positive charge through hydrogen bonding of an hydronium ion.



The decrease in mobility giving maxima at both high and low pH follows as a consequence of increased screening at high ionic strength.

In addition, most coals have mineral matter incorporated into their structures in various degrees. These are classified into three categories, 1) admixed minerals of larger size, 2) incorporated minerals as a result of metamorphic processes and 3) inherent minerals uniformly distributed within the organic matrix (21, 22). Demineralization procedures probably do not remove all of the mineral matter. For example, treated coal had as much as 10 percent of the ash content of untreated samples in Fuerstenau's work (9). Table 1 shows the ash content of untreated coals used in this work. The degree of entrapment determines how easily coal can be cleaned and is of current interest in beneficiation.

The extensive pore structure of coal will contain embedded water with dissolved salts, minerals, humic acids and organic matter. The release and subsequent adsorption of various species from these pores is likely to be a function of pH. One of the techniques used to determine the moisture retention and pore structure is to observe the behavior of metallic ion adsorption on coal (23).

Such selectivity will allow the transport of only certain materials into and out of those pores, analogous to a molecular sieve. Evidence for this behavior is shown in Figure 3, where the average mobility for several samples is plotted as a function of pH units away from the iep. Two features can be noted: first, the maximum negative mobilities are all similar in value, and secondly, the maximum positive mobilities have a larger amount of variation.

We interpret the above as follows: at high pH, the carboxylic and phenolic groups on the carbon skeleton of coal are mainly responsible for the negative charge. The organic framework is basically similar for the fully oxidized surfaces in this work and will result in similar electrophoretic mobility. This interpretation is supported by recent results obtained by Sequential Elution by Specific Solvents Chromatography, SESC (24). Findings indicated that although different coals varied greatly in overall structure, many of the same chemical groups were always present.

At low pH, positive functionalities, metallic oxides and adsorption of metal ions leached from pores all contribute to the observed mobility. The larger amount of variability expected in these processes will be reflected in a greater difference in the mobility that is observed from sample to sample.

This is in agreement with the results of Wen and Sun (25) who showed that at

lower pH, the zeta potential of oxidized coal was controlled by the presence of electrolytes such as Fe^{+2} and Al^{+3} ; both of which form hydroxides at pH values below 8. Above this pH, the metal ions behaved much like an indifferent electrolyte with little or no effect on the zeta potential. In addition, they also suggested that variations due to oxidation, shown to be small above pH 7 as compared to larger variation below pH 7, might be explainable due to the solubility of humic acids on the coal surface.

It is important to note that the measurements will be very sensitive to the solids concentration of the slurry. Previous workers have not specified this important parameter. In addition, the aging effects will be most pronounced in the high concentration region. Conditioning and aging procedures are generally not reported in the literature either. In this work, care was taken to properly condition a dilute stock solution for three days followed by further dilution to a very low particle concentration at a given pH in order to avoid any high concentration anomalies. By avoiding excessive leaching of inorganic ions, we are seeing the electrophoretic mobility of the coal surface and not a layer on inorganic hydrolysis precipitate. This could account for the generally high iep observed in this work as compared to other values in the literature (9, 25).

The composition of the uvb sample, while not completely understood, appears to consist of condensed polynuclear ring systems which have alkyl side chains containing heteroatoms such as nitrogen, oxygen and sulfur (7). Limited data suggests that oxygen is present as non-hydrogen bonded phenolic groups.

The concentration of mineral oxide in the uvb material is very low; it was found to be 0.9 percent for the sample reported in this work. The observed amphoteric behavior may then be explainable in terms of zwitterionic surface groups. It the uvb materials are really primarily asphaltenes, then this is in agreement with the conclusions of Cratin, who has suggested that the amphoteric nature of the asphaltenes might be similar to amino acids (26).

ACKNOWLEDGEMENTS

This work was supported by a Grant from the Atlantic Reserach Corporation of Alexandria, Virginia. Technical assistance and instrument support was provided by Pen Kem, Inc. of Bedford Hills, New York.

REFERENCES

1. Report to the APS by the study group on research planning for coal utilization and synthetic fuel production, Rev. Mod. Phys., 53, No. 4, part II, Oct. 1981.
2. B.J. Marlow and R.L. Rowell, in Third International Symposium on Coal-Oil Mixture Combustion, Orlando, FLA., April 1-3, 1981, CONF-810498 (Vol. 2) pp 640-650, National Technical Information Service, U.S. Dept. of Commerce, Springfield, VA 22161 (1981).
3. R.L. Rowell, S.R. Vasconcellos, R.J. Saia and R.S. Farinato, I&EC Process Design & Development 20, 283-288 (1981).
4. R.L. Rowell, S.R. Vasconcellos, R.J. Saia, A.I. Medalia, B.S. Yarmoska and R.E. Cohen, I&EC Process Design & Development 20, 289-294 (1981).
5. R.L. Rowell, EPRI Final Report, Projects RP-1030 and RP-1455-6, Electric Power Research Institute, RRC, Box 50490, Palo Alto, CA 94303 (1981).
6. J.J. Kosman and R.L. Rowell, Colloids and Surfaces, 4, 245-254 (1982).
7. R.B. Long, Advan. Chem. Ser., 195, 17 (1981).
8. The Pen Kem 3000 Electrokinetics Analyzer Reference Manual, 1982, Pen Kem, Inc., 341 Adams St., Bedford Hills, NY, 10507.

9. D.W. Fuerstenau, J.M. Rosenbaum and J. Laskowski, *Colloids and Surfaces*, 8, 153 (1983).
10. P.A. Arp, *J. Colloid Interface Sci.*, 96, 80 (1983).
11. A.L. Smith in "Dispersions of Powders in Liquids, 3d ed.", G.D. Parfitt ed., Applied Science Publishers, NJ (1981).
12. S. Levine and A.L. Smith, *Disc. Faraday Soc.*, 52, 290 (1971).
13. A.L. Smith, *J. Colloid Interface Sci.*, 55, 525 (1976).
14. R.E. Marganski and R.L. Rowell, *ACS/PMSE Preprints* 52, 399 (1985).
15. R.J. Hunter, "Zeta Potential in Colloid Science, Principles and Application", Academic Press, New York, NY, 1981.
16. R.E. Marganski and R.L. Rowell, *J. Disp. Sci. Tech.* 4, 415 (1983).
17. G.L. Tingley and J.A. Morrey in "Coal Structure and Reactivity", a Battelle Energy Report, Battelle Pacific Northwest Laboratories, Richland, Washington, 1973.
18. T.W. Healy and L.R. White, *Adv. Colloid Interface Sci.*, 9, 303 (1978).
19. S. Kelebek, T. Salman and C.W. Smith, *Canadian Metallurgical Quarterly*, 21, 205 (1982).
20. R.H. Yoon, T. Salman and G. Donnay, *J. Colloid Interface Sci.*, 70, 483 (1979).
21. R.A. Strechlow, L.A. Harris and C.S. Yust, *Fuel* 57, 185 (1978).
22. E.L. Fuller Jr., *J. Colloid Interface Sci.*, 89, 309 (1982).
23. O. P. Mahajan in "Coal Structure", R.M. Meyers ed., Academic Press, NY (1982).
24. C & E News, August 9, 1982.
25. W.W. Wen and S.C. Sun, *Soc. Min. Eng., AIME*, 262, 174 (1977).
26. P.D. Cratin, in "Chemistry and Physics of Interfaces II", ACS Publications (1971).

Table 1. Ash Content and Sieve Fractions

<u>Sample (#)</u>	<u>% Ash*</u>	<u>Sieve mesh</u>
Island Creek (c26)	16.0	200 x 325
Gen. Motors (c8)	4.8	-200
Bishop (c28)	4.7	200 x 325
Chyoda uvb (c27)	0.9	-200

*Determined by the University of Massachusetts Microanalysis Laboratory at 1000°C in oxygen.

Table 2. Elemental Analysis* of Chyoda uvb

<u>Element</u>	<u>Weight %</u>
Carbon	86.5
Hydrogen	6.0
Nitrogen	1.5
Sulfur	5.3
Oxygen	0.7

*Determined by the University of Massachusetts Microanalysis Laboratory.

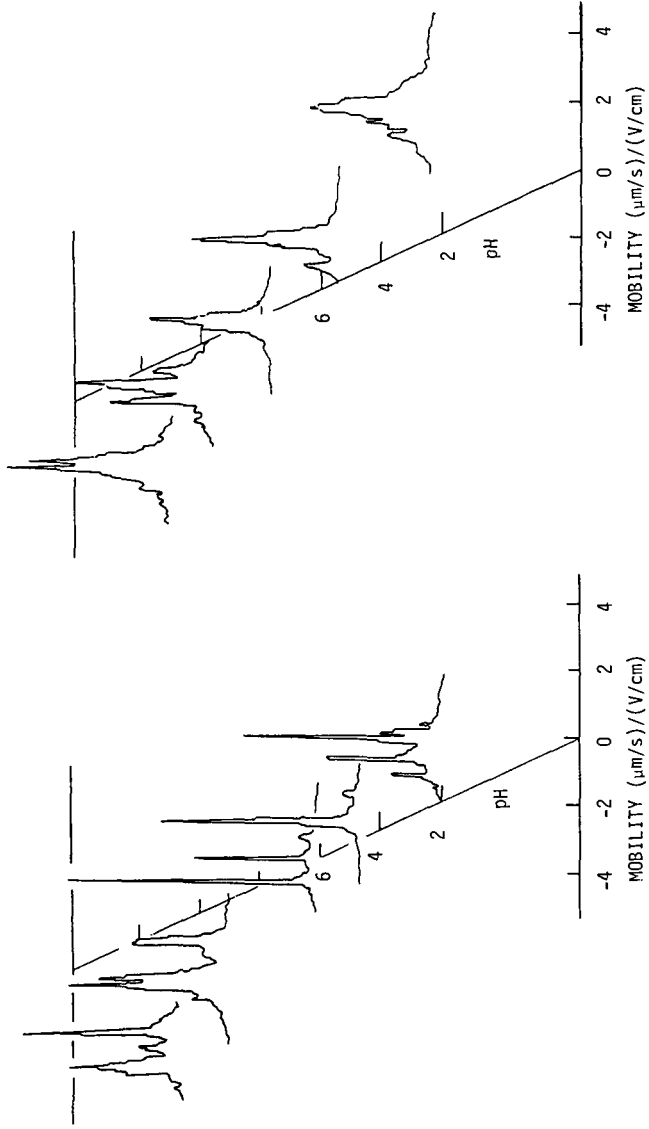


Figure 1. Electrophoretic mobility distribution as a function of pH for General Motors coal sample C8.

Figure 2. Electrophoretic mobility distribution as a function of pH for Chiyoda uvb sample C27.

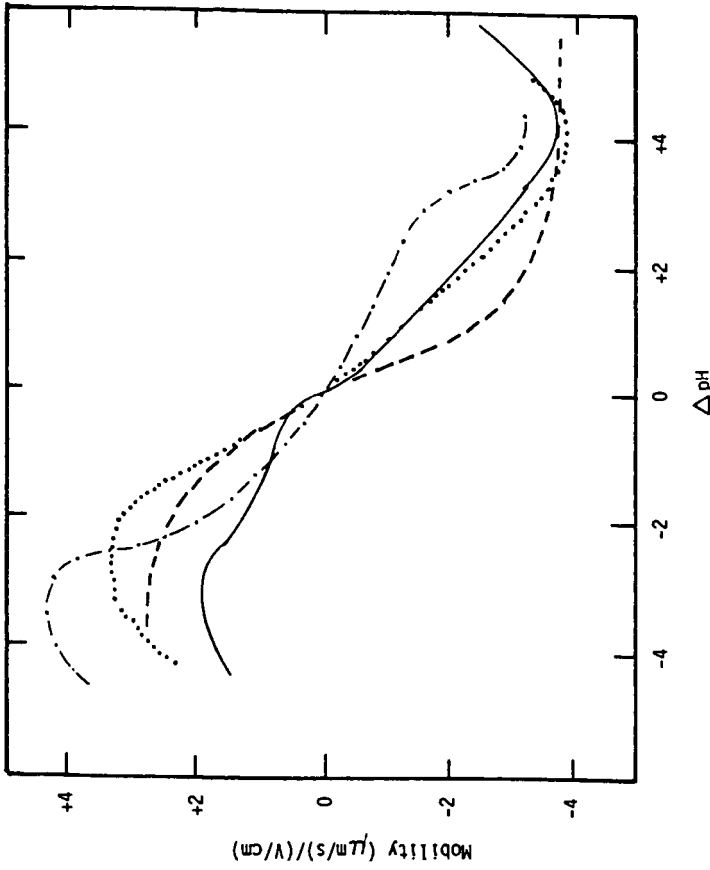


Figure 3. Average electrophoretic mobility as a function of pH shift from the isoelectric point for unconverted vacuum bottoms (uvb) and several coals. Samples (and isoelectric points) are: solid line, General Motors coal C8 (6.0); dashed line, Bishop coal C28 (6.4); dotted line, Island Creek coal C26 (6.2); and dash/dotted lines, Chyoda uvb C27 (6.8).

A COMPARISON OF THE ACOUSTIC MOBILITY AND THE ELECTROPHORETIC MOBILITY OF COAL DISPERSIONS

B.J. Marlow

Pen Kem, Inc.
Bedford Hills, NY 10507

R.L. Rowell

Department of Chemistry
University of Massachusetts
Amherst, MA 01003

INTRODUCTION

Aqueous coal dispersions play a major role from mining to the utilization of coal. The properties of these dispersions, such as stability towards aggregation, rheology, etc., are controlled by two major factors, namely, the particle size and interfacial chemistry. The interfacial chemistry is controlled by the interactions of the coal surface with the aqueous phase.

Coal surface-aqueous phase interactions are controlled by rank, mineral content, surface functional groups, pore structure, adsorption, pH, ionic strength, etc. These interactions can be probed using electrokinetic techniques (1-11). Electrokinetic techniques presently used to investigate aqueous coal dispersions include microelectrophoresis and streaming potential (12). Although both of these techniques are invaluable to study coal surface interactions they cannot be used for process condition dispersions. As a result, questionable extrapolations to process conditions must be performed.

Below, we describe a new electrokinetic technique that utilizes ultrasonics and preliminary data on the application of this technique to coal dispersions. The advantage of ultrasonics are (i) virtually any particle size can be used from ions to aggregates, (ii) any concentration of the dispersed phase can be used from the ppm range to volume filling networks, (iii) samples can be optically opaque or photosensitive, and (iv) measurements can be made on flowing systems.

THEORY

In 1933, Debye (13) predicted that subjecting an electrolytic solution to a sound wave of ultrasonic frequencies would result in an alternating potential, the IVP or ion vibration potential, having the same frequency as the sound wave. The potential is detected with two electrodes placed normal to the sound propagation separated by a phase distance other than an integral multiple of the wavelength; the optimum separation being $(2n+1) \lambda/2$. The basis of the "Debye effect" is that the effective masses and frictional drag coefficients of anions and cations are different due to composition and solvation. These differences result in different degrees of displacement amplitude and phase. The relative displacement of anion and cation produces a separation of charge centers creating a vibrating dipole. The original theory of Debye has since been modified (14) and experimentally verified, a review of which can be found in reference (15).

In 1938, Hermans (16) and Rutgers (17) reported an effect similar to the Debye effect when ultrasonic waves were propagated through a colloidal dispersion. In contrast to the IVP where the displacement of anion

and cation produce an alternating potential, the relative displacement of a charged particle from its surrounding "ion atmosphere" induces the potential termed the colloid vibration potential or CVP. Since this time many colloidal systems have been investigated qualitatively using this technique (18-23). The first quantitative measurements were performed by Marlow et al (24) where the dilute theory of Enderby and Booth (25,26) is verified and extended to concentrates using the Levine et al (27) cell model theory.

Pictorially, the mechanism of the CVP is shown in Figure 1. To understand the mechanism of the CVP it is useful to point out that the CVP is analogous to the sedimentation potential or Dorn effect (28) and reflects the same intrinsic phenomena. Figure 1a shows a charged colloidal particle at rest with its accompanying "ion atmosphere" of "thickness" $1/\kappa$. If this particle is acted on by a gravitational field as shown in Figure 1b, the ion atmosphere is perturbed from equilibrium resulting in polarization and the formation of a static dipole. In contrast, if the particle is acted on by an acoustic field as shown in Figure 1c, a dynamic or vibrating dipole results. It is important to point out that in the Dorn effect the particle is caused to move relative to the medium but in the acoustic effect both particle and medium move and it is the relative motion that produces the effect.

As with the sedimentation potential, the acoustically produced dipole results in a potential that is immeasurably small for a single particle but a macroscopic measurable potential results in a swarm of particles such as in a colloid. Figure 2 shows the general technique used to measure the CVP. Two inert metal electrodes A and B are placed normal to the sound propagation and spaced at one-half a wavelength.

The relationship between the measured CVP and pertinent electrokinetic parameters for dilute aqueous dispersions ($\phi < 1$) can be expressed as (24)

$$CVP = \frac{2P\phi}{\lambda_0} \frac{(\rho_1 - \rho_2)}{\rho_1} \frac{\epsilon_0 D \zeta}{\eta} \quad [1]$$

where P is the sound pressure amplitude, ϕ the volume fraction of particles, λ_0 the conductivity of the medium, ρ_2 the particle density, ρ_1 the medium density, ϵ_0 the permittivity of free space, D the dimensionless dielectric constant, ζ the zeta or electrokinetic potential, and η the viscosity of the medium. Normalizing the CVP for P, λ_0 , ϕ , and $(\rho_2 - \rho_1)/\rho_1$ leads to an acoustic mobility AM having the same units as the electrophoretic mobility EM, i.e.,

$$AM = \frac{CVP \lambda_0}{2P\phi(\rho_2 - \rho_1)/\rho_1} = \frac{\epsilon_0 D \zeta}{\eta} = EM \text{ (m}^2/V_s) \quad [2]$$

Thus, measurements of the CVP, P, and λ_0 as well as knowledge of the relative particle density and concentration leads to the same information as obtainable from electrophoresis.

In concentrated dispersions particle-particle hydrodynamic and electrical interactions occur. Applying the Levine et al (27) cell model theory of the Dorn effect to the CVP results in an interaction parameter $F(\kappa a, \phi)$ on the right hand side of equation [1] where a represents the electrokinetic radius or the particle size a divided by the "thickness" of the ion atmosphere. Figure 3 shows a plot of the interaction parameter $F(\kappa a, \phi)$ as a function of ϕ for the case where $\kappa a \gg 1$ and $a > 0.5 \mu\text{m}$

which will invariably be the case in aqueous coal dispersions. Thus, instead of the CVP increasing linearly with ϕ as predicted by the dilute theory, the CVP will initially rise linearly and then gradually level off and go through a maximum.

EXPERIMENTAL

Materials

A bituminous coal used as a reference sample in previous work (29-32) obtained from General Motors Corporation was used in this work. The coal was air ground to 100% minus 200 mesh and stored in a sealed container. The ash content was 4.8%.

The water used was distilled and ion exchanged and had a specific volume conductivity of $2E-4$ S/m. Solution acidity and alkalinity was adjusted with 1N KOH or 1N HCl obtained standardized from Fisher Scientific Company.

Methods

Aqueous coal dispersions were prepared by first outgassing the desired quantity of coal at 30 C under vacuum. The desired quantity of distilled water was then added by back filling under vacuum. The samples were then rolled in polyethylene containers for 24 hr on a mill. Five dispersions were prepared, namely, 0.04, 0.1, 0.2, 0.3, and 0.4 weight percent coal.

Acoustic measurements were performed with the Pen Kem System 7000 Acoustophoretic (tm) Titrator. The System 7000 measures the CVP, P , λ_0 , pH, T , and titrant volume accurate to 1 microliter. All measurements were performed at 25 C. A description of the apparatus can be found in reference (24). All pH titrations were performed by starting at the equilibrated pH and adding acid to one aliquot of sample and then base to another aliquot of sample and then combining the data.

Electrophoretic mobility measurements were performed with the Pen Kem System 3000 Automated Electrokinetics Analyzer some of which are reported in reference (11).

RESULTS AND DISCUSSION

The dependence of the CVP on GM coal concentration for a pH adjusted to 6.2 is shown in Figure 4. The CVP initially rises linearly with concentration and then levels off and goes through a maxima at a coal concentration of 30% by volume. Also shown in Figure 4, are the calculated values based on the dilute theory and cell model. These values were calculated by using measured values of the dispersions supernatant conductivity, particle density 1.22 g/cm³, and the particles electrophoretic mobilities determined by sampling the supernatant of the settled dispersions, all of which are given in Table 1. The high supernatant conductivities are the result of both dissolution of material from the coal and electrolyte added to adjust the pH to 6.2. The correlations shown in Figure 4, show good agreement between experiment and theory. Thus, ultrasonic electrokinetic measurements can be applied to concentrated coal dispersions to obtain meaningful information about the electrokinetic properties of the dispersion. Figure 5, shows a plot comparing both electrophoretic and acoustic mobilities as a function of pH for GM coal. The acoustic mobilities were obtained at a particle concentration of 4% whereas the electrophoretic mobilities were obtained by adding a few drops of this dispersion to a solution of the desired pH (11). Thus, the acoustic mobilities are

determined with an aqueous phase containing any leached materials whereas the electrophoretic data is taken with approximately a 200-fold dilution in the leached materials.

Good agreement is shown between electrophoresis and ultrasonics as shown in Figure 5 Irrespective of the seemingly different preparation techniques. The mobility is positive below a pH=5.8, the isoelectric point η_{ep} , and negative above this pH. Most researchers believe the negative potential at high pH is the result of the dissociation of carboxylics, phenolics, etc. on the coals surface (3,11) or alternatively due to the adsorption of metal hydroxides formed from the mineral present in coal (2). A positive potential below the isoelectric point is described as the result of protonation of the acid groups on the surface of the coal (10), the adsorption of cations (6), or the adsorption of hydronium ions (11).

Figure 6. shows a plot of the acoustic mobilities of GM coal as a function of pH at two particle concentrations, namely, 0.04 and 0.40% by volume. The behavior in the concentrated dispersion no longer resembles that obtained in the dilute dispersion. The mobilities at the higher concentration are generally lower, the isoelectric point is shifted to a significantly lower value, and maxima and minima are seen at high and low pH.

We believe that the concentration effect shown in Figure 6. results from the fact that in the concentrated dispersion the equilibrated supernatant conductivity is greater than in the dilute case. Thus, in the concentrate significantly more material is leached from the coal pores and surface. As a result, the double layer is compressed in the concentrate and the potentials accordingly lowered. Also, the dissolved materials of the coal become "specifically" adsorbed.

A shift to a lower pH as well as a maxima and a reversal of potential with lowering pH as shown in Figure 6. results from the chemisorption of anions (12). A maxima and reversal at high pH also seen in Figure 6. is the result of the adsorption of cations (12). Thus, in concentrated aqueous coal dispersions deviation of the electrokinetic properties from ppm studies will be significant. The deviations are the result of chemically adsorbed anions at low pH values and adsorbed cations at higher pH values. The adsorbed materials are produced from leaching of the coal surface and pores with subsequent deposition.

We believe that the results described above show that the application of ultrasonic electrokinetic techniques to aqueous coal dispersions will be of great practical significance in the future when attempting to characterize charged coal particles in concentrates.

Table 1. Comparison of cell model calculations of the CVP and experiment as a function of GM coal concentration at a pH=6.2.

Coal Volume Fraction	EM (m^2/Vs) $\times 10^8$	λ_0 (S/m)	F(ka, ϕ)	-CVP(mV)	
				Exp.	Cal.
0.04	-1.00	0.18	0.95	0.016	0.019
0.10	-0.97	0.18	0.88	0.049	0.042
0.20	-0.97	0.19	0.75	0.072	0.067
0.30	-0.96	0.21	0.63	0.074	0.078
0.40	-0.95	0.24	0.51	0.072	0.069

REFERENCES

1. R.E. Marganski and R.L. Rowell, *J. Dispersion Sci. and Tech.*, 4(4), 415-424 (1983).
2. C.W. Angle, W.M. Leung, R.J. Mikula, and H.A. Hamza, "Processing and Utilization of High Sulfur Coals", ed. Y.A. Attia, Elsevier, Amsterdam, 67-87 (1985).
3. D.W. Fuerstenau, J.M. Rosenbaum, and J. Laskowski, *Colloids and Surfaces*, 8, 153 (1983).
4. S.C. Sun and J.A.L. Cambell, *Adv. Chem. Series*, 55, 363-375 (1965).
5. J.A.L. Cambell and S.C. Sun, *SME AIME Trans.*, 247, 120-122 (1970); 247, 111-114 (1970).
6. W.W. Wen and S.C. Sun, *Soc. Min. Eng. AIME*, 262, 174 (1977).
7. M. Parsad, *J. Inst. Fuel*, 2, 174 (1974).
8. J. Coca, J.L. Bueno, and H. Sastre, *L. Chem. Tech. Biotechol.*, 2, 637-642 (1982).
9. S. Mori, T. Hara, and K. Aso, *Powder Technology*, 40, 161-165 (1984).
10. S. Kelebek, T. Solman, and G.W. Smith, *Canadian Metall. Eng. Quarterly*, 21(2), 205-209 (1982).
11. R.E. Marganski, "The Dependence of the Electrophoretic Mobility Distribution on pH, Ionic Strength and Surfactant Concentration for Aqueous Dispersions of Alumina and Coal Slurries", Ph.D. Thesis, University of Massachusetts, Amherst MA (1984).
12. R.J. Hunter, "Zeta Potential in Colloid Science", Academic Press, New York (1981).
13. P. Debye, *J. Chem. Phys.*, 1, 13 (1933).
14. J. Buggosh, E. Yeager, and F. Hovorka, *J. Chem. Phys.*, 15(8), 542 (1947).
15. R. Zana and E. Yeager, *Mod. Aspects of Electrochem.*, 14, 1 (1982).
16. J. Hermans, *Phil. Mag.*, 25, 426 (1938); 26, 674 (1938).
17. A. Rutgers, *Physica*, 5, 46 (1938); *Nature*, 157, 74 (1946).
18. E. Yeager, J. Buggosh, F. Hovorka, and J. McCarthy, *J. Chem. Phys.*, 17, 411 (1949).
19. E. Yeager, H. Dietrick, and F. Hovorka, *J. Acoust. Soc. Am.*, 25, 456 (1953).

20. E. Yeager, J. Dereska, and F. Hovorka, Tech. Report No. 23, Western Reserve University, Ultrasonic Research Laboratory, Cleveland, OH.
21. R. Zana and E. Yeager, J. Phys. Chem., 71, 3502 (1967).
22. U. Beck, R. Zana, and E. Rohloff, TAPPI, 61(9), 63 (1978).
23. R. Zana and E. Yeager, U.S. Clearing House Fed. Sci. Tech. Inform., AD-681063, Case Western Reserve University, Cleveland, OH.
24. B.J. Marlow, D. Fairhurst, T. Oja, and H. Pendse, Submitted to Langmuir, December (1986).
25. J. Enderby, Proc. Phys. Soc., 207A, 321 (1951).
26. F. Booth and J. Enderby, Proc. Phys. Soc., 208A (1952).
27. S. Levine, G. Neale, and J. Epstein, J. Colloid and Interface Sci., 57, 424 (1976).
28. B.J. Marlow and R.L. Rowell, Langmuir, 1, 83 (1985).
29. B.J. Marlow and R.L. Rowell, in Third International Symposium on Coal-Oil Mixture Combustion, Orlando, FLA., April 1-3, 1981, CONF-810498 (Vol. 2) p. 640-650, National Technical Information Services, U.S. Dept. of Commerce, Springfield, VA 22161 (1981).
30. R.L. Rowell, S.R. Vasconcellos, R.J. Saia, and R.S. Farinato, I&EC Process Design & Development, 20, 283-288 (1981).
31. R. L. Rowell, S.R. Vasconcellos, R.J. Saia, A.I. Medalia, B.S. Yamoska and R.E. Cohen, I&EC Process Design & Development, 20, 289-294 (1981).
32. R.L. Rowell, EPRI Final Report, Projects Rp-1030 and Rp-1455-6, Electric Power Research Institute, RRC, Box 50490, Palo Alto, CA 94303 (1981).

Figure 1. Mechanism of Dorn effect and CVP

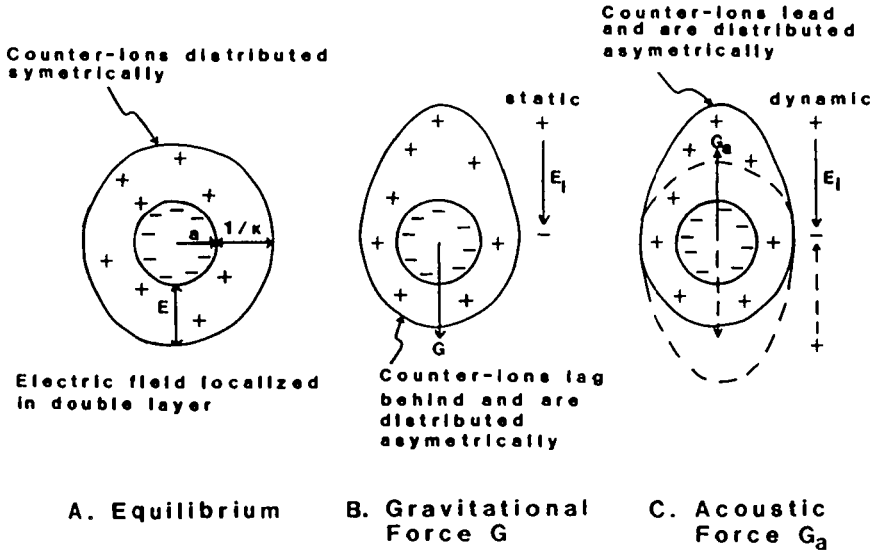


Figure 2. Measurement of CVP

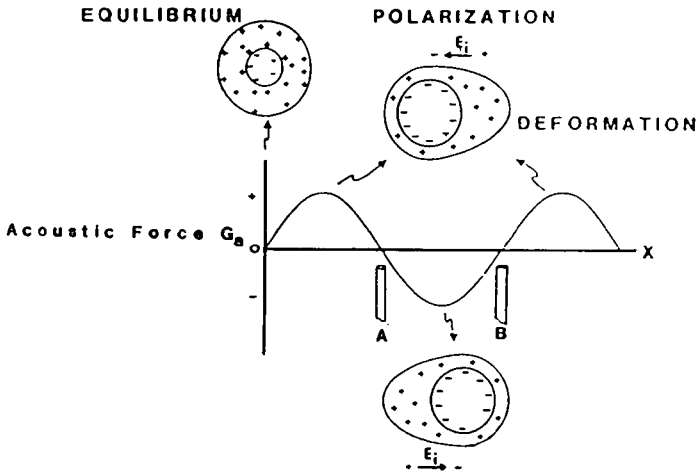


Figure 3. Interaction parameter as a function of volume fraction.

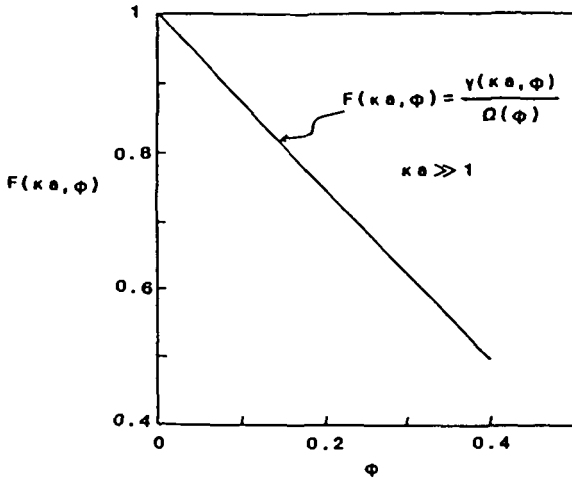


Figure 4. CVP as a function of coal concentration at a pH of 6.2.

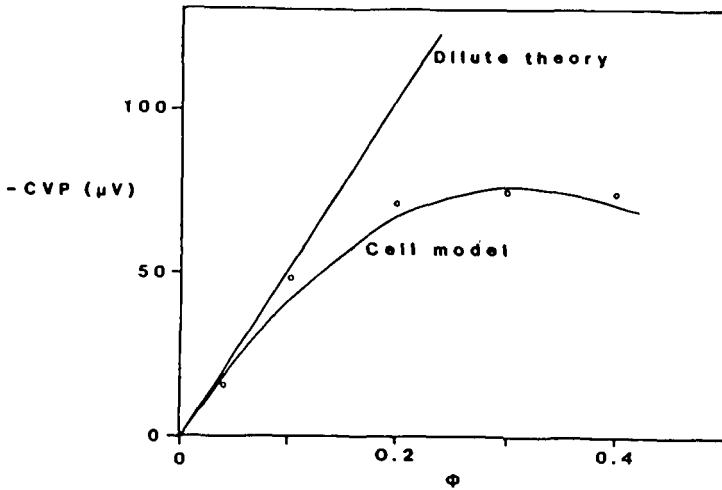


Figure 5. Comparison of acoustic and electrophoretic mobilities for GM coal.

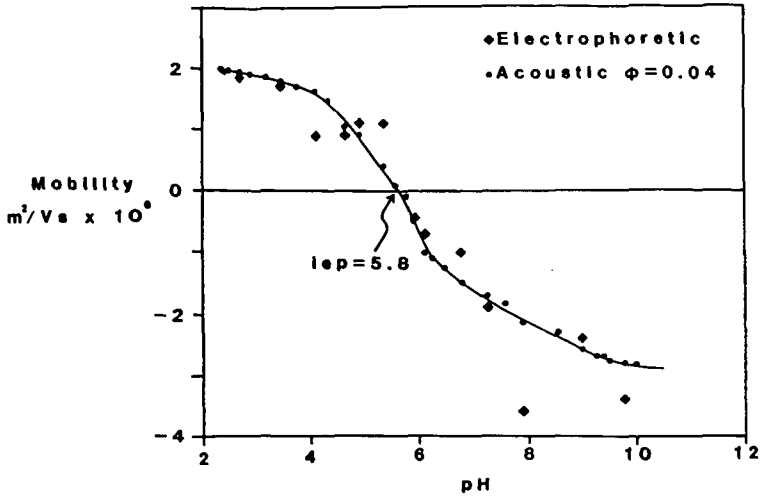
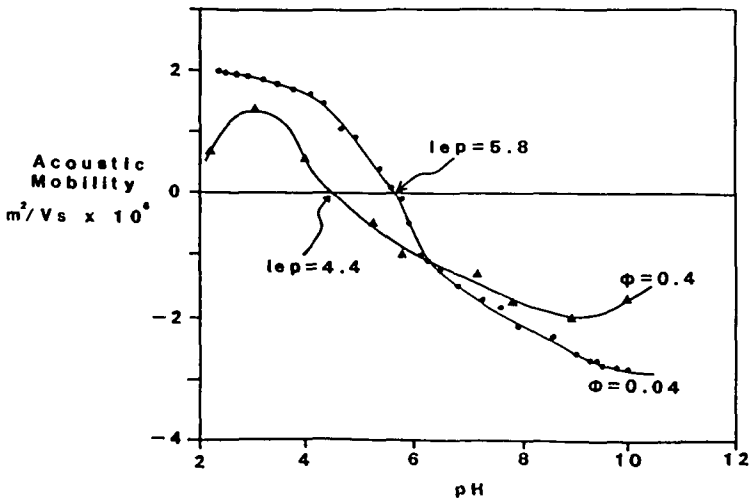


Figure 6. Effect of GM coal concentration on acoustic mobility.



**COAL ELECTROKINETICS: THE ORIGIN OF CHARGE AT
COAL/WATER INTERFACE**

J.S. Laskowski

Department of Mining and Mineral Process Engineering
The University of British Columbia
Vancouver, B.C., Canada

Introduction

Electrokinetic measurements provide valuable information on the properties of coal aqueous suspensions that depend on the charge of the particles; examples include coal particles floatability, coal suspensions stability and rheology, coal fines filtrability, etc. Such measurements reveal the relationship of charge to the nature of coal and how the charge is effected by the liquid phase composition. It may also serve as an additional tool in the studies on coal surface composition.

For any solid/liquid system both the composition of the solid and the concentration and valency of ions in the solution contribute to the sign and value of the electrokinetic potential. In the case of very dilute suspensions containing a small number of individual particles in a large amount of solution, as in microelectrophoretic experiment, the contribution from the value of surface potential is more important. For the concentrated suspensions, however, as in the case of electrophoretic mass transfer experiment, the value of the zeta potential, depends to a large extent, on the concentration of ions in the liquid phase.

The results discussed in this paper all pertain to the conditions of conventional microelectrophoretic experiment conducted at extremely low solid concentration.

Recent analysis of the available data on electrokinetics of coal/water suspensions [1] has led to a general relationship (Fig. 1) which shows schematically the microelectrophoretic mobility - pH curves for the coals of different rank. The shift of the curves for lower rank coals towards more acidic pH ranges resembles the shift caused by oxidation [2].

As seen from Fig. 1, the zeta potential - pH curves for coals clearly exhibit iso-electric points; thus coal particles have both negative and positive sites.

Coal particles are extremely heterogenous: various heteroatoms and functional groups along with inorganic impurities are present in the hydrocarbon matrix. These surface sites exhibit various electrochemical characteristics and they all contribute to the overall electrical surface charge of coal particles. The basic concept of this paper is that under the conditions of a microelectrophoretic experiment, in which small number of solid particles is suspended in a large volume of solution, there are three main effects contributing to the surface charge of coal particles:

- (i) coal hydrocarbon matrix,
- (ii) coal heteroatoms and functional groups,
- (iii) coal inorganic impurities.

In experiments at higher solid/solution ratio, a fourth effect, the effect of dissolved species, may play a more important role in determining surface charge.

Model Systems

Hydrocarbons. Fig. 2 shows Mehrishi and Seaman's [3] data obtained for anionic (RCOOH), nonionic (ROH) and cationic (RNH₂) hydrocarbons. The electrophoretic mobility versus pH curves confirm the presence of carboxyl group for the acid with pK estimated to be about 4.3, as the pH at which the microelectrophoretic mobility is one-half of the plateau value, similarly for n-octadecylamine pK is 8.8. The

electrophoretic mobility curve for the non-ionogenic but polar compound, octadecanol, reveals that this hydrocarbon is negatively charged over the whole pH range. Hollinshead et al. found [4], however, that the purified octadecanol showed lower electrophoretic mobility which may suggest the influence of trace contaminants.

Nujol (medical paraffin) droplets in water were shown by many researchers to be negatively charged over the whole pH range [5,6]. This is consistent with Wen and Sun's results obtained for six hydrocarbons between hexane to octadecane [7] (Fig. 3). Droplets of kerosene in water are also negatively charged over the entire pH range [7,8]. It is of interest to observe that Perreira and Schulman [9] found that pure paraffin wax was negatively charged above pH 5. The zeta potential values for paraffin wax reported by Arbiter et al. [10] were negative in the pH range 3 to 10.

Our measurements with aromatic hydrocarbon, anthracene (Aldrich, purity 98%+), show similar mobility-pH relationship: anthracene crystals are negatively charged over the whole pH range. It seems then that the H^+ and OH^- ions play predominant role in charging a neutral hydrocarbon wall.

Nujol oil droplets with adsorbed polysaccharide molecules, containing no acidic or basic groups, were found not to acquire any charge [5].

Such results as received above suggest that while the effect of ionic groups can be satisfactorily predicted, the contribution of the hydrocarbon matrix to the overall particle charge needs to be reexamined.

Graphite. Spurny and Dobias [11] reported that pure Ceylon graphite was negatively charged in aqueous solution, with the zeta potential increasing continuously over the pH range 2 to 10. Similar results were obtained by Chander et al [12].

Fig. 4 shows our results obtained for Ceylon graphite [13]. In our experiments, an original finely ground graphite sample, as well as sample purified by leaching were utilized in microelectrophoretic experiments. The leached sample was prepared by conditioning 10 g of finely ground graphite (below 38 μ m) in 100 ml of 1 N HCl solution at 45°C for 16 hours, followed by filtration, thorough washing with distilled water and drying at 50°C. 62 ppm Fe, 12 ppm Al, 9 ppm Mg and 17 ppm Ca were detected in the pregnant solution. ICP analysis of the original sample revealed the following major impurities: 0.14% Fe, 0.02% Ca, 0.01% Mg, 0.01% Ti, 0.01% Al, 0.01% Na, 0.01% K and 0.01% P. All other impurities present in the sample assayed less than 50 ppm. Examination of both samples under a scanning microscope (ETEC, Autoscan) gave no indication of alterations of the mineralogical structure introduced by the leaching. Specific surface area measurements carried out with the use of a Quantsorb (Quantachrome Corp.) apparatus and nitrogen gave 5.08 and 5.25 m^2/g for the original and leached -38 μ m graphite samples, respectively.

As it can be seen from Fig. 4, both graphite samples exhibit negative zeta potential values over the whole pH range. The leached sample is more negative points to the role the cationic surface centers like Fe^{3+} , Ca^{2+} and Mg^{2+} may play.

Graphite particles which are handled in air are claimed to be partially oxidized [14] which probably explains the graphite particles behavior in the electrokinetic experiments.

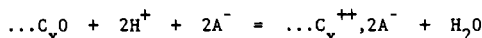
Carbon Black. Carbon black is a form of elemental carbon prepared by partial combustion of various carbon-containing substances (cone sugar, liquid or gaseous hydrocarbons, etc). They contain above 90% carbon, with oxygen and hydrogen being the other two major constituents [15]. Carbon blacks can be graphitized by heating in the absence of oxygen. This process leads to the elimination of functional groups and growth of graphitic layers. High temperature treatment (up to 3000 °C) provides a solid structure closely resembling that of graphite [16].

The origin of charge on carbon black particles has attracted the attention of many researchers. Miller [17,18] studied adsorption from aqueous solutions on the charcoal prepared from purified cane sugar by prolonged heating at 1200 °C followed by activating heating for 24 to 48 hrs at the same temperature in the presence of a

limited supply of air. Such a charcoal was found in the adsorption studies to cause decomposition of neutral salts with the base set free and the equivalent amount of acid adsorbed onto charcoal. The process is referred to as hydrolytic adsorption. Frumkin and his co-workers [19,20,21] showed that carbons outgassed at 950 °C did not adsorb mineral acid from a dilute solution and that adsorption could be restored in the presence of oxygen. They also found an exponential relationship between the oxygen pressure and the acid adsorption. In Frumkin's electrochemical theory the oxygen adsorbed on carbon surface is assumed to ionize to some extent with the formation of hydroxyl ions; the carbon surface acquires positive sign in this process and the solution becomes more alkaline:

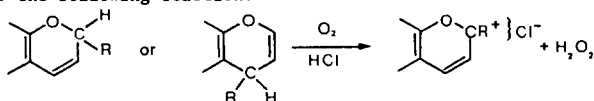


where $\dots C_x O, 2A^-$ stands for positively charged carbon surface with adsorbed anions. In acidic solution

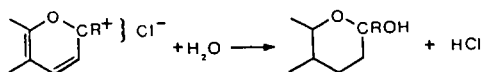


The carbon then acquires positive charge in the presence of oxygen [22,23,24], but the same carbon exposed to oxygen for long periods, or at elevated temperatures, oxidizes and dissociation of the oxygen functional groups imposes a negative charge on the system in an aqueous environment [25,26].

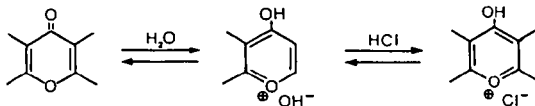
Garten and Weiss [27] postulated that the carbons contain chromene structures. A characteristic reaction of this group is the formation of a carbonium ion according to the following reaction:



The benzopyrylium(carbonium) ion is a weak base having a dissociation constant of the order of 10^{-10}



Garten and Weiss [27] pointed out that chromene structures on the surface of an H-carbon would function as a redox system. In the presence of oxygen and acid the carbon is oxidized so that it acquires the potential of the oxygen-hydrogen peroxide couple with which it is in equilibrium, and, hence, the adsorption of acid anions at the carbonium ion sites is a function of the oxygen partial pressure and the pH value of the solution. This chromene-carbonium ion couple may then be regarded as a chemical background for Frumkin's electrochemical theory.



Voll and Boehm [28] found evidence for a different cyclic ether structure, pyrone-like structure, characterized by basic properties. According to them each basic site contains two oxygen atoms, but they may be located in two different rings of a graphitic layer.

Arbiter et al [10] came to a conclusion that for hydrophobic solids, the double layer is entirely on the water side of the interface and is then analogous to that at the water/air interface. James in his review [29] showed a straight line

which approximates the experimental curve for Nujol as a typical mobility versus pH relationship for a nonionogenic surface.

Coal Electrokinetics

Coal is heterogenous at a number of levels [30]. At the simplest level it is a mixture of organic and inorganic phases, but because mineral matter originated from the inorganic constituents of the precursor plant organic materials (syngenetic mineral matter), and from the inorganic components transported to the coal bed (epigenetic and epiclastic mineral matter [31]), its textures and liberation characteristics differ. Mineral matter may occur as deposits in the cracks and cleats, but also in the form of very finely disseminated discrete mineral particles. Coal also contains inorganic matter in the form of chemically-bonded elements (such as organic sulfur and nitrogen).

The most important common coal minerals include [32]: clay minerals (kaolinite, illite), silicates (quartz), carbonates (dolomite, siderite), disulfides (pyrite, marcasite), sulfates (gypsum), and sulfides (galena, pyrrhotite). Aluminosilicates make up as much as 50% of the total mineral matter content, and quartz usually accounts for up to 20% of all mineral content.

Physical separation of mineral matter from coal depends mainly on its uniformity of distribution. Epigenetic minerals, which are typically concentrated along cleats are preferentially exposed during breaking of coal and thus are physically separable from coal.

Recent findings indicate that most of the mineral matter included in coal to the micron particle size range is a distinct separable phase which can be liberated by crushing and very fine grinding. Separation of coal particles from such a liberated gangue can lead to clean coal concentrate containing about 1% of ash [33]. Usually cleaned coal contains 6-8% ash. Cleaned coal has then considerably reduced the content of silicates, carbonates, disulfides and sulfates, but still contains various chemically bonded inorganic elements as well as finely disseminated minerals incorporated in the hydrocarbon matrix. In one of the first papers on coal electrokinetics, Sun and Campbell [34] demonstrated that the zeta potential versus pH curves are very sensitive to inorganic impurities content.

The coal minerals have very different electrokinetic characteristics. Aluminosilicates develop negative charge at basal planes as a result of isomorphous substitution, but the edges are characterized by $pH_{i.e.p.} = 9.1$, as for Al_2O_3 .

Quartz is negatively charged practically over entire pH range, while i.e.p. of dolomite and calcite is claimed to be situated in the slightly alkaline pH range.

Fig. 5 shows that for some coals demineralization by leaching, which in this particular case decreased ash content from about 11% to below 1%, can alter coal electrokinetic properties very significantly [35]. Apparently not only the content of ash but also its chemical composition must be important. It is therefore very doubtful whether the empirical equation that interrelates the zeta potential value with the coal chemical composition, and among other factors the ash content, as recently was proposed by Mori et al [36], can reflect true effect of the inorganic matter on the coal zeta potential.

Fig. 6 reveals one of typical problems facing researchers in the area of fine coal beneficiation [37]. While upper curves were obtained with the use of fresh fine material produced by crushing coarser pieces selected manually from the investigated coal samples, the bottom curve shows the zeta potential values for the same three coal samples which, however, were not produced by crushing coarser lumps, but rather by sieving the samples. In the latter case the experimental points for all three samples practically lay on the same zeta potential pH curve. This curve is not very different from the one obtained for precipitated humic acid (purified Aldrich sodium salt of humic acid was used). This interesting result, although not discussed here, shows again how misleading results can be produced in this area.

The Charge at Coal/Water Interface

Coalification and coal rank are synonymous with progressive enrichment of coal in organically bonded carbon.

Coal is a highly crosslinked polymer, which consists of a number of stable fragments connected by relatively weak crosslinks. The average number molecular weight per cross link increases with the rank of coal and that can be ascribed to the presence of larger molecules assembled together to form the macromolecules or to fewer cross links in higher rank coals. The aromatic carbon content, which is about 50% for subbituminous coals, increases to over 90% for anthracite [38].

Electrochemical properties of the coal/aqueous interface are mainly determined by coal functional groups and heteroatoms. Therefore, the effect of oxidation on coal electrokinetic potential as reported by many researchers [39,40,41,42], is very consistent. The content of phenolic groups decreases gradually with increasing coal rank [43], while carboxylic groups are of little importance in coals with greater than 80% carbon content [44,45]. The zeta potential versus pH curves for low rank coals can be approximated with two straight lines, while for fresh high rank coals the same relationship can be approximated with a single line (Fig. 1). The former indicates that the oxidized coal contains various acidic groups, while the latter behaves similarly to a nonionogenic solid as already discussed. It is likely that oxidized coal contains not only carboxylic groups with $pK = 4.7$ as for carboxylic acids, but probably also more acidic carboxyls, as for instance the carboxylic groups in position ortho to phenolic hydroxyl (for such carboxyls, as in salicylic acid, $pK = 3.0$).

Another important heteroatom, sulfur, appears in three forms: organic sulfur, pyritic sulfur and sulphatic sulfur. Sulfate sulfur is usually of only minor importance and occurs mainly as gypsum which is to a large extent removed in physical cleaning of coal. The same physical separation removes only coarse pyrite leaving with coal finely disseminated pyrite.

Some researchers found [46] that when pyrite is present in the coal in high concentrations, its oxidation products control the surface charge on coal particles. What is then the origin of the electrical charge at a coal/water interface?

There is no doubt that negative sites on coal surface are provided by carboxylic and phenolic groups (Fig. 7), and also by inorganic impurities such as silica. Much more complicated is the nature of the sites that generate positive charges.

The positive sites can be generated by inorganic impurities, such as for example Al_2O_3 . Coal also contains nitrogen [47]: bituminous coals typically 1.5-1.75% and anthracites less than 1%. It is believed that most of the nitrogen in coal is present in ring compounds, predominantly pyridine and quinoline derivatives. These groups, as well as Voll and Boehm's pyrone-like cyclic structures, can also contribute to the creation of a positive surface charge.

The role of oxygen as discussed by Frumkin [19-24], and Garten and Weiss [27], may also be very important in creating positive charge. It is interesting to recall here some electrochemical tests carried out with anthracite in the 60's [48,49]. They included two series of measurements carried out with a freshly prepared anthracite electrode, and with the same electrode exposed to air for a few days under room conditions.

As seen the potential of a freshly prepared unoxidized electrode, measured in aqueous solution versus saturated calomel electrode (Fig. 8), was increasing with time (during the first 30-60 minutes), but decreased abruptly on addition of an electrolyte. This decrease depended on the anion and suggested that the electrode was positively charged.

For the oxidized anthracite electrode the potential was steadily decreasing with time during the first 60-120 minutes, but sharply increased on addition of an electrolyte and this time the increase depended on the valency of the cation

(Al³⁺>Ca²⁺>K⁺). It seems then that while the fresh anthracitic surface was positively charged in water, the same electrode exposed to air for several days acquired negative charge obviously due to its oxidation. These experiments suggest that the same phenomena that occur on carbon black, may also be involved in the creation of electrical potential on surface of coal. Such positive sites on coal surface would then be generated by electrochemical mechanism which may operate only in the presence of oxygen and only if surface is freshly prepared. It is still, however, unclear whether such an electrochemical mechanism may only be involved in setting up the charge on anthracite surface, or also on lower rank coals.

References

1. J.S. Laskowski and G.D. Parfitt, Electrokinetics of Coal Water Suspensions, In Interfacial Phenomena in Coal Technology (G.D. Botsaris and Y. Glazman, eds.), Marcel Dekker, in press.
2. J.S. Laskowski, Proc. 1st Meeting of the Southern Hemisphere on Mineral Technology, Rio de Janeiro, December 1982, Vol. 1, p. 59.
3. J.N. Mehrishi and G.V.F. Seaman, Trans. Faraday Soc., **64**, 3152 (1968).
4. S. Hollinshed, G.A. Johnson and B.A. Pethica, Trans. Faraday Soc., **61**, 577 (1965).
5. H.W. Douglas and D.J. Shaw, Trans. Faraday Soc., **53**, 512 (1957).
6. J.M.W. Mackenzie, Trans. AIME, **244**, 393 (1969).
7. W.W. Wen and S.C. Sun, Separation Sci., **16**, 1491 (1981).
8. J.S. Laskowski and J.D. Miller, in Reagents in the Minerals Industry (M.J. Jones and R. Oblatt, eds.), Inst. Min. Met., London, 1984, pp. 145-154.
9. H.C. Parreira and J.H. Schulman, in Solid Surfaces (R.F. Gould, ed.), Advances in Chemistry Series, No. 33, Amer. Chem. Soc., Washington, D.C., 1961, p. 160.
10. N. Arbiter, Y. Fujii, B. Hansen and A. Raja, in Advances in Interfacial Phenomena of Particulate/Solution/Gas Systems: Applications to Flotation Research, (P. Somasundaran and R.B. Grieves, eds.), AIChE Symposium Series 150, Vol. 71, 1975, p. 176.
11. J. Spurny and B. Dobias, Coll. Czechoslov. Chem. Comm., **27**, 931 (1962).
12. S. Chander, J.M. Wie and D.W. Fuerstenau, in Advances in Interfacial Phenomena of Particulate/Solution/Gas Systems: Application to Flotation Research, (P. Somasundaran and R.B. Grieves, eds.), AIChE Symposium Series 150, Vol. 71, 1975, p. 183.
13. J.A. Solari, A.C. De Araujo and J.S. Laskowski, Coal Preparation, **3**, 15 (1986).
14. A.J. Groszek, Far Disc. Chem. Soc., **59**, 109 (1975).
15. A.I. Medalia and D. Rivin, in "Characterization of Powder Surfaces" (G.D. Parfitt and K.S. Sing, eds.), Academic Press, 1976, pp. 279-351.
16. M.H. Polley, W.D. Schaeffer and W.R. Smith, J. Phys. Chem., **57**, 469 (1953).
17. E. Miller, J. Am. Chem. Soc., **46**, 1150 (1924).
18. E. Miller, J. Am. Chem. Soc., **47**, 1270 (1925).
19. A. Bruns and A. Frumkin, Z. Phys. Chem., **141**, 141 (1929).
20. R. Burstein and A. Frumkin, Z. Phys. Chem., **141**, 158 (1929).
21. R. Burstein, A. Frumkin and D. Lawrowskaya, Z. Phys. Chem., **150**, 421 (1930).
22. N. Bach and A. Frumkin, Kol. Z., **46**, 89 (1928).
23. N. Bach, Kol. Z., **64**, 153 (1933).
24. A. Pilojan, N. Kriworutschko and N. Bach, Kol. Z., **287** (1933).
25. H.R. Kruyt and G.S. de Kadt, Kol. Z., **47**, 44 (1928).
26. E.J.W. Verwey and J.H. de Boer, Rec. Trav. Chem., **55**, 675 (1936).
27. V.A. Graten and D.E. Weiss, Austr. J. Chem., **10**, 309 (1957).
28. M. Voll and H.P. Boehm, Carbon, **9**, 481 (1971).
29. A.M. James, in Surface and Colloid Science (E. Matijevic, ed.), Plenum Press, New York, 1981, Vol. 11, p. 121.
30. A.C. Cook, Separation Science, **16**, 1981, 1545.
31. M.T. Mackovsky, in Coal and Coal Bearing Strata (D. Murchison and T.S. Westoll, eds.), Elsevier, New York, 1968, p. 309.

32. J.J. Renton, in Coal Structure (R.A. Meyers, ed.), Academic Press, New York, 1982, p. 283.
33. D.V. Keller, The Separation of Mineral Matter from Pittsburgh Coal by Wet Milling, ACS Symposium on Chemistry of Mineral Matter and Ash in Coal, Am. Chem. Soc. Vol. 29, No. 4, pp. 326-336.
34. S.C. Sun and J.A.L. Campbell, in Coal Science (P. Given, ed.), Advances in Chemistry Series, No. 55, Amer. Chem. Soc., Washington, D.C., 1966, p. 363.
35. J.M. Rosenbaum, D.W. Fuerstenau and J. Laskowski, Colloids and Surfaces, **8**, 153 (1983).
36. S. Mori, T. Hara, K. Aso, and H. Okamoto, Powder Technology, **40**, 161 (1984).
37. Qi Liu and J.S. Laskowski, Coal Flotation Promoters and their Mechanism of Action, 191st ACS Meeting, New York, April, 1986, Paper No. 325.
38. D.D. Whitehurst, T.O. Mitchell and M. Farcasiu, Coal Liquefaction, Academic Press, New York, 1980.
39. W.W. Wen and S.C. Sun, Trans. AIME, **262**, 174 (1977).
40. S. Sobieraj and B. Majka-Myrcha, Physicochemical Problems of Mineral Processing, Wroclaw, 1980, No. 12, p. 165. In Polish.
41. B. Yarar and J. Leja, Proc. 9th Int. Coal Preparation Congress, New Delhi, 1982, paper C5.
42. K.C. Teo, S. Finora and J. Leja, Fuel, **61**, 71 (1982).
43. Z. Abdel-Baset, P.H. Given and R.F. Yazab, Fuel, **57**, 95 (1978).
44. A. Ihnatowicz, Bull. Central Research Mining Institute, No. 125, Katowice, 1952. In Polish.
45. L. Blom, L. Edelhausen and D.W. van Krevelen, Fuel, **36**, 135 (1957).
46. W.W. Wen, Electrokinetic Behavior and Flotation of Oxidized Coal; Ph.D. Thesis, Pennstate University, (1977).
47. A. Attar and G.G. Hendrickson, in Coal Structure (R.A. Meyers, ed), Academic Press, New York, 1982, p. 132.
48. J.S. Laskowski and V.I. Klassen, Dokl. Akad. Nauk SSSR, **145**, 857 (1962).
49. V.I. Klassen and J.S. Laskowski, Koll Zh., **25**, 549 (1963).

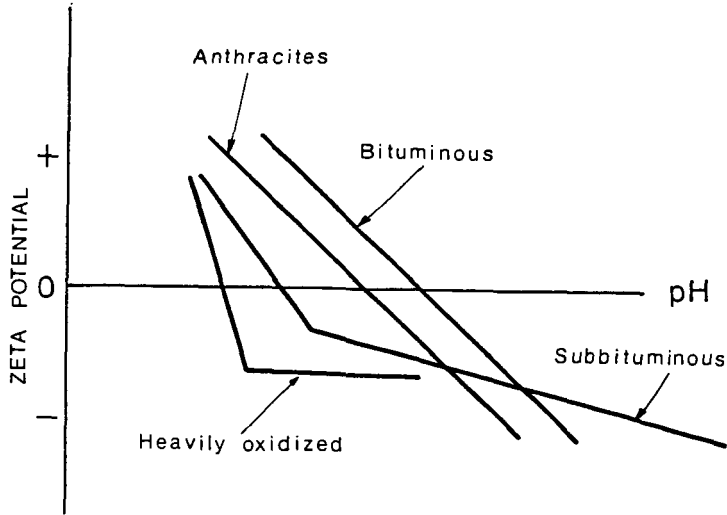


Fig. 1. Schematic microelectrophoretic mobility versus pH curves for different coals [1].

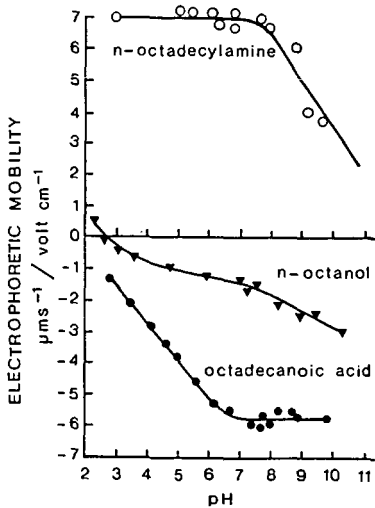


Fig. 2. Electrophoretic mobility against pH relationship for n-octadecylamine, n-octadecanol and n-octadecanoic acid in 0.02 N NaCl [3].

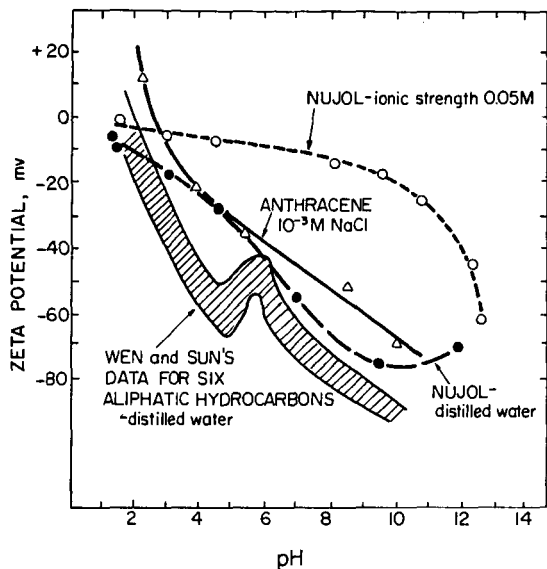


Fig. 3. Zeta potential of Nujol droplets [6], six aliphatic hydrocarbons [7] and anthracene.

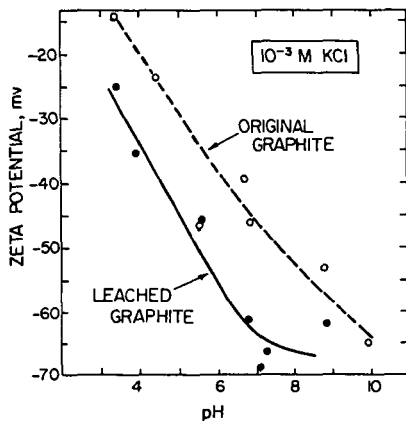


Fig. 4. Zeta potential vs. pH curve for graphite [13].

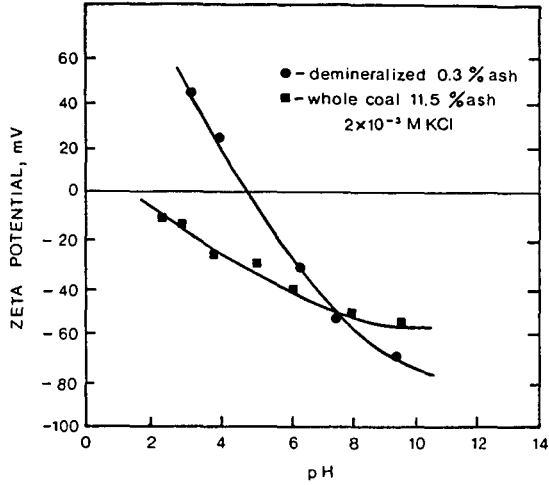


Fig. 5. Zeta potential vs. pH curves for raw and demineralized Somerset mine coal [35].

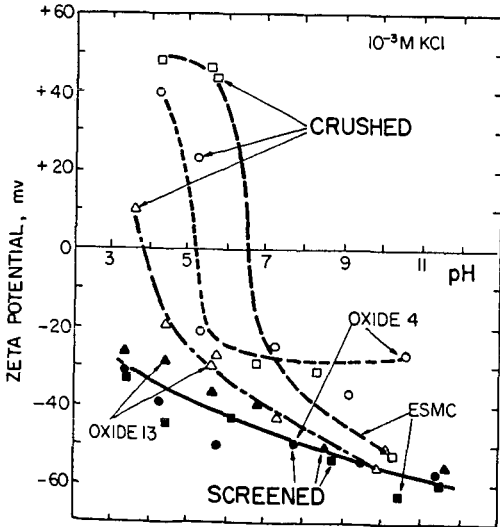


Fig. 6. Zeta potential vs. pH curves for unoxidized metallurgical coal (ESMC), and Fording metallurgical coal: slightly oxidized (Oxide 4) and severely oxidized (Oxide 13) [37].

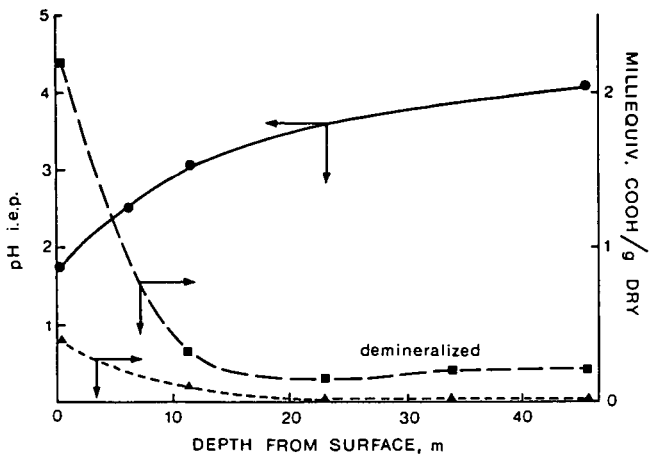


Fig. 7. Iso-electric points and carboxylic group content of coal samples collected from Seam No. 7 of the Fording River Deposit, B.C., at various distances from the surface (adapted after [41,42]).

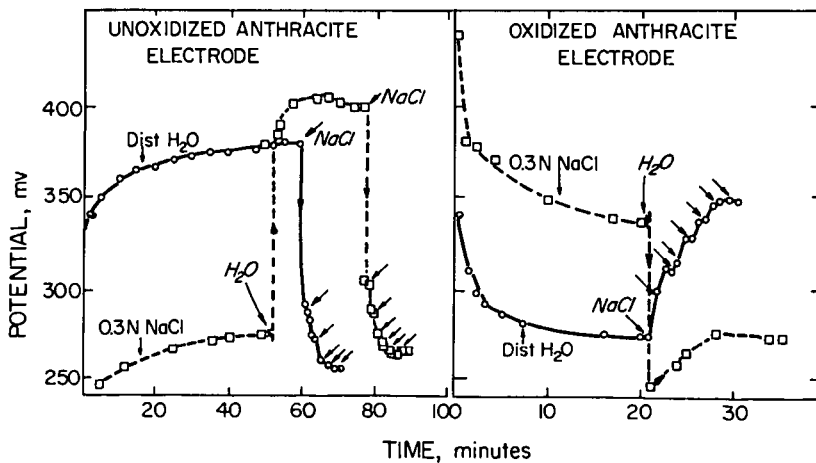


Fig. 8. Potential of fresh and oxidized anthracite electrodes measured versus saturated calomel electrode [48,49].

ELECTROKINETIC BEHAVIOR OF COAL

D. W. Fuerstenau, J. M. Rosenbaum and Y. S. You

Department of Materials Science and Mineral Engineering
University of California
Berkeley, CA 94720

ABSTRACT

Electrokinetic measurements show that coals generally exhibit a charge reversal at a certain pH because the surface charge on coal is controlled by the dissociation/ionization of oxygenated functional groups on the coal matrix and by the presence of siliceous contaminants. The lower the ash mineral content of a coal, the higher is the pH at which the charge is reversed (that is, its PZR). De-ashing a coal causes it to exhibit a higher PZR. Increased oxidation causes the pH for charge reversal to decrease due to the higher concentration of oxygen functional groups.

INTRODUCTION

When a solid such as coal is immersed in a liquid environment, a charge is developed on the surface by dissociation of functional groups (COOH, C=O, COH) from the surface or by adsorption of ions from solution. The surface charge on the coal together with the counter ions constitute the electrical double layer. For the study of charged systems, three interfacial potentials are of interest: i) the surface potential (or total double layer potential), ii) the Stern layer potential (the potential at the first layer of counter ions) and iii) the zeta potential. The electrokinetic or zeta potential is the potential at the shear plane, where slip must occur when the solid moves relative to the liquid. The behavior of the solid particle in a liquid under these conditions is governed by the charge density at the shear plane, not the charge density at the solid surface. The measurement of electrokinetic potentials is relatively easy and this often is the only direct electrical measurement that can be conducted. Although interpretation of the results is not straight-forward, often the useful assumption is made that the slipping plane and the Stern plane coincide. Since the zeta potential can be manipulated through adsorption of inorganic or organic ions at the Stern plane, the study of the electrokinetic behavior of solid is of practical importance in flotation, dispersion, flocculation, etc.

Important parameters for characterizing the surface of a solid in water is the condition when the surface charge and the surface potential is zero. Ions that constitute the surface charge are called potential-determining ions, and their activity in solution when the surface is uncharged is called the point of zero charge (PZC). Another condition of importance is when the Stern layer potential is zero. This can either be the PZC or can result if counter ions have such a strong affinity for the surface that more counter ions can adsorb than there are surface charges. The reversal of the zeta potential, which is often called the isoelectric point (IEP) of the solid, therefore can result either from the reversal of the surface potential or of the Stern potential. Because there is also an isoelectric point of a solution in equi-

librium with a solid, the term point of zeta potential reversal (PZR) is less confusing and that term will be used here.

The electrokinetic behavior of coal is difficult to study because of the complex mineralogy and heterogeneity of coal and, more significantly, it has the tendency to undergo substantial alterations upon exposure to various environments (1). The literature does not contain many papers on the electrokinetic behavior of coal (1-13). Campbell and Sun (2,3) studied the electrokinetic behavior of anthracite and bituminous coal by streaming potential methods, and H^+ and OH^- ions were found to be the potential-determining ions. The PZC of anthracite (whole coal) was found to occur at about pH 4 and that of its vitrain at pH 5.0 to 5.2. The PZC of bituminous coal was found to occur at around pH 4.6. Substantial variations of zeta potential were observed with pH for the various macerals. More recently, Wen and Sun (7,8) investigated the electrokinetic behavior of fine coals of different rank and oxidation degree by an electrophoretic technique. They suggested that H^+ and OH^- are the potential-determining ions for most of the coals. The PZR of anthracite, bituminous and lignite coal decreased in the reverse order of the rank and occurred at pH 5.0, about 4.5 and 2.3, respectively. The magnitude of the zeta potential increases as the rank of the coal decreases because the lower rank coal contains a greater fraction of oxygen functional groups which provide more negatively charged sites on the surface of the coal (7,8).

The objectives of our investigations were to delineate factors that control the zeta potential of coal, including coal rank, degree of oxidation and ash mineral content. An attempt to evaluate the PZC of coals is also presented.

MATERIALS AND METHODS

The coal samples used in this investigation included a Wyoming bituminous steam coal, a Colorado bituminous metallurgical coal, two samples of Pennsylvania anthracite, and a hand-picked sample of vitrain bands from a West Virginia bituminous seam supplied by the Coal Research Bureau, West Virginia University. Coal specimens were protected from atmospheric oxidation during transport and storage. Table 1 presents proximate and ultimate analyses of the samples. To study de-ashed coal, the siliceous ash-forming minerals were removed by leaching with an HF-HCl procedure, which removes over 90% of the contained mineral matter without attacking the coal substance according to Bishop and Ward (14). Table 2 summarizes the mineral matter content of the de-ashed samples studied. The other samples were oxidized by passing oxygen at 125°C through the bed of coal particles for up to 260 hours.

Electrophoretic mobilities of particles were measured with a microelectrophoresis apparatus manufactured by Zeta-Meter Inc., using their Pyrex/Teflon electrophoresis cell. For most of the mobility measurements, about 0.02 gram of coal that had been ground to minus 400 mesh was suspended in 100 ml of solution for about 9 hours while agitating. Streaming potentials were evaluated using plugs containing 48 x 65-mesh coal particles in an apparatus identical to that described by Ball and Fuerstenau (15).

Table 1 - Analyses of Coal Samples by Percent (dry basis)

	Penna. (I) Anthracite	Wyoming Bitum. (Steam)	Colorado Bitum. (metal.)	Penna. (II) Anthracite	HF-Treated Penna. (II) Anthracite	Vitrain
Carbon	88.24	72.91	71.68	79.83	93.03	81.93
Hydrogen	2.11	---	5.10	2.10	1.96	5.38
Nitrogen	0.65	---	1.60	0.94	0.74	1.24
Chlorine	0.00	---	0.02	0.02	0.52	0.02
Total Sulfur	0.75	0.68	0.60	0.86	0.78	1.03
Pyritic S	0.10	0.06	---	---	---	0.24
Organic S	0.61	0.62	---	---	---	0.78
Sulfate S	0.04	0.00	---	---	---	0.01
Oxygen	---	---	9.02	2.94	1.54	1.46
Moisture (as received)	2.93	---	2.94	2.08	1.42	---
Ash	1.67	5.53	11.50	13.31	1.43	3.33
Volatile Matter	4.02	41.35	39.49	---	---	37.91
8tu/lb	13,700	12,800	12,800	12,600	14,400	14,700

Acid-base titrations to estimate the surface charge density were carried out utilizing an automatic titrator with minus 37- μ m Wyoming bituminous coal, using the Onoda-deBruyn "fast titration" method to estimate external charge density (16). A simple check of the pzc of the coal sample was carried out by the solids addition method, worked out by Fuerstenau (17).

RESULTS AND DISCUSSION

The PZR of high-ash anthracite II was found to occur at about pH 2.8. A series of leaching experiments was performed wherein various amounts of siliceous material were removed from the coal. Figure 1 gives the zeta potential, as measured by electrophoresis, of anthracite containing 13.3, 9.0, 2.0 and 1.4% ash content. As the amount of ash is reduced, the point of zeta potential reversal is increased to about pH 4.5, which is the same as found for anthracite I, a low-ash coal. The zeta potential of silica generally exhibits a reversal at pH 1-2 and that of graphite at about pH 4. Thus, coal behaves somewhat as a composite material. The Colorado bituminous coal containing 11.5% ash has a PZR less than pH 2, but after reducing the ash content to 0.3% the pH of the zeta potential reversal is increased to about 4.5 (Figure 2). Clearly, any studies involving raw coal must take into account the distribution of various components at the surface, that is silica, carbonaceous matrix, and oxygen functional groups.

The zeta potential of the low-ash Wyoming bituminous coal was determined by streaming potential measurements and the results are given in Figure 3. The PZR of this coal appears to occur at pH 4.5. Is this reversal in the zeta potential a surface charge reversal? The results of the titration of this same coal are presented in Figure 4, which shows that the isotherms cross at about pH 5. This cross point represents the PZC (16). Furthermore, experiments were carried out using the dry-solids addition method. If a dry solid is added to water, adsorption of the potential-determining ions will

Table 2 - The ash and silicon contents of various coals before and after HF-treatment

Coal		Percent Ash in Coal	Si content as percent of ash
Pennsylvania Anthracite II	Untreated	13.3	45.3
	HF-treated	1.4	0.7
Colorado Bituminous	Untreated	11.5	35.1
	HF-treated	0.3	6.6

cause their activity to shift towards the PZC (17). In the case of coal, if H^+ and OH^- are potential-determining, as more surface area is added to the system, adsorption of H^+ and OH^- occurs, shifting the solution pH towards the PZC. The results of such experiments, given in Figure 5, show that the PZC occurs at pH 4.8, indicating that the PZR given in Figure 3 is indeed also the PZC.

Oxidation of the coal causes the zeta potential to shift to more acidic pH's. Figure 6 shows the electrokinetic behavior of anthracite I after it had been oxidized in oxygen at 125°C for various time periods. As for an explanation of this shift, the surface composition and orientations of surface functional groups in coals are generally not known, and must be inferred from analyses of the bulk coals. Acidity of surface sites in charcoals and carbon blacks has been attributed to carboxyl groups, phenolic groups and cyclic esters called lactones (18,19). As coals oxidize, large amounts of polymeric hydroxy-carboxylic acids called humic acids are formed which may further oxidize to phenolic aldehydes and water-soluble acids (20). It is the production of these acidic groups on the coal surface which is primarily responsible for the decrease in flotation recovery and the decrease in zeta potential of oxidized coals. It is likely that the majority of the observed change in electrophoretic properties upon oxidation is due to the formation of more and stronger acidic functional groups on the coal surface.

A vitrain sample was oxidized at 125°C and at this temperature, this particular sample was partially burned up. Gray ash could be seen in the oxidizing vessel during sampling. The electrophoretic mobility was found to change drastically with such severe oxidation. Subsequent experiments showed the mobility to be about the same as that of a sample of the ash itself. In order to oxidize the vitrain without combusting it, the temperature in the oxidizing oven was lowered to 80°C and another sample oxidized. Under these more mild conditions, the pronounced shift of the PZC to lower values with oxidation was observed and the results are shown in Figure 7.

It can be seen from the results that anthracite (Fig. 6) does not oxidize readily, even at 125°C, while the vitrain oxidizes quite easily at 80°C. This is principally due to the difference in rank of the two coals. The anthracite is 88.2% carbon versus 72.9% for the vitrain, and contains considerably fewer reactive functional groups that may be susceptible to oxidation.

SUMMARY

Because the charge on the surface of coal results from the dissociation/ionization of various oxygenated functional groups, H^+ and OH^- appear to be potential-determining. Electrokinetic experiments show that pH controls the charge reversal on coals, depending upon the ash content and the degree of oxidation. High-ash coals exhibit charge reversal at lower pH's. When the coal is de-ashed, its PZR increases. Similarly, oxidation reduces the pH at which the surface charge is reversed, due to the increase in the concentration of oxygen functional groups.

ACKNOWLEDGEMENT

This research was sponsored by grants from Lawrence Berkeley Laboratory (Grant No. 4736) sponsored by DOE and from the Dept. of the Interior, Grant No. G5195008.

REFERENCES

1. Celik, M.S. and Somasundaran, P., *Colloids and Surfaces*, 1, 121, 1980.
2. Campbell, J.A.L. and Sun, S.C., *Trans. AIME*, 247, 111, 1970.
3. Campbell, J.A.L. and Sun, S.C., *Trans. AIME*, 247, 120, 1970.
4. Baker, A.F. and Miller, K.J., *Mining Congress J.*, 54, 43, 1968.
5. Brown, D.J., in *Froth Flotation*, D.W. Fuerstenau, ed., AIME, N.Y. 1962.
6. Jessop, R.R. and Stretton, J.L., *Fuel*, 41, 317, 1968.
7. Wen, W.W. and Sun, S.C., *Trans. AIME*, 262, 172, 1977.
8. Wen, W.W., Ph.D. Thesis, Pennsylvania State University, 1977.
9. Rosenbaum, J.M., M.S. Thesis, University of California, Berkeley, 1980.
10. You, Y.S., Ph.D. Thesis, University of California, Berkeley, 1983.
11. Yarar, B., *Trans. AIME*, 272, 1978, 1983.
12. Kelebek, S., Salman, T., and Smith, G.W., *Canadian Met. Quart.*, 21, 205, 1982.
13. Mori, S., Hara, T., and Aso, K., *Powder Technology* 40, 161, 1984.
14. Bishop, M. and Ward, D.L., *Fuel*, 37, 191, 1958.
15. Ball, B. and Fuerstenau, D.W., *Mineral Science and Engineering*, 5, 267, 1973.
16. Onoda, G.Y. and deBruyn, P.L., *Surface Sci.*, 4, 48, 1966.
17. Fuerstenau, D.W., *Pure and Applied Chem.*, 24, 135, 1970.
18. Fuerstenau, D.W. and Pradip, *Colloid and Surfaces*, 4, 229, 1982.
19. Medeiros, D. and Petersen, E.E., Lawrence Berkeley Laboratory Report LBL-4439, University of California, Berkeley, 1975.
20. Toda, Y., *Fuel*, 52, 36, 1973.

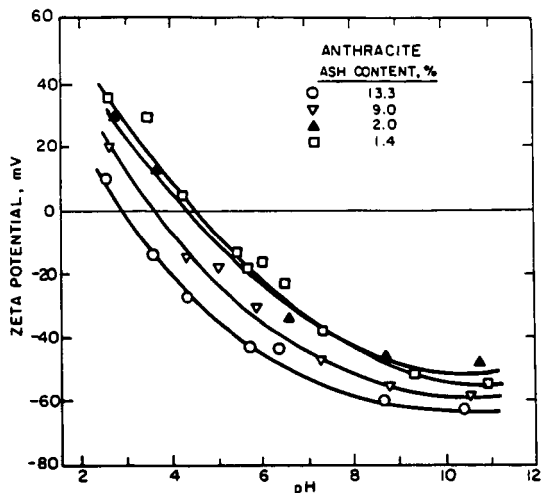


Fig. 1 - The effect of removal of silica by leaching from coal on the zeta potential of anthracite.

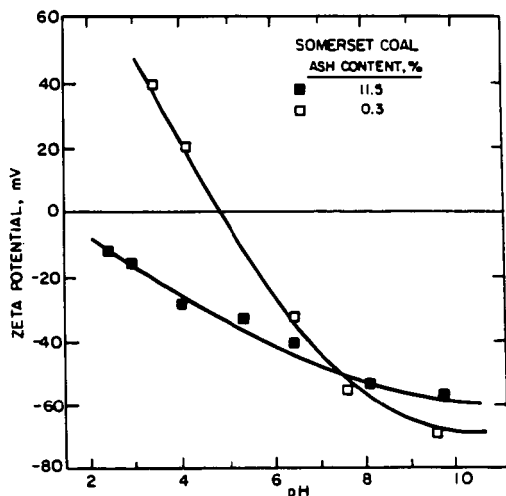


Fig. 2 - Effect of ash content on electrokinetic behavior of HF-treated and untreated Colorado bituminous (Somerset) coal as a function of pH.

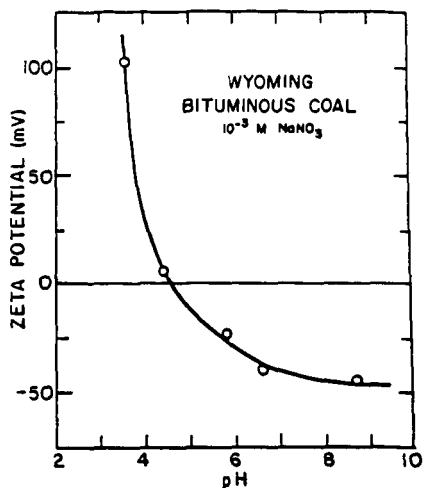


Fig. 3- The zeta potential of Wyoming bituminous coal as measured by streaming potential methods.

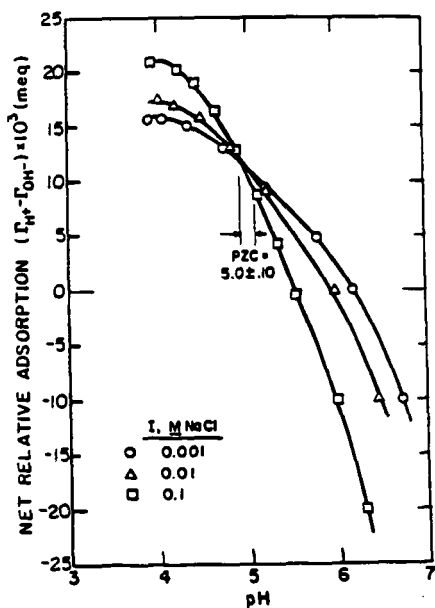


Fig. 4- Determination of the point of zero charge of Wyoming bituminous coal by potentiometric titration.

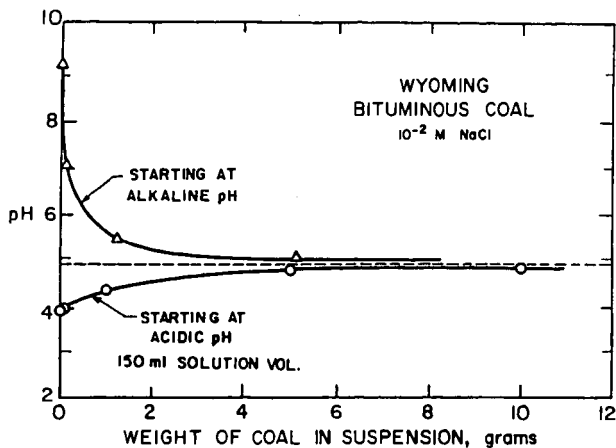


Fig. 5 - Determination of the point of zero charge of Wyoming bituminous coal by the dry-powder addition method.

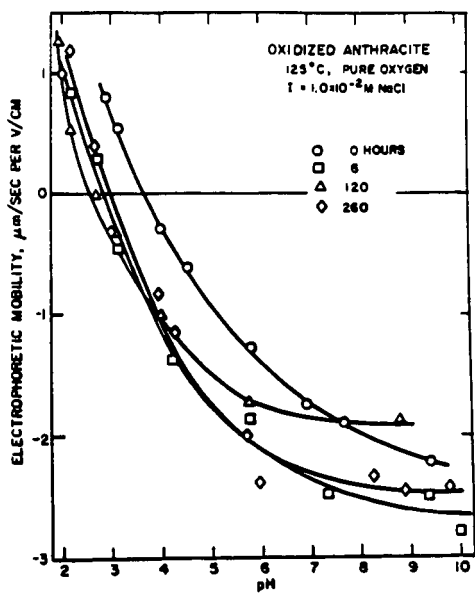


Fig. 6 - Electrophoretic mobility versus pH for dry ground oxidized anthracite.

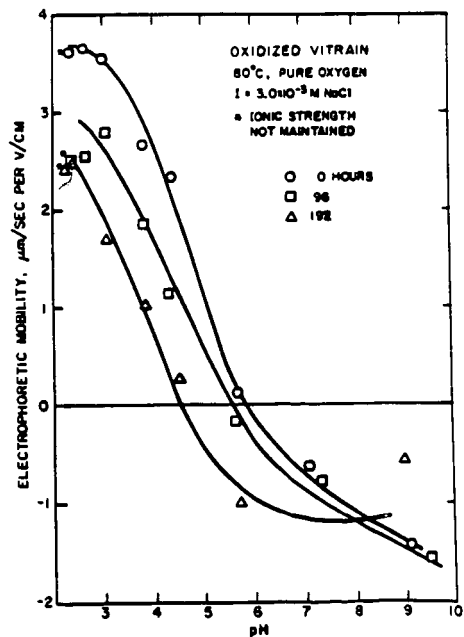


Fig. 7 - Electrophoretic mobility versus pH of vitrain oxidized at 80°C.

ELECTROPHORETIC MOBILITY OF CONCENTRATED COAL SUSPENSIONS

E. Z. Casassa and E. W. Toor, Department of Chemical Engineering, Carnegie Mellon University, Pittsburgh, PA. 15213

Abstract: A variety of properties of dry coal powders and of coal/water slurries have been measured for ten bituminous coals, some available as both ROM and beneficiated samples. Slurry rheology, maximum solids content and stability towards sedimentation are in general related to the electrophoretic mobility measured in concentrated suspensions, rather than to the microelectrophoretic mobility determined in very dilute suspensions of the coals. The influence on slurry properties of coal particle median size, BET surface area with nitrogen as adsorbate, ash content, soluble ash content, and degree of oxidation will be discussed.

Introduction: The objective of this study has been to relate the surface chemistry of a coal to its beneficiation and oxidation history in order to develop the hypothesis that coal/water slurry properties depend upon surface charge, wettability, and additive adsorption from solution. Previous work^[1] with four bituminous coals had suggested that, in general, particle surface charge controls slurry rheology, sedimentation stability and maximum solids content of coal/water slurries. High interparticle repulsion results in low viscosity, high solids content, poor sedimentation stability and hard-packed sediments. Low interparticle repulsion is associated with good sedimentation stability but increased viscosity and lower solids content. Incomplete wetting of a coal powder leads to hydrophobic aggregation, and decreases stability toward sedimentation. Additives may be employed to improve wetting and dispersion or to improve slurry properties by manipulating surface charge. The current work is intended to increase understanding of the contributions to slurry behavior made by the different types of materials present on heterogeneous coal surfaces.

Experimental: Properties of dry coal powders and of coal/water suspensions have been examined for six eastern bituminous coals, both freshly ground and after several months storage under air or under nitrogen. For three coals run-of-mine (ROM) samples have been compared to physically beneficiated samples. The six coals were chosen from among those surveyed as part of a large study of coal slurryability and combustion performance sponsored by the Pittsburgh Energy Technology Center of the U. S. Department of Energy.^[2]

The dry powder of each coal has been characterized as to its median size, particle size distribution, B. E. T. surface area with nitrogen as adsorbate, moisture content, degree of oxidation determined by the U. S. Steel alkali

extraction test^[3], critical surface tension for wetting, and wettability in solutions of three surfactants^[4]. The density of each coal powder in water has been determined by pycnometry and suspensions of each coal have been titrated with hydrochloric acid and sodium hydroxide solutions. For five of the six coals Gulf Research and Development Company provided surface analyses by XPS for samples recently ground under air and in some cases under nitrogen. In addition, proximate, ultimate and mineral ash analyses are available for each coal.

The microelectrophoretic mobility of each coal sample has been measured as a function of pH, in dilute potassium nitrate and in slurry supernatant, and compared to the electrophoretic mobility determined as a function of pH for 50%(wt) slurries of the coal in water, and in solutions of the nonionic surfactant Triton X-100 and of the anionic dispersant Lomar D. The apparent viscosity of the same 50%(wt) slurries was measured as a function of pH at shear rates between 2.7 and 90 s⁻¹. Apparent viscosity has also been determined as a function of coal concentration in water, at the natural pH of each coal. The sedimentation behavior of each coal has been measured as a function of pH for 25%(wt) slurries in water and as a function of coal concentration, in water and in solutions of the surfactant Triton X-100, at the natural pH of the coal. Surface tension of the slurry supernatant determined after the completion of sedimentation experiments in Triton X-100 solution is a measure of the amount of surfactant adsorbed from solution by the particles. The concentration of nine inorganic ions dissolved from the coal surface into the slurry liquor was also determined.

Results and Discussion:In Table 1 some pertinent properties of the powdered coals are compared. Except for the 6.4% ash Splash Dam coal, the median size of all samples lies between 42 and 57 μm , and in addition, these samples have similar particle size distribution widths. The Illinois #6 and Upper Freeport coals have relatively high surface areas, while the other samples have surface areas between 1.0 and 2.6 m²g⁻¹. The results of the U.S. Steel alkali extraction oxidation test indicate that most of the coals show little sign of oxidation of the carbonaceous surface. However the 6.2% ash Lower Kittanning Coal and the Illinois #6 sample are significantly oxidized, and the aged 8.7% ash Lower Kittanning and Black Creek samples show less marked oxidation.

For samples freshly ground under air, and for samples aged under air, the pyrite content reported when proximate, ultimate, mineral ash and forms of sulfur analyses were performed is compared in Table 2 to the soluble iron content found in the liquor from 10%(wt) slurries of the coals each at its natural pH, and to the ionic strength of the same samples, as calculated

Table 1

ANALYTICAL DATA FOR COAL POWDERS

Coal	Median Size μm	Surface Area m^2g^{-1}	U.S. S. Oxidation Test	
			% Transmission	
			Fresh	Aged
<u>Splash Dam</u>				
17.0% ash	43	1.3	100	96
6.4% ash	26	2.3	98	98
5.3% ash	44	1.0	92	99
1.6% ash	43	1.6	99	96
<u>Lower Kittanning</u>				
8.7% ash	47	2.1	92	87
6.2% ash	48	2.5	47	15
2.3% ash	42	2.6	96	95
<u>Illinois #6</u>				
9.7% ash	57	44.0	—	36
<u>Black Creek</u>				
5.8% ash	57	2.1	97	92
<u>Upper Freeport</u>				
21.9% ash	48	11.6	95	97
<u>Pittsburgh Seam #8</u>				
30.8% ash	52	2.2	100	100
6.0% ash	53	1.1	100	99

from the analyses for sodium, potassium, magnesium, calcium, iron, aluminum, silicon, chloride and sulfate ions in the slurry liquor. The reported pyrite (or pyrite plus sulfate) content is not a good indicator of either the quantity of soluble iron found or of the ionic strength of the slurry. Slurries high in soluble iron also fall in the high ionic strength group, though calcium and magnesium salts also contribute significantly to the ionic strength, particularly in the case of Pittsburgh Seam #8. In most cases, aging and oxidation appear to increase the ionic strength, but for Black Creek and Upper Freeport coals aging under air appears to decrease the solubility of the inorganic minerals present. The critical surface tension for wetting tends to be somewhat higher for high ash coals than for beneficiated coals, indicating that, as expected, the high ash coals are more hydrophilic. The Black Creek and Upper Freeport coals show marked increases in critical surface tension for wetting, again suggesting that aging under air has affected the inorganic minerals present on the surfaces of these coals.

The major result of this study is the confirmation of the hypothesis that coal/water slurry properties depend upon coal particle surface charge, as measured by electrophoretic mobility. Figure 1 shows the apparent viscosity at a shear rate of 9 s^{-1} as a function of electrophoretic mobility for two of

the Splash Dam coals freshly ground under air as well as data for Illinois #6 and Hiawatha coals, as received, from our previous study⁽¹⁾ of four bituminous coals. High viscosity occurs at mobilities close to zero, the effect being more marked for the coals with smaller median diameter.

Table 2. PYRITE AND SOLUBLE IRON CONTENT, IONIC STRENGTH AND CRITICAL SURFACE TENSION FOR WETTING

Coal	Pyrite %(wt)	Soluble Iron mmole dm ⁻³	Ionic Strength mmole dm ⁻³	Critical Surface Tension for Wetting mN m ⁻¹
<u>Splash Dam</u>				
17.0% ash, fresh	0.11	0.003	2.3	46
17.0% ash, aged		0.007	2.4	46
6.4% ash, fresh	0.15	<0.001	1.3	41
6.4% ash, aged		<0.001	1.1	40
5.3% ash, fresh	0.04	<0.001	1.0	40
5.3% ash, aged		<0.001	3.8	40
1.6% ash, fresh	0.06	0.007	1.0	40
1.6% ash, aged		<0.001	1.0	40
<u>Lower Kittanning</u>				
8.7% ash, fresh	0.05	<0.001	1.1	42
8.7% ash, aged		0.100	7.1	42
6.2% ash, fresh	0.68	<0.001	1.7	42
6.2% ash, aged		<0.001	2.3	43
2.3% ash, fresh	0.08	<0.001	0.9	41
2.3% ash, aged		<0.001	1.0	41
<u>Illinois #6</u>				
9.7% ash, fresh	1.30	0.25	26.1	50
9.7% ash, aged		3.93	61.0	50
<u>Black Creek</u>				
5.8% ash, fresh	0.14	1.25	13.6	45
5.8% ash, aged		0.50	7.3	49
5.6% ash, aged and washed		0.32	1.7	..
<u>Upper Freeport</u>				
21.9% ash, fresh	0.35	0.66	43.6	43
21.9% ash, aged		0.43	24.5	46
<u>Pittsburgh Seam #8</u>				
30.8% ash, fresh	1.17	<0.001	14.6	43
30.8% ash, aged		<0.001	19.4	43
6.0% ash, fresh	0.50	<0.001	5.6	42
6.0% ash, aged		<0.001	5.0	42

When the maximum viscosity found for a coal in a 50%(wt) slurry at two different shear rates is plotted versus median size of the dry coal powder in Figure 2 it can be seen that the viscosity is markedly more dependent upon shear rate at low median size, that is, that non-Newtonian behavior is more extensive when the total surface area is high. For smaller median size effective void space can be reduced to a greater extent when flocculation occurs. The scatter of the data in Figure 2, however, indicates that the surface chemistry of a coal affects the extent of flocculation even when

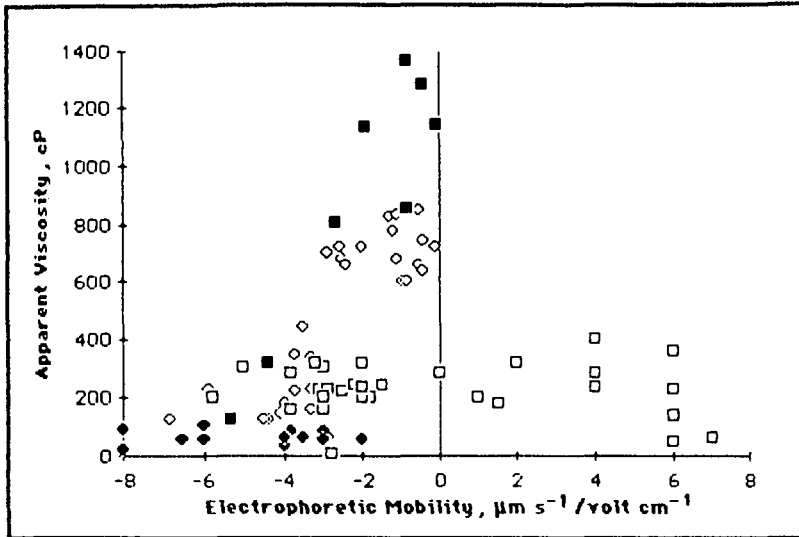


Figure 1. Apparent Viscosity as a Function of Electrophoretic Mobility at a Shear Rate of 9 s^{-1} for: ■ Splash Dam 6.4% ash, ● Hiawatha, ◇ Splash Dam 17% ash, □ Illinois #6

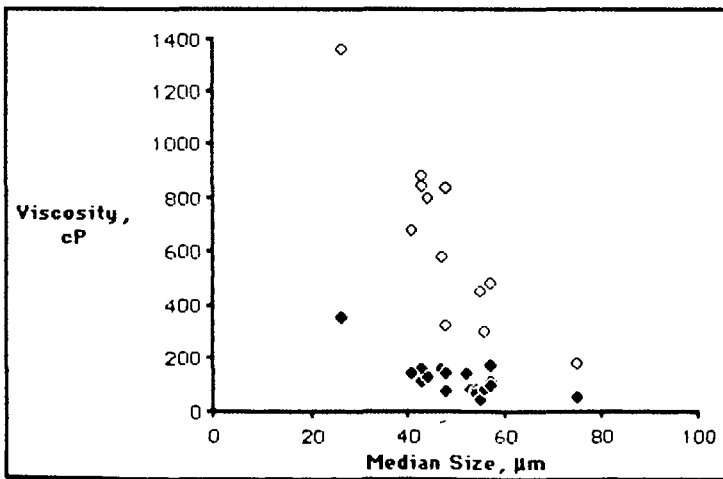


Figure 2. Maximum Viscosity as a Function of Median Size, for 50%(wt) Slurries of Sixteen Coals, at a Shear Rate of: ◇ 9 s^{-1} , ● 90 s^{-1}

particles of the same median size and size distribution width are compared. The two lowest outliers of the shear rate 9 s^{-1} curve are the two most oxidized coal samples, Lower Kittanning 6.2% ash and Hiawatha, coals which have a strongly negative mobility, and strong interparticle repulsion, over most of the pH range. On the other hand, Illinois #6, Upper Freeport and San Juan with surface areas of 44, 12 and $10 \text{ m}^2\text{g}^{-1}$ respectively, lie on the high side of the curve, suggesting that at least a portion of the pore space is accessible to the fluid, thus decreasing the effective void space and increasing apparent viscosity for these coals.

Figure 3 demonstrates the dependence on surface charge of the median agglomerate size calculated from sedimentation data, relative to the dry particle median size. Sedimentation stability is good when there is extensive flocculation and therefore a high apparent viscosity at very low shear rates. The highly oxidized coals with low apparent viscosities show very poor stability toward sedimentation, and form hard-packed sediments, as a result of the strong interparticle repulsion. The strongly shear-thinning San Juan coal shows a high calculated agglomerate size.

In Figure 4 sedimentation rate is plotted as a function of coal concentration for three coals each at its natural pH, to demonstrate the effect of ionic strength upon stability toward sedimentation. In solutions of high ionic strength the electrical double layer is compressed towards the particle surface, decreasing interparticle repulsion and the magnitude of the electrophoretic mobility, thus promoting flocculation. As a result, sedimentation rate is decreased, and final sediment volume is increased. However at shear rates between 2.6 and 90 s^{-1} the ionic strength has little effect on the apparent viscosity measured for these slurries. This suggests that weak flocs existing at the very low shear rates occurring in sedimentation under gravity are broken apart at higher shear rates.

Figure 5 shows several patterns for the dependence of electrophoretic mobility upon pH. In Figure 5(a),(b) and (c) each pair of coals compared is similar in median particle size of the dry coal powders and in ionic strength of the slurries. In Figure 5(a) the high ash Splash Dam and Lower Kittanning samples both have a point of zero charge near pH 3, where kaolin has been reported to have a point of zero charge⁽⁵⁾. In Figure 5(b), the low ash Splash Dam and Lower Kittanning coals are compared. Both these samples have a positive electrophoretic mobility up to at least pH 6. This appears to be the pattern of mobility associated with an unoxidized mainly carbonaceous surface. The two high ash samples of the same coals in Figure 5(a) show behavior very similar to that of the beneficiated coals at high pH, but the

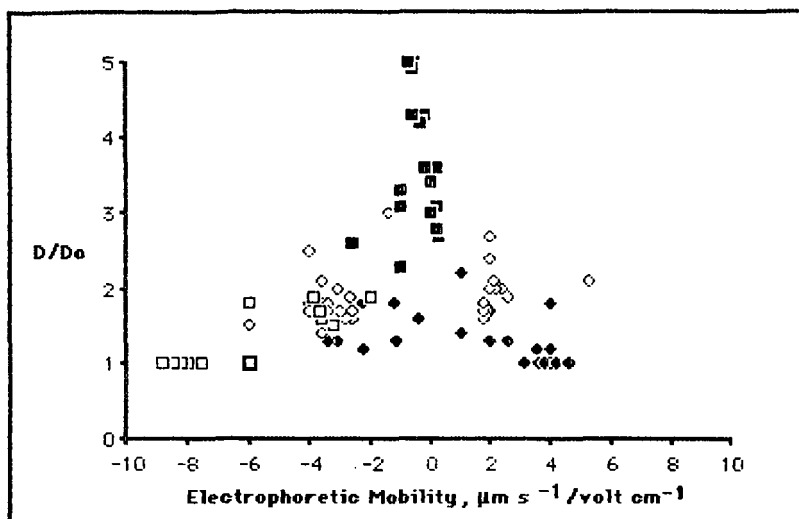


Figure 3. Ratio of Median Size D Calculated from Sedimentation Data to Median Size D_0 of Dry Powder, as a Function of Electrophoretic Mobility for: \blacklozenge Pittsburgh Seam #8-3, $D_0 = 41 \mu\text{m}$; \blacksquare San Juan, $D_0 = 55 \mu\text{m}$; \diamond Illinois #6, $D_0 = 57 \mu\text{m}$; \square Hiawatha, $D_0 = 56 \mu\text{m}$

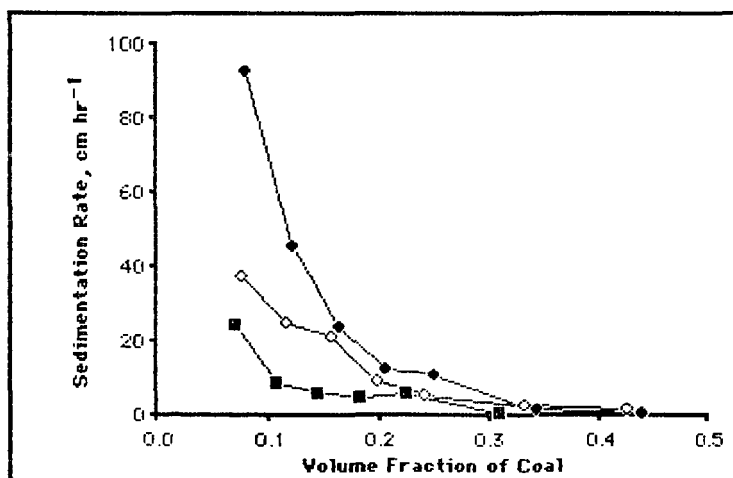


Figure 4. Sedimentation Rate as a Function of Coal Concentration for:
 \blacklozenge Lower Kittanning Coal, 2.3% ash, Ionic Strength = $0.9 \text{ mmole dm}^{-3}$
 \diamond Black Creek Coal, 5.8% ash, Ionic Strength = 14 mmole dm^{-3}
 \blacksquare Upper Freeport Coal, 21.9% ash, Ionic Strength = 44 mmole dm^{-3}

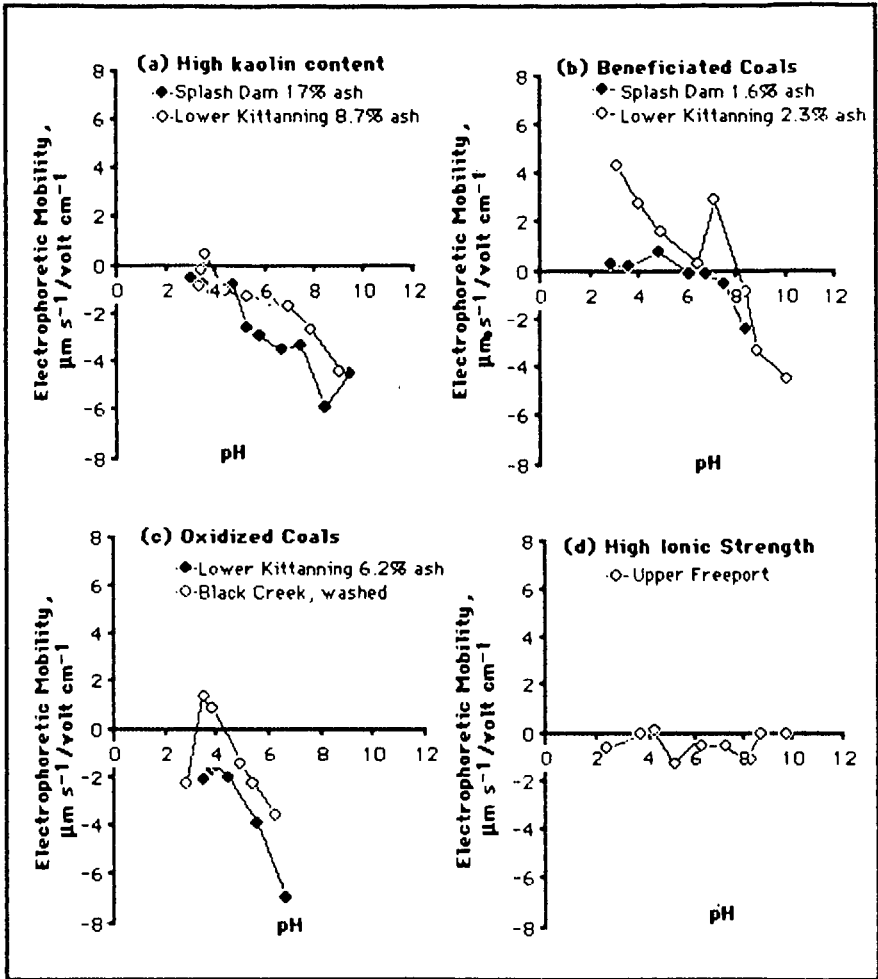


Figure 5. Electrophoretic Mobility as a Function of pH for 50%(wt) Slurries of Freshly Ground Coals, in Deionized Water

clay dominates the pattern at low pH. In Figure 5(c) the pattern for two oxidized coals is shown. Measurements could not be made above about pH 6 for either of these coals, because their slurries settled too rapidly, indicating very high interparticle repulsion and high surface charge. The patterns seen in Figure 5(b) and (c) are consistent with the observations reported by Wen and Sun^[6] of electrophoretic mobility versus pH curves for very dilute suspensions of unoxidized and oxidized Pittsburgh Seam #8 vitrain. Finally Figure 5(d) shows the electrophoretic mobility observed for the high ionic strength slurries of Upper Freeport coal. The pattern for this high ash coal might be expected to resemble Figure 5(a) were it not for the high ionic strength of the slurries, which increases with pH since sodium hydroxide was added to change the slurries from their natural pH of 3. For such slurries, electrophoretic mobility is not a good predictor of the variation of viscosity with pH, though it does predict sedimentation stability and final sediment volume. High soluble iron content tends to make coal particle electrophoretic mobility less negative in the pH range from 4 to 8, but in coal/water slurries high soluble iron is usually associated with high ionic strength which decreases the absolute value of the electrophoretic mobility and makes any effects of soluble iron difficult to detect.

Conclusions: Median particle size, particle size distribution width and particle internal volume accessible to water have a strong influence upon coal/water slurry viscosity and stability. At a given median size, size distribution and surface area, slurry properties can be predicted from the electrophoretic mobility of concentrated suspensions. The effects upon surface charge, and therefore upon slurry viscosity and stability, of oxidation, beneficiation and slurry ionic strength can also be predicted, although slurry viscosity is less sensitive to ionic strength than slurry stability toward sedimentation.

REFERENCES:

- [1] G. D. Parfitt et al., "A Program of Basic Research on the Utilization of Coal-Water Mixture Fuels", Final Report to the U. S. Department of Energy, Pittsburgh Energy Technology Center, DOE/PC/40285, (1984)
- [2] E. W. Albaugh, B. E. Davis and A. A. Levasseur, "Coal and CWM Selection for the DOE Characterization Project", *Proceedings of the Sixth International Symposium on Coal Slurry Combustion and Technology*, 282, (1984)
- [3] D. E. Howenhaupt and R. J. Gray, "The Alkali-Extraction Test as a Reliable Method of Detecting Oxidized Metallurgical Coal", *International Journal of Coal Geology*, 1, 63, (1980)
- [4] J. O. Glanville and J. P. Wightman, "Actions of Wetting Agents on Coal Dust", *Fuel*, 58, 819, (1979)
- [5] G. A. Parks, "Aqueous Surface Chemistry of Oxides and Complex Oxide Minerals", *Advances in Chemistry Series*, 67, 121 (1967)
- [6] W. W. Wen and S. C. Sun, "An Electrokinetic Study on the Oil Flotation of Oxidized Coal", *Separation Science and Technology*, 16, 1491 (1981)

SURFACE CHARGE OF ILLINOIS COAL AND PYRITES FOR DRY ELECTROSTATIC CLEANING

A. Mukherjee, D. Gidaspow, and D. T. Wasan

Chemical Engineering Department
Illinois Institute of Technology
Chicago, Illinois 60616

Introduction

Most of Illinois coal cannot be burned directly because its sulfur content is too high to meet present air pollution requirements. The Institute of Gas Technology Data Book on coal conversion (21) lists the pyrite, sulfate and organic sulfur content of various Illinois coals. Generally more than 50% of the sulfur contained in Illinois coal is in the form of iron pyrites. The organic sulfur content of some Illinois coals, such as Illinois No. 2 coal, is sufficiently low, that the removal of iron pyrites will produce compliance coal that can be burned in pulverized form.

Coal beneficiation techniques were recently reviewed by Tsai (11) and Liu (20). Physical beneficiation methods can be classified into wet and dry processes. Wet processes such as froth flotation have gained commercial status. However, dry methods of pyrite removal such as electrostatic or magnetic methods are potentially more energy efficient since they avoid the need of drying the coal before combustion and also do not use expensive surfactants.

Electrostatic methods used in the past involved expensive rotor type machines and were designed based on only limited fundamental measurements (Inculet, et al., (7), Moore, (13). Gidaspow, et al. (4) have recently shown that an electrofluidized bed can continuously remove iron pyrites from coal. The design and scale up of such a system is based on the fact that the electrophoretic mobility of pyrites is much greater than coal, since the surface charge of pyrites is ten times that of coal. The surface charge of pyrites and coal is used in a mathematical model of electrofluidization (Shih, et al.(17) ; Shih, (16)) to predict the extent of segregation in an electrofluidized bed. The objective of the present study is to obtain charge measurements of coal and pyrites which should be useful in the design of electrostatic separators.

Apparatus and Procedure

For measuring the charge of the particles a closed loop pneumatic system, shown in Figure 1, was constructed. The lift line, 7.62 cm in diameter and 6 meters high, was made of plexiglas. The particles whose charge we wish to measure, were loaded in the top hopper. Air was blown through the bottom of the lift line by a compressor via a honeycomb distributor. The solids were lifted by the air through the transport line and were subsequently returned to this line by means of a 2.54 cm. downcomer by gravity. Earlier a screwfeeder (Gidaspow, et al., (4)) was used, but the screwfeeder has a tendency to break up the particles and thereby creating excessive amounts of dust. Another problem with the screwfeeder was that its motor heats up very quickly, and subsequently jams, when large throughputs were used or when the air flow rates were low. The solids flow rate could be adjusted by controlling valve 1, while the gas flow rate could be controlled by adjusting valve 2. A cyclone with a dust bag was installed at the top to remove any dust, which could otherwise create a fire hazard. Flow rates through the system could be measured by opening a sampling valve 4. The charge of the particles was measured by using a ball probe, the details of which are shown in Figure 2. Other methods for charge measurement are available (Boschung and Glor, (1); Gajewski and Szaynor, (3); Kittaka et al., (8) and Saunders et al., (15)), but the ball probe is simple, reliable and makes in-situ on line measurements possible. The probe which is similar to that used by Soo et al. (8), is inserted into the flow stream of the

particles. The probe picks up a current which is proportional to the charge of the particles. The electrometer is a high impedance instrument which can measure currents up to 10^{-13} amperes. The lead to the ball probe was enclosed in a ceramic tube in order to avoid leakage of current. To reduce background current, the ceramic tube was again enclosed in a copper tube such that the lead to the probe, the ceramic tube and the copper tube formed concentric cylinders. The copper tube acts like a Faraday cage and reduces any disturbances due to build up charges on the walls of the conveyor. The tip of the ball probe was always kept at the axis of the lift line unless otherwise indicated. When measurements of current were taken in the pneumatic conveyor, air was first blown, and the current setting of the electrometer was set to zero. Particles were then blown along with the air, and the reading of the current by the electrometer was taken as the absolute current due to the impact of the particles on the ball probe. The probe and all other electrical connections were stored in alcohol when they were not in use, and just before use, they were cleaned with alcohol, acetone and finally, with distilled water.

The relation between current and the average charge of the particles is

$$i = qn \quad 1)$$

where i is the current measured by the electrometer, q is the average charge of the particle, and n is the number of particles striking the probe per second. From the above relation it is clear that the number of particles striking the probe per second is still unknown. To measure the quantity n , the output of the electrometer was connected to a Hewlett Packard oscilloscope, and an IBM personal computer with an A/D interface. The Keithley electrometer has a built in amplifier so that its output is amplified to a maximum of three volts. Anytime a particle impacts on the probe, a spike was observed on the oscilloscope. The number of peaks per second gave the frequency of particles impacting the probe. This number was obtained in two different ways using the IBM PC. In the first method, a power spectrum of the output of the electrometer was computed by using a Fast Fourier Transform algorithm (FFT), and the frequency of the maximum of the power spectrum gave the value of n . In the second method, whenever the voltage level of the output of the electrometer crossed a certain threshold value, a Schmidt trigger in the A/D converter was activated, which in turn incremented a count. The number of times the trigger was activated per second, gave the frequency of particles striking the probe per second. Both these methods produced a value of n which agreed with each other quite closely. The use of the Schmidt trigger was preferred, since it was less time consuming, and occupied less memory storage space in the computer. The use of the FFT procedure was also complicated by the fact that parasitic frequencies also produced maxima in the power spectrum, which could sometimes be confused with the frequencies of the particles.

The porosity or the volume fraction of particles flowing in the pneumatic conveyor, was measured by an X-ray absorption densitometer. The X-ray densitometer assembly consists of an X-ray source, a detector, and a recording system. A schematic diagram of the system is shown in Figure 3. The X-ray source and the detector were kept on either side of the transport line on a movable table. The table was mounted on a vertical screw shaft, which was driven by a reversible electric motor. The X-ray motor could be moved anywhere up and down by means of the motor. The 200 mCi X-ray source consists of a tiny capsule of Curium-244 isotope having a half life of 17.8 years. The source was well enclosed in a stainless steel container 2.0 centimeters in diameter. The container had a small window in the front for X-ray emissions. The principal emissions of the source were X-rays, of photoenergy between 12 and 23 KeV. A sodium iodide scintillation detector measured the intensity of the X-rays transmitted through the pneumatic line. A schematic diagram of the detector recorder assembly is shown in Figure 4. The output of the scintillation detector was connected sequentially to a preamplifier, a delay line amplifier, a single channel analyzer, and a timer counter unit. This assembly could

count the number of photons of X-rays striking the scintillation detector per unit time. As the counting time was fixed at 10 seconds, the reading on the counter could be interpreted on an arbitrary scale, as the intensity of the transmitted X-rays. This arbitrary scale was calibrated to read the voidage or porosity directly. To calibrate this scale to give values of porosity, particles were placed between rectangular containers of known volume, and the X-ray count was recorded. This step was repeated for various different containers to give a calibration curve of known porosity. The details of the calibration are reported by Luo (12) and Gidaspow et al., (4).

The humidity of the carrier gases was measured by inserting a digital General Eastern model 1200 AP dew point hygrometer in the flow stream of the particles. The materials used for measurement of charge were iron pyrites and coal. The pyrites were obtained from Fischer Scientific Company. The coal used was Illinois 6 coal, supplied by the Illinois State Geological Survey. The average size of both types of particles used were 270 μm . The charge of these particles was measured without any further treatment.

The mass flow rate of particles can be computed by using the relation

$$\frac{\dot{m}}{\pi R^2} = \frac{\frac{4}{3}\pi r^3 \rho_p n}{\pi \frac{d^2}{4}} \quad 2)$$

where \dot{m} is the mass flow, r is the radius of the particle, ρ_p is the particle density, d is the diameter of the probe, and R is the radius of the pipe. In the above equation, it is assumed that the local mass flow rate is constant across the diameter of the pipe.

The velocity of the particle can be computed by using the mass balance equation for steady feed rate

$$\frac{\dot{m}}{\pi R^2} = \rho_p \epsilon_s v_s \quad 3)$$

where ϵ_s is the measured volumetric concentration of the solid phase, v_s is the solid velocity to be computed, and R is the radius of the transport line. All measurements reported here were obtained in the fully developed flow region where volumetric concentration did not change with height.

Results and Discussion

Figure 5 shows the charge of pyrite and coal as a function of solid velocity at a constant gas velocity and humidity. The sign of charges shown here and in subsequent figures is negative. Although the charges of both pyrite and coal are negative, there is an order of magnitude difference in their values. This shows that pyrites and coal get charged selectively and that electrostatic separation of particles is feasible. The electric charge of both coal and pyrites increase as a function of solid velocity, as expected for triboelectric charging. In a related electrostatic separation experiment (Gidaspow et al., (4)), pyrites always moved to the positive electrode in greater amounts than coal, indicating that pyrites were more negatively charged than coal.

Figures 6 and 7, show the effect of varying the gas velocities for transport of pyrite and coal. Since the range of gas velocities is small due to the limitations of the present experimental setup, no observable difference in charging due to variations in gas velocity was noticed. The present experimental set up is being redesigned so that the velocities could be varied over much larger ranges.

Figures 8 and 9, show the effect of humidity on the charging of coal and pyrite. When a particle gets charged by triboelectrification, the amount of charge that a particle is capable of retaining is dependent on the ambient atmospheric conditions. Under dry conditions, most of the charge acquired by the particles, is retained. However, when the humidity content of the surrounding atmosphere is high, the charges accumulated on the particle begin to leak back into the atmosphere due to the bombardment of water molecules. The higher the humidity, the greater is the leakage of charge from the particles to the atmosphere. This shows that electrostatic separation of coal would be optimum under dry conditions.

The effect of particle concentration on charge of pyrites is shown in Figure 10. It is observed that as the concentration increases the charge drops. This could be due to the fact that under dilute conditions, more particle-wall interactions are possible than under concentrated conditions, where particle-particle interactions are more common. Under the assumption that all particles are nearly homogeneous, they would also have similar work functions. Therefore particle-particle contacts will have little bearing on the charging of particles. On the other hand, the work functions of the particle and the wall are much different, hence the probability of the particle getting charged on contact with the wall is much larger.

The amount of charge a particle is capable of carrying is dependent on the size of the particle as seen in Figure 11. These data were taken in the pneumatic conveying system shown in Figure 12. This apparatus is similar to that shown in Figure 1, except that it is of rectangular cross-section. Larger particles are capable of carrying much higher charges. However when particle charge is normalized by the particle surface area, the variation of charge as a function of particle size is minimal, as seen in Figure 13. This shows that only those electrons on the surface of the particles take part in the triboelectrification process.

The radial charge profile in the conveyor is shown in Figure 14. The charge at the center of the tube is constant, while it drops off at the wall. There could be two reasons for this observation. The first is that the probe is influenced by the accumulated charge on the wall of the conveyor, which is opposite to that of the particles. The second reason is that the velocity of the particles close to the wall is much lower than at the center of the pipe (Nakamura and Capes, (14); Syamlal (19)), thus the charge is smaller close to the wall, consistent with the variation of the charge with velocity shown in Figure 5.

Conclusions

We have shown that the electric charge of iron pyrites is generally an order of magnitude higher than that of coal. This higher charge is the basis of electrostatic separation of iron pyrites from coal. Humidity of the carrier gases has the most significant effect on the particle charge. The solid velocity, porosity and the particle size also influence the charge of the particles. The nearly linear dependence of the charge of pyrites and coal on particle velocity suggests that the electric charge is acquired by triboelectrification which is analogous although not identical to streaming current found in colloidal suspensions in liquid.

Acknowledgement

This study was sponsored by the Department of Energy and Natural Resources of the State of Illinois and the Coal Research Board, project ENR-6CR6.

Literature Cited

1. Boscung, P., and Glor, M. "Methods for Investigating the Electrostatic Behavior of Powders," *Journal of Electrostatics* 8, 205 (1980).

2. Fasso L., Chao, S., and Soo, S. L. "Measurement of Electrostatic Charges and Concentration of Particles in the Freeboard Fluidized Beds," *Powder Technology*, 33, pp. 211-221 (1982).
3. Gajewski, J. B., and Szaynor, A. "Charge Measurements of Dust Particles in Motion," *Journal of Electrostatics* 10, 229 (1981).
4. Gidaspow, D., Wasan, D. T., Saxena, S., Shih, Y. T., Gupta, K. P., and Mukherjee, A. "Electrostatic Desulfurization of Coal in Fluidized Beds and Conveyors," Presented at Miami Beach Annual AIChE meeting, Paper No. 58c, preprinted in Microfiche, November (1986).
5. Gidaspow, D., Wasan, D. T., Saxena, S., and Mukherjee, A. "Electrostatic Desulfurization of Coal," Annual report to the Coal Research Board and the Department of Energy and Natural Resources, Springfield, Illinois, December, (1985).
6. Gidaspow, D., Syamlal, M., Seo, Y. and Luo, K. M., "Dilute, Dense-Phase and Maximum Solid Gas Transport," Proceedings of the Advanced Research and Technology Development, Direct Utilization Contractors Meeting, U.S. Department of Energy, pp 180-189, (1985).
7. Inculet, I. I., Berganou, M. A., and Brown, J. D., "in Physical Cleaning of Coal: Present and Developing Methods," ed. Y. A. Liu, Marcel Dekker Inc. New York, (1982).
8. Kittaka, R., Masui, N., and Murata, Y. "A Method for Measuring the Charging Tendency of Powders in Pneumatic Conveyance through Pipes," *Journal of Electrostatics* 6, pp 181-190 (1979).
9. Kittaka, S., and Murata, Y. "A New System for Measuring the Charging Tendency of Solid Particles," *Journal of Electrostatics* 2, pp 111-119 (1976).
10. Kuczynski, R., Przekwas, A., and Kucinski, W. "The Static Electrification of Particles in Gas Solids Pipe Flow," *Journal of Electrostatics* 10, 309 (1981).
11. Liu, Y. A., "Physical Cleaning of Coal" Marcel Dekker, Inc. (1982).
12. Luo, K. M., "Ph.D. Thesis in progress," Illinois Institute of Technology, Chicago, (1986).
13. Moore, A. D., *Electrostatics and its Applications*, John Wiley and sons, (1973).
14. Nakamura, K., and Capes, C. E., "Vertical Pneumatic Conveying: A Theoretical Study of Uniform and Annular Particle Flow Models," *Can. J. Chem. Eng.* 51, pp 39-46 (1973).
15. Saunders, J. H., Chao, B. T., and Soo, S. L. "Performance of a Device for Entrainment Reduction and Smoother Operation of a Fluidized Bed," *Powder Technology* 35, pp 233-239 (1983).
16. Shih, Y. T., "Hydrodynamics of Separation of Particles: Sedimentation and Fluidization," Ph.D. Thesis, Illinois Institute of Technology, Chicago, (1986).
17. Shih, Y. T., Gidaspow, D., and Wasan, D. T., "Sedimentation of Fine Particles in Nonaqueous Media," *Colloids and Surfaces*, accepted for publication (1986).
18. Soo, S. L., Cheng L., and Tung S. K. "Electric Measurements of Flow Rate of Pulverized Coal," *ASME Journal of Engineering for Power*, April (1970).

19. Syamlal, M., "Multiphase Hydrodynamics of Gas-solid Flow," Ph.D. Thesis, Illinois Institute of Technology Chicago (1985).
20. Tsai, S. C., "Fundamentals of Coal Beneficiation and Utilization," Elsevier (1982).
21. Institute of Gas Technology, "Coal Conversion Systems Technical Data Book". Prepared for the U.S. Department of Energy (1982).

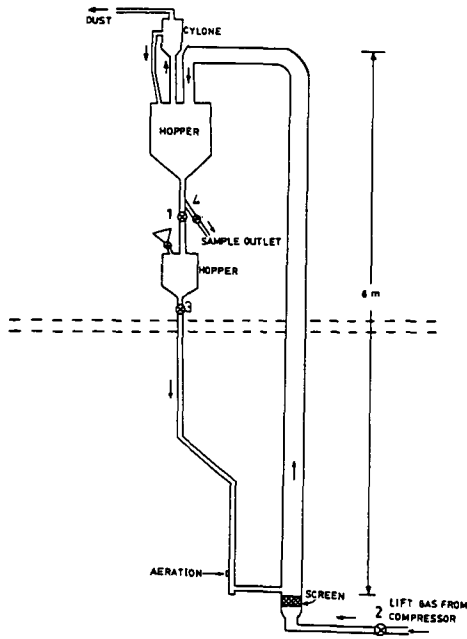


Figure 1. Pneumatic Conveying System.

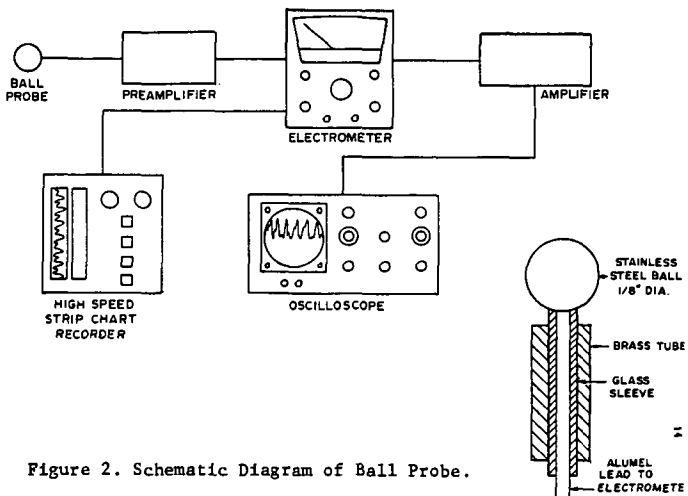


Figure 2. Schematic Diagram of Ball Probe.

1. X-ray Source 2. X-ray Detector
 3. Recorder System 5. Motor

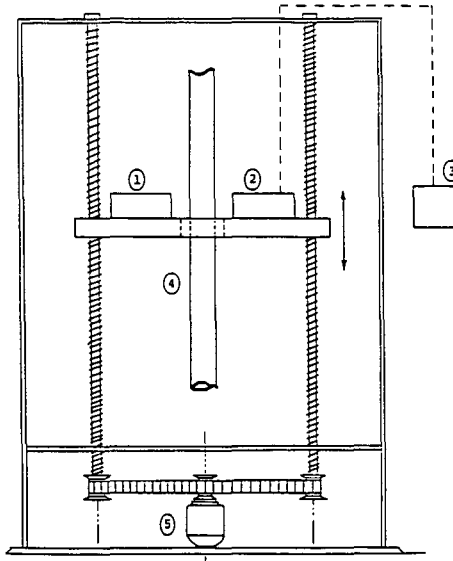


Figure 3. Schematic Diagram of X-ray Densitometer.

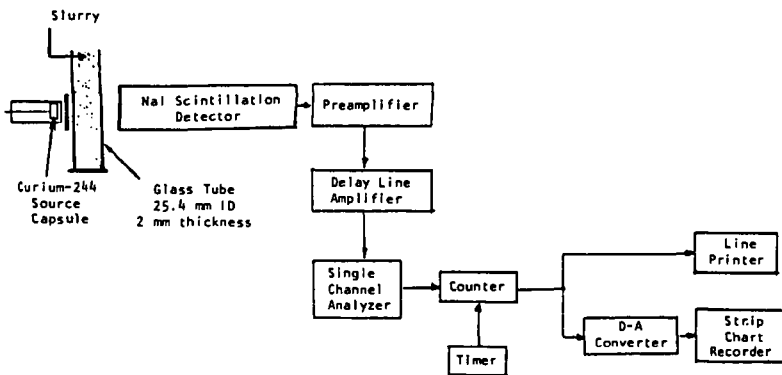


Figure 4. Line Diagram for X-ray Recorder Assembly.

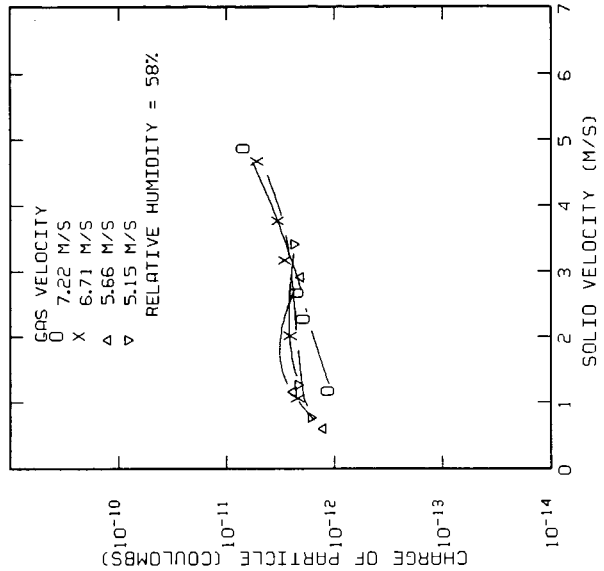


Figure 5. Charge of Pyrite and Illinois No. 6 Coal.

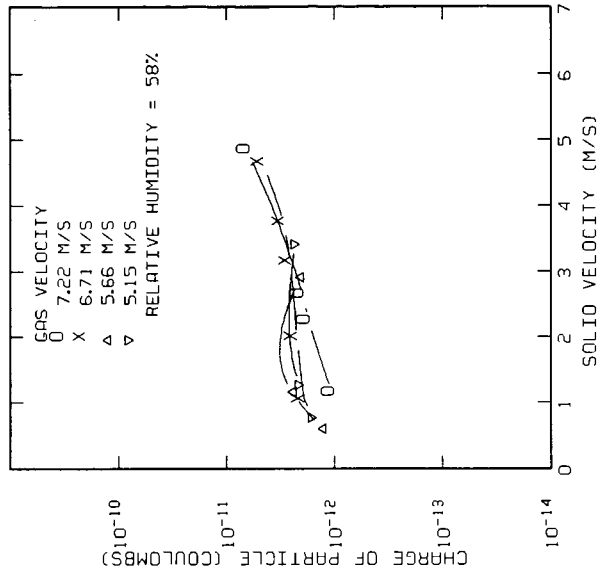


Figure 6. Effect of Gas Velocity on Charge of Pyrites.

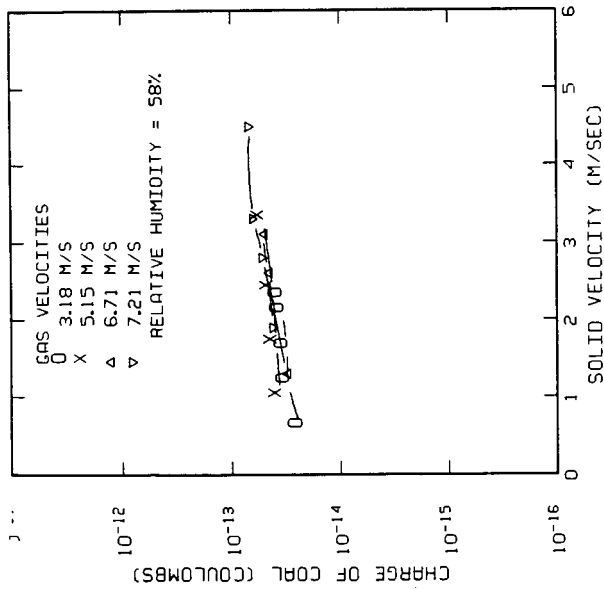


Figure 7. Effect of Gas Velocity on Charge of Coal.

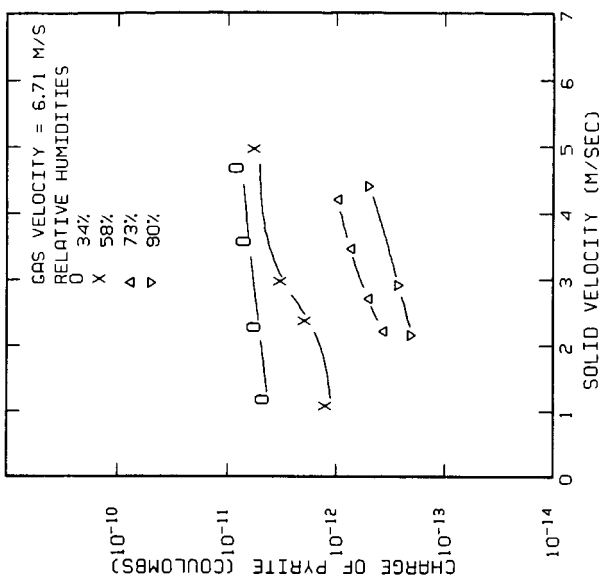


Figure 8. Effect of Humidity on Charge of Pyrites.

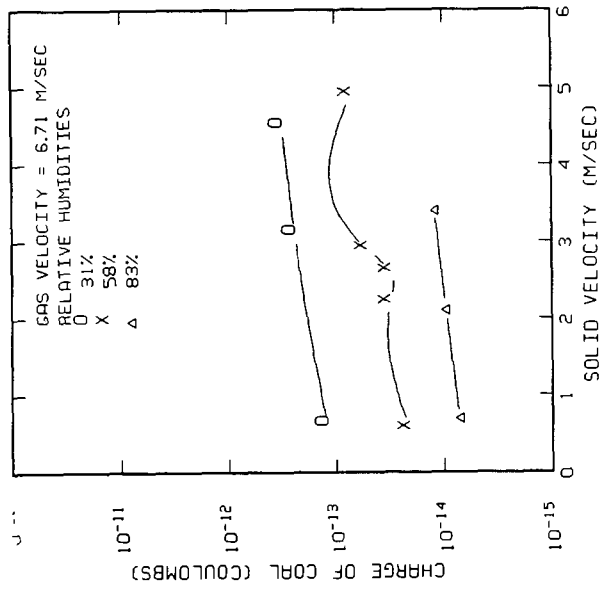


Figure 9. Effect of Humidity on Charge of Illinois No. 6 Coal.

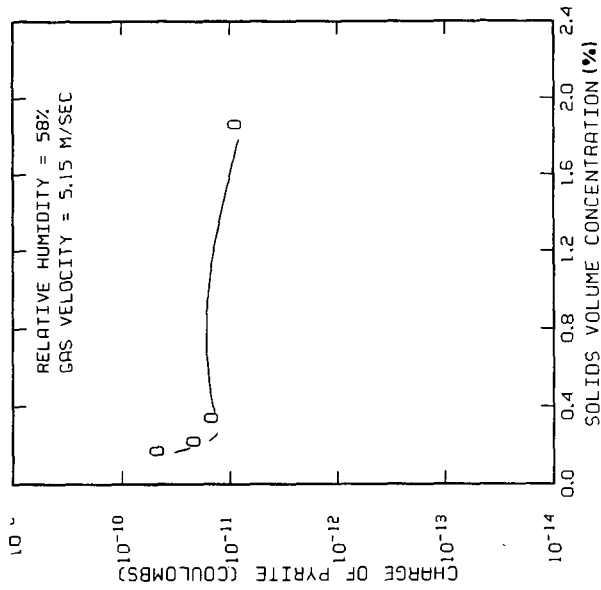


Figure 10. Effect of Particle Concentration on Charge of Pyrite.

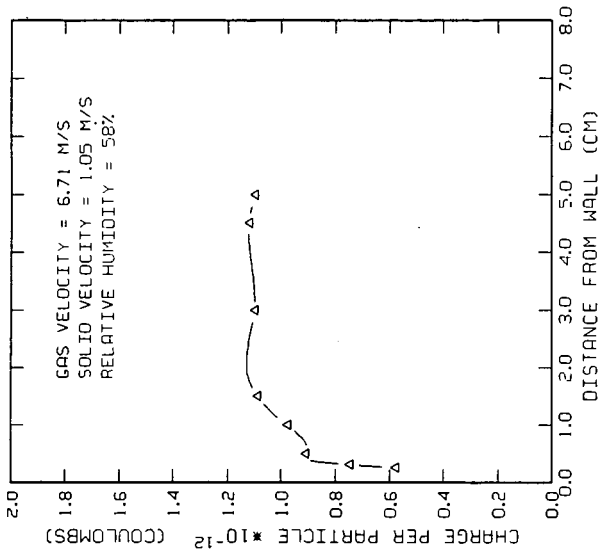


Figure 14. Radial Charge Profile of Pyrite.

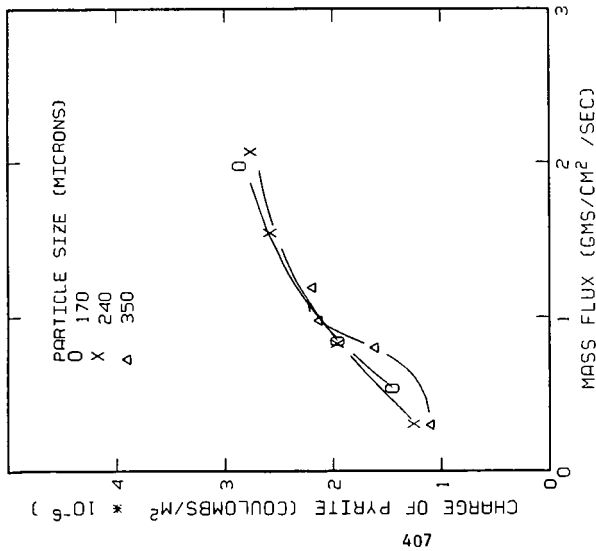


Figure 13. Charge of Pyrite Normalized by Surface Area.

THE EFFECTS OF WEATHERING ON FLOTATION AND THERMOPLASTIC PROPERTIES OF COAL

M. M. Wu, G. A. Robbins, R. A. Winschel and F. P. Burke

CONOCO COAL RESEARCH DIVISION
4000 Brownsville Road
Library, PA 15129

INTRODUCTION

Weathering can affect the behavior of coal in many production and end-use processes (1). Extensive laboratory research has been performed to determine the chemical nature of coal weathering. Most reported coal weathering simulation experiments have been conducted at temperatures greater than 100°C to accelerate the oxidation rate. Carboxyl, carbonyl, ether and phenolic groups have been reported to form upon coal oxidation (2,3). The oxidation mechanism is reportedly different at temperatures above and below about 70°C (4). In addition, recent studies indicate that the chemical nature of coal oxidation may be different at the lower temperatures more typical of natural coal weathering ($\leq 80^\circ\text{C}$) (5). The work reported here is a systematic laboratory study of coal weathering at realistic conditions of temperature and time using different ranks of coal. The objectives of this study are 1) to determine the effects of weathering on coal properties with emphasis on froth flotation and thermoplastic properties, 2) to compare the abilities of various techniques to measure the degree of weathering, 3) to better define the chemical nature of low-temperature coal weathering. In this paper, weathering is defined as the progressive changes in coal properties that occur as coal is exposed to humid air at temperatures of 80°C or less.

Medium and high volatile bituminous coals were weathered at temperatures of 25°C, 50°C and 80°C in flowing humid air for as long as 369 days. Absolute humidity, which was constant for all experiments, was equal to 80% relative humidity at 20°C. Weathered coals were sampled periodically and characterized by a variety of relevant techniques, including ultimate and proximate analyses, forms of sulfur, Gieseler plastometer, free swelling index (FSI), Audibert-Arnu dilatometer, heat of combustion, slurry pH, alkaline extraction and petrography. The froth flotation performance of the fresh and weathered coals was measured as a function of weathering time at several collector dosages. The weathered coals were also characterized by Fourier Transform infrared spectroscopy (FTIR) and X-ray photoelectron spectroscopy (XPS) to study the chemical nature of weathering.

Properties of laboratory weathered coals were compared with those of a naturally weathered coal.

EXPERIMENTAL

Weathering Unit. A schematic diagram of the weathering unit is shown in Figure 1. The coal (1.2 kg, -28 mesh) used in the study was dispersed in a fixed-bed reactor (3" ID) using 3/8" Intalox ceramic saddles (ca. 1.2 kg) to prevent air channeling. The temperature of the coal bed was controlled by circulating water from a thermostated bath through the reactor's outer jacket. The water circulator maintained the coal bed at temperatures up to 80°C to within 1°C. Two thermocouples were located at 1/3 and 2/3 of the coal bed height to monitor bed temperature. Air was introduced to the bottom plenum of the reactor at 1.7 SCFH. A third thermocouple was inserted in the reactor bottom to monitor the temperature of the incoming air. Air humidity (80% relative humidity at 20°C) was controlled by dividing the air into two controlled-flow parallel streams with one stream passing through two water saturators in series. Feed air and reactor off-gas, sampled

several times for gas chromatographic analysis, showed no significant difference in oxygen composition, thus indicating that these reactors are being operated at differential conditions and that the air flow is sufficient for uniform coal weathering. Periodic samples were taken from the weathering units as follows. The entire reactor contents were emptied over a screen to remove the saddles. The entire coal sample was riffled ten times and sampled for analyses. The remaining coal was re-mixed with the saddles, then re-packed into the reactor. The reactor was tapped while being packed to settle the bed. Bed back-pressure, typically 0.5 psig, was monitored to ascertain the absence of channelling.

Coals. The high-volatile bituminous coal used in this study was freshly mined run-of-mine (ROM) Pittsburgh seam coal from West Virginia. The coal was ground to -28 mesh before use. The medium-volatile coal used was the natural -28 mesh portion of freshly mined ROM Horsepen seam coal from West Virginia. The mine from which the coal was obtained extracts both the upper and middle Horsepen seams. The "naturally weathered" medium-volatile bituminous coal used in this study was obtained from an adjacent mine that also extracts the Horsepen seam coal, except in this case the seams are very near the surface. The "naturally weathered" coal examined here was the natural -28 mesh portion of the coal. Analyses and properties of these coals are listed in Table 1.

Analyses. Gieseler plastometer and free swelling index (FSI) measurements followed ASTM procedures. Audibert-Arnu dilatometer measurements followed the ISO procedure. The alkaline extraction test was performed by the published procedure (6). Ultimate and proximate analyses, forms of sulfur and heat of combustion were measured by standard procedures. Fourier Transform infrared (FTIR) spectra were collected of the neat samples (not ground further after removal from weathering unit) using diffuse reflectance with a Nicolet Model 7199 FTIR spectrometer. X-ray photoelectron spectroscopy (XPS) was performed with a Perkin-Elmer PHI Model 560 ESCA/SAM spectrophotometer with a magnesium X-ray source.

Froth Flotation Tests. Froth flotation tests were made using a Denver Model D1 flotation cell. Coal slurry (5 wt % coal) was first charged to the cell and conditioned at 1500 rpm for three minutes to ensure thorough wetting of the coal. Collector (No. 2 fuel oil), when used, was added and conditioned for 15 seconds. Frother (methyl isobutyl carbinol) was then added and conditioned for 15 seconds. The air valve was opened and the froth was manually removed for two minutes. Froth concentrate and tails were filtered, dried, then analyzed.

RESULTS AND DISCUSSION

Medium-Volatile Bituminous Coal. Horsepen seam coal (-28 mesh) was weathered at 80°C. Only slight changes in chemical composition were observed upon weathering. For example, there was a small but significant decrease in heating value (14446 vs 14809 Btu/lb, dry), an increase in oxygen content (5.6% vs 3.0%, by difference) and a slight increase in sulfate sulfur content (0.06% vs 0.02%) as weathering time increased to 84 days. In contrast, the thermoplastic properties, i.e., Gieseler maximum fluidity and Audibert-Arnu dilatation, exhibited very rapid decreases with weathering time. These two properties, log Gieseler maximum fluidity and Audibert-Arnu dilatation, are plotted as fractions of their initial value and as a function of weathering time in Figure 2. After 30 to 40 days, % dilatation became negative, indicating that there was no dilatation, only contraction. After 50 to 60 days, log Gieseler maximum fluidity became negative, indicating Gieseler maximum fluidity was below 1 DDPM (essentially no fluidity). In contrast to these two thermoplastic properties, coal recovery (% MAF) in the froth flotation tests using frother (9.6 mg MIBC/L slurry, 0.38 lb MIBC/ton coal) but no collector showed a more gradual decrease with weathering time (Figure 2). Clearly, coking/caking properties are lost more rapidly than flotation recovery. Flotation recovery of the

weathered coal can be restored to a large extent by use of small amounts of collector oil. For example, flotation recovery of the coal weathered for 84 days at 80°C increased from 14% (no collector) to 66% when collector (0.08 lb fuel oil/ton coal) was used.

Similar to flotation recovery, FSI decreased much less rapidly during early weathering than the Gieseler plastometer and Audibert-Arnu dilatometer measurements. At 80°C, FSI decreased from 8 1/2 to 5 1/2 after 44 days and to 2 1/2 after 84 days weathering. This decrease in FSI correlated fairly well with the loss in flotation recovery. FSI is obviously less responsive to early weathering than the Gieseler and Audibert-Arnu measurements. However, FSI may be a more meaningful measurement for the severely weathered coals because the plastometer and dilatometer values decreased to such low values with extensive weathering. FSI may show less responsiveness to early weathering partially as a result of the sample preparation required by the ASTM test. For FSI measurements, the coal must be ground to -60 mesh (as opposed to -35 mesh for the Gieseler), thus opening up fresh, less weathered surfaces. However, the Audibert-Arnu test, which requires a -100 mesh grind size, still shows excellent responsiveness to weathering.

The diffuse reflectance FTIR spectra (neat) of the fresh coal and coal weathered for 51 days are shown in Figure 3. The difference spectrum clearly indicates an increase in the carbonyl peak intensity at about 1700 cm^{-1} and a decrease in the C-H stretch intensity at about 2900 cm^{-1} upon weathering. The carbonyl peak can be assigned to carboxylic acids or ketones (7). An oxidation index developed by U.S. Steel (7), based on the FTIR spectra, is plotted as a function of weathering time in Figure 4. The index consists of the ratio of the integrated intensity of the carbonyl band (1635 cm^{-1} to 1850 cm^{-1}) to that of the aromatic and aliphatic C-H stretch band (2746 cm^{-1} to 3194 cm^{-1}). Since the index includes the C-H stretch band, it is sensitive to the loss of C-H intensity from weathering as well as to carbonyl production (7). Figure 4 indicates a fairly consistent increase from an index value of 0.45 for the fresh coal to 1.45 after 84 days weathering at 80°C. Others have attributed such changes to the oxidation of C-H groups to carbonyl groups (3,7).

The surface elemental compositions (C, total and organic O, S, N, Si, Al) by XPS of the coal weathered at 80°C for various times were obtained by XPS. Organic oxygen was calculated by subtracting inorganic oxygen from total oxygen, assuming that inorganic oxygen is associated with Si and Al in the oxide forms (2,8). The surface organic oxygen content increased from 4.8% to 8.5% after 84 days weathering. This increase is consistent with the carbonyl production determined by FTIR. The atomic ratio of organic oxygen to carbon (organic O/C ratio) obtained by XPS has been used as an indication of coal surface oxidation (8). The organic O/C ratios obtained by XPS (surface) and by ultimate analyses (Bulk) along with the ratio of oxidized to unoxidized surface sulfur (by XPS) at various weathering times are shown below.

Weathering Time (Days at 80°C)	Organic O/C		Surface Sulfur (Oxidized/Unoxidized)
	Surface	Bulk	
0	0.056	0.026	0.6
31	0.072	0.032	---
51	0.090	0.042	---
84	0.105	0.051	1.7

The surface organic O/C ratio increased more rapidly than the bulk organic O/C ratio, indicating the sensitivity of the coal surface to oxidation (weathering). The ratio of oxidized to unoxidized surface sulfur was calculated using the XPS S_{2p} peaks shown in Figure 5. Two distinct S_{2p} peaks were resolved, one at a low binding energy (164 eV) and one at a high binding energy (169 eV). The peak at

164 eV can be assigned to unoxidized sulfur species (pyritic sulfur and perhaps some organic sulfur) (9) and the peak at 169 eV can be assigned to oxidized sulfur species (sulfate) (9,10). The relative intensity (atomic percentage) of the S_{2p} peak at 169 eV to the S_{2p} peak at 164 eV increased after 84 days weathering at 80°C, indicating that surface pyritic sulfur was oxidized to sulfate.

High-Volatile Bituminous. Pittsburgh seam coal (-28 mesh) was weathered at 25°C, 50°C and 80°C for up to 369 days. As with the Horsepen seam coal, small decreases in heating value and small increases in oxygen and sulfate contents were observed with increased weathering time. For example, heating value decreased from 13335 to 12940 Btu/lb (dry), oxygen content (by difference) increased from 6.5 to 8.6% and sulfate sulfur content increased from 0.06 to 0.09% after 45 days weathering at 80°C. As shown in Figures 6 and 7, the rates of change with time (slopes) of both the Gieseler maximum fluidity and FSI are strongly dependent on weathering temperature. Similar changes in maximum fluidity and FSI with time and temperature have also been reported by others (7,13). Interestingly, the rate of change of maximum fluidity with time shows a first-order Arrhenius dependence on temperature. Using the Arrhenius expression, an energy of activation of about 40 kJ/mol is calculated. The exact physical significance of this result is unknown. However, observations of relationships between multiple parameters such as this should permit better understanding of the effects and mechanisms of weathering.

FTIR was used to characterize the chemical nature of weathering on Pittsburgh seam coal at 25, 50 and 80°C. The U.S. Steel oxidation index was used to represent the extent of organic matrix oxidation. At 80°C, the oxidation index increased from 0.72 (fresh coal) to 1.63 after 20 days and to 2.05 after 45 days. At 50°C, the oxidation index increased to 1.29 after 229 days and to 1.30 after 268 days. At 25°C, the oxidation index showed little change from the fresh coal, being 0.82 and 0.71 after weathering 268 days and 313 days, respectively. These data show that the rate of production of carbonyl groups and loss of C-H stretch intensity upon weathering is strongly temperature dependent, consistent with the temperature dependence of the change in maximum fluidity upon weathering (Figure 6).

Fresh and weathered coals were characterized by XPS. An asymmetric C_{1s} peak with a shoulder at high binding energy was observed after weathering at 80°C, indicating that some oxyhydrocarbon was generated. This is consistent with the FTIR results showing carbonyl production. As with the Horsepen Seam coal, two distinct S_{2p} peaks were resolved with binding energies of 164 eV and 169 eV. The relative intensity (atomic percentage) of the S_{2p} peak at 169 eV to the S_{2p} peak at 164 eV increased after 45 days weathering at 80°C, indicating that surface pyritic sulfur was oxidized to sulfate. Froth flotation performance depends on surface interactions (11). Flotation recovery is compared below to the ratio of oxidized/unoxidized sulfur and to the atomic ratios of organic O/C obtained by XPS. Organic oxygen was calculated as with the Horsepen seam coal.

Weathering Time (Days at 80°C)	Flotation Recovery (% MAF) Using 0.5 lb Fuel Oil/ Ton Coal	Surface Sulfur (Oxidized/ Unoxidized)	Organic O/C	
			Surface	Bulk
0	94.5	0.62	0.077	0.066
45	25.1	2.98	0.156	0.088

Flotation recovery decreased with increasing surface oxidation of both the organic matrix and the pyrite. The surface organic O/C ratio increased more rapidly than the bulk organic O/C ratio (obtained from ultimate analysis), indicating the sensitivity of the coal surface to oxidation (weathering). In contrast to the coal weathered at 80°C for 45 days, a symmetric C_{1s} peak, similar to that of fresh coal, was observed in XPS spectrum of the coal weathered at 25°C for 313 days, thus

showing little oxyhydrocarbon production (2,8). This is also consistent with the FTIR results which show no evidence for significant carbonyl production at 25°C. Two distinct S_{2p} peaks were resolved (164 eV and 169 eV) for the coal weathered at both 80°C and 25°C, indicating surface pyritic sulfur was oxidized to sulfate at both temperatures. The ratio of oxidized to unoxidized sulfur for the coal weathered at 25°C for 313 days is 1.70. For this weathered coal, pyrite oxidation was evident but little organic oxidation was apparent. This may suggest that for the 25°C weathered coal, the loss of flotation recovery is primarily caused by pyrite oxidation instead of organic matrix oxidation (12). A similar conclusion was reached in an assessment of a stockpile sample of the same Pittsburgh seam coal which showed poor flotation performance (14).

The froth flotation results with this coal were qualitatively similar to those using the Horsepen seam coal. Coal recovery (% MAF) decreased with the extent of weathering (time and temperature) and could be significantly improved by increasing the collector dosage. Even for the coal most severely weathered at 80°C (45 days), flotation recovery was restored to over 90% by increasing the collector dosage from 0.5 to 2.0 lbs fuel oil/ton coal. Substantial losses in flotation recovery occurred only after very large decreases in fluidity had occurred; however, the relationship between fluidity and flotation recovery appears to be temperature dependent as shown below.

T (°C)	Weathering		Flotation Recovery (% MAF)	Maximum Fluidity (DDPM)
	Time (days)			
Fresh	0		94.5	30,600
80	30.9		78.2	2.6
80	45		25.1	1.5
50	268		69.4	70.6
25	313		46.4	3,442

These flotation data were obtained using 0.5 lbs fuel oil/ton coal as collector. At each temperature, the degree of weathering that produced substantial loss of flotation recovery results in different reductions in maximum fluidity. This would suggest that the loss of flotation recovery and loss of fluidity result from different causes. Weathering temperature apparently affects not only the rate of weathering, but also the relative change of the different properties affected by weathering. Thus, it would appear that the use of high temperature, e.g., over 100°C, to accelerate weathering may produce coal with properties different from those produced at lower temperatures and longer times.

Naturally Weathered Coal. A "naturally weathered" Horsepen seam coal was characterized for comparison with the laboratory weathered coals. Properties of this coal, listed in Table 1, indicate that it is at least moderately weathered. The Gieseler maximum fluidity measurement was low at 30 DDPM, the % dilatation (Audibert-Arnu) was negative (-22%) and the alkaline extraction test gave a low transmittance of 13.8%. The flotation recovery (% MAF) was extremely low at 10.1% using frother (0.38 lb MIBC/ton coal) but no collector. FTIR and XPS indicated that there was mild oxidation of the organic matrix. The surface organic O/C ratio was extremely high at 0.29. This compares to a bulk ratio of 0.07 obtained by ultimate analysis. The relatively large surface organic O/C ratio occurring in the presence of only moderate carbonyl production suggests that chemisorbed oxygen may be present on the coal surface (probably peroxide)(4). XPS characterization showed a ratio of oxidized/unoxidized sulfur of 3.8, indicating that pyrite was highly oxidized. It appears that oxidation of both pyrite and the organic matrix is responsible for the poor froth flotation performance of this naturally weathered coal.

SUMMARY AND CONCLUSION

The Gieseler plastometer and Audibert-Arnu dilatometer are the most responsive tests to the early stage of weathering, thus demonstrating that relatively moderate weathering will destroy coal thermoplasticity. Other parameters measured are much less responsive to weathering. FSI appears to be a useful indicator only for relatively severely weathered coal. Substantial loss in flotation recovery upon weathering occurred only after the Gieseler maximum fluidity was greatly reduced. The rate of decrease in Gieseler maximum fluidity with time shows an Arrhenius temperature dependence. FTIR shows production of carbonyl groups at 80°C (fast) and 50°C (slow), but carbonyl production is small or nonexistent even after 313 days at 25°C. XPS shows that the surface organic O/C ratio increased more rapidly than the bulk O/C ratio obtained by ultimate analysis, indicating the sensitivity of the coal surface to oxidation (weathering). Pyritic sulfur was also oxidized to sulfate on the coal surface. Froth flotation recovery of the weathered coals deteriorated with increasing degree of weathering and showed a different dependence on temperature than maximum fluidity. Flotation recovery can be largely restored by increasing the collector dosage used. The relative importance of the effects of organic matrix and pyrite oxidation on flotation recovery appear to be dependent on the weathering temperature. If this is the case, it would appear imperative to use realistically low temperatures to model natural weathering.

ACKNOWLEDGMENT

The authors gratefully acknowledge the contributions of H. B. Oblad, D. E. Lowenhaupt, and D. H. Ralston. Conoco Coal Research Division is the research branch of Consolidation Coal Co.

REFERENCES

1. Cox, J. L. and Nelson, C. R., ACS Div. Fuel Chem. Prepr. 29 (1), 102 (1984).
2. Perry, D. L. and Grint, A., ACS Div. Fuel Chem. Prepr. 31 (1), 107 (1986).
3. Rhoads, C. A., Senftle, J. T., Coleman, M. M., David, A., and Painter, P. C., Fuel, 62, 1387 (1983).
4. Yohe, G., Illinois State Geological Survey Report of Investigations, 207, 1958.
5. Larsen, J. W., Lee, D., Schmidt, T. and Grint, A., Fuel, 65, 595 (1986).
6. Lowenhaupt, D. E. and Gray, R. J., Int. J. Coal Geol., 1, 63 (1983).
7. Huffman, G. P., Huggins, F. E., Dunmyre, G. P., Pignoco, A. J., Lin, M-C, Fuel, 64, 849 (1985).
8. Perry, D. L. and Grint, A., Fuel, 62, 1024 (1983).
9. Frost, D. C., Leeder, W. R. and Tapping, R. L., Fuel, 53, 206 (1974).
10. Wagner, C. D., "Handbook of X-ray Photoelectron Spectroscopy", Perkin-Elmer, Eden Prairie, MN, 1979.
11. Celik, M. S. and Somasundaran, P., Sep. Sci. Tech., 21 (4), 393, (1986).
12. Firth, B. A. and Nicol, S. K., Coal Preparation, 1, 53 (1984).
13. Larsen, J. W., Lee, D., Shawver, S. E. and Schmidt, T. E., Annual Report, GRI Contract No. 5081-361-0562, Feb., 1984.
14. Robbins, G. A., Oblad, H. B. and Meenan, G. F., "FTIR Characterization of Fine Coals Exhibiting Froth Flotation or Dewatering Problems", Proceedings, Third Annual Pittsburgh Coal Conference, Sept., 1986, Pittsburgh, PA.

TABLE 1

ANALYSES AND PROPERTIES OF HORSEPEN AND PITTSBURGH SEAM COALS

	Horsepen Seam	Pittsburgh Seam	Horsepen Seam "Naturally Weathered"
<u>Proximate Analysis (wt % As Det.)</u>			
Moisture	0.61	2.29	1.75
Volatile Matter	24.59	36.57	25.52
Ash	5.82	10.41	9.83
Fixed Carbon (By Difference)	68.98	50.73	62.90
<u>Ultimate Analysis (wt % Dry Basis)</u>			
Carbon	84.06	74.04	78.75
Hydrogen	4.69	4.93	4.28
Nitrogen	1.33	1.39	1.19
Sulfur, Total	1.11	2.54	0.98
Pyritic	0.41	1.37	0.15
Sulfate	0.02	0.06	0.15
Organic (By Difference)	0.68	1.11	0.68
Oxygen (By Difference)	2.96	6.48	4.79
Ash	5.86	10.66	10.01
Heating Value (Btu/lb, Dry)	14,809	13,335	13,790
<u>Gieseler Plastometer</u>			
Maximum Fluidity (DDPM)	1,836	30,600	30
Softening Temperature (°C)	387	348	398
Resolidification Temperature (°C)	511	481	498
Maximum Fluidity Temperature (°C)	472	434	440
Plastic Range (°C)	124	133	106
Free Swelling Index	8 1/2	7 1/2	7
<u>Audibert-Arnu Dilatometer</u>			
Contraction (%)	28	27	24
Dilatation (%)	191	103	-22
T ₁ , °C	377	334	384
T ₂ , °C	418	404	442
T ₃ , °C	496	454	475
T ₂ -T ₃ , °C	78	50	33
Alkaline Extraction (% Transmittance)	88.8	90.0	13.8
<u>Flotation Recovery (% MAF)</u>			
Without Collector	94.1	-	10.1
With Collector (0.5 lb Fuel Oil/ Ton Coal)	-	94.5	49.1
<u>Wet Screen Analysis, wt %</u>			
<u>Tyler Mesh</u>			
28 x 48 mesh	39.4	36.3	34.0
48 x 100 mesh	26.4	23.7	24.9
100 x 200 mesh	14.3	17.7	15.0
-200 mesh	19.9	22.3	26.1

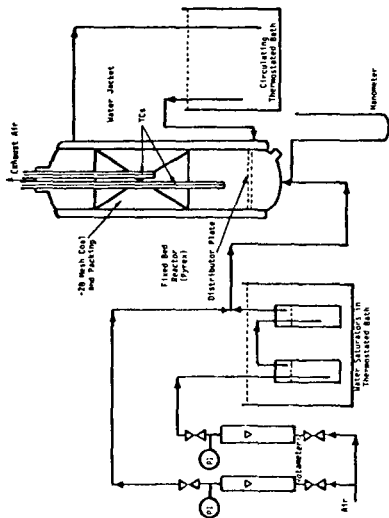


Figure 1. Coal Weathering Unit.

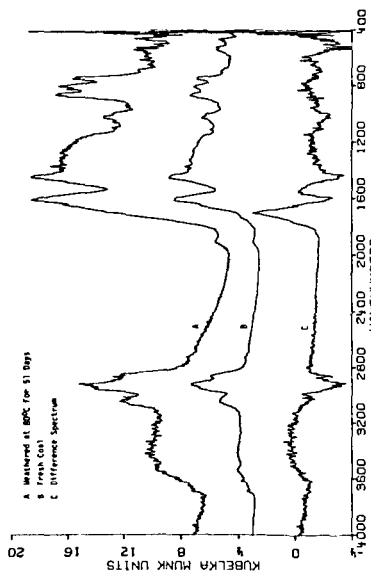


Figure 3. FIR Spectra of Horsepen Seam Coal.

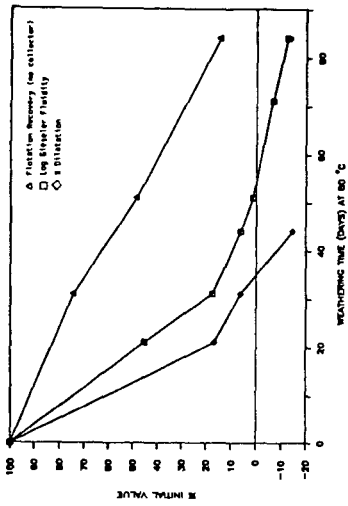


Figure 2. Thermoplastic and Flotation Properties of Horsepen Seam Coal as a Function of Weathering Time at 80°C.

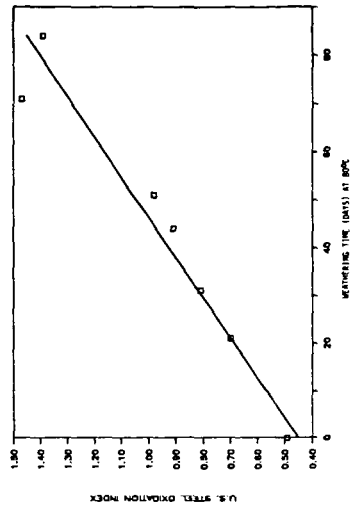


Figure 4. Oxidation Index of Horsepen Seam Coal as a Function of Weathering Time at 80°C.

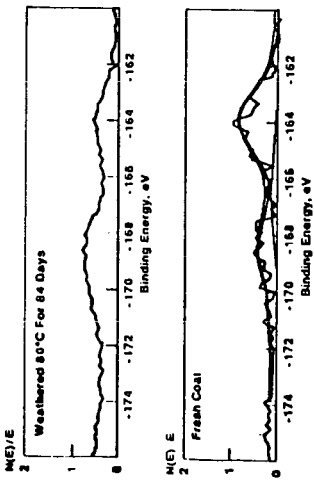


Figure 5. XPS S_{2p} Spectra of Horsepen Seam Coal.

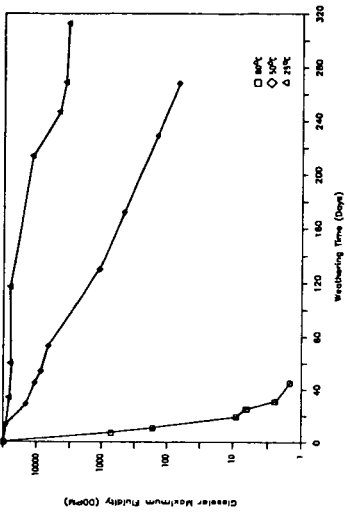


Figure 6. Gieseler Maximum Fluidity of Pittsburgh Seam Coal as a Function of Weathering Time and Temperature.

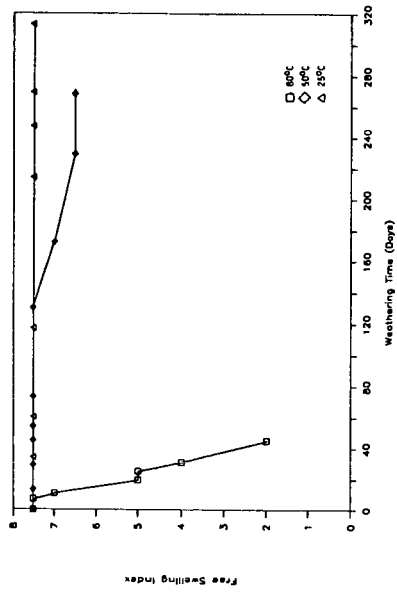


Figure 7. Free Swelling Index of Pittsburgh Seam Coal as a Function of Weathering Time and Temperature.

ASSESSING OXIDATION AND THE WETTABILITY OF COAL BY A FILM FLOTATION TECHNIQUE

D. W. Fuerstenau, M. C. Williams, K. S. Narayanan and J. L. Diao

Department of Materials Science and Mineral Engineering
University of California
Berkeley, CA 94720

ABSTRACT

The wettability of various as-received and oxidized coals can be quantified by a film flotation technique developed in our laboratories. Film flotation response curves yield an average wetting tension, ($\bar{\gamma}_c$), that can be used as an index for correlating the behavior of coals with their composition, treatment, process behavior, etc. The shift in $\bar{\gamma}_c$ with oxidation provides a quantitative measure of the change in surface energy of the coal induced by the increase in oxygen functional groups.

INTRODUCTION

With the exception of anthracite, almost all coals are very sensitive to oxidation. Addition of oxygen even in amounts too small to quantify will alter the properties of coal. Oxidation can proceed in-situ for coal deposits at shallow depths or may occur during mining, transportation, storage and processing. Whether oxidation takes place in the bulk of the coal or is limited to a thin surface layer, can affect drastically the surface properties of coal. The rate of oxidation is further enhanced as the specific surface area of coal is increased through comminution. Much effort is being directed towards elucidating the effect of oxidation on wettability or flotability.

An earlier study by Sun (1) indicated that the flotability of coal decreases with oxidation. Others (2,3) have also observed the flotability of oxidized coals to decrease even in the presence of collectors. Yarar (4) found that the flotation yield decreases for coals mined from deposits closer to the surface of the earth. This is attributed to higher probability of oxidation in shallow beds.

Despite these useful observations, delineation of the alteration in surface characteristics (wettability) due to oxidation remains imprecise. Contact angle measurements are strongly influenced by the pronounced heterogeneity of coal. Immersion time measurements, which have been used quite extensively for this purpose are extremely arbitrary and are theoretically ambiguous. Hornsby and Leja (5) first published papers on the use of normal flotation tests in a series of methanol-water solutions of decreasing surface tension to characterize coal flotability. In this paper, we describe a new film flotation method for determining the wettability of coal particles and illustrate its use in assessing oxidation effects with various coals.

Materials and Methods:

The coals used in this study along with their proximate analysis (ash,

volatile matter and fixed carbon) are listed in Table 1. The coal samples, which were received in large lumps, were first crushed in a jaw-crusher and then ground in a small coffee-grinder to minimize contamination. After fractionating the sample by sieving, the material was stored in a glove box in air-tight glass bottles. The glove box was further purged with inert gas to minimize oxidation. For the film flotation experiments 48 x 65 mesh (295 x 210 μm) particles were used.

Table 1 - Proximate Analysis (dry basis) of Raw Coals

Coal	Volatile Matter % wt.	Ash % wt.	Fixed Carbon % wt.	dmmf Carbon % wt.
Cambria #33	17.15	6.47	76.38	87.3
Geneva	40.96	8.23	50.81	82.2
Springfield	31.32	31.99	36.69	74.3
Kittanning	25.84	43.06	31.10	71.4
Anthracite	2.95	5.25	91.80	91.8

Film flotation, discussed in detail elsewhere (6,7), involves placing a monolayer of particles onto the surface of a liquid of given surface tension. The liquids used were solutions made of analytical grade methanol and triply distilled water. With this procedure, the particles are partitioned into lyophobic and lyophilic fractions which are filtered, dried and weighed. Similar tests are repeated using solutions having different surface tensions. The weight percent of the lyophobic fraction plotted as a function of solution surface tension yields what is called the wetting tension distribution diagram. The coal samples were oxidized in a natural convection oven at different temperatures (150°C, 200°C, and 244°C) for 19 hours. The oxygen functional groups were determined by wet potentiometric titration methods outlined by Schafer (8).

RESULTS AND DISCUSSION

Extensive experiments have been carried out to investigate the film flotation response of coal and the use of the results for characterizing coal behavior. Figure 1a, in which the cumulative percentage of particles not imbibed by the liquid is plotted as a function of the surface tension of that liquid, illustrates the film flotation response of 210 x 295 μm particles of Cambria #33 coal (a hydrophobic Pennsylvania bituminous coal). This figure clearly shows that there is a distribution in the wettability of the coal particles. We consider the cumulative plot given in Figure 1a to be a surface-based partition curve, which gives the cumulative distribution of particles in relation to their effective surface energy or hydrophobicity. We have defined three parameters from the kind of results given in Figure 1a: the surface tension of the solution that wets all particles, $\gamma_c(\text{min})$, the mean surface tension of particles in the distribution, $\bar{\gamma}_c$, and the surface tension of the solution above which none of the particles are wetted, $\gamma_c(\text{max})$. Initially, we consider that particles are imbibed at a given surface tension when the contact angle of those particles has just reached a value of zero. However, due to gravitational effects, sinking occurs at contact angles slightly greater than zero. Thus, the surface tension of the solution that imbibes all the particles represents those

particles with the lowest surface free energy, that is $\gamma_c(\min)$. The mean critical wetting surface tension of particles in the assembly is designated as $\bar{\gamma}_c$, and this then must represent an average of the γ_c 's of the particles being tested.

Using the data from Figure 1a, the mass fraction of the particles which are lyophobic is plotted in Figure 1b as a function of the surface tension of the imbibing solution. This figure indicates the existence of a surface parameter distribution, even for a closely-graded size distribution of the coal. The average surface tension parameter for each distribution, $\bar{\gamma}_c$, can be calculated from the histogram.

Coal oxidation is known to proceed in stages, which lead progressively through the production of gases, changes in the properties of gases, and changes in the properties of the remaining solid (9). Surface oxidation is caused when coal is exposed to an oxidizing atmosphere. The initial stages of oxidation are characterized by chemisorption of oxygen and the formation of acidic functional groups, specifically carboxylic (-COOH), ketone (C=O) and phenolic (-OH). Prolonged oxidation under high severity conditions can result in substantial uptake of oxygen deep into the coal matrix. Oxidation in laboratory investigations has been carried either with chemical oxidants or by thermal oxidation. For the work reported here we have used the thermal oxidation procedure described.

In this work, the effect of oxidation on the wettability of powdered coal was investigated through film flotation response, by varying the surface tension of the liquid between that of pure methanol (22.5 mN/m) and distilled water (72.8 mN/m). The wetting surface tension distribution of Cambria #33 coal oxidized at 150, 200 and 244°C for 19 hours is shown in Figure 2. From the results presented here, it is clearly seen that the curves are shifted to the right with increased oxidation, indicating an increase in the average wetting surface tension ($\bar{\gamma}_c$) as the coal becomes more oxidized. In an ideal unoxidized coal, the carbonaceous material (macerals) is responsible for its natural hydrophobicity with the inorganic minerals generally being hydrophilic. Upon oxidation the carbonaceous substrate produces oxygenated functional groups (-COOH, -OH) at the surface, which increase the hydrophilicity of coal due to their interaction with polar water molecules.

The curves in Figure 2 suggest that different components of the hydrophobic fraction in this coal tend to oxidize at different degrees since $\bar{\gamma}_c$ changes markedly without $\gamma_c(\min)$ shifting appreciably. To test this, some contact angle results obtained by Yang (10) on the same sample of coal are reproduced in Figure 3, which gives plots of the cosine of the contact angle (θ), measured on coal samples oxidized at different temperatures, as a function of the surface tension of the aqueous methanol solution. These so-called Zisman plots yield the critical wetting surface tension, γ_c , by extrapolation of the line to cosine $\theta = 1$. The results given in Figure 2 indicate that γ_c for the coal is essentially independent of the extent of oxidation. Yet the contact angle in water indeed reflects oxidation behavior rather markedly with the contact angle being 90 degrees for as-received coal, 50 degrees when oxidized at 150°C and 40 degrees when oxidized at 200°C.

In regard to sensitivity of contact angle behavior, Parekh and Aplan (11) also observed that γ_c is the same for a wide range of coals, namely 45 mN/m.

This indicates probably some insensitivity in the contact angle technique for determining the critical wetting tension of coals and serving as a comparative index for differentiating coal subjected to different degrees of oxidation.

We believe that the mean wetting surface tension, $\bar{\gamma}_C$, provides a useful index with which to correlate process response among various coals or between degrees of oxidation of the same coal. To test this, the percentage of oxygen in functional groups was determined by wet potentiometric titration method outlined by Schafer (8). Figure 4 shows the correlation between the concentration of oxygen functional groups with $\bar{\gamma}_C$. In addition, Fuerstenau et al. (12) determined the flotation behavior of this same coal in 0.5M NaCl solutions and their results for maximum flotation yield are also included in Figure 4. This figure shows that the coal is rendered hydrophilic as the percentage of oxygen groups in the coal increases. This is also very well reflected by the film flotation results which show the γ_C to increase with oxidation, thus establishing its applicability in quantifying hydrophilicity.

The fact that the increase in hydrophilicity for a given coal is due to the increase in oxygen functional groups is further elucidated by determining the acidic and phenolic groups in the lyophilic and lyophobic fractions produced by film flotation. Film flotation of Geneva Mine coal (a Utah bituminous coal) was performed in 30% methanol solution ($\gamma = 45$ mN/m). Potentiometric titrations of the lyophobic and lyophilic fractions indicate that the particles imbibed into the solution (58% of the feed) have a considerably higher concentration of carboxylic and phenolic functional groups than the floating particles. The original feed was also titrated to determine the functional group closure. The results are presented graphically in Figure 5. There is a 99 percent closure on the phenolic and a 97 percent closure on the carboxylic groups. It is apparent from these studies that the presence of oxygen functional groups increases the hydrophilicity of coals, which in turn alters their processing response.

This procedure was extended to ascertain how a range of coals having wide range of proximate analysis (Table 1) were affected when oxidized and film floated. Table 2 presents the values of $\bar{\gamma}_C$ (or γ_{50}) obtained from the wetting tension diagrams for both as-received and oxidized (at 200°C, 19 hrs) coals used in this investigation. For some of the as-received coals and oxidized coals complete wetting tension distribution diagrams could not be obtained, because the most hydrophilic particles were engulfed into pure water. However, analysis of the curves for coals for which the full distribution could be obtained indicated that the $\bar{\gamma}_C$ is reasonably close to γ_{50} , that is the 50% point on the cumulative distribution plots. Some preliminary observations are that, of the bituminous coals, those with highest ash content are the most hydrophilic and the one with the highest volatile matter content is the most hydrophobic. Interestingly, anthracite is the least hydrophobic of the as-received coals and exhibits great resistance to oxidation. The initial behavior of coal and its susceptibility to oxidation will depend on the characteristics of the different carbonaceous species present in a given coal. This depends on the conditions of coalification to which the decaying plant matters are subjected.

Table 2 - Average Wetting Surface Tension from the Film Flotation of Raw Coal and Coal Oxidized for 19 hours at 200°C.

Coal	Average Wetting Tension (mN/m)	
	Raw	Oxidized
Cambria #33	46.8	75.5
Geneva	31.0	66.0
Springfield	51.5	76.5
Kittanning	49.0	90.0
Anthracite	69.0	71.0

SUMMARY AND CONCLUSIONS

In summary, by conducting film flotation with a series of alcohol-water solutions, the wettability of as-received and oxidized coals can be quantified. This quantification is achieved by estimating the mean wetting surface tension ($\bar{\gamma}_c$) for a given sample of coal. All the coals tested showed a marked increase in hydrophilicity on oxidation. The sensitivity of $\bar{\gamma}_c$ as an index for predicting the flotation response of coal is established through a correlation between oxygen content, $\bar{\gamma}_c$ and flotation yields. Potentiometric titrations of the hydrophilic and hydrophobic fractions of coal confirm that the concentration of oxygen functional groups is much higher in the hydrophilic fraction than in the hydrophobic fraction.

ACKNOWLEDGEMENT

This material was prepared with the support of the U.S. Department of Energy, Grant No. DE-FG22-84PC70776.

REFERENCES

1. Sun, S. C., Trans. AIME, 199, 396, 1954.
2. Wen, W. W., and Sun, S. C., Trans. AIME, 262, 174, 1977.
3. Celik, M. S., and Somasundaran, P., Colloids and Surfaces, 1, 121, 1980.
4. Yasar, B., Trans. AIME, 272, 1978, 1983.
5. Hornsby, D. T., and Leja, J., Coal Preparation, 1, 1, 1984.
6. Fuerstenau, D. W., Williams, M. C., and Diao, J. L., AIME Annual Meeting, New Orleans, March 1986.
7. Fuerstenau, D. W., Williams, M. C., and Urbina, R. H., Proceedings, Conference on Coal Science, Pergamon Press, 517, 1985.
8. Schafer, H. N. S., Fuel, 49, 271, 1970.
9. Tsai, S. C., Fundamentals of Coal Beneficiation and Utilization, Coal Science and Technology - 2, Elsevier, New York 1982.
10. Yang, G. C. C., Ph.D. Thesis, University of California, Berkeley, 1983.
11. Parekh, B. K., and Aplan, F. F., Recent Developments in Separation Science, 4, 107, 1974.
12. Fuerstenau, D. W., Yang, G. C. C., and Laskowski, J. S., Coal Preparation, in press, 1986.

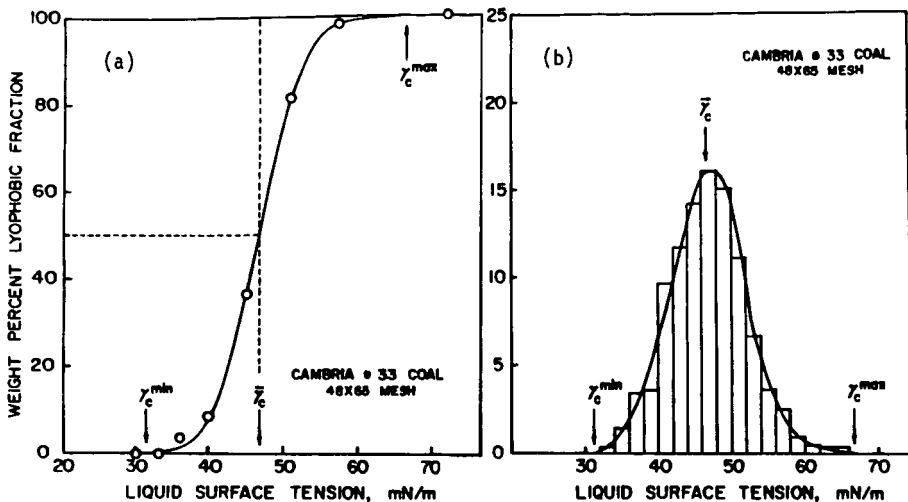


Fig. 1- a) Film flotation partition curve for Cambria #33 bituminous coal, and b) Frequency histogram for the lyophobicity of Cambria #33 coal.

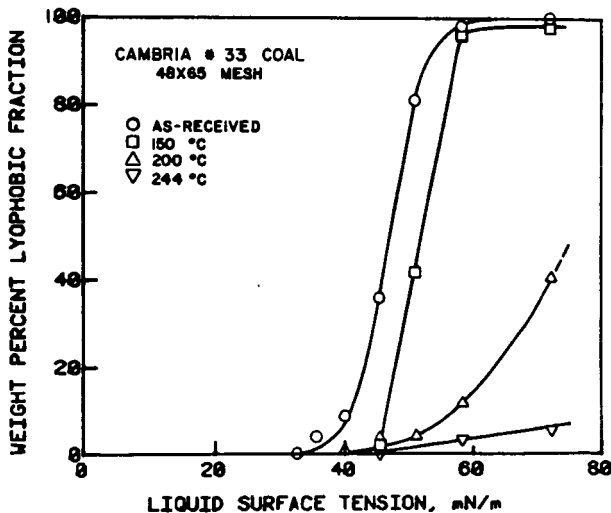


Fig. 2- Film flotation partition curves for as-received and oxidized Cambria #33 coal.

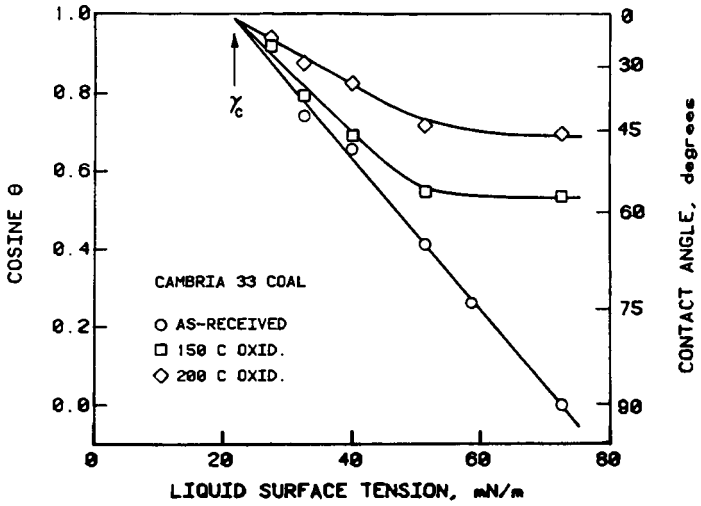


Fig. 3 - Zisman plots of the cosine of the contact angle of aqueous methanol solutions on as-received and oxidized Cambria #33 bituminous coal.

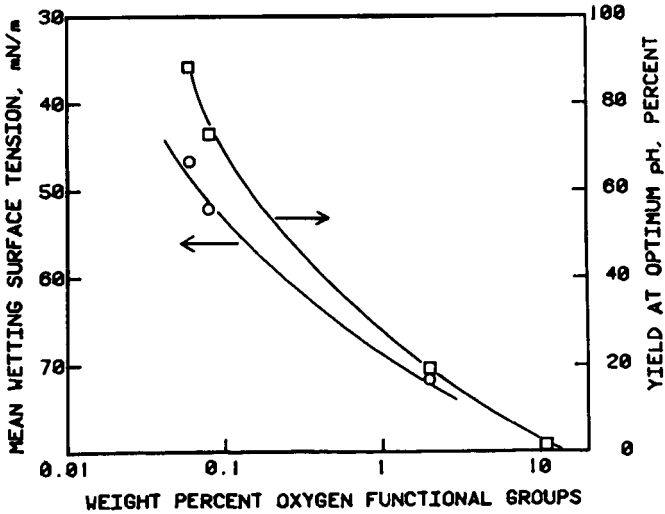


Fig. 4 - Correlation between the concentration of oxygen functional groups, average wetting tension and flotation yield for Cambria #33 coal.

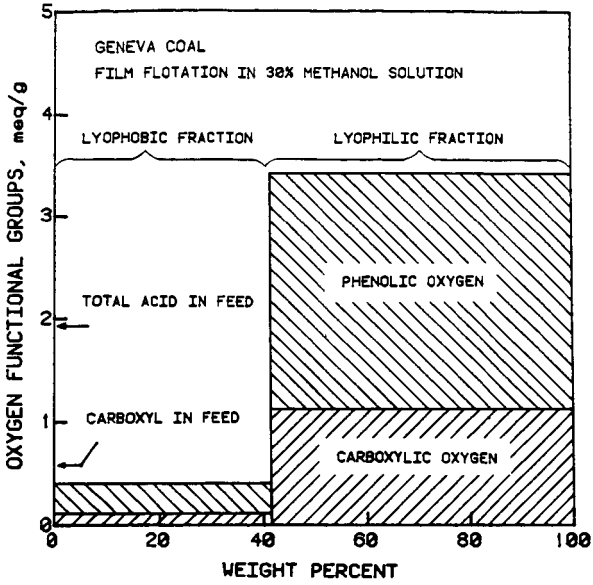


Fig. 5 - Graphical representation of the distribution of functional groups between the lyophobic and lyophilic fractions from the film flotation of Geneva coal.

AGGLOMERATION CHARACTERISTICS OF HYDROPHILIC COALS AND PYRITE/COAL MIXTURES

R. Venkatadri, R. Markuszewski, and T. D. Wheelock

Ames Laboratory and
Chemical Engineering Department
Iowa State University
Ames, Iowa 50011

Introduction

The need for industry to clean fine-size coal is increasing steadily. Selective oil agglomeration of coal fines suspended in water is a practical technique for beneficiating hydrophobic coals, but the technique is less well developed for beneficiating weakly hydrophobic and hydrophilic coals such as Illinois No. 6 coal and oxidized Upper Freeport coal. The oil agglomeration characteristics of the latter were investigated in this study and compared to those of two hydrophobic materials, unoxidized Upper Freeport coal and graphite. Also, since there is a general need to improve the separation of coal particles from iron pyrite particles for all types of coal, consideration was given to this problem. In addition, the effect of sodium oleate, a well-known anionic surfactant, on the agglomeration characteristics of these materials was studied.

Materials

Handpicked samples of coal were obtained to minimize their ash content. A sample of Illinois No. 6 coal was obtained from a fresh underground face at the River King Mine No. 1 in St. Clair county, Illinois, and a sample of Upper Freeport coal from the Lucerne No. 6 mine in Indiana county, Pennsylvania. The Illinois coal had an ash content of 7-10% and the Pennsylvania coal an ash content of 6-7%. The rank of the Illinois coal was high volatile bituminous C and that of the Pennsylvania coal medium volatile bituminous. The fresh Illinois coal was weakly hydrophobic and the fresh Pennsylvania coal highly hydrophobic. Pure graphite from Sri Lanka and pure iron pyrite from Peru were obtained from Ward's Natural Science Establishment. All of these materials were ground in the dry state by a high-speed impact mill. Various portions of the ground Upper Freeport coal were spread in thin layers on watch glasses and oxidized in a laboratory oven with natural air convection at 150°C for up to 144 hr.

Pure n-heptane (b.p. = 98°C) from Eastman Kodak Company was used as the agglomerating oil. Sodium oleate (SOL) from J. T. Baker Company was used as an anionic surfactant. Deionized water prepared by passing steam condensate through a Barnstead NANOpure II cartridge system was used in all experiments. The resistivity of the purified water was 17.9 megohm-cm. The pH of the particle suspensions was adjusted with either reagent grade hydrochloric acid or ammonium hydroxide.

Experimental Methods

Special procedures were used for measuring particle recovery by oil agglomeration and the zeta potential of suspended particles. A specially designed closed system was used for the agglomeration experiments in order to eliminate air from the system because air had been found previously to affect the results (1). This system utilized the motor and agitator from a 14-speed kitchen blender, but a 500-ml. canning jar was substituted for the open vessel furnished with the blender. The jar was inverted and a hole was drilled in the bottom. The hole was plugged with a rubber septum through which oil could be introduced with a

hypodermic syringe. For each experiment, the jar was filled with a suspension containing 10 g. of particles, and the suspension was conditioned for 3 min. at the highest speed. The oil was introduced quickly and mixing was continued at the highest speed for another 3 min. The agglomerated solids were recovered on a 100-mesh screen (U.S. Standard), dried overnight in an oven at 100-110°C, and weighed to determine the recovery.

To determine the zeta potential of suspended particles, 0.02 g. of material was mixed with 100 ml. of 0.001 M sodium chloride, and the pH was adjusted to the desired level with hydrochloric acid or ammonium hydroxide. Next the suspension was stirred vigorously for 2 hr. and the final pH measured. The suspension was then placed in an ultrasonic bath and agitated for 5 min. The zeta potential of the particles was subsequently measured with a Zeta-Meter 3.0 unit.

Results and Discussion

Electrokinetic Properties

The measured zeta potential for different materials in 0.001 M sodium chloride is shown as a function of pH in Figure 1. The zeta potential of pyrite at any given pH was similar to that reported previously (2, 3). Above pH 3.5 the zeta potential of graphite was similar to that reported for unleached graphite by Solari et al. (4). However, these workers did not report any values below pH 3.5 where graphite was found to have a strong electropositive charge in the present investigation. The zeta potential curve for unoxidized Upper Freeport coal was found to lie slightly below the curve for graphite up to pH 4 and slightly above the curve for graphite beyond pH 4. The isoelectric point for the Upper Freeport coal occurred at pH 3.3 and for graphite at pH 3.7. The zeta potential curve for Upper Freeport coal which had been oxidized at 150°C for 120 hr. lay below that of the unoxidized coal. Although the zeta potential of Illinois No. 6 coal was similar to that of oxidized Upper Freeport coal at pH 3.5-4, it was affected less by pH so that at higher pH the zeta potential of Illinois No. 6 coal was noticeably greater than that of oxidized Upper Freeport coal.

For bituminous coal the variation of zeta potential with pH as indicated in Figure 1 was attributed by Campbell and Sun (5) to the adsorption of electro-positive hydronium ions at low pH and electronegative hydroxyl ions at high pH. The present results for graphite suggest that the same mechanism may have accounted for the variation in zeta potential of this material. The greater electronegativity of the oxidized Upper Freeport coal compared to the unoxidized material may have been due to the introduction of carboxylic acid groups through oxidation which upon ionization would tend to increase the negative charge. Although this explanation could account for the difference in zeta potential at high pH, it would not account for the difference at low pH where the carboxylic acid groups would not be ionized. At low pH, oxidation of the coal surface seemed to interfere with the adsorption of hydronium ions. This may also explain why the zeta potential of the Illinois No. 6 coal was negative at low pH, because this coal is known to have a relatively high oxygen content.

Agglomeration Characteristics of Individual Materials

The results of agglomerating various materials with heptane are shown in Figure 2. The oxidized Upper Freeport coal used for this set of results was treated at 150°C for 144 hr. The -325 mesh materials were agglomerated separately at the natural pH of the respective aqueous suspensions. The recovery curves for graphite and unoxidized Upper Freeport coal were very similar and characteristic of hydrophobic materials. In each case only a relatively small amount of heptane

was required to achieve a high recovery of solids. Thus a recovery of 98% or more was achieved with 10 w/w % heptane (i.e., 1 g. heptane/10 g. solids) in the case of graphite and 15 w/w % heptane in the case of Upper Freeport coal. As expected, the weakly hydrophobic and hydrophilic materials responded less well to oil agglomeration. The maximum recovery of Illinois No. 6 coal was 62% and oxidized Upper Freeport coal 57%, and to achieve these recoveries an oil dosage of 27 w/w % was required. The recovery of pyrite was even lower with a maximum recovery of 15% being realized. With a large amount of heptane the recovery of these materials declined, which may seem surprising. However, Capes and Germain (6) also observed a decrease in coal recovery with excessive amounts of oil and attributed the decline to the formation of a weak coal-oil amalgam which passed through the collecting screen. It is also known that hydrophilic powders can stabilize oil-in-water emulsions (7) and such emulsions would be likely to pass through the collecting screen leading to the loss of both the hydrophilic material and oil.

Effect of Sodium Oleate

The effect of small amounts of sodium oleate on the agglomeration recovery of Illinois No. 6 coal and Upper Freeport coal (oxidized for 144 hr.) is shown in Figure 3. For these results only 5 w/w % heptane was used in treating the suspensions of the individual materials at their natural pH. Without sodium oleate, coal recovery was slight, but with an initial concentration of 2.5×10^{-4} M in the suspension, the recovery of -200 mesh Illinois No. 6 coal or -325 mesh Upper Freeport coal (oxidized for 144 hr.) increased sharply. On the other hand, the recovery of -325 mesh Illinois No. 6 coal was not affected by sodium oleate over the indicated range of concentration. However, in a subsequent experiment when the concentration of sodium oleate was increased to 8×10^{-4} M, the recovery of -325 mesh Illinois No. 6 coal increased to 85%.

These results appear to have been strongly affected by either the adsorption or deposition of oleic acid on the coal surface with a corresponding increase in hydrophobicity of the material. In the pH range of the coal suspensions, nonionized oleic acid should have been the predominant oleate species present (8). Furthermore, because of the low solubility of oleic acid in water at pH 4 it is quite likely that a colloidal deposit would have formed which could have coated the coal particles and rendered them more hydrophobic. Alternatively, oleic acid molecules may have been adsorbed by the coal surface due to hydrogen bonding between the carboxylic acid heads of the molecules and carboxylic acid groups on the coal surface or possibly due to hydrophobic interaction between the hydrophobic tails of the molecules and hydrophobic regions on the coal surface.

Sodium oleate was also found to have a remarkable effect on the agglomeration of -325 mesh pyrite with 5 w/w % heptane (see Figure 4). When pyrite was suspended in plain water and agglomerated, the maximum recovery was only 11%, but when pyrite was suspended in 10^{-4} M or higher concentrations of sodium oleate and agglomerated, the recovery jumped to 92-97%. Increasing the concentration of sodium oleate broadened the pH range over which pyrite recovery was enhanced. Also, at the highest concentration (5×10^{-4} M) spherical agglomerates were produced whereas at lower concentrations less compact, irregular-shaped agglomerates were formed.

In Figure 4 it can be seen that for any given sodium oleate concentration there was a sharp drop in recovery when a certain pH was exceeded. Moreover, the upper limit of pH for agglomeration to occur increased with increasing sodium oleate concentration. The shift in the pH limit suggests that precipitation onto the pyrite surface may have played a dominant role. Morgan *et al.* (8) have

pointed out that for oleic acid the pH of precipitation is a sensitive function of concentration. Thus by reducing the pH from 8 to 6, the oleate activity is reduced about 100 fold. Consequently the upper agglomeration limits indicated in Figure 4 could very well correspond to the pH of oleic acid precipitation. Another possibility at high pH would be the adsorption of various anionic oleate species.

Separation of Particle Mixtures

The separation of various mixtures of carbonaceous materials and pyrite was attempted by selective agglomeration with heptane. For this series of experiments all of the solids were ground to pass a 200 mesh screen (U.S. Standard). Equal amounts by weight of ground pyrite and either ground graphite or coal were introduced into the agglomeration apparatus. The heptane dosage was based on the total weight of solids (10 g.). For graphite/pyrite mixtures, the agglomerated product was analyzed by leaching with a hot solution containing equal parts of concentrated nitric and hydrochloric acids which dissolved the pyrite but not the graphite (9). For coal/pyrite mixtures the agglomerated product was analyzed for total sulfur and a sulfur balance was used in estimating the recovery of each component. The separation efficiency achieved was based on the following relation between the carbonaceous material (C.M.) and pyrite:

$$\text{Sepn. Eff. (\%)} = \text{C.M. Recovered (\%)} - \text{Pyrite Recovered (\%)}$$

The results of agglomerating various particle mixtures are presented in Table 1. A good separation of graphite and pyrite was achieved, and the separation efficiency or selectivity of the process improved as the amount of heptane was increased because the amount of pyrite recovered decreased. This result was similar to that observed previously (9). However, a good separation of coal and pyrite was not achieved with either unoxidized Upper Freeport coal or Illinois No. 6 coal. When either of these coals was mixed with pyrite, the recovery of pyrite generally exceeded the recovery of coal. Moreover, the recovery of pyrite

Table 1. Separation of a 50:50 mixture of a carbonaceous material and pyrite by selective agglomeration. All solid materials were -200 mesh

Carbonaceous material	Heptane, w/w %	Final pH	Recovery, %			Separation Eff., %
			Overall	C.M.	Pyrite	
Graphite	5	5.1	58.3	96.2	20.4	75.8
Graphite	10	5.1	56.2	96.5	16.3	80.2
Graphite	15	5.1	50.7	96.5	5.2	91.3
Up. Freep. coal	10	2.2	97.0	94.0	100.0	-6.0
Up. Freep. coal	10	4.9	97.1	97.8	96.2	1.6
Up. Freep. coal	10	9.6	93.1	86.1	100.0	-13.9
Ill. No. 6 coal	1	4.2	8.8	0.5	17.1	-16.6
Ill. No. 6 coal	3	4.2	28.3	12.7	43.9	-31.2
Ill. No. 6 coal	5	4.2	47.9	25.0	70.7	-45.7
Ill. No. 6 coal	10	4.1	52.7	34.8	70.6	-35.8
Ill. No. 6 coal	15	4.0	63.4	39.2	87.8	-48.6
Ill. No. 6 coal	5	10.4	6.1	4.1	8.0	-3.9
Ill. No. 6 coal	10	10.2	29.5	21.8	37.1	-15.3
Ill. No. 6 coal	15	10.2	22.8	20.2	25.2	-5.0

with a given amount of heptane was usually greater than the recovery obtained when pyrite alone was treated under similar conditions. Therefore, the presence of coal in the system promoted the agglomeration of pyrite whereas the presence of graphite did not. Furthermore, under some conditions the recovery of Upper Freeport coal was lower than it would have been if agglomerated by itself. Hence, the pyrite either monopolized more of the oil or suppressed coal agglomeration. An explanation for these results cannot be traced to the electrokinetic properties or to the agglomeration characteristics of the individual materials. On both counts graphite and Upper Freeport coal exhibited similar properties and characteristics. This intriguing phenomenon is being investigated further.

Conclusions

When various carbonaceous materials and pyrite were agglomerated individually, the recovery with a given amount of heptane increased in the following order: pyrite, oxidized Upper Freeport coal, Illinois No. 6 coal, unoxidized Upper Freeport coal, and graphite. This order seems indicative of the relative hydrophobicity of the materials. Adding traces of sodium oleate to the agglomeration system markedly increased the recovery of pyrite, oxidized Upper Freeport coal, and Illinois No. 6 coal. The results suggest that deposition of oleic acid onto the coal or pyrite surface or possibly adsorption of various oleate species may have accounted for an increase in hydrophobicity and recovery. An attempt to separate mixtures of carbonaceous materials and pyrite produced divergent results which require further explanation. On the one hand, a good separation of graphite and pyrite was achieved by selective agglomeration with heptane whereas, on the other hand, a similar separation was not achieved with coal and pyrite.

Acknowledgement

Ames Laboratory is operated for the U.S. Department of Energy by Iowa State University under contract No. W-7405-Eng-82. This work was supported by the Assistant Secretary for Fossil Energy, through the Pittsburgh Energy Technology Center. The experimental work of L. Kotlarz and D. Clark is gratefully acknowledged.

Literature Cited

1. J. Drzymala, R. Markuszewski, and T. D. Wheelock, "Influence of Air on Oil Agglomeration of Carbonaceous Solids," *International Journal of Mineral Processing*, (in press).
2. K. A. S. Osoka, L. M. Kye, R. Markuszewski, and T. D. Wheelock, "Flocculation of Pyrite and Silica with Either Polyacrylic acid or Xanthated Polyacrylic Acid," presented at 60th Colloid and Surface Science Symposium, Atlanta, GA, June 15-18, 1986.
3. M. C. Fuerstenau, M. C. Kuhn, and D. A. Elgillani, "The Role of Dixanthogen in Xanthate Flotation of Pyrite," *Transactions Society of Mining Engineers*, 241, 148-156 (1968).
4. J. A. Solari, A. C. De Araujo, and J. S. Laskowski, "The Effect of Carboxymethyl Cellulose on the Flotation and Surface Properties of Graphite," *Coal Preparation*, 3, 15-31 (1986).
5. J. A. L. Campbell and S. C. Sun, "Bituminous Coal Electrokinetics," *Transactions Society of Mining Engineers*, 247, 111-122 (1970).

6. C. E. Capes and R. J. Germain, "Selective Oil Agglomeration in Fine Coal Beneficiation," in: Physical Cleaning of Coal, Y. A. Liu (ed.), Marcel Dekker, Inc., New York, 1982, pp. 293-351.
7. M. Adams-Viola, G. C. Botsaris, and Yu M. Glazman, "An Investigation of the Hydrophilic/Oleophilic Nature of Various Coals: Its Importance to the Stability and Rheological Properties of Coal-Oil Mixtures," presented at 179th National Meeting, American Chemical Society, Houston, TX, March 27, 1980.
8. L. J. Morgan, K. P. Ananthapadmanabhan, and P. Somasundaran, "Oleate Adsorption on Hematite: Problems and Methods," International Journal of Mineral Processing, 18, 139-152 (1986).
9. J. Drzymala, R. Markuszewski, and T. D. Wheelock, "Selective Oil Agglomeration of Graphite in the Presence of Pyrite," Coal Preparation, (in press).

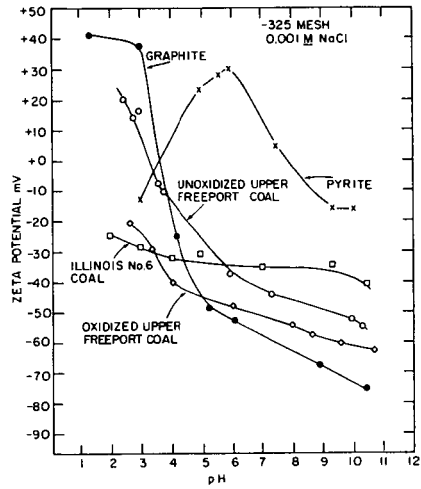


Figure 1. Zeta potential of various materials.

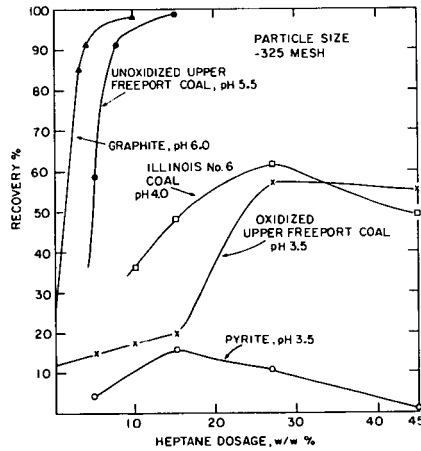


Figure 2. Effect of heptane dosage on agglomeration recovery of various materials.

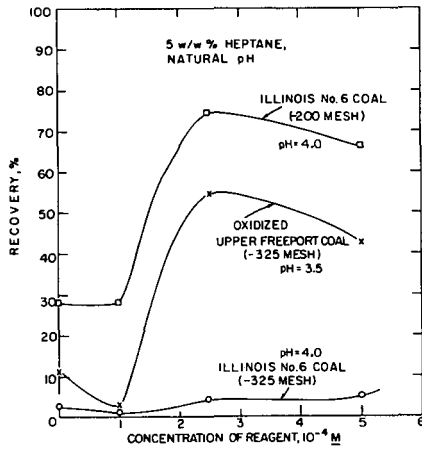


Figure 3. Effect of sodium oleate concentration on agglomeration recovery of coal.

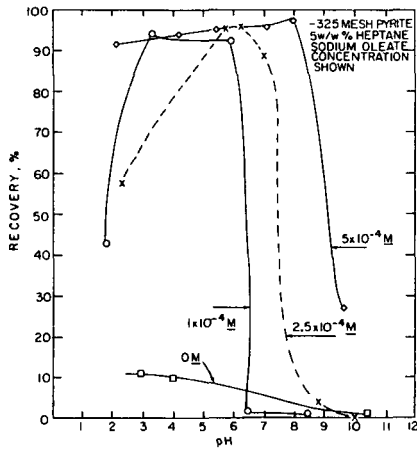


Figure 4. Effects of sodium oleate concentration and pH on agglomeration recovery of pyrite.

A STUDY OF INTERFACIAL PROPERTIES IN THE LIQUID CO₂-WATER-COAL SYSTEM

BOBBY CHI, B. I. MORSI, G. E. KLINZING AND S.-H. CHIANG

Chemical and Petroleum Engineering Department
University of Pittsburgh
Pittsburgh, PA 15261 USA

INTRODUCTION

During the past few years, a great deal of interest has developed in fine coal cleaning techniques. The concerns about the environmental effect of sulfur dioxide emissions and the efficient use of clean-burning fuel for utility boilers provide the main impetus for the increased research in this area. Currently, several advanced surface-property-based techniques [1,2,3,4] are under development. Among these, the LICADO (Liquid Carbon Dioxide) process [4], which utilizes liquid CO₂ at about 6 MPa and room temperature to separate mineral matter from coal, is currently being investigated as a new technique for cleaning coal.

The LICADO process relies on the relative wettability of "clean" coal and mineral particles with liquid CO₂ and water, respectively. When liquid CO₂ is dispersed into a coal-water slurry, it tends to form agglomerates with the clean coal particles and float them to the liquid CO₂ phase. The mineral particles, on the other hand, remain in the aqueous phase as refuse. Since the surface/interfacial properties of fine coal particles play such an important role in this coal cleaning operation, an understanding of their behavior becomes indispensable. Therefore, basic measurements must be made on the surface/interfacial properties of coal particles under conditions similar to those encountered in actual operation of the LICADO process.

BACKGROUND

It is generally postulated that the differences in surface/interfacial properties between the coal maceral and coal mineral (hydrophobic vs. hydrophilic) form the basis for the separation of these two components in the CO₂-water system. One of the most important surface/interfacial properties is the contact angle. In 1805, Young proposed that the equilibrium contact angle (θ) of a liquid drop resting on a flat solid surface be expressed in terms of three interfacial tensions - γ_{LV} at the interface of the liquid and vapor, γ_{SL} at the interface of the solid and liquid, and γ_{SV} at the interface of the solid and vapor. As Baughman and Razouk [5] pointed out, the term γ_{SV} can be related to the surface tension of the solid γ_S by adding the film pressure, π_{SV} , due to adsorbed vapor. Hence the surface tension of the solid γ_S , which is free from any adsorbed surface film, can be described as

$$\gamma_S = \gamma_{SL} + \gamma_{LV} \cos \theta + \pi_{SV} \quad 1)$$

The measurement of π_{SV} is likely to be difficult, but could conceivably be done [6] by measuring the amount of vapor (Γ , mole of vapor adsorbed per unit solid surface area) adsorbed at pressures ranging from near zero up to the saturated vapor pressure of the liquid, and using the integrated form of the Gibbs adsorption equation

$$\pi_{SV} = RT \int_{P_0}^P \Gamma \, d \ln P \quad 2)$$

where P_0 is the saturated vapor pressure of the liquid. At 298 K, P_0 is 3.13 KPa for water and is 6.42 MPa for liquid CO₂.

Coal is a heterogeneous material composed of many different components which exhibit their own solid surface tension on the coal surface. Thus, the γ_S of the coal surface is actually a statistical average value. The surface area of each component and its surface tension on the coal surface can supply valuable information in determining the coal surface tension. It is due to the heterogeneity of coal that Neumann et al [7,8] have recently reported the duality of coal surface tension (based on the assumptions of negligible π_{SV} and of $\gamma_{SL}=0$ at the critical wetting condition) in the two different

ranges of 0.03 - 0.04 N/m and 0.06 - 0.07 N/m. According to Neumann [9], γ_{sl} can be determined from the known contact angle and liquid surface tension through the use of Young's equation and the following equation of state:

$$\gamma_{sl} = [(\gamma_{sv})^{1/2} - (\gamma_{lv})^{1/2}]^2 / [1 - 15(\gamma_{sv} \gamma_{lv})^{1/2}] \quad 3)$$

where 15 has the unit of m/N. In the case of the coal-liquid CO₂-gaseous CO₂ system, coal samples were observed to be completely wetted by liquid CO₂ (cos θ =1). This was predicted from Zisman plot [6] based on the very low surface tension of liquid CO₂ ($\gamma_{lv} \approx 0.0005$ N/m). Consequently, γ_{sl} was estimated to be negligible (≈ 0). This fact suggests that the CO₂ adsorption film pressure, π_{sv} , can be used to approximate the coal surface tension γ_s . However, the determination of π_{sv} depends on the measurements of the high pressure CO₂ adsorption isotherm and the specific surface area of the coal. The coal surface area can be determined using the Dubinin-Polanyi (DP) equation with CO₂ adsorption data at 298 K and vacuum conditions [10,11].

In order to understand the separation mechanism involved in the LICADO process, it is necessary to study the interfacial interactions occurring in the CO₂-water-coal system. Young's equation can be applied to the water-liquid CO₂-coal system at 298 K and 6.42 MPa with the following designations: o - the liquid CO₂ phase saturated with dissolved water; w - the water phase saturated with dissolved liquid CO₂; s - the solid surface of the coal samples. The equation which relates the interfacial tensions and contact angles among the phases can be expressed as:

$$\gamma_{so} = \gamma_{sw} + \gamma_{wo} \cos \theta_{wo} \quad 4)$$

where γ_{ij} is the interfacial tensions between phase i and phase j, and θ_{wo} is the contact angle of the water on the solid surface surrounded by liquid CO₂.

The postulate of relative hydrophobicity of coal and mineral surfaces leads to the following inequality of contact angles for the clean coal (c), the feed coal (f), and the refuse (r):

$$(\theta_{wo})^c > (\theta_{wo})^f > (\theta_{wo})^r \quad 5)$$

and using Equation 4, this inequality can be expressed in terms of interfacial tensions:

$$(\gamma_{so} - \gamma_{sw})^c < (\gamma_{so} - \gamma_{sw})^f < (\gamma_{so} - \gamma_{sw})^r \quad 6)$$

It should be emphasized that these are equilibrium equations and that they do not reveal how the particle initially comes into contact with different fluid media. The body force and the shear force are usually required to initiate this contact. Since the shear and body forces are determined by the physical properties (such as particle size, specific gravity) of the coal particles as well as the hydrodynamic conditions in the separation system, it is therefore believed that a relationship between the process performance and the wetting characteristics of the coal/refuse particles can be understood through the following experimental studies.

EXPERIMENTAL Batch Research Unit

The Batch Research Unit was used to obtain process performance data and to collect coal/refuse samples for surface/interfacial property studies. The unit consists of two high pressure cells (2-inch I.D.) connected by a 2-inch ball valve so that the clean coal and refuse can be removed completely without remixing of the products when the system is depressurized. The system is provided with two variable speed mixers (up to 1200 rpm) for agitation of both the aqueous and liquid CO₂ phases. Hence, the effect of mixing on the separation process can be studied. In the experiment, approximately one liter of coal-water slurry was used for each test run. Liquid CO₂ was injected from the bottom while both phases were mixed. After a pre-determined time, the liquid CO₂ injection and the agitation were stopped and phases were allowed to separate. The center valve was then closed and the clean coal product and the refuse fraction were removed.

High Pressure Interfacial Property Measuring Device

A high pressure apparatus (Figure 1), equipped with necessary optical and photographic accessories, was constructed for the measurement of interfacial properties in the coal-liquid CO₂-water system. The measurement cell, equipped with two-inch windows on opposite sides, was mounted on a rotary table capable of ±180 degree rotation. The connections from this cell were high pressure flexible metal tubes. This apparatus was used to perform the following kinds of measurements:

- Vapor-liquid and liquid-liquid interfacial tensions for the vapor CO₂-liquid CO₂-water system.
- Equilibrium, advancing or receding contact angles of water on coal samples in an environment that can be either liquid CO₂ or gaseous CO₂ at various pressures.

An overhead mixing cell was used to equilibrate both immiscible phases so that both the liquid CO₂ and water could be fed from the mixing cell to the measurement cell by gravity. Hence, a stable pendant drop could be hung from the tip of a S.S. tube for photography. Two high-pressure pycnometers were used to determine the density of water and CO₂ at room temperature and various pressures.

For the contact angle measurement, a liquid drop (sessile drop) was deposited on a 1" diameter x 1/4" thick coal pellet sample, which was held by a specimen holder. This specially designed specimen holder could be mounted, from the side of a two-inch flanged opening, on the tip of a shaft assembly. The shaft assembly was designed in such a way that both rotational and translational movement can be externally controlled. The horizontal rotation of the specimen holder enabled the measurements of the contact angle from any direction of the sessile drop. The vertical movement permitted the adjustment of distance between coal sample and the tip of the feed tube during the formation of the sessile drop. The contact angle could be measured either in-situ using the angular protractor inside the eyepiece of the microscope or from the photograph of the drop.

Photographic image could be analyzed either by Andreas' manual method [12] or by Rotenberg's numerical method [13]. Using the latter method, the images were digitized using the LEITZ TAS-plus image analyzer connected to a macroviewer. A computer program written in TAS-plus language was developed to digitize the contour of the drop and to transfer the coordinate data to the University VAX/VMS system, where Rotenberg's program was implemented to calculate either the interfacial tension or the contact angle.

Dubinin-Polanyi Coal Surface Area and CO₂ Adsorption Isotherm

The surface area of coal was determined from the adsorption of CO₂ using a BET apparatus operated at 298 K. The Dubinin-Polanyi plot could be constructed from the amount of CO₂ adsorbed on the coal surface at various vacuum pressures in order to obtain the CO₂ adsorption surface area.

The equilibrium unit used for studying CO₂ adsorption on coal was a high pressure cell in which a precision quartz spring held the coal sample in a porous thimble. Adsorption experiments were performed by introducing a known weight (~2g) of coal sample in the system and then degassing the sample under vacuum. This was followed by the introduction of liquid CO₂. Once equilibrium had been attained, the elongation of the quartz spring was measured to determine the amount of CO₂ adsorbed on coal. By incorporating the integration of the adsorption isotherm and the surface area data from the DP plot, a computer program written in FORTRAN 77 language was developed to determine the film pressure (π_{sv}).

RESULTS AND DISCUSSION

Upper Freport coal from Indiana County, PA with 23.5% ash content was selected for the experimental work. Primarily, -200 mesh samples were used in this study while other size fractions such as -28 mesh, -28+100 mesh, and -100 mesh were used only for comparison purposes. The coal samples for interfacial property measurements were obtained from the LICADO batch cleaning experiments under specified operating conditions.

Wetting Characteristics and Mixing of the LICADO process

The clean coal and refuse samples from each stage of the multistage cleaning experiments were analyzed. The ash content of the coal samples together with the measured contact angles of water under various CO₂ pressures are presented in Table 1. Based on the deposition technique of the sessile drop, two cases were studied:

1. The coal surface was saturated with CO₂ gas at a desired pressure followed by placing the saturated water drop on the surface (CO₂-first-wet).
2. A water sessile drop was first formed on the coal surface at its own vapor pressure. Then, CO₂ gas was introduced into the system at the desired pressure. After equilibrium was established, the contact angle was measured (water-first-wet).

Table 1: CONTACT ANGLE OF WATER AT TWO DIFFERENT DEPOSITION TECHNIQUES

Ash Content (Stage No.)		(P, θ)	(P, θ)	(P, θ)	(P, θ)	(L, θ)
2.7% (4c)	1*	(0, 110)	(2.1, 118)	(4.1, 134)	(6.2, 146)	(L, 154)
	2**	(0, 110)	(2.1, 113)	(4.1, 122)	(6.2, 130)	(L, 128)
3.4% (3c)	1	(0, 111)	(2.1, 115)	(4.3, 133)	(6.2, 143)	(L, 152)
	2	(0, 111)	(2.6, 118)	(5.2, 127)	(6.2, 127)	(L, 117)
5.0% (2c)	1	(0, 105)	(2.1, 113)	(4.8, 138)	(6.2, 142)	(L, 152)
	2	(0, 105)	(2.1, 108)	(4.1, 118)	(6.2, 132)	(L, 123)
6.9% (4r)	1	(0, 97)	(2.2, 104)	(4.7, 114)	(6.2, 128)	(L, 154)
	2	(0, 97)	(2.1, 100)	(4.1, 108)	(6.2, 115)	(L, 105)
8.4% (1c)	1	(0, 103)	(2.2, 113)	(4.3, 128)	(6.3, 128)	(L, 138)
	2	(0, 103)	(2.2, 110)	(4.7, 118)	(6.3, 126)	(L, 120)
11.6% (3r)	1	(0, 85)	(1.4, 81)	(2.8, 99)	(6.3, 128)	(L, 137)
	2	(0, 85)	(2.8, 88)	(5.6, 92)	(6.0, 97)	(L, 92)
18.1% (2r)	1	(0, 71)	(3.2, 80)	(5.2, 102)	(6.0, 112)	(L, 130)
	2	(0, 71)	(2.2, 72)	(4.8, 75)	(6.3, 84)	(L, 80)
23.5% (f)	1	(0, 84)	(2.2, 88)	(5.2, 113)	(6.3, 119)	(L, 145)
	2	(0, 84)	(2.8, 88)	(4.5, 91)	(6.3, 94)	(L, 82)
54.2% (1r)	1	(0, 0)	(1.5, 80)	(4.6, 93)	(6.3, 94)	(L, 89)
	2	DOES NOT EXIST				

*1: CO₂-First-Wet; **2: Water-First-Wet; c: Clean Coal; f: Feed; r: Refuse;
P in MPa; θ in Degree; L: Liquid CO₂ Phase.

It is shown that the water contact angle on the feed coal surface (CO₂-first-wet) increases from 84° at atmospheric CO₂ pressure to 120° at a gaseous CO₂ pressure of 6.2 MPa. When the water drop is in the liquid CO₂ environment, the contact angle increases further to 145°. This similar trend can also be observed for the first stage clean coal (1c). On the other hand, the water contact angle on the refuse sample (1r) decreases from 94° to 89° as the environment changes from equilibrium gaseous CO₂ to liquid CO₂. Hence, the largest contact angle difference between the clean coal (8.4% ash) and refuse (54.2% ash) samples is in the liquid CO₂ phase, which accordingly, indicates that clean coal particles show a hydrophobic behavior (145°) that results in their agglomeration and transfer to the liquid CO₂ phase while refuse particles, more hydrophilic, remain in the water phase. Measurements made from other stage samples display a similar phenomenon. Generally, it is observed that when the ash content of the coal sample increases, the water contact angle decreases. A strong support for the use of liquid CO₂ as the processing medium for fine coal cleaning is therefore confirmed.

It was observed that the mixing in the LICADO process helped to improve the effectiveness of separation between the coal and mineral matter. In an attempt to understand the relationship between

the shear force and interfacial force, the effect of mixing speed in both the liquid CO₂ and water phases was studied. As depicted in Figure 2, it appears that an intermediate agitation speed between 300 to 900 rpm will be best for the separation. It is possible to explain the effect of agitation on the LICADO process from the data obtained from the contact angle measurement on the feed coal. Since the coal sample was prepared in a water slurry form before feeding to the LICADO system, the wetting characteristic of the feed coal/water slurry is similar to that of the water-first-wet case as the CO₂ pressure is raised to the LICADO operating pressure. Consequently, a smaller contact angle (94°) can explain the poor separation result (13% ash content, 11% yield) at zero mixing speed, where no shear force is supplied to expose the water-first-wet coal surface to the liquid CO₂ medium. On the other hand, an optimum mixing speed in both phases will provide enough shear force to expose the clean coal particles to the liquid CO₂ droplets. It follows that a good separation (8.6% ash content, 67% yield) at 800 rpm can be interpreted by the larger contact angle (145°) when coal particles are in contact with liquid CO₂ (CO₂-first-wet case). As the mixing speed increases beyond 1200 rpm, the very strong agitation action, which overwhelms the interfacial force, may cause the entrainment of refuse particles into large clean coal agglomerates. This results in a higher ash content (12.3% ash content) in the product coal.

Table 2: SURFACE AND PHYSICAL PROPERTIES OF COAL SAMPLES

Ash %	Particle Size μm	Specific Gravity	Surface Area $\text{m}^2/\text{g-coal}$	g-CO ₂ adsorbed ^a per g-coal	Film Pressure N/m $\times 10^3$
2.7 (4c)	15.2	1.27	163	0.097	61.3
3.4 (3c)	16.0	1.28	156	0.088	65.0
5.0 (2c)	16.2	1.30	156	0.097	65.0
6.9 (4r)	17.1	1.32	143	0.095	79.5
8.4 (1c)	18.8	1.31	138	0.085	81.2
11.6 (3r)	18.8	1.32	136	0.090	80.9
18.1 (2r)	17.4	1.40	82	0.055	88.0
23.5 (f)	18.4	1.45	109	0.082	81.8
54.2 (1r)	25.6	1.88	52	0.046	93.7

^aAt CO₂ pressure of 6.2 MPa.

Adsorption and Agglomeration of the LICADO Process

The measurements of CO₂ adsorption on samples from each cleaning stage were performed at pressures ranging from vacuum pressure to the vapor pressure of CO₂ at room temperature. The results are presented in Table 2. It can be seen that the use of carbon dioxide in fine coal cleaning produces clean coal with a relatively larger specific surface area (136 ~ 163 m²/g-coal) than that of the corresponding refuse (52 ~ 143 m²/g-coal). The mean particle size and the specific gravity increase as the ash content of the coal sample increases. In addition, the CO₂ adsorption data, obtained at various elevated pressures to construct a complete adsorption isotherm, shows that the amount of CO₂ adsorbed on the clean coal samples (0.085 ~ 0.097 g-CO₂/g-coal) is greater than the amount adsorbed on the corresponding refuse (0.046 ~ 0.095 g-CO₂/g-coal). Consequently, the film pressure of each coal sample increases from 0.0613 to 0.0937 N/m as the ash content of the coal sample increases from 2.7% to 54.2%. Due to the low surface tension of liquid CO₂, it has been deduced that the CO₂ adsorption film pressure is suitable to represent the solid surface tension of the coal. Thus, the surface tension (γ_s) of these coal/refuse samples increases from 0.0613 to 0.0937 N/m as the ash content increases from 2.7% to 54.2%. It is believed that this large amount of adsorbed CO₂ will help to agglomerate the clean coal particles, which further confirms the validity of using liquid CO₂ for fine

coal cleaning.

Effect of Particle Size on Coal Surface Properties

Since the clean coal samples have relatively larger surface areas and smaller particle sizes than those of the refuse samples, three factors were envisioned to contribute to these adsorption results: (1) surface property (ash content); (2) mean particle size; (3) specific surface area.

In order to understand the role that the mean particle size plays on the coal/refuse surface properties, portions of Upper Freeport -28 mesh and -28+100 mesh coal were ground to -200 mesh and -100 mesh coal respectively. Hence within each of these two tested groups (-28 mesh and -200 mesh; -28+100 mesh and -100 mesh), the coal samples differ only in their particle size while the other physical properties such as the ash content, sulfur content and specific gravity remain the same. The contact angles, surface areas, and adsorption isotherms for these samples were experimentally determined.

The results (Table 3) show that the contact angles in the large particle size fractions (-28+100 mesh and -28 mesh) are slightly smaller than those in the small particle size fractions (-100 mesh and -200 mesh). This may be attributed to the apparent differences in surface condition of the compressed coal pellet samples formed with large and small particle sizes. Hence the apparent contact angle measured for the large particle size coal tends to underestimate the true contact angle. This phenomenon was also observed by Murata [14]. By considering the small contact angle differences between these two size fractions of each group, it can be said that the particle size has only a minor effect on the contact angle.

Table 3: EFFECT OF PARTICLE SIZE ON COAL SURFACE/INTERFACIAL PROPERTIES

	(Ash=28.6%, S.P.=1.52)		(Ash=23.5%, S.P.=1.45)	
	-28+100 mesh	-100 mesh	-28 mesh	-200 mesh
θ in Liquid CO ₂	140	149	138	145
Surface Area (m ² /g-coal)	87	98	95	108
π_{sv} (N/m) $\times 10^3$	90.4	88.8	85.2	81.6
g-CO ₂ /g-coal at P=P ₀	0.057	0.065	0.069	0.082
g-CO ₂ /m ² -coal at P=P ₀	0.0655	0.0663	0.0726	0.0752

As expected, the surface area is smaller for the large size fraction of coal samples, but the difference of 12 ~ 14 m²/g-coal indicates that a certain portion of the internal micropore exists in these coal samples. By incorporating the data of the adsorption isotherm and the specific surface area, the film pressure of each size fraction of coal sample was measured and compared. Since the CO₂ adsorption film pressure is only a function of temperature, pressure and composition, little difference between the two size fractions of coal samples is perceived for both of the tested groups. It is thus concluded that the particle size has little effect on the CO₂ adsorption film pressure of the coal.

It is also found that coal with the larger size fraction adsorbed less CO₂ on a unit weight basis. This can be explained by the fact that when the coal particles are ground into smaller sizes, the increase in the total surface area is mostly due to the increase in the external surface area (assuming very few dead pores in the original coal particles), while the internal micropore surface area is the same for both the larger and smaller sizes of coal particles. The increase in the external surface area for the finer coal particles is known to be the reason for the increased amount of CO₂ adsorption on a unit weight basis. However when expressed on a unit surface area basis, the same amount of adsorption is observed. Again, it reveals that the mean particle size has a minor effect on the CO₂ adsorption.

CONCLUSIONS

From the above discussion, it is clear that the LICADO process is a surface-property-driven process that belongs to the physical cleaning category. The work performed so far indicates that the mechanism of the LICADO process is governed by the interactions among the interfacial, shear and body forces present in the coal particle-liquid CO₂-water system. The shear and body forces are determined by the physical properties of the coal particles as well as the hydrodynamic conditions in the separation process, which subsequently control the manner that the surfaces of coal particles are exposed to processing media. Therefore, it is possible to optimize the performance of the LICADO process by improving the quality of mixing.

ACKNOWLEDGMENTS

The authors wish to gratefully acknowledge the financial support for this work by the U.S. Department of Energy (DE-AC22-83PC63048).

BIBLIOGRAPHY

1. Yoon, R.H., Cleaning of Ultrafine Coal by Microbubble Flotation, presented at the First Annual Pittsburgh Coal Conference, September 1984.
2. Capes, C.I., McIlhenny, N.E., McKeever, R.E., and Massor, L., Application of Spherical Agglomeration to Coal Preparation, Paper Presented at the 7th International Coal Preparation Congress, Sydney, Australia, 1976.
3. Keller, D.V., The Otisca Process of Preparation and Dewatering of Fine Coal, pp. 152-171 Proceeding of the Consolidation and Dewatering of Fine Particles Conference, University of Alabama, August 10-12, 1982.
4. Chiang, S.H. et al., Process for Removing Mineral Matter From Coal, Patent Number: 4,613,429, September 23, 1986.
5. Bikerman, J.J., J. Phys. Colloid. Chem. 64, 1292 (1960).
6. Burnett, M.K., Zisman, W.A., J. Phys. Chem. 64, 1292 (1960).
7. Neumann, A.W., Good, R.J., Hope, C.F. and Sejpal, M., J. of Colloid and Interface Science, Vol. 49, No. 2, Nov. 1974.
8. Neumann, A.W., et al., "Surface Properties of Coal Particles in Aqueous Media. I. Solidification Front Measurements", Dept. of Mechanical Engineering, Univ. of Toronto, Ontario, Canada, 1984.
9. Neumann, A.W., et al., "Surface Tension Effects in the Sedimentation of Coal Particles in Various Liquid Mixtures", Dept. of Mechanical Engineering, Univ. of Toronto, Ontario, Canada, 1984.
10. Marsh, H., Siemieniowska, T., Fuel 44, pp. 355-367, 1965.
11. Honda, H., Yoshida, Y., Toyada, S., Hatami, M. and Toda, Y., Fuel 50, No. 2, pp. 187-200, 1971.
12. Andreas, J.M., Hauser, E.A., Tucker, W.B., J. Phys. Chem., 42, pp. 1001-1019, 1938.
13. Rotenberg, Y., Boruvka, L., and Neumann, A.W., J. of Colloid and Interface Science, Vol. 93, No. 1, pp. 169-183 (1983).
14. Murata, T., "Wettability of Coal Estimated from the Contact Angle," Fuel 1981, Vol. 60, Aug. pp 744-746.

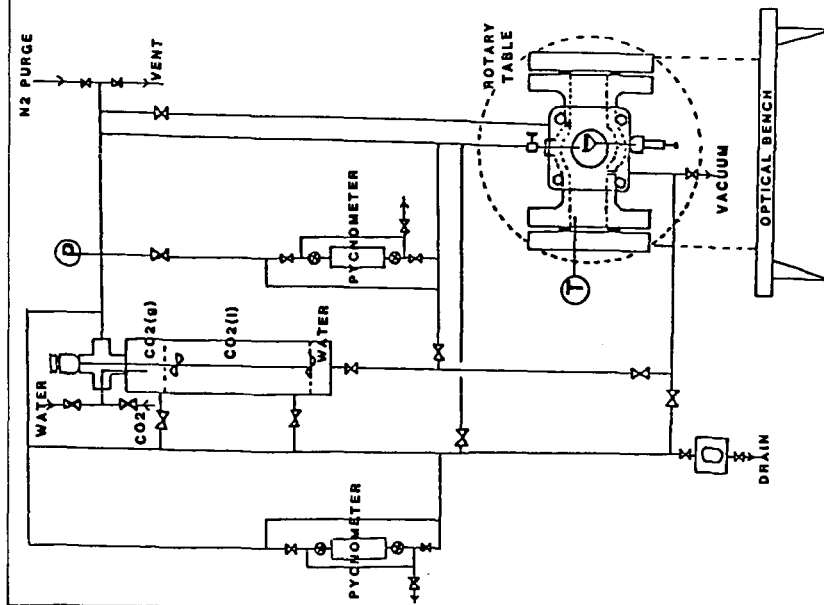


Figure 1: High Pressure Contact Angle Apparatus

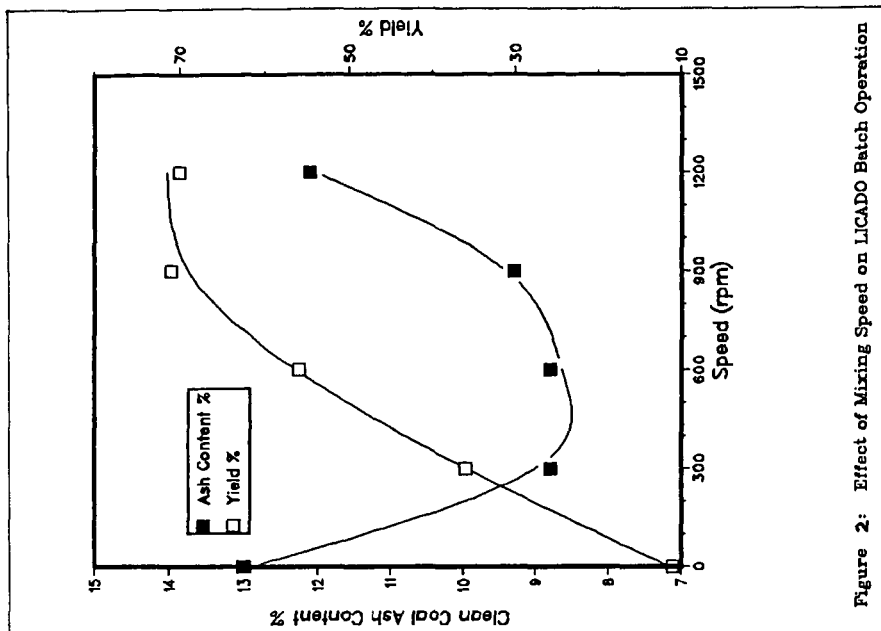


Figure 2: Effect of Mixing Speed on LICADO Batch Operation

MEASUREMENT OF SURFACE PROPERTIES OF COAL USING A MODIFIED
WASHBURN TECHNIQUE

Geatesh K. Tampy, Wen-Jia Chen, Michael E. Prudich and
Robert L. Savage

Department of Chemical Engineering
Ohio University
Athens, Ohio 45701

Abstract

Several physical coal cleaning processes, e.g. oil agglomeration and flotation, are dependent on the surface properties of coal. One conventional method of surface characterization involves measurement of the contact angle. The Washburn method of contact angle measurement has advantages over most other techniques used to measure the contact angle of solids in powder form. This technique involves filling a vertical cylindrical tube with the powdered solid and allowing a liquid to penetrate the powder bed by capillary driving forces.

The Washburn method has been modified using fundamental equations governing fluid transport through a packed bed. The experimental methodology itself has been extended to allow for the application of an external pressure differential to supplement the capillary forces. The addition of the applied pressure differential simplifies computation of the contact angle. Contact angles for different coal/oil systems have been measured and the interfacial free energy changes have been quantified. These results have been related to performance of the coals in the oil agglomeration process.

INTRODUCTION

There are several different methods for characterizing the interaction of nonpolar and nonionic liquids with polydisperse, heterogeneous solids (like coal) in powder form. These characterization techniques often result in the calculation of a contact angle. Unfortunately, the results produced from these varying techniques often do not agree. Two of the more popular quantitative methods for measuring the contact angle in such systems are the Bartell plug method(1) and the Washburn capillary rise method(2). More recently Heertjees and Kossen(3) have suggested a different approach which involves making a compressed pellet out of the powdered solid, and measuring the height of a drop of liquid placed on the pellet. The contact angle is measured based on the height of the drop and the porosity of the plug as measured by mercury intrusion. However, Neumann and Good(4) have indicated that pelletization changes the nature of the solid surface. The Bartell method, which involves the application of an external pressure to resist the penetration of a liquid into a plug of the solid powder, is extremely cumbersome. The Washburn method, which also involves a plug of the solid powder, is much simpler to perform and involves filling a vertical glass tube with the powder and allowing the liquid to penetrate the plug aided purely by capillary forces. The rate of penetration is measured and the contact angle calculated.

The Washburn method, though simple in execution, has two major drawbacks: 1) The computation of the contact angle is based on the assumption that the powder in the tube can be described as a bundle of capillaries with circular cross-section. The Hagen-Poiseuille equation is then applied to yield,

$$\frac{dh}{dt} = \frac{R^2 \Delta P}{8\nu h} \quad 1)$$

where t is time, h is the height of the column of liquid in the capillary, R is the radius of the capillary, ν is the viscosity, and ΔP is the Laplace pressure, given as,

$$\Delta P = \frac{2 \delta_{lv} \cos \theta}{R} \quad 2)$$

where δ_{lv} is the liquid-vapor interfacial tension and θ is the contact angle. 2) The capillary radius, R, in the equation above, has to be calculated in order to determine the contact angle. The suggested methods for doing this include either conducting an experiment with a liquid which "completely wets" the surface of the powder (then the $\cos \theta$ value is forced to unity and R can be directly computed) or using mercury porosimetry data to estimate the value of R (5). There are problems with both of these approaches. For a heterogeneous substance like coal, it is not easy to find a liquid which completely wets all of the chemically different fractions (both organic and mineral). Furthermore, at least two experiments are required in order to quantify the contact angle, the experiment with the completely wetting liquid and the experiment with the liquid to be characterized. The packing of the powder plug in the two experiments might not be the same, resulting in an erroneous estimation of R.

Using mercury porosimetry to estimate R has its own unique problems. The contact angle for mercury with most solids is known to lie between 130 and 140 degrees(5). Therefore, the "wetting" of coal by mercury is accompanied by an increase in the surface free energy. In oil agglomeration, we are looking for oils which will wet the coal surface and cause a decrease in the surface free energy. Keeping these conditions in mind, in the absence of an applied external force oils will spontaneously penetrate the interstices of the plug to a much greater degree, and more quickly, than mercury. The effective interstitial structure that mercury sees is not the same effective interstitial structure that the oils sees. It is this effective structure that defines the behavior of the draw up of oil by the plug.

Figure 1 shows the results of mercury porosimetry tests on two powdered coal samples, PSOC 276 and PSOC 751. The volume of mercury intrusion per gram of sample was found to increase from 0.18 ml to 1.16 ml for PSOC 276 and from 0.15 ml to 1.15 ml for PSOC 751 as the applied pressure was increased from 0 psia to 48,000 psia. Table 1 indicates the volumes per gram drawn into the same two coals for different agglomerating oils. Comparing Figure 1 and Table 1 it can be seen that a pressure of about 100 psia would have to be applied to the mercury system to cause the same amount of mercury draw-up that occurs spontaneously (at 0 psia) for the hydrocarbon oil systems.

TABLE 1
Specific Oil Draw-up for Coal Samples.

Specific Draw-up, ml oil per gram coal			
Coal Sample	No.2 Fuel Oil	Varsol	Pentane
PSOC 276	0.88	0.90	0.92
PSOC 305	0.88	0.87	0.82
PSOC 751	0.85	0.83	0.82

EXPERIMENTAL METHOD

It is evident that before reasonable results can be expected, both limitations indicated above have to be eliminated. To do this, we first follow a procedure which has been successfully adopted to define the flow of fluid through a packed bed. These results are well documented in the literature(6,7) and are applicable for laminar flow (low Reynolds number, so that inertial forces can be neglected). This condition can be expected to exist when Laplace pressure drives the fluid. The analysis essentially involves two modifications to the Washburn procedure: 1) The radius of the circular capillary, R, is replaced by a "hydraulic radius", r, which is defined as the ratio of the area of cross-section of the pore through which the liquid penetrates to the wetted perimeter. The advantage of doing this is that r may subsequently be eliminated from the equation by using a relationship between r and the "average" particle diameter, D.

$$r = (De\phi) / 6 \cdot (1-e) \quad 3)$$

where ϕ is the sphericity and is assumed to equal 0.73 for pulverized coal(8). e is the interstitial void space per unit volume of the bed, or bed porosity. 2) A tortuosity factor is used to modify the distance of fluid flow upward through the packed bed. The tortuosity factor is required because the actual distance through which the liquid flows is greater than the measured height, h. Values for this factor have been experimentally determined to lie between 2.0 and 2.5, as long as the porosity of the bed is not much greater than 0.5, and the flow is laminar. A value of 25/12 was used for the tortuosity factor in our calculations(6).

If the Laplace pressure accounts for the only force causing the draw-up of then liquid, then substitution and integration yields,

$$\frac{h^2}{t} = \frac{D \cdot \phi \cdot e \cdot \delta_{lv} \cos \theta}{12.5 \sqrt{1-e}} \quad 4)$$

The above equation is not based on the assumption that the bed is a bundle of cylindrical capillaries, and also, more importantly, the velocity can be related to the particle diameter and the porosity, which is determined by measuring the quantity of liquid drawn up into the bed per unit weight of solid for each bed used.

For heterogeneous, polydisperse systems, the average diameter to be used in Equation 4 may be difficult to measure. This

difficulty may be overcome by repeating the capillary plug experiment with the addition of an external pressure driving force applied in the same direction as the capillary pressure. The additional applied pressure driving force is added linearly to the Laplace pressure driving force which appears implicitly in Equation 4. This treatment results in a system of two equations with two unknowns and a new h^2/t slope is obtained which permits D to be eliminated from the resulting single equation.

RESULTS AND DISCUSSION

Three coals, PSOC 276 (Ohio #8, hvAb, 13.5% initial ash), PSOC 305 (Ohio #11, hvBb, 22.5% initial ash), and PSOC 751 (Ohio #6, hvBb, 6.0% initial ash) were chosen for use in this study. These coals are among a group of Ohio coals currently being evaluated for their physical beneficiation potential at Ohio University. Upon receipt from the Penn State Coal Sample Bank, the coals were carefully stored under nitrogen, were wet ground and vacuum dried. In performing the capillary rise experiments, the dried samples were put into glass tubes (120mm long x 10mm ID) with fritted glass bottoms, to form packed beds. A standard tapping procedure was adopted to insure that the packing, and hence the porosity, did not vary too much from one bed to the another. It was found that after 500 taps, dealt out in sets of 50 interspersed with the addition of more coal to the tube, the variation in the final height of sample in the column did not change more than 2mm (1.7% of total bed height). The tubes were weighed before and after the filling and the weight of sample per unit volume of the tube was computed. The sides of the tubes were marked with graduations, and the tubes placed vertically so that the bottom of the tube was just in contact with the liquid in a beaker. If the liquid were to wet the solid, it would rise up the tube at a rate dictated by Equation 4. This rise could clearly be observed. At the conclusion of the experiment, the tube was weighed once again and the weight of the liquid drawn up per unit volume of the tube, and the porosity were evaluated. It was found that for all the tests, the porosity fell within the range 0.5 ± 0.02 .

The change in height of the liquid in the column was recorded as a function of time and an h^2 versus t graph plotted. A good straight line fit was observed in every case, and the reproducibility was very good (Figure 2). The D values were calculated using the slopes obtained from experiments performed with and without an external applied pressure. These values are depicted in Table 2. Also shown are the particle volume mean diameters which were measured using a Horiba CAPA 300 centrifugal particle size analyzer (the assumed particle density was 1.35 g/ml). Both sets of particle size readings show the same trend with the "capillary" readings being, on the average, 28% greater than the centrifugal sizing readings. The $\cos \theta$ and θ values for the three coals with Varsol and pentane are also computed, using the calculated D values. Young's equation (Equation 5) was applied to the data and the product, $\delta_{1V} \cos \theta$ calculated.

$$\delta_{sv} - \delta_{sl} = \delta_{1V} \cos \theta \quad 5)$$

The term $\delta_{1V} \cos \theta$ represents the difference between the coal-air interfacial energy and the coal-oil interfacial energy, that is, the decrease in free energy that occurs when the coal is wetted by the oil. Calculated values for these three terms can be found in Table 3.

The three coals, PSOC 276, PSOC 305, and PSOC 751 have been subjected to oil agglomeration testing using No.2 fuel oil, Varsol, and pentane as the agglomerating oils. The results of several oil agglomeration tests are given in Table 4. A comparison of Tables 3 and 4 illustrate that the coal/oil combinations which yield the best ash reductions are also the combinations having the larger surface free energy decreases. Therefore, the wettability results do provide some indication of the oil agglomeration performance that may be expected for a given coal/oil combination.

TABLE 2

Particle Diameters.

Coal	Mean particle diameters, microns	
	From Capillary Calc.	From CAPA 300
PSOC 276	11.3	8.4
PSOC 305	11.9	9.5
PSOC 751	10.1	8.1
Standard Dev.	0.8	0.8

TABLE 3

Contact Angle Results.

Coal	No. 2 Fuel Oil			Varsol			Pentane		
	θ	$\cos\theta$	$\delta_{lv}\cos\theta$	θ	$\cos\theta$	$\delta_{lv}\cos\theta$	θ	$\cos\theta$	$\delta_{lv}\cos\theta$
PSOC 276	74.6	0.26	7.3	83.3	0.12	3.3	83.7	0.11	2.0
PSOC 305	83.7	0.11	3.1	87.2	0.05	1.4	89.3	0.04	0.7
PSOC 751	79.8	0.18	5.0	84.6	0.09	2.4	85.8	0.07	1.2

Free energies reported in units of dyne/cm.

TABLE 4
Results of Oil Agglomeration Testing.

Coal	Oil	Feed Ash, wt%	Product Ash, wt%	% Ash Reduction
PSOC 276	No. 2	15.5	9.0	41.9
PSOC 276	Varsol	13.7	7.7	43.8
PSOC 276	Pentane	13.6	7.2	47.1
PSOC 305	No. 2	22.7	12.4	45.4
PSOC 305	Varsol	22.4	17.2	23.2
PSOC 305	Pentane	22.7	17.1	24.7
PSOC 751	No. 2	6.1	3.6	41.0
PSOC 751	Varsol	5.7	3.5	38.6
PSOC 751	Pentane	5.7	4.4	22.8

CONCLUSIONS

A modified Washburn technique of contact angle measurement has been proposed that does not suffer from some of the inadequacies of the original technique. Using the modified method, the decrease in free energy associated with the replacement of a solid-air interface by a solid-liquid interface can be measured. Such measurements are useful in predicting the efficiencies that may be expected in the oil agglomeration process and possibly in other surface-based physical beneficiation processes. Additional processing information, such as degree of mineral matter liberation, is required in order to make quantitative predictions of beneficiation performance.

ACKNOWLEDGEMENTS

The authors would like to acknowledge the State of Ohio for its financial support. The authors would also like to thank the Penn State Coal Sample Bank for supplying the coal samples used and Dr. W. Kneller of the University of Toledo for his help in obtaining the mercury porosimetry data.

REFERENCES

1. Bartell, F.E., and Merrill, E.J., J. Phys. Chem., **36**, 1178 (1932); Bartell, F.E., and Whitney, C.E., ibid., p. 3115.
2. Washburn, E.W., Phys. Rev., **17**, 273 (1921).
3. Heertjes, P.H., and Kossen, N.W.F., Powder Technology, **2**, 33 (1967).
4. Neumann, A.W., and Good, R.J., in Surface and Colloid Science, Vol. **11**, Good, R.J., and Stromberg, R.R., eds., Plenum, NY (1979).
5. Hiemenz, P.C., Principles of Colloid and Surface Chemistry, 2nd ed., Marcel Dekker, NY (1986).
6. Bird, R.B., Stewart, W.E., and Lightfoot, E.N., Transport Phenomena, John Wiley, NY (1960).
7. McCabe, W.L., and Smith, J.C., Unit Operations of Chemical Engineering, 3rd ed., McGraw-Hill, NY (1976).
8. Perry, R.H., and Chilton, C.H., eds., Chemical Engineers' Handbook, 5th ed., McGraw-Hill, NY (1973).

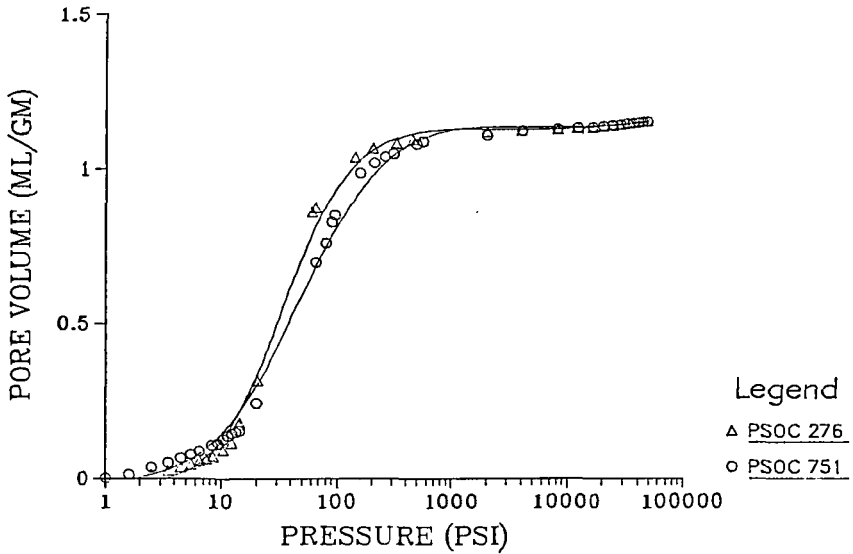


Figure 1. Mercury intrusion data for two Ohio coals.

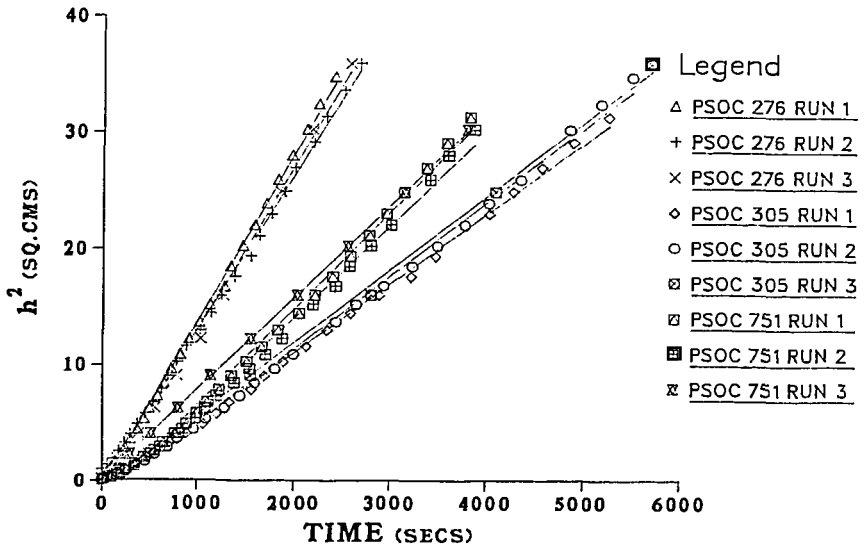


Figure 2. Capillary rise data for the intake of No. 2 Fuel oil by three Ohio coals. Three runs for each coal.